Contents

Chapter 6

Waves in Laser-Produced Plasma

6.1 Foreword to Parametric Instabilities

The dispersion relation for electron plasma waves is developed in section 2.6. Some changes in the dispersion relation of electron and ion waves due to ponderomotive force are given in section 4.3. In this chapter we discuss mainly the parametric instabilities in laser–plasma interactions.

All material substances, including plasma, interact nonlinearly with high-power lasers leading to parametric instabilities. A **parametric instability** is defined in general by the nonlinear phenomenon where a periodic variation in the medium induces growing oscillations at a different frequency. In solids, liquids and gases these instabilities arise due to the nonlinear polarizability of the material. In a plasma medium the nonlinear effects are caused by such terms as $\mathbf{v} \times \mathbf{B}$, $\mathbf{v} \cdot \nabla \mathbf{v}$, $\nabla \cdot (n\mathbf{v})$, ponderomotive forces, changes of mass due to relativistic velocities, velocity-dependent collision frequency, etc. These terms can cause a large amplitude wave, called the **pump wave**, which provides the driving force to excite other wave modes in the plasma.

In the absence of a pump wave and a magnetic field, three modes of propagation are possible in plasma:

(a) **electromagnetic wave**;
(b) **electron wave**, known as **plasmon** or **Langmuir wave** (sometimes denoted by '**high frequency electrostatic plasma wave**'); and
(c) **ion wave**, also called **acoustic wave** (sometimes denoted by '**low frequency electrostatic ion-acoustic wave**').

Neglecting the ponderomotive forces, the dispersion relations of these waves are

$$\textbf{electromagnetic wave}: \quad \omega^2 = \omega_{pe}^2 + c^2 k^2 \tag{6.1}$$

$$\textbf{electron wave} = \textbf{plasmon}: \quad \omega^2 = \omega_{pe}^2 + 3k^2 v_e^2 \tag{6.2}$$

$$\textbf{ion wave} = \textbf{acoustic wave}: \quad \omega = kc_s = k\left(\frac{Zk_B T_e}{m_i}\right)^{1/2} \tag{6.3}$$

where ω and k are the wave frequency and wave number respectively and $\omega_{pe} = (4\pi e^2 n_e/m_e)^{1/2}$ is the electron plasma frequency. m_e and m_i are the electron and ion mass respectively, Z is the degree of ionization, c is the speed of light and c_s is the sound velocity, T_e, v_e and n_e are the electron temperature, velocity and density respectively, and k_B is the Boltzmann constant. T_e much larger than the ion temperature is assumed. Equations (6.1) and (6.2) were derived in sections 2.7 and 2.6 respectively, while equation (6.3) is developed in section 6.6 of this chapter (the soliton section).

A high-power laser wave (denoted by the incoming 'photon'), serving as a pump, can induce the following parametric instabilities in plasma:

Wave–wave interaction

photon → photon + acoustic	(stimulated Brillouin scattering = SBS)
photon → photon + plasmon	(stimulated Raman scattering = SRS)
photon → acoustic + plasmon	(decay instability)
photon → plasmon + plasmon	(two-plasmon instability)

Wave–particle interaction

photon + particle → photon + particle	(stimulated Compton scattering)
photon + particle → plasmon + particle	(stimulated Compton scattering)
photon + particle → acoustic + particle	(stimulated Compton scattering)

(6.4)

In (6.4) 'photon', 'acoustic' and 'plasmon' mean electromagnetic, ion and electron waves respectively. The **energy and momentum conservation** in the wave–wave interaction is described by

$$\omega_0 = \omega_1 + \omega_2, \qquad \mathbf{k}_0 = \mathbf{k}_1 + \mathbf{k}_2 \tag{6.5}$$

where ω_0 and $\mathbf{k}_0$ are the frequency and wave number of the pumping laser field that decays into two waves (ω_1, $\mathbf{k}_1$) and (ω_2, $\mathbf{k}_2$). Using these conservation laws and the dispersion relations (6.1), (6.2) and (6.3), the wave–wave interactions are induced in the following domain:

1. A laser pump with frequency near the plasma frequency, $\omega_0 \approx \omega_{pe}$, may decay into a plasmon and an ion wave, resulting in absorption of the laser. This effect happens near the critical surface since $\omega_0 \approx \omega_{pe}$ implies $n_e \approx n_{ec}$, where n_{ec} is the critical density.
2. A laser pump with frequency $\omega_0 > 2\omega_{pe}$ may decay into a photon and a plasmon (SRS), leading to laser scattering, including backscattering.

This instability reduces the laser absorption. $\omega_0 > 2\omega_{pe}$ implies that this instability occurs at $n_e < \frac{1}{4} n_{ec}$.

3. A laser pump with frequency $\omega_0 > \omega_{pe}$ may decay into a photon and an acoustic wave (SBS), resulting in backscattering and thus reduced laser

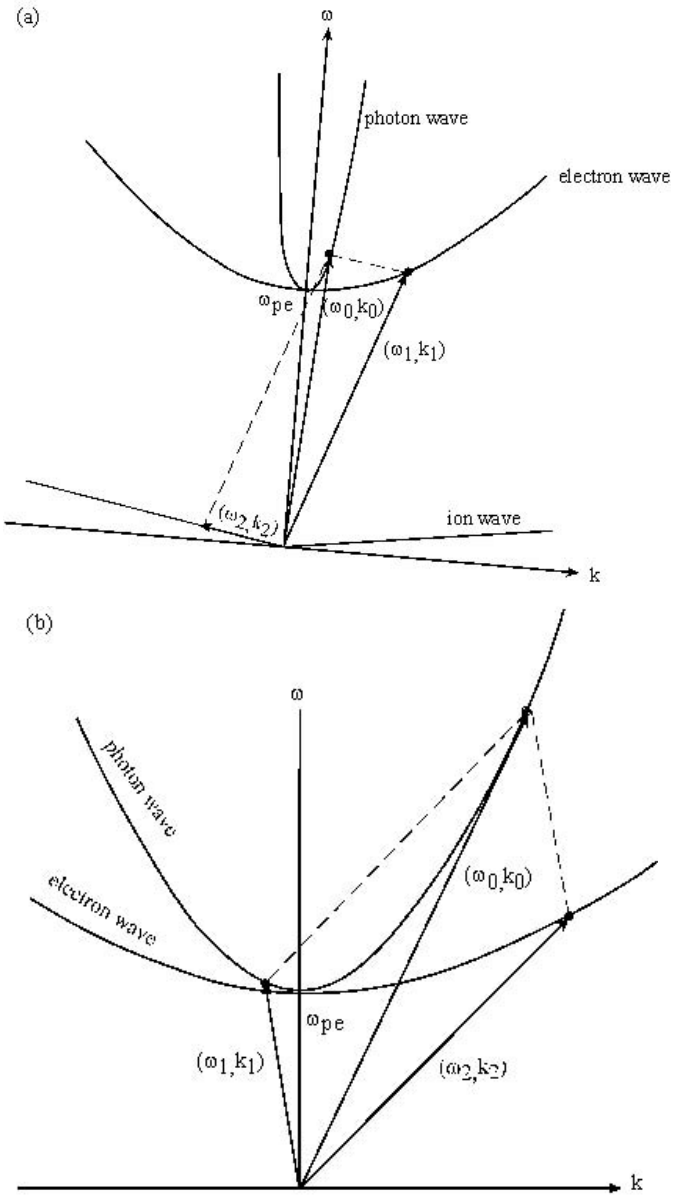

Figure 6.1—continues.

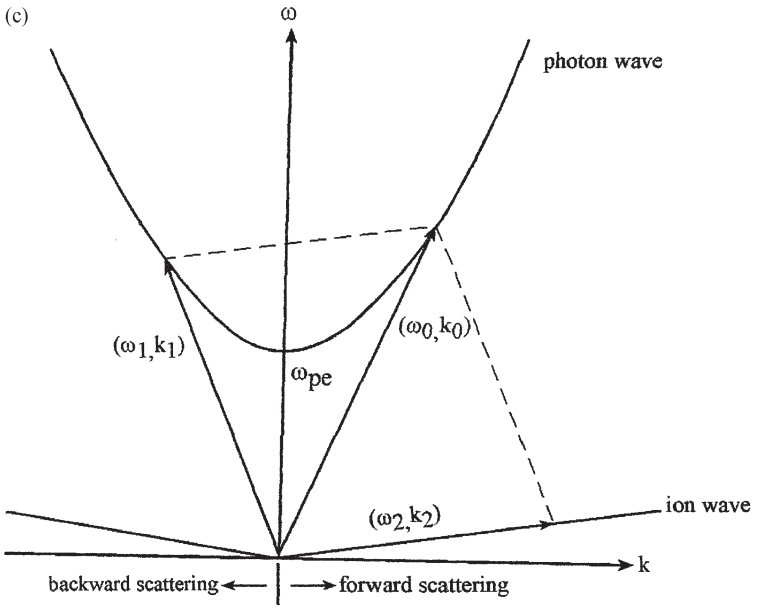

Figure 6.1. Schematic description in the ω-k space of the conservation laws given in equations (6.5), taking into account the dispersion relations (6.1), (6.2) and (6.3) for (a) decay instability, (b) stimulated Raman instability and (c) stimulated Brillouin instability.

absorption. SBS contains a low-energy ion wave that takes only a small fraction of the laser energy, while the rest of the energy can be scattered out of the plasma. $\omega_0 > \omega_{pe}$ implies that this instability occurs at $n_e < n_{ec}$.

4. A laser pump with frequency $\omega_0 = 2\omega_{pe}$ may decay into two plasmons, inducing laser absorption. This phenomenon happens at an electron density $n_e = \frac{1}{4}n_{ec}$.

A schematic description of the conservation laws given in equations (6.5) are given in figure 6.1 (Hughes 1980), taking into account the dispersion relations (6.1), (6.2) and (6.3) for (a) decay instability, (b) stimulated Raman instability and (c) stimulated Brillouin instability. The wave is described by a point vector on the appropriate dispersion relation line in the ω-k space and equations (6.5) are satisfied by adding the vectors according to the decay under consideration.

The possible absorption mechanisms and the domain of wave–wave interactions are summarized in figure 6.2 along a density profile typical of laser–plasma interaction.

Parametric instabilities in plasma have been studied for the past 40 years. Since the first analytic analysis (Dubois and Goldman 1965, Silin

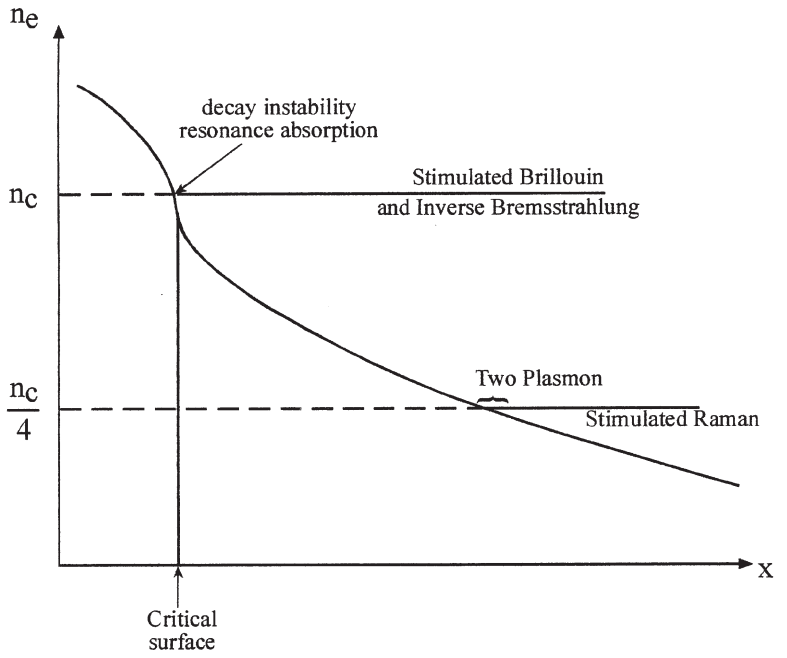

Figure 6.2. Possible absorption mechanisms and the domain of wave–wave interactions along the density profile.

1965a), general treatment of the parametric instabilities were developed (Nishikawa 1968, Rosenbluth 1972, Chen 1974, Dawson and Lin 1974, Kaw *et al.* 1976, Hughes 1980, Cairns 1983, Kruer 1988) and the experimental status summarized (Baldis *et al.* 1991). Since the 1960s at almost every conference on high-power laser–plasma interactions, the subject of parametric instabilities has been on the agenda.

In section 6.2 the forced harmonic oscillator is summarized in an elementary introduction (Crawford 1968) to the general formalism of parametric instabilities. As is demonstrated in this section, energy cannot be absorbed by a wave without the existence of damping. In non-relativistic plasma the electromagnetic wave suffers only collisional damping. However, the electron and ion waves experience in addition to collision the collisionless damping due to wave particle interactions. In order to clarify this physically important phenomenon, discovered by Landau (Landau 1946), a physical picture of Landau damping (Stix 1992, Kruer 1988) is given in section 6.3. In section 6.4 the formalism of the parametric decay instability is given and in section 6.5 the stimulated Brillouin scattering is developed. We end this chapter with section 6.6, where the soliton equation is obtained for ion plasma waves.

6.2 The Forced Harmonic Oscillator

In this section the harmonic motion of a point mass oscillating in the x direction is summarized (Crawford 1968). This is instructive for understanding the more complex problem of parametric instabilities. The displacement from equilibrium is denoted by $x(t)$. The forces acting on the mass m are:

(a) The return force, $-m\omega_0^2 x(t)$, due to a spring constant $K = m\omega_0^2$.
(b) A frictional drag force, $-m\Gamma(\mathrm{d}/\mathrm{d}t)x$, where Γ is the damping constant per unit mass (Γ has the dimension of s^{-1}).
(c) An external force $F(t)$.

First, the special case where $F = 0$ is considered. The equation describing the motion for the displacement from equilibrium $x_1(t)$ is

$$\frac{\mathrm{d}^2 x_1}{\mathrm{d}t^2} + \Gamma \frac{\mathrm{d}x_1}{\mathrm{d}t} + \omega_0^2 x_1 = 0. \tag{6.6}$$

The solution of (6.6) with the initial conditions $x_1(0)$ and $v_1(0) = (\mathrm{d}/\mathrm{d}t)x_1(0)$ is

$$x_1(t) = \exp\left(-\frac{\Gamma t}{2}\right)\left\{x_1(0)\cos\omega_1 t + \left[\frac{v_1(0) + 0.5\Gamma x_1(0)}{\omega_1}\right]\sin\omega_1 t\right\} \tag{6.7}$$
$$\omega_1^2 = \omega_0^2 - \tfrac{1}{4}\Gamma^2.$$

The oscillations are weakly damped if $\frac{1}{2}\Gamma \ll \omega_0$. The oscillations are critically damped if $\frac{1}{2}\Gamma \approx \omega_0$, in this case $\omega_1 \to 0$, $\cos\omega_1 t \to 1$ and $(1/\omega)\sin\omega_1 t \to t$. If $\frac{1}{2}\Gamma > \omega_0$ the oscillations are over-damped, $\omega_1 = \pm\mathrm{i}|\omega_1|$ and $\cos\omega_1 t \to \cosh\omega_1 t$, $\sin\omega_1 t \to \sinh\omega_1 t$.

Next, the forced oscillation is introduced by taking $F(t) = F_0\cos\omega t$. This case is representative for functions that can be described by Fourier transform. Therefore, the equation of motion in this case is given by

$$\frac{\mathrm{d}^2 x}{\mathrm{d}t^2} + \Gamma\frac{\mathrm{d}x}{\mathrm{d}t} + \omega_0^2 x = \left(\frac{F_0}{m}\right)\cos\omega t. \tag{6.8}$$

The **steady-state** solution of this equation describes the motion of the oscillator after the harmonic driving force has been applied for a very long time compared with the free oscillation mean decay time $\tau_\mathrm{f} = 1/\Gamma$. In this case the harmonic oscillations are at frequency ω. The steady-state solution of equation (6.8) is

$$\begin{aligned} x_\mathrm{s} &= X_\mathrm{ab}\sin\omega t + X_\mathrm{el}\cos\omega t \\ X_\mathrm{ab} &= \left(\frac{F_0}{m}\right)\left\{\frac{\Gamma\omega}{(\omega_0^2-\omega^2)^2 + \Gamma^2\omega^2}\right\} \\ X_\mathrm{el} &= \left(\frac{F_0}{m}\right)\left\{\frac{\omega_0^2-\omega^2}{(\omega_0^2-\omega^2)^2 + \Gamma^2\omega^2}\right\}. \end{aligned} \tag{6.9}$$

It is important to point out that $X_{ab}(\Gamma = 0) = 0$. One can see that X_{ab} is the amplitude of power absorption. On the other hand, X_{el} does not contribute to the power absorption (see equation (6.10)) but contributes only to the energy of the system; thus it describes an elastic amplitude.

The time-averaged input power $P(\omega)$ into the oscillator is

$$P(\omega) = \left\langle F(t)\frac{dx}{dt}\right\rangle = \frac{1}{2}F_0\omega X_{ab}$$
$$= \left(\frac{F_0^2}{2m\Gamma}\right)\frac{\Gamma^2\omega^2}{(\omega_0^2-\omega^2)^2+\Gamma^2\omega^2} \tag{6.10}$$

where $\langle\ \rangle$ denotes time average, and $\langle\cos^2\omega t\rangle = \frac{1}{2}$, $\langle\cos\omega t\sin\omega t\rangle = 0$ was used. We emphasize again that $P = 0$ if $\Gamma = 0$.

The frequencies $\omega(\pm\frac{1}{2})$, where the power decreases to half its value, are

$$\omega(\pm\tfrac{1}{2}) = \sqrt{\omega^2+\frac{\Gamma^2}{4}} \pm \frac{\Gamma}{2}. \tag{6.11}$$

The frequency interval between the two half-power points, $\Delta\omega_{res} = \omega(+\frac{1}{2}) - \omega(-\frac{1}{2})$ is defined as the 'full-frequency width at half maximum' and equals Γ. Therefore, one has the following very important relation between the resonance 'full-width' for forced oscillations and the mean decay time for free oscillations τ_f:

$$\Delta\omega_{res}\tau_f = 1, \qquad \Delta\omega_{res} = \Gamma, \qquad \tau_f = \frac{1}{\Gamma}. \tag{6.12}$$

It is important to note that even for a system with many degrees of freedom the resonant width and the free decay time for each mode satisfy equation (6.12), assuming that the resonances are well separated, i.e. they do not overlap.

The time-averaged stored energy $W(\omega)$ is given by

$$W(\omega) = \frac{1}{2}m\left\langle\left(\frac{dx}{dt}\right)^2\right\rangle + \frac{1}{2}m\omega_0^2\langle x^2\rangle = \frac{1}{4}m(\omega_0^2+\omega^2)(X_{ab}^2+X_{el}^2)$$
$$= \left(\frac{F_0^2}{4m}\right)\frac{(\omega_0^2+\omega^2)}{(\omega_0^2-\omega^2)^2+\Gamma^2\omega^2}. \tag{6.13}$$

The general solution of equation (6.8) is

$$x(t) = x_1(t) + x_s(t)$$
$$= \exp\left(-\frac{\Gamma t}{2}\right)(X_1\sin\omega_1 t + X_2\cos\omega_1 t) + X_{ab}\sin\omega t + X_{el}\cos\omega t \tag{6.14}$$

where X_1 and X_2 are arbitrary constants fixed by the initial conditions of displacement and velocity. Taking $x(0) = 0$, and $v(0) = 0$ the solution

(6.14) can be rewritten

$$x(t) = X_{\mathrm{ab}}\left[\sin\omega t - \exp\left(-\frac{\Gamma t}{2}\right)\sin\omega_1 t\right] + X_{\mathrm{el}}\left[\cos\omega t - \exp\left(-\frac{\Gamma t}{2}\right)\cos\omega_1 t\right]. \tag{6.15}$$

Two special solutions are of interest, one at the eigenvalue frequency,

$$x(t, \omega = \omega_1) = \left[1 - \exp\left(-\frac{\Gamma t}{2}\right)\right] x_{\mathrm{s}}(t) \tag{6.16}$$

(note that for $t \gg 1/\Gamma$ one gets the steady-state solution as given above) and the second, more important, is the resonance solution (for $\Gamma = 0$)

$$x(t, \omega = \omega_0) = \left(\frac{F_0}{2m\omega_0}\right) t \sin\omega_0 t. \tag{6.17}$$

In the resonant case the amplitude of oscillations is unbounded as $t \to \infty$ because the oscillator continuously absorbs energy from periodic external force. This system is in resonance with the external force.

6.3 Landau Damping

Landau damping is discussed in almost every book on plasma physics. However, in most of the literature this collisionless damping appears in an abstract mathematical formalism. An electron or ion wave can be damped without collisions. Since this phenomenon is not a mathematical trick, but has a concrete physical reality, it is also important to explain it in a physical picture supported by mathematics. We shall follow a picture suggested by Stix (Kruer 1988, Stix 1992).

In the simplest one-dimensional model, the motion of the particles (electrons or ions) in an electric field are described by Newton's law:

$$\frac{\mathrm{d}^2 x}{\mathrm{d}t^2} = \frac{\mathrm{d}v}{\mathrm{d}t} = \frac{qE}{m}\sin(kx - \omega t) \tag{6.18}$$

where x is the coordinate of the particle, q and m are the charge and mass of the particle, and E, k and ω are the amplitude, the wave number and the angular frequency of the electric field. Equation (6.18) is nonlinear and very complex.

Following the previous section it seems that without damping it is impossible to damp energy into (or out) of the particles. This statement is correct only for one particle, or for a system of particles whose velocity distribution is constant. However, by considering a non-constant velocity distribution of the particles, one can divide the particles into two groups: one with velocity v significantly different from the wave phase velocity

ω/k, and the second with a velocity in the range of the electric field phase velocity, $v \approx \omega/k$. For v very different from ω/k, equation (6.18) implies that these particles oscillate without any gain or loss of energy. However, particles with a velocity $v \approx \omega/k$ feel a nearly constant electric field and therefore can be accelerated or decelerated. If the velocity distribution of the particles is not constant in the surrounding $v \approx \omega/k$, then the wave can exchange energy with the particles.

Equation (6.18) is solved using the iteration method, by expanding the solutions for $x(t)$ about a position x_0 and a free streaming velocity v_0 ($\approx \omega/k$):

$$x(t) = x_0 + v_0 t + x_1(t) + x_2(t), \qquad v(t) = \frac{\mathrm{d}x}{\mathrm{d}t} = v_0 + v_1 + v_2. \tag{6.19}$$

The zeroth-order solution of (6.18) is obtained by taking $E = 0$:

$$x(t, E = 0) = x_0 + v_0 t. \tag{6.20}$$

Substituting (6.20) into (6.18), one obtains the first-order contributions v_1 and x_1:

$$\begin{aligned} v_1 &= \frac{qE}{m\alpha}[\cos(kx_0 - \alpha t) - \cos kx_0] \\ x_1 &= -\frac{qE}{m\alpha^2}[\sin(kx_0 - \alpha t) - \sin kx_0 + \alpha t \cos kx_0] \\ \alpha &\equiv \omega - kv_0 \end{aligned} \tag{6.21}$$

where the initial conditions $v_1(0) = 0$ and $x_1(0) = 0$ were chosen. Substituting $x = x_0 + v_0 t + x_1$ into the right-hand side of equation (6.18), one gets $(\mathrm{d}/\mathrm{d}t)v_1 + (\mathrm{d}/\mathrm{d}t)v_2$ on the left-hand side of this equation. Using v_1 and x_1 from (6.21) yields

$$\begin{aligned} \frac{\mathrm{d}v_2}{\mathrm{d}t} &= \frac{qE}{m}\{\sin[(kx_0 - \alpha t) + kx_1] - \sin(kx_0 - \alpha t)\} \\ &= \frac{2qE}{m}\left\{\cos\left(kx_0 - \alpha t + \frac{kx_1}{2}\right)\sin\left(\frac{kx_1}{2}\right)\right\} \\ &\approx \frac{qE}{m}\{kx_1 \cos(kx_0 - \alpha t)\} \\ &= \frac{kq^2E^2}{m^2\alpha^2}\cos(kx_0 - \alpha t)[\sin(kx_0 - \alpha t) - \sin(kx_0) + \alpha t \cos kx_0]. \end{aligned} \tag{6.22}$$

Now the formulae are available to calculate the rate of change of the particle energy, $P(t)$. Denoting by $\langle\ \rangle_{x_0}$ the average over the initial positions and assuming that the particles are initially at random (i.e. $\langle \cos kx_0 \rangle_{x_0} = \langle \sin kx_0 \rangle_{x_0} = 0$, $\langle \cos^2 kx_0 \rangle_{x_0} = \frac{1}{2}$, etc.), one gets for $P(t; v_0)$:

$$P(t; v_0) = \left\langle \frac{\mathrm{d}}{\mathrm{d}t}\left(\frac{1}{2}mv^2\right)\right\rangle_{x_0} = m\left(\left\langle v_0 \frac{\mathrm{d}v_2}{\mathrm{d}t}\right\rangle_{x_0} + \left\langle v_1 \frac{\mathrm{d}v_1}{\mathrm{d}t}\right\rangle_{x_0}\right). \tag{6.23}$$

The term $\langle v_0 v_1 \rangle_{x_0} = 0$, while terms with a higher order than E^2 were neglected. Substituting (6.21) and (6.22) into (6.23) and averaging over the initial positions of the particles, one gets

$$P(t; v_0) = \frac{q^2 E^2}{2m} \left[\frac{\sin \alpha t}{\alpha} + k v_0 \left(\frac{\sin \alpha t}{\alpha^2} - \frac{t \cos \alpha t}{\alpha} \right) \right]$$
$$= \frac{q^2 E^2}{2m} \left[\frac{\sin \alpha t}{\alpha} - \frac{\partial}{\partial \alpha} \left(\frac{\sin \alpha t}{\alpha} \right) \right]. \tag{6.24}$$

We are interested in the vicinity of $\omega - k v_0 = \alpha \approx 0$, therefore the main contribution to the power given above is achieved for very large times. Therefore, it seems justifiable to take the limit $t \to \infty$ (Kruer 1988) in equation (6.24). Using in (6.24) the following representation for the Dirac delta function:

$$\delta(\alpha) = \frac{1}{\pi} \lim_{t \to \infty} \frac{\sin \alpha t}{\alpha} \tag{6.25}$$

and the identity

$$\delta(\alpha) = \delta(\omega - k v_0) = \frac{1}{|k|} \delta \left(v_0 - \frac{\omega}{k} \right) \tag{6.26}$$

one gets

$$P(v_0) = \frac{\pi q^2 E^2}{2m|k|} \frac{\partial}{\partial v_0} \left[v_0 \delta \left(v_0 - \frac{\omega}{k} \right) \right]. \tag{6.27}$$

The last step is to average over the initial velocity distribution of the particles $f(v_0)$, in order to obtain the desired energy rate exchange between the wave and the particles:

$$\langle P(v_0) \rangle_{v_0} = \int_{-\infty}^{+\infty} \mathrm{d}v_0 f(v_0) P(v_0) = -\frac{\pi q^2 E^2}{2m|k|} \left(\frac{\omega}{k} \right) \left[\frac{\partial f(v_0)}{\partial v_0} \right]_{(v_0 = \omega/k)}. \tag{6.28}$$

Note that $\langle P(v_0) \rangle_{v_0}$ is the average power given to the particles. For positive values the particles gain energy, while for negative values the particles lose energy, and all this without collisions between the particles. From this result one can see that the collisionless energy exchange between the wave and the particles occurs for particles having a velocity almost equal to the wave phase velocity. Particles with $v_0 < \omega/k$ (but in the vicinity of ω/k) gain energy from the wave, while particles with $v_0 > \omega/k$ (but in the vicinity of ω/k) lose energy to the wave. If $f(v_0)$ decreases with increasing velocity, i.e. the slope of $f(v_0)$ is negative at ω/k, then the wave loses energy to the particles. If $f(v_0)$ increases with increasing velocity, i.e. the slope of $f(v_0)$ is positive at ω/k, then the wave gains energy from the particles.

The power density balance (energy given by the wave = energy taken by the particles) between the wave and the particles can be written by

$$n\langle P(v_0)\rangle_{v_0} = -\frac{\mathrm{d}}{\mathrm{d}t}\left(\frac{E^2}{8\pi}\right) = -\frac{\Gamma_{\mathrm{EM}}E^2}{4\pi} \tag{6.29}$$

where n is the particle density, $E \propto \cos(\omega t)$, and Γ_{EM} (the wave damping constant) is the imaginary part of ω. Using (6.28) and (6.29), one gets

$$\frac{\Gamma_{\mathrm{EM}}}{\omega} = \frac{\pi\omega_{\mathrm{pe}}^2}{2n_{\mathrm{e}}k^2}\left[\left(\frac{\partial f(v_0)}{\partial v_0}\right)_{v_0=\omega/k}\right]. \tag{6.30}$$

In the last equation an electron wave is assumed, where ω_{pe} is the electron plasma frequency and $n = n_{\mathrm{e}}$ is the electron density. Landau has derived equation (6.30) by using the Vlasov equation (see section 3.4). Using a Maxwellian distribution for the electrons, $f(v) \approx \exp(-v^2/2v_{\mathrm{e}}^2)$, where $mv_{\mathrm{e}}^2 = k_{\mathrm{B}}T_{\mathrm{e}}$ (T_{e} = the electron temperature), equation (6.30) yields

$$\frac{\Gamma_{\mathrm{EM}}}{\omega} = -\sqrt{\frac{\pi}{8}}\,\frac{\omega_{\mathrm{pe}}^2\omega}{k^2|k|v_{\mathrm{e}}^3}\exp\left(-\frac{\omega^2}{2k^2v_{\mathrm{e}}^2}\right). \tag{6.31}$$

6.4 Parametric Decay Instability

The energy-momentum conservation of an electromagnetic wave decaying into a plasma wave is described schematically in figure 6.1(a). This decay is called the parametric decay instability. This instability is described in a formalism (Nishikawa 1968) of two harmonic oscillators with damping (see section 6.1), where the electromagnetic wave times the 'other oscillator' are acting as a driving force. The electromagnetic wave is the pump, where A_0 and ω_0 denote its amplitude and frequency:

$$A_0 = E_0\cos\omega_0 t = \frac{E_0}{2}[\exp(\mathrm{i}\omega_0 t) + \exp(-\mathrm{i}\omega_0 t)]. \tag{6.32}$$

The electron and ion density fluctuation amplitudes are A_1 and A_2; their appropriate frequencies are ω_1 and ω_2 and $\omega_1 > \omega_2$. More explicitly, the equations of motion describing the electron wave (denoted by index 1) and the ion wave (denoted by index 2) are

$$\begin{aligned}\frac{\mathrm{d}^2A_1}{\mathrm{d}t^2} + \Gamma_1\frac{\mathrm{d}A_1}{\mathrm{d}t} + \omega_1^2A_1 &= c_1A_2A_0\\ \frac{\mathrm{d}^2A_2}{\mathrm{d}t^2} + \Gamma_2\frac{\mathrm{d}A_2}{\mathrm{d}t} + \omega_2^2A_2 &= c_2A_1A_0.\end{aligned} \tag{6.33}$$

The coefficients Γ_j ($j = 1$ or 2) describe the collision plus collisionless (Landau) damping, ω_j ($j = 1$ or 2) are the eigenvalue of equations (6.33) with the neglect of damping and coupling ($c_1 = c_2 = 0$), and it is assumed

that the pump amplitude A_0 is unaffected by the decay waves 1 and 2. These nonlinear equations are transformed to algebraic equations by Fourier transform:

$$A(\omega) = \frac{1}{2\pi} \int \mathrm{d}t \exp(\mathrm{i}\omega t) A(t). \tag{6.34}$$

Note that in the case of nonlinear equations it is not permitted to make the substitution $(\partial/\partial t) \rightarrow -\mathrm{i}\omega$. For example, using (6.32) and (6.34) one gets

$$\begin{aligned} &\frac{1}{2\pi} \int \mathrm{d}t\, A_0(t) \exp(\mathrm{i}\omega t) A_2(t) \\ &\quad = \frac{E_0}{4\pi} \int \mathrm{d}t [\exp(\mathrm{i}\omega_0 t) + \exp(-\mathrm{i}\omega_0 t)] \exp(\mathrm{i}\omega t) A_2(t) \\ &\quad = \frac{E_0}{2} [A_2(\omega + \omega_0) + A_2(\omega - \omega_0)]. \end{aligned} \tag{6.35}$$

Assuming constant damping rates, the Fourier transform of equations (6.33) yields the following algebraic equations:

$$\begin{aligned} D_1(\omega) A_1(\omega) + \frac{c_1 E_0}{2} [A_2(\omega + \omega_0) + A_2(\omega - \omega_0)] &= 0 \\ D_2(\omega - \omega_0) A_2(\omega - \omega_0) + \frac{c_2 E_0}{2} [A_1(\omega) + A_1(\omega - 2\omega_0)] &= 0 \\ D_2(\omega + \omega_0) A_2(\omega + \omega_0) + \frac{c_2 E_0}{2} [A_1(\omega) + A_1(\omega + 2\omega_0)] &= 0 \end{aligned} \tag{6.36}$$

where $D_j(\omega)$ is defined by

$$D_j(\omega) = \omega^2 - \omega_j^2 + \mathrm{i}\omega\Gamma_j \quad \text{for } j = 1, 2. \tag{6.37}$$

In the first equation of (6.36) one can see that mode 1 at a frequency $\omega[A_1(\omega)]$ couples with mode 2 $[A_2]$ at $\omega + \omega_0$ and $\omega - \omega_0$, as demonstrated in (6.35). Therefore, in order to obtain $A_2(\omega + \omega_0)$ and $A_2(\omega - \omega_0)$, one has to take a Fourier transform like (6.35) for modes 1 at frequencies ω, $\omega + 2\omega_0$ and $\omega - 2\omega_0$, leading to the second and third equations of (6.36). Assuming that mode 1 is resonant only near ω, one can neglect $A_1(\omega + 2\omega_0)$ and $A_1(\omega - 2\omega_0)$ in equations (6.36), yielding three algebraic equations with three unknowns $A_1(\omega)$, $A_2(\omega - \omega_0)$ and $A_2(\omega + \omega_0)$, written in matrix form:

$$\begin{pmatrix} D_1(\omega) & c_1 E_0/2 & c_1 E_0/2 \\ c_2 E_0/2 & D_2(\omega - \omega_0) & 0 \\ c_2 E_0/2 & 0 & D_2(\omega + \omega_0) \end{pmatrix} \begin{pmatrix} A_1(\omega) \\ A_2(\omega - \omega_0) \\ A_2(\omega + \omega_0) \end{pmatrix} = \begin{pmatrix} 0 \\ 0 \\ 0 \end{pmatrix}. \tag{6.38}$$

A solution is obtained only if the determinant of the coefficients vanish. Since A_1 describes the electron wave, where $\omega_0 \approx \omega \approx \omega_1$, one can neglect the parametric decay instability for the off-resonance amplitude $A_2(\omega + \omega_0)$. In

this case the zero determinant of the coefficients of (6.38) yields

$$D_1(\omega)D_2(\omega-\omega_0)-\frac{c_1c_2E_0^2}{4}$$
$$\approx -4\omega_1\omega_2\left(\omega-\omega_1+\mathrm{i}\frac{\Gamma_1}{2}\right)\left(\omega-\omega_0+\omega_2+\mathrm{i}\frac{\Gamma_2}{2}\right)-\frac{c_1c_2E_0^2}{4}=0 \quad (6.39)$$

where the following relations have been used: $\omega_0-\omega\approx\omega_2$, $\omega+\omega_1\approx 2\omega_1$ and $\Gamma_1\omega\approx\Gamma_1\omega_1$. Defining the real and complex parts of ω by ω_R and Γ respectively,

$$\omega=\omega_\mathrm{R}+\mathrm{i}\Gamma. \quad (6.40)$$

Equation (6.39) yields two equations (the first by equating the real part to zero and the second by equating the imaginary part to zero):

$$\begin{aligned}(\omega_\mathrm{R}-\omega_1)(\omega_\mathrm{R}-\omega_1-\delta)+\alpha E_0^2&=(\Gamma+\tfrac{1}{2}\Gamma_1)(\Gamma+\tfrac{1}{2}\Gamma_2)\\ \omega_\mathrm{R}&=\omega_1+\frac{(\Gamma+\frac{1}{2}\Gamma_1)\delta}{2\Gamma+\frac{1}{2}\Gamma_1+\frac{1}{2}\Gamma_2}\\ \delta&\equiv\omega_0-\omega_1-\omega_2\\ \alpha&\equiv\frac{c_1c_2}{4\omega_1\omega_2}.\end{aligned} \quad (6.41)$$

Substituting the second equation of (6.41) into the first one we get

$$E_0^2=\frac{1}{\alpha}\left\{(\Gamma+\tfrac{1}{2}\Gamma_1)(\Gamma+\tfrac{1}{2}\Gamma_2)\left[1+\frac{\delta^2}{(2\Gamma+\frac{1}{2}\Gamma_1+\frac{1}{2}\Gamma_2)^2}\right]\right\}. \quad (6.42)$$

Note that $E_0^2/(8\pi)$ is the (time-averaged) laser field energy density, i.e. the pump energy density in our case. For E_0 defined in (6.32) the laser irradiance I_L (erg cm^{-2} s^{-1}) is $cE_0^2/(8\pi)$. The pump energy can be invested into the electron and ion waves only if the damping Γ is positive, $\Gamma\geq 0$. The threshold pumping, i.e. the threshold laser field $E_{0,\mathrm{th}}$, is obtained by substituting $\Gamma=0$ in equation (6.42):

$$E_{0,\mathrm{th}}^2=\frac{\omega_1\omega_2\Gamma_1\Gamma_2}{c_1c_2}\left[1+\frac{4\delta^2}{(\Gamma_1+\Gamma_2)^2}\right]. \quad (6.43)$$

The threshold energy of the pump goes to zero when the damping (collisional or Landau) of either the electron wave or the ion wave goes to zero. The minimum pumping amplitude $E_{0,\mathrm{min}}$ is obtained for the exact resonance condition, i.e. $\delta=0$:

$$E_{0,\mathrm{min}}^2=\frac{\omega_1\omega_2\Gamma_1\Gamma_2}{c_1c_2}. \quad (6.44)$$

The maximum growth rate $\Gamma_{\max}$ of the parametric instability is given from (6.42), by substituting in this equation $\Gamma_1 = \Gamma_2 = 0$ and $\delta = 0$:

$$\Gamma_{\max} = \left(\frac{c_1 c_2}{4\omega_1 \omega_2}\right)^{1/2} E_0. \tag{6.45}$$

At this stage it is important to point out that the vanishing of the 3×3 determinant of (6.38) also has an imaginary eigenvalue

$$\omega = \mathrm{i}\Gamma. \tag{6.46}$$

In this case one of the modes has a zero frequency and the second mode has the pump frequency ω_0. This instability is known as the **oscillating two-stream** instability. This phenomenon acquired this name because the electrons (or the ions) have a time-averaged particle distribution function with two peaks, as in the two-stream instabilities. The following scenario can explain this instability (Chen 1974) if the pump frequency is smaller than the plasma frequency: an ion density fluctuation causes a charge separation, which induces an electric field oscillating with the pump frequency. Even if the pump is homogeneous in space, the induced electric field is not homogeneous and thus applies a ponderomotive force on the electrons, which are moving from the low-density to the high-density region. The created d.c. (low frequency) electric field drags the ions and the ion density perturbation grows. The density ripple does not propagate since $\mathrm{Re}\,\omega = 0$.

We now calculate the values of c_1 and c_2 in the above equations by analysing the more (algebraic) simple oscillating two-stream instability. Note that in Gaussian units the dimension of $[c_j]$ is $[\mathrm{s}^{-1}\,(\mathrm{cm/g})^{1/2}]$. Since c_1 and c_2 are model-independent, we can choose the simplest relevant model. In particular, the Poisson equation and the fluid equations for ions and electrons are used; where the collision frequencies are neglected, $\Gamma_1 = \Gamma_2 = 0$, the electron and ion temperatures also vanish, $T_\mathrm{e} = T_\mathrm{i} = 0$, and the degree of ionization is taken as $Z = 1$.

The electron motion is described by a superposition of a high-frequency motion and a low-frequency motion. The high-frequency motion is independent of the ion motion, while the low-frequency motion describes electrons and ions moving together in a quasi-neutral motion. The induced electric field, as explained above, also has low- and high-frequency components. The indices l and h are used for low- and high-frequency components, while the index 0 is used for the pump component or the zeroth-order approximation. The electric field E, the ion and electron densities n_i and n_e, and the fluid ion and electron velocities v_i and v_e have the components

$$\begin{gathered} E = E_0 + E_\mathrm{h} + E_\mathrm{l}, \qquad n_\mathrm{i} = n_0 + n_\mathrm{l}, \\ n_\mathrm{e} = n_0 + n_\mathrm{l} + n_\mathrm{h}, \qquad v_\mathrm{i} = v_\mathrm{l}, \qquad v_\mathrm{e} = v_0 + v_\mathrm{l} + v_\mathrm{h}. \end{gathered} \tag{6.47}$$

It is assumed that the space perturbation is oscillatory, of the form $\exp(\mathrm{i}kx)$, and the equations are linearized, so that in the equations describing the plasma one can use the Fourier transform result for linear equations:

$$\frac{\partial}{\partial x} = \mathrm{i}k. \tag{6.48}$$

The equations describing the plasma system under consideration are:

(a) The ion force (momentum) and continuity equations

$$\frac{\partial v_\mathrm{l}}{\partial t} = \frac{eE_\mathrm{l}}{m_\mathrm{i}}, \qquad \frac{\partial n_\mathrm{l}}{\partial t} + n_0 \frac{\partial v_\mathrm{l}}{\partial x} = 0. \tag{6.49}$$

(b) The electron force (momentum) and continuity equation

$$\frac{\partial v_\mathrm{e}}{\partial t} + v_\mathrm{e} \frac{\partial v_\mathrm{e}}{\partial x} = -\frac{e}{m_\mathrm{e}}(E_0 + E_\mathrm{h} + E_\mathrm{l}), \qquad \frac{\partial n_\mathrm{e}}{\partial t} + n_\mathrm{e} \frac{\partial v_\mathrm{e}}{\partial x} = 0. \tag{6.50}$$

(c) The Poisson equation

$$\frac{\partial E}{\partial x} = -4\pi e n_\mathrm{h} \;\Rightarrow \mathrm{i}kE_\mathrm{h} = -4\pi e n_\mathrm{h}. \tag{6.51}$$

Taking the time derivative of the continuity ion equation and using the force equation, both of (6.49) and using (6.48), one gets

$$\frac{\partial^2 n_\mathrm{l}}{\partial t^2} = -\frac{\mathrm{i}ken_0 E_\mathrm{l}}{m_\mathrm{i}}. \tag{6.52}$$

Note that E_l is induced by the ponderomotive force, proportional to $\nabla(E_0 + E_\mathrm{h})^2 \approx 2E_0 \nabla E_\mathrm{h}$. Therefore, E_l is determined by the knowledge of E_h. Linearizing the electron force equation in (6.50) about the zeroth-order electron velocity, and using a Poisson equation, one gets for the fast and low frequency components

$$-\mathrm{i}\omega_0 v_\mathrm{h} = \frac{4\pi e^2 n_\mathrm{h}}{\mathrm{i}km_\mathrm{e}}, \qquad \mathrm{i}k\left(\frac{eE_0 \cos\omega_0 t}{\mathrm{i}\omega_0 m_\mathrm{e}}\right) v_\mathrm{h} = -\frac{eE_\mathrm{l}}{m_\mathrm{e}}. \tag{6.53}$$

From these last two equations one gets the low-frequency electric field E_l, which is substituted into (6.52) to get the ion (i.e. low-frequency) driven equation:

$$\frac{\partial^2 n_\mathrm{l}}{\partial t^2} = c_2 n_\mathrm{h} E_0 \cos\omega_0 t, \qquad c_2 \equiv -\frac{\mathrm{i}ek}{m_\mathrm{i}}\left(\frac{\omega_\mathrm{pe}^2}{\omega_0^2}\right) \approx -\frac{\mathrm{i}ek}{m_\mathrm{i}}. \tag{6.54}$$

Equation (6.54) describes how a high-frequency density (n_h) times the pump drives a low-frequency (n_l) density with a coupling c_2.

The electron continuity equation of (6.50), with the use of (6.48) and (6.51), yields

$$\frac{\partial n_\mathrm{h}}{\partial t} + \mathrm{i}kn_0 v_\mathrm{h} + \mathrm{i}kv_0 n_\mathrm{l} = 0. \tag{6.55}$$

Taking the time derivative of this equation, neglecting $\partial n_l/\partial t$, and using

$$\frac{\partial v_0}{\partial t} = -\frac{eE_0 \cos\omega_0 t}{m_e}, \qquad \frac{\partial v_h}{\partial t} = -\frac{4\pi e^2 n_h}{ikm_e} \tag{6.56}$$

one obtains the high-frequency (electron) wave equation driven by the low-frequency (ion) density times the pump:

$$\frac{\partial^2 n_h}{\partial t^2} + \omega_{pe}^2 n_h = c_1 n_l E_0 \cos\omega_0 t, \qquad c_1 = \frac{ike}{m_e}. \tag{6.57}$$

Substituting c_2 and c_1 from (6.54) and (6.57) into (6.43), (6.44) and (6.45), we get for the **parametric decay instability** the threshold and minimum pump amplitudes, as well as the maximum possible growth of the instability:

$$\begin{aligned} E_{0,th}^2 &= \frac{m_e m_i \omega_1 \omega_2 \Gamma_1 \Gamma_2}{e^2 k^2}\left[1 + \frac{4\delta^2}{(\Gamma_1+\Gamma_2)^2}\right] \\ E_{0,min}^2 &= \frac{m_e m_i \omega_1 \omega_2 \Gamma_1 \Gamma_2}{e^2 k^2} \\ \Gamma_{max} &= \left(\frac{1}{m_e m_i \omega_1 \omega_2}\right)^{1/2} \frac{ekE_0}{2} \\ I_0 &= \frac{cE_0^2}{8\pi} \end{aligned} \tag{6.58}$$

where I_0 is the pump (laser) energy flux (in erg s^{-1} cm^{-2}).

6.5 Stimulated Brillouin Scattering

The general equations (6.33) can also be used to analyse the stimulated Brillouin or Raman instabilities. However, in this section we are using a different approach (Cairns 1983). The formalism of this section is sometimes more easily generalized to inhomogeneous systems, and occasionally the physics is more transparent. Neglecting damping and couplings, the solutions of (6.33) amplitudes and the unaffected pump amplitude can be written as

$$A_j = a_j \exp(i\omega_j t) + \text{c.c.} \quad \text{for } j = 1, 2, 3 \tag{6.59}$$

where a_j are constants and c.c. denotes complex conjugate. It is assumed that by the introduction of damping and couplings the amplitudes can still be presented by (6.59) but with a_j ($j = 1, 2$) functions of time, but the time variation scale of these functions is small in comparison with the oscillation frequency time. This implies that d^2a_j/dt^2 and $\Gamma\, da_j/dt$ ($j = 1, 2$) can be neglected when substituting (6.59) into (6.33). The pump amplitude a_0 is not affected by the instability. In this approximation the following equations

are derived from (6.33):

$$2\omega_1 \frac{\mathrm{d}a_1}{\mathrm{d}t} + \omega_1 \Gamma_1 a_1 = -\mathrm{i}c_1 a_0 a_2, \qquad 2\omega_2 \frac{\mathrm{d}a_2}{\mathrm{d}t} + \omega_2 \Gamma_2 a_2 = \mathrm{i}c_2 a_0 a_1. \tag{6.60}$$

First-order differential equations of the form of (6.60) are now directly derived for the stimulated Brillouin scattering (Dawson and Lin 1974). The following notation is used: E_0 is the (laser) pump amplitude; E is the scattered electromagnetic field moving in the opposite direction to the pump wave (i.e. reflection out of the plasma); T_e is the electron temperature, assumed to be much larger than the ion temperature; n_ia is the ion density perturbation associated with the acoustic wave; and n_0 is the background plasma density. Plasma charge neutrality requires that the electron density associated with the acoustic wave n_ea equals the ion density perturbation, defined by

$$n_\mathrm{ea} = n_\mathrm{ai} = n_\mathrm{a} \cos k_\mathrm{a} x \tag{6.61}$$

where k_a is the wave number of the acoustic wave. The electron energy density is $k_\mathrm{B} T_\mathrm{e} n_\mathrm{ei}$ and a fraction n_ai/n_0 (n_0 is the background density) of this energy is acquired by the ion acoustic wave. The (space average) energy density conservation of the Brillouin process (i.e. photon wave $\rightarrow$ photon wave + ion acoustic wave) is

$$\frac{E_0^2}{8\pi} = \frac{E^2}{8\pi} + \frac{1}{2} k_\mathrm{B} T_\mathrm{e} n_\mathrm{a} \left(\frac{n_\mathrm{a}}{n_0} \right). \tag{6.62}$$

The momentum density Π in the wave is related to the energy density of a wave W by

$$\Pi = \left(\frac{W}{\omega} \right) \mathbf{k}. \tag{6.63}$$

The simplest proof of (6.63) is in the quantum picture, $W = \hbar \omega n$, where $\hbar = h/2\pi$ and h is the Planck constant, ω is the (angular) wave frequency and n is the appropriate density. $\Pi = \hbar \mathbf{k} n$, where $\mathbf{k}$ is the wave number vector. The ratio of Π to W gives (6.63). Therefore, the momentum density conservation of the Brillouin process is

$$\left(\frac{E_0^2}{4\pi} \right) \left(\frac{\mathbf{k}_0}{\omega_0} \right) = \left(\frac{E^2}{4\pi} \right) \left(\frac{\mathbf{k}}{\omega} \right) + \left(\frac{k_\mathrm{B} T_\mathrm{e} n_\mathrm{a}^2}{n_0} \right) \left(\frac{\mathbf{k}_\mathrm{a}}{\omega_\mathrm{a}} \right). \tag{6.64}$$

Substituting (6.62) into (6.64), one gets

$$\frac{E^2}{4\pi} \left(\frac{\mathbf{k}_0}{\omega_0} - \frac{\mathbf{k}}{\omega} \right) = \frac{k_\mathrm{B} T_\mathrm{e} n_\mathrm{a}^2}{n_0} \left(\frac{\mathbf{k}_\mathrm{a}}{\omega_\mathrm{a}} - \frac{\mathbf{k}_0}{\omega_0} \right). \tag{6.65}$$

Since $(\mathbf{k}, \omega)$ describes a backscatter electromagnetic wave, and $\omega_\mathrm{a} \ll \omega_0$, one can use

$$\mathbf{k} \approx -\mathbf{k}_0, \qquad \omega \approx \omega_0, \qquad \frac{k}{\omega} \approx \frac{k_0}{\omega_0} = \frac{1}{c}, \qquad \frac{k_\mathrm{a}}{\omega_\mathrm{a}} = \frac{1}{v_\mathrm{a}} = \sqrt{\frac{m_\mathrm{i}}{k_\mathrm{B} T_\mathrm{e}}} \gg \frac{1}{c} \tag{6.66}$$

into (6.65) to obtain

$$E = \left(\frac{2\pi c}{n_0}\sqrt{m_i k_B T_e}\right)^{1/2} n_a = \sqrt{2\pi n_0 m_i c v_a}\left(\frac{n_a}{n_0}\right). \tag{6.67}$$

From energy and momentum conservation the important result has been obtained that an ion acoustic wave induces an electromagnetic field; this field is proportional to the ion density wave amplitude. In order to calculate the rate of growth of E as a function of n_{ia} (and vice versa), the dynamical equations, i.e. Maxwell's equations and the fluid (or Vlasov–Boltzmann) plasma equations, must be used.

The electric wave equation, derived from Maxwell's equations (see Appendix A), is

$$\nabla^2 \mathbf{E} - \frac{1}{c^2}\frac{\partial^2 \mathbf{E}}{\partial t^2} - \nabla(\nabla \cdot \mathbf{E}) = \frac{4\pi}{c^2}\frac{\partial \mathbf{J}}{\partial t}. \tag{6.68}$$

For the Brillouin instability the source current $\mathbf{J}$ is given by

$$\mathbf{J} = -e n_{ea} \mathbf{v}_e = -e \mathbf{v}_e n_a \cos k_a x \tag{6.69}$$

where (6.61) was used in the second equality. The zeroth-order equation for the electron velocity $\mathbf{v}_e$, induced by the pump wave E_0, is

$$\frac{\partial v_e}{\partial t} = -\frac{eE_0}{m_e}\cos(k_0 x - \omega_0 t). \tag{6.70}$$

Taking the solution of (6.70), i.e. $v_e = -v_0 \sin(k_0 x - \omega_0 t)$, $v_0 = eE_0/(m_e\omega_0)$, and inserting it into (6.69) yields a source current

$$J = \frac{n_a e^2 E_0}{2m_e\omega_0}\{\sin[(k_0 + k_a)x - \omega_0 t] + \sin[(k_0 - k_a)x - \omega_0 t]\}. \tag{6.71}$$

The electromagnetic backscattered wave is described by the second term of the source current, $\mathbf{k}_0 - \mathbf{k}_a = \mathbf{k} \approx -\mathbf{k}_0$, and therefore only the second term is kept for further analysis. From (6.68), the back-reflected electromagnetic wave equation is derived by using the second term of (6.71):

$$\frac{\partial}{\partial t}\sin[(k_0 - k_a)x - \omega_0 t] = -\omega_0 \cos[(k_0 - k_a)x - \omega_0 t] \approx -\omega_0 \cos(-k_0 x - \omega t)$$

$$= -\omega_0 \cos(k_0 x + \omega t)$$

$(\partial^2/\partial x^2)E = -k^2 E$, and the transversal property ($\mathbf{k} \cdot \mathbf{E} = 0$) of the electromagnetic wave

$$\frac{\partial^2 E}{\partial t^2} + k^2 c^2 E = \frac{\omega_{pe}^2 n_a E_0}{2n_0}\cos(k_0 x + \omega_0 t) \tag{6.72}$$

where ω_{pe} is the electron plasma frequency. For the resonant case, $kc = \omega = \omega_0$, equation (6.72) has the solution (6.17):

$$E = E(t)\sin(k_0 x + \omega_0 t), \qquad E(t) = \frac{\omega_{pe}^2 E_0 t}{4\omega_0}\left(\frac{n_a}{n_0}\right). \tag{6.73}$$

Taking the time derivative of the amplitude $E(t)$,

$$\frac{dE(t)}{dt} = \left(\frac{\omega_{pe}^2}{4\omega_0 n_0}\right) E_0 n_a \tag{6.74}$$

and substituting n_a/n_0 from (6.67), one gets

$$\frac{dE}{dt} = \left(\frac{\omega_{pe}^2 E_0}{4\omega_0\sqrt{2\pi n_0 m_i c v_a}}\right) E \equiv \Gamma_{Bril} E, \qquad E(t) = \exp(\Gamma_{Bril} t). \tag{6.75}$$

Using the values of the energy flux of the pump, $I_0 = cE_0^2/(8\pi)$, we get for the growth rate of the backscattered wave amplitude, Γ_{Bril},

$$\Gamma_{Bril} = \frac{1}{\sqrt{2}}\,\frac{\omega_{pe}^2}{\omega_0}(n_0 m_i c^2 v_a)^{-1/2}(I_0)^{1/2}. \tag{6.76}$$

Generalizing (6.74) to include damping due to electron–ion collisions Γ_{EM}, one has the following equation for the backscattered wave amplitude:

$$\frac{dE(t)}{dt} + \Gamma_{EM} E(t) = \frac{\omega_{pe}^2}{4n_0\omega_0} E_0 n_a. \tag{6.77}$$

This equation has the structure generally developed in (6.60). Γ_{EM} can be related to the electron–ion collision frequency ν_{ei}, by assuming that the coherent oscillations of the electrons are converted to thermal motion at the rate of electron–ion collisions. The energy conservation rate in this case implies the relation between Γ_{EM} and ν_{ei}:

$$\Gamma_{EM}\frac{E^2}{8\pi} = \nu_{ei}\left[\frac{1}{2} n_e m_e \left(\frac{eE}{m_e\omega}\right)^2\right] \;\Rightarrow\; \Gamma_{EM} = \nu_{ei}\left(\frac{\omega_{pe}^2}{\omega^2}\right). \tag{6.78}$$

A similar equation to (6.77) for dn_a/dt has to be developed in order to solve the problem.

From equation (6.67) one has that $dn_a/dt \propto dE/dt$ and from (6.75) that $dE/dt \propto E_0 E$, thus implying the desired equation $dn_a/dt \propto E_0 E$. Substituting explicitly (6.75) into (6.67) gives

$$\frac{dn_a}{dt} = \frac{\omega_{pe}^2}{8\pi\omega_0 m_i c v_a} E_0 E. \tag{6.79}$$

Including collisional and Landau damping in this equation, one gets

$$\frac{dn_a}{dt} + \Gamma_a n_a = \frac{\omega_{pe}^2}{8\pi\omega_0 m_i c v_a} E_0 E. \tag{6.80}$$

This is the second equation with a structure as in (6.60). Using the relationship $\mathrm{d}n_a/\mathrm{d}t = \Gamma_{Bril} n_a$ and $\mathrm{d}E/\mathrm{d}t = \Gamma_{Bril} E$, the differential equations (6.77) and (6.80) yield the algebraic equations:

$$\begin{pmatrix} \Gamma_{Bril} + \Gamma_{EM} & -\dfrac{\omega_{pe}^2 E_0}{4 n_0 \omega_0} \\ -\dfrac{\omega_{pe}^2 E_0}{8\pi\omega_0 m_i c v_a} & \Gamma_{Bril} + \Gamma_a \end{pmatrix} \begin{pmatrix} E \\ n_a \end{pmatrix} = \begin{pmatrix} 0 \\ 0 \end{pmatrix}. \tag{6.81}$$

A solution of these equations is possible only if the determinant of the coefficients vanish, which implies

$$\Gamma_{Bril} = \frac{1}{2}\left\{ -(\Gamma_{EM} + \Gamma_a) \pm \left[(\Gamma_{EM} + \Gamma_a)^2 + \left(\frac{\omega_{pe}^4 I_0}{\omega_0^2 n_0 m_i c^2 v_a} - 4\Gamma_{EM}\Gamma_a \right) \right]^{1/2} \right\} \tag{6.82}$$

where $(\Gamma_{EM}\Gamma_a)^2$ was neglected. The threshold for the pump irradiance I_0 is obtained by taking $\Gamma_{Bril} = 0$:

$$I_0 \geq I_{0,th} = \frac{4\Gamma_{EM}\Gamma_a \omega_0^2 n_0 m_i c^2 v_a}{\omega_{pe}^4}. \tag{6.83}$$

For pump intensities large compared with threshold, (6.82) and (6.83) give

$$\Gamma_{Bril}(I_0 \gg I_{0,th}) = \frac{\omega_{pe}^2}{2\omega_0}\sqrt{\frac{I_0}{n_0 m_i c^2 v_a}}. \tag{6.84}$$

A similar formalism for stimulated Raman instability yields

$$\begin{aligned} \Gamma_{Ram}(I_0 \gg I_{0,th}) &= \frac{\omega_{pe}^2}{2\omega_0}\sqrt{\frac{I_0}{2 n_0 m_e c^2 v_p}} \\ I_{0,th} &= \frac{4\Gamma_{EM}\Gamma_p \omega_0^2 n_0 m_e c^2 v_p}{\omega_{pe}^4} \end{aligned} \tag{6.85}$$

where $v_p = \omega_p/k_p$; v_p, ω_p and k_p are the phase velocity, the angular frequency and wave number of the plasmon (electron) wave respectively. Γ_p is the collisional and Landau damping for the plasmon wave.

6.6 A Soliton Wave

6.6.1 A historical note

J. Scott Russell, who made observations on water waves on the Edinburgh to Glasgow canal, first realized the phenomenon of solitary wave in 1834. These observations together with laboratory experiments, where solitary waves

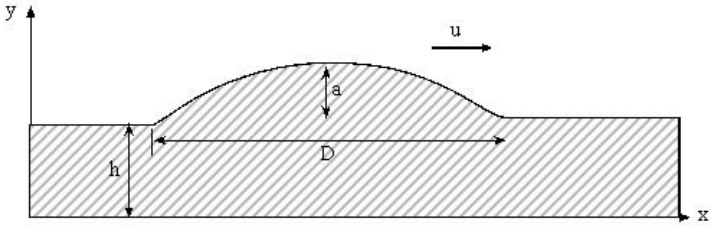

Figure 6.3. A solitary wave moving with a steady velocity u. h is the height of the undisturbed water, a is the amplitude of the wave and g is the gravitational acceleration constant, satisfying $D \gg h \gg a$.

were generated by dropping a weight at one end of a shallow water channel, were published (Russell 1844) in 1844 before the British Association for the Advancement of Science. Russell suggested the following empirical formula in order to explain the steady state velocity u of the solitary wave:

$$u^2 = g(h + a) \tag{6.86}$$

where h is the height of the undisturbed water, a is the amplitude of the wave (figure 6.3) and g is the gravitational acceleration constant. Equation (6.86) was later deduced by Boussinesq in 1871 (Boussinesq 1871) and independently by Rayleigh (Rayleigh 1876), by using the equations of motion for an incompressible fluid and assuming a wavelength $\sim D$ much greater than the height h of the water in the channel. They also derived the displacement $(y - h)$ of the wave above the level h:

$$y(x,t) - h = a\,\mathrm{sech}^2\left[\frac{(x - ut)}{D}\right], \qquad D^2 = \frac{4h^2(h + a)}{3a}. \tag{6.87}$$

In 1895 Korteweg and de Vries (**KdV**) developed (Korteweg and de Vries 1895) the equation

$$\frac{\partial y}{\partial t} = \frac{3}{2}\sqrt{\frac{g}{h}}\left[\left(y - h + \frac{2\alpha}{3}\right)\frac{\partial y}{\partial x} + \frac{\beta}{3}\frac{\partial^3 y}{\partial x^3}\right] \tag{6.88}$$

in order to describe the motion of weakly nonlinear long transversal waves. In equation (6.88), α is a small arbitrary parameter and β is given by

$$\beta = \frac{h^3}{3} - \frac{\sigma_{\mathrm{st}} h}{g\rho} \tag{6.89}$$

where σ_{st} is the surface tension and ρ is the density of the liquid. Equation (6.87) is a solution of the KdV equation (6.88).

The modern development in the theory of the KdV equation starts with the work of Fermi, Pasta and Ulam in 1955 (Fermi *et al*. 1955). They studied a nonlinear discrete mass string, and to their surprise the thermalization of the energy in such a nonlinear system could not be achieved. Kruskal and

Zabusky (1965) solved this paradox by modelling the nonlinear spring with the KdV equation, yielding (numerically) the soliton solution. The Fermi–Pasta–Ulam problem suggests that a nonlinear interaction does not necessarily cause the destruction of oscillations, causing randomization. This type of phenomenon and the KdV equation have since been derived in many physical problems, such as an ion acoustic wave in plasma (Washimi and Taniuti 1966).

6.6.2 What is a soliton?

A soliton is a localized nonlinear wave of steady-state form. If it interacts with other solitons, after the interaction these structures separate in such a way that their original structure is preserved and their velocities are unchanged. The positions of the solitons are slightly shifted from where they would have been without the existence of the interaction. The solitons are solitary waves but the solitary waves are not necessarily solitons (Eliezer 1985).

6.6.3 What is a solitary wave?

The solitary waves are a one-parameter family of shaped pulses, moving with a velocity u proportional to the wave amplitude a, and their width D is inversely proportional to the square root of the amplitude (see figure 6.3). Therefore, the larger the amplitude the faster is their velocity and the narrower is their width.

6.6.4 The wave equation

The wave equation in one space dimension is

$$\frac{1}{u^2}\frac{\partial^2\psi}{\partial t^2} - \frac{\partial^2\psi}{\partial x^2} = 0. \tag{6.90}$$

This equation describes the propagation of waves in homogeneous media with a constant velocity u. In deriving this equation, one has to make three main assumptions:

(a) There is no **dissipation**.
(b) The amplitude of oscillation ψ is small so that one can **neglect nonlinear terms**.
(c) There is no **dispersion**, i.e. the velocity of the wave propagation does not depend on the frequency of the wavelength.

If one does not assume the absence of dissipation, nonlinearity and dispersion, then the universal wave equation (6.90) is not applicable and each medium has to be described by a different system of equations.

If the initial value of ψ and its time derivative are given, i.e. $\psi(x,0)$ and $(\partial/\partial t)\psi(x,0)$ are known, then the wave equation (6.90) is a well-defined initial value problem. This equation, like any other linear differential equation, obeys the **superposition principle**. That is, if $f(x-ut)$ and $g(x+ut)$ solve equation (6.90), then $\psi(x,t)=f(x-ut)+g(x+ut)$ is also a solution of this equation. $f(x-ut)$ and $g(x+ut)$ represent waves of fixed shape, travelling to the right and left respectively. The general solution $\psi=f+g$ describes two waves that can pass through each other without changing their shape. In general, this superposition principle does not occur in physical systems described by nonlinear differential equations. However, a number of nonlinear differential equations have been discovered which allow waves to pass through each other without changing their shapes and velocities. Moreover, some principle of superposition can be defined for these nonlinear equations. These equations are called 'solitary wave equations', and the KdV equation belongs to this class of equations.

Next we show that an ion plasma wave with a wavelength much larger than the Debye length satisfies the KdV equation; thus a soliton solution exits in laser–plasma interaction.

6.6.5 Ion plasma wave and the KdV equation

We consider the fluctuation in the ion density of two component plasma (electrons and ions), i.e. the ion acoustic waves. This problem is described by the following fluid-Poisson equations:

$$\begin{aligned}
\frac{\partial n_\mathrm{i}}{\partial t}+\frac{\partial (n_\mathrm{i}v_\mathrm{i})}{\partial x}&=0\\
n_\mathrm{i}m_\mathrm{i}\frac{\mathrm{d}v_\mathrm{i}}{\mathrm{d}t}&=Zen_\mathrm{i}E\\
n_\mathrm{e}m_\mathrm{e}\frac{\mathrm{d}v_\mathrm{e}}{\mathrm{d}t}&=-en_\mathrm{e}E-\frac{\partial (n_\mathrm{e}k_\mathrm{B}T_\mathrm{e})}{\partial x}\approx 0\\
\frac{\partial E}{\partial x}&=4\pi e(Zn_\mathrm{i}-n_\mathrm{e})
\end{aligned} \tag{6.91}$$

where n_i is the ion density and v_i their velocity, n_e is the electron density and v_e the electron fluid velocity, m_i and m_e are the ion mass and the electron mass, and Z is the charge ionization of the ions. The electron pressure is $n_\mathrm{e}k_\mathrm{B}T_\mathrm{e}$. The electron temperature is much larger than the ion temperature, and in this case for simplicity one can take a zero ion temperature, $T_\mathrm{i}=0$. In the third equation of (6.91), the right-hand side is taken as zero by neglecting the inertia of the electrons relative to that of the ions. Since $m_\mathrm{i}\gg Zm_\mathrm{e}$, the inertia term $(n_\mathrm{e}m_\mathrm{e}\,\mathrm{d}v_\mathrm{e}/\mathrm{d}t)$ in the electron momentum equation can be neglected when $\mathrm{d}v_\mathrm{e}/\mathrm{d}t\approx \mathrm{d}v_\mathrm{i}/\mathrm{d}t$, i.e. when the high-frequency plasma oscillations are neglected. Since we are interested in the regime of density and

velocity fluctuations near the ion plasma frequency, the above approximation is justified.

In solving equations (6.91) we introduce the dimensionless variables

$$\begin{aligned}
&\xi = \frac{x}{\lambda_D}, \qquad \lambda_D = \left(\frac{k_B T_e}{4\pi e^2 Z n_0}\right)^{1/2}, \qquad \tau = \omega_{pi} t \\
&\omega_{pi} = \left(\frac{4\pi n_0 Z^2 e^2}{m_i}\right)^{1/2}, \qquad v = \frac{v_i}{\omega_{pi}\lambda_D}, \qquad F = \frac{e\lambda_D E}{k_B T_e} \\
&N = \frac{n_i}{n_0}, \qquad N_e = \frac{n_e}{Z n_0}, \qquad \Omega = \frac{\omega}{\omega_{pi}} \\
&\kappa = k\lambda_D, \qquad k = \frac{2\pi}{\lambda}
\end{aligned} \tag{6.92}$$

where n_0 and Zn_0 are the ion and electron initial (undisturbed) densities accordingly, and k is the wave number. The fluid-Poisson equations (6.91) in these dimensionless variables are

$$\begin{aligned}
\frac{\partial N}{\partial \tau} + \frac{\partial (Nv)}{\partial \xi} &= 0 \\
\frac{\partial v}{\partial \tau} + v\frac{\partial v}{\partial \xi} - F &= 0 \\
\frac{1}{N_e}\frac{\partial N_e}{\partial \xi} + F &= 0 \\
\frac{\partial F}{\partial \xi} + N_e - N &= 0.
\end{aligned} \tag{6.93}$$

At this stage it is convenient to define the Fourier modes:

$$\begin{aligned}
N_e &= 1 + \delta N_e \exp[\mathrm{i}(\kappa\xi - \Omega\tau)] \\
N &= 1 + \delta N \exp[\mathrm{i}(\kappa\xi - \Omega\tau)] \\
v &= \delta v \exp[\mathrm{i}(\kappa\xi - \Omega\tau)] \\
F &= \delta F \exp[\mathrm{i}(\kappa\xi - \Omega\tau)].
\end{aligned} \tag{6.94}$$

Substituting (6.94) into (6.93) and linearizing the equations (i.e. neglecting powers of δ greater than one), one gets

$$\begin{pmatrix} -\mathrm{i}\kappa & 0 & 0 & -1 \\ 0 & -\Omega & \kappa & 0 \\ 0 & 0 & -\mathrm{i}\Omega & -1 \\ 1 & -1 & 0 & \mathrm{i}\kappa \end{pmatrix} \begin{pmatrix} \delta N_e \\ \delta N \\ \delta v \\ \delta F \end{pmatrix} = \begin{pmatrix} 0 \\ 0 \\ 0 \\ 0 \end{pmatrix}. \tag{6.95}$$

A non-trivial solution of (6.95) requires the vanishing of the determinant of the coefficients, yielding the dispersion relation

$$\kappa = \frac{\Omega}{\sqrt{1-\Omega^2}} \qquad \text{for } \Omega \ll 1: \quad \kappa \approx \Omega + \tfrac{1}{2}\Omega^3, \quad \Omega \approx \kappa \approx \frac{\lambda_D}{\lambda}. \tag{6.96}$$

As can be seen from this dispersion relation, one has an ion wave with large wavelength (in comparison with the Debye length) if $\Omega \ll 1$. It is worth mentioning that to the lowest order one has for the ion wave the dispersion relation

$$\kappa = \Omega \;\Rightarrow\; \frac{\omega}{k} = \left(\frac{Zk_B T_e}{m_i}\right)^{1/2} = v_a \tag{6.97}$$

where v_a is the phase velocity. The dispersion relation given in equation (6.97) was used in (6.66) for $Z = 1$ and throughout the book for (the linear) ion acoustic phase velocity.

The soliton solution is obtained by taking into account the nonlinear dispersion relation (6.96). The phase term in the Fourier transform of equations (6.94) is

$$\mathrm{i}(\kappa\xi - \Omega\tau) = \mathrm{i}[\Omega(\xi - \tau) + \tfrac{1}{2}\Omega^3\xi]. \tag{6.98}$$

The term $\frac{1}{2}\Omega^3\xi$ is called the dispersive term. It is convenient to introduce new variables that incorporate this effect:

$$\zeta = \Omega(\xi - \tau), \qquad \eta = \Omega^3\xi. \tag{6.99}$$

We rewrite equations (6.93) in terms of these variables. For this purpose we use

$$\frac{\partial}{\partial\xi} = \Omega\frac{\partial}{\partial\zeta} + \Omega^3\frac{\partial}{\partial\eta}, \qquad \frac{\partial}{\partial\tau} = -\Omega\frac{\partial}{\partial\zeta} \tag{6.100}$$

so that the fluid-Poisson equations to be solved are

$$\begin{aligned}
\frac{\partial N}{\partial\zeta} + \frac{\partial(Nv)}{\partial\zeta} + \Omega^2\frac{\partial(Nv)}{\partial\eta} &= 0 \\
\Omega\frac{\partial N_e}{\partial\zeta} + \Omega^3\frac{\partial N_e}{\partial\eta} + FN_e &= 0 \\
-\Omega\frac{\partial v}{\partial\zeta} + \Omega v\left(\frac{\partial v}{\partial\zeta} + \Omega^2\frac{\partial v}{\partial\eta}\right) - F &= 0 \\
\Omega\frac{\partial F}{\partial\zeta} + \Omega^3\frac{\partial F}{\partial\eta} + N_e - N &= 0.
\end{aligned} \tag{6.101}$$

Equations (6.101) are solved by the following perturbation series:

$$\begin{aligned} N &= 1 + \Omega^2 N_1 + \Omega^4 N_2 + \cdots \\ N_e &= 1 + \Omega^2 N_{e1} + \Omega^4 N_{e2} + \cdots \\ v &= \Omega^2 v_1 + \Omega^4 v_2 + \cdots \\ F &= \Omega^3 F_1 + \Omega^5 F_2 + \cdots . \end{aligned} \tag{6.102}$$

The leading terms of the expansion are evident from equations (6.101). The Ω^2 expansion of N and N_e is necessary in order to have a consistent perturbation theory in the small parameter Ω. Equations (6.101) to lowest order in Ω are (first and last equations to order Ω^2 and second and third equations to order Ω^3)

$$\begin{aligned} -\frac{\partial N_1}{\partial \zeta} + \frac{\partial v_1}{\partial \zeta} &= 0 \\ \frac{\partial v_1}{\partial \zeta} - F_1 &= 0 \\ \frac{\partial N_{e1}}{\partial \zeta} + F_1 &= 0 \\ N_1 &= N_{e1}. \end{aligned} \tag{6.103}$$

The solution of these equations is

$$N_1 = N_{e1} = v_1 = \phi(\zeta, \eta), \qquad F_1 = -\frac{\partial \phi}{\partial \zeta}. \tag{6.104}$$

An arbitrary function of η was neglected by integrating the first equation of (6.103). In the next order in Ω, equations (6.101) are (first and last equations to order Ω^4 and second and third equations to order Ω^5)

$$\begin{aligned} -\frac{\partial N_2}{\partial \zeta} + \frac{\partial}{\partial \zeta}(v_2 + \phi^2) + \frac{\partial \phi}{\partial \eta} &= 0 \\ -\frac{\partial v_2}{\partial \zeta} + \phi \frac{\partial \phi}{\partial \zeta} - F_2 &= 0 \\ \frac{\partial N_{e2}}{\partial \zeta} + \frac{\partial \phi}{\partial \eta} + \phi F_1 + F_2 &= 0 \\ \frac{\partial F_1}{\partial \zeta} - N_2 + N_{e2} &= 0. \end{aligned} \tag{6.105}$$

Equations (6.105) are linearly combined ($\partial/\partial\zeta$ [last eq.] + [second eq.] − [first eq.] − [third eq.] = 0) and F_1 is substituted by using (6.104) to yield

an equation for ϕ:

$$\frac{\partial \phi}{\partial \eta} + \phi \frac{\partial \phi}{\partial \zeta} + \frac{1}{2} \frac{\partial^3 \phi}{\partial \zeta^3} = 0. \tag{6.106}$$

This equation is the famous **KdV equation** describing a **soliton**. Equation (6.106) admits a solution of a solitary wave that is a single pulse, which retains its shape as it propagates with a velocity u^* in (ζ, η) space. Thus we are looking for a solution of the variable $(\zeta - u^*\eta)$, or equivalently in the usual space (x, t) the solution is a function of $(x - ut)$, where u is the speed of the solitary wave. The following relations between the coordinates

$$\zeta = \Omega\xi - \Omega\tau = \Omega\lambda_D^{-1}x - \Omega\omega_{pi}t, \qquad \eta = \Omega^3\xi = \Omega^3\lambda_D^{-1}x \tag{6.107}$$

imply

$$x - ut = K(\zeta - u^*\eta) \Rightarrow \begin{cases} u^* = \dfrac{1}{\Omega^2}\left(1 - \dfrac{\omega_{pi}\lambda_D}{u}\right) \\ u = \dfrac{\omega_{pi}\lambda_D}{1 - \Omega^2 u^*} \\ K = \dfrac{u}{\Omega\omega_{pi}} \end{cases}. \tag{6.108}$$

Looking now for a solution of equation (6.106) in the variable z,

$$z = \zeta - u^*\eta \tag{6.109}$$

one gets from (6.106)

$$-u^* \frac{\partial \phi}{\partial z} + \phi \frac{\partial \phi}{\partial z} + \frac{1}{2} \frac{\partial^3 \phi}{\partial z^3} = 0. \tag{6.110}$$

This equation can be integrated to yield

$$u^*\phi - \frac{1}{2}\phi^2 - \frac{1}{2}\frac{\mathrm{d}^2\phi}{\mathrm{d}z^2} = 0 \tag{6.111}$$

where the constant of integration is assumed to vanish. Multiplying equation (6.111) by $\mathrm{d}\phi/\mathrm{d}z$ and integrating once more (again with a zero constant of integration), one has

$$\left(\frac{\mathrm{d}\phi}{\mathrm{d}z}\right)^2 = \frac{2}{3}\phi^2(3u^* - \phi). \tag{6.112}$$

The solution of this equation is

$$\phi(z) = 3u^* \operatorname{sec} \mathrm{h}^2\left[\left(\sqrt{\frac{u^*}{2}}\right)z\right]. \tag{6.113}$$

One can verify the solution (6.113) by direct substitution into (6.111) by using the identities

$$\frac{\mathrm{d}(\operatorname{sech} z)}{\mathrm{d}z} = -(\operatorname{sech} z)(\tanh z), \qquad \operatorname{sech}^2 z + \tanh^2 z = 1. \tag{6.114}$$

The solution ϕ of (6.113) has a peak at $z = 0$ with a maximum $\phi_{\max} = 3u^*$. ϕ vanishes at $z = \pm\infty$, it moves with a velocity u^* in (ζ, η) coordinates, and it has a width of $\sqrt{2/u^*}$. This solution has only one parameter, u^*, and has the characteristic properties of a solitary wave, i.e. the larger the speed the greater is the amplitude and the narrower is the width.

Recalling that $\phi = v_1 = N_1 = N_{e1}$, we return to the dimensional variables $x - t$. From (6.92), (6.102) and (6.113) one gets

$$n_i - n_0 = \Omega^2 n_0 N_1 = (\delta n) \operatorname{sech}^2\left(\frac{x - ut}{D}\right), \qquad \delta n = 3\Omega^2 n_0 u^*. \tag{6.115}$$

Using (6.108) and (6.115) yields

$$u = \frac{\omega_{pi}\lambda_D}{1 - \Omega^2 u^*} = \frac{\omega_{pi}\lambda_D}{1 - (\delta n/3n_0)} \approx \omega_{pi}\lambda_D\left(1 + \frac{\delta n}{3n_0}\right). \tag{6.116}$$

Using the relations (6.108), the solution (6.113) and δn from (6.115), one gets the width of the soliton wave D,

$$D = \sqrt{\frac{2}{u^*}}\,\frac{u}{\Omega\omega_{pi}} = \frac{\lambda_D}{1 - (\delta n/3n_0)}\sqrt{\frac{6n_0}{\delta n}} \approx \lambda_D\sqrt{\frac{6n_0}{\delta n}}. \tag{6.117}$$

The standard properties of a solitary wave can be seen from equations (6.116) and (6.117):

(a) The width of the solitary wave D decreases with increasing δn.
(b) The velocity of the solitary wave u increases with increasing δn.

We end this section with a note on the KdV equation. Equation (6.106) is a special case of the general KdV equation

$$\frac{\partial\phi}{\partial t} + \mu\phi\frac{\partial\phi}{\partial x} + \nu\frac{\partial^3\phi}{\partial x^3} = 0 \tag{6.118}$$

where μ and ν are two coefficients. The solution of the KdV equation is

$$\begin{aligned} \phi &= \phi_0 \operatorname{sech}^2[(x - ut)/D] \\ D &= 2\sqrt{\frac{3\nu}{\phi_0\mu}} \\ u &= \frac{\phi_0\mu}{3}. \end{aligned} \tag{6.119}$$

In our equation (6.106) the coefficients are $\mu = 1$ and $\nu = \frac{1}{2}$, implying $\phi_0 = 3u$ and $D = (2/u)^{1/2}$ (see equation (6.113)).

The soliton concept has also attracted interest and speculation in laser–plasma interactions. In particular the solitary waves were associated with the ponderomotive force. Cavity structures, measured experimentally near the critical surface, were related to solitary waves. However, it seems that the very interesting phenomena of the soliton have not yet been fully and successfully investigated in laser–plasma interactions.

Chapter 7

Laser-Induced Electric Fields in Plasma

7.1 High- and Low-Frequency Electric Fields

In laser–plasma interaction the electric field, or rather the various macroscopic electric fields, plays a major role in defining the properties of the plasma system. First, the laser electric field, $E_L \cos \omega_L t$, is propagating into the plasma, where part of it is reflected and the other part is absorbed. The laser electric field amplitude and its frequency are given by

$$\begin{aligned} E_L\,(\mathrm{V/cm}) &= 2.75 \times 10^9 \left(\frac{I_L}{10^{16}\,\mathrm{W/cm^2}} \right)^{1/2} \\ \omega_L\,(\mathrm{s^{-1}}) &= \frac{2\pi c}{\lambda_L} = 1.88 \times 10^{15} \left(\frac{\mu\mathrm{m}}{\lambda_L} \right) \end{aligned} \tag{7.1}$$

where I_L is the laser energy flux and λ_L is the laser wavelength. ω_L sets the scale for high-frequency phenomena and the period of one laser oscillation $(2\pi/\omega_L)$ is about 3.3 fs for a 1 μm laser wavelength.

The propagating and reflected electric fields in different plasma media were calculated in chapter 5. The electric fields associated with the possible waves in the plasma were calculated in chapter 6. Two classes of electric fields were derived: the high-frequency one, of the order of the laser frequency or the electron–plasma frequency, $\omega \approx \omega_{pe} \approx 10^{15}\,\mathrm{s^{-1}}$ (for electron density $\sim 10^{21}\,\mathrm{cm^{-3}}$), and the low-frequency electric field of the order of the ion–plasma frequency $\omega \approx 10^{12}\,\mathrm{s^{-1}}$. The appropriate time scales are about 1 fs for the high-oscillation fields and about 1 ps for the low-oscillation fields.

Another interesting case of a slowly-varying (in time) electric field is the one induced by the ponderomotive force and developed in chapter 4. This 'd.c.' (i.e. very slow varying in time) electric field E is in the direction of the gradient of E_L^2 and the magnitude of this electric field (E) is of

the order

$$en_e E \approx \left(\frac{\omega_{pe}^2}{\omega_L^2}\right)\frac{E_L^2}{16\pi r_L}$$

$$\Rightarrow\ E\,(\mathrm{V/cm}) \approx 1.0\times 10^7\left(\frac{I_L}{10^{16}\,\mathrm{W/cm^2}}\right)\left(\frac{10^{21}\,\mathrm{cm^{-3}}}{n_{ec}}\right)\left(\frac{100\,\mu\mathrm{m}}{r_L}\right) \qquad (7.2)$$

where n_e is the electron density, n_{ec} is the electron critical density, r_L is the laser radius defined by $I_L \approx \exp(-r^2/2r_L^2)$, and it is assumed that $\mathrm{grad}\, E_L^2 \approx E_L^2/r_L$. As discussed in chapter 6, an electric field can also be induced by the ponderomotive forces associated with the wave–wave instabilities.

In general, the electric field in laser–plasma interactions is discussed in the previous three chapters. In this chapter we shall add two cases of slowly varying electric fields: in section 7.2 the electric field of an expanding plasma into the vacuum is calculated and in section 7.3 an electric field in the double layers is calculated. An example of charge particle acceleration due to these electric fields is given in section 7.4.

7.2 Expansion of Plasma into the Vacuum

A laser-created plasma is expanding into the vacuum, towards the laser irradiation (Gurevich *et al.* 1965, 1968, 1969, Crow *et al.* 1975, Anisimov *et al.* 1979, Sigel 1979). When a laser irradiates a target, the electrons are heated and they expand towards the vacuum. The ions follow the electrons that expand towards the vacuum. In this section the hydrodynamic problem of plasma expansion is calculated, by assuming that the electrons and the ions are treated as separate fluids with different temperatures.

We assume the simplest one-dimensional problem with plane geometry. For a laser spot on target $2r_L = D$ (r_L, the laser radius, is defined in the previous section), this approximation is valid as long as $D \gg v_i t$, where v_i is the streaming velocity of the ions and t is the expansion time. The continuity equation for the ions and the momentum equations for the electrons and ions are

$$\begin{aligned}\frac{\partial n_i}{\partial t} + \frac{\partial (n_i v_i)}{\partial x} &= 0\\ \frac{\partial P}{\partial x} + en_e E &= 0\\ m_i n_i\left(\frac{\partial v_i}{\partial t} + v_i\frac{\partial v_i}{\partial x}\right) &= eZn_i E\end{aligned} \qquad (7.3)$$

where E is the electric field in the expanding plasma, n_i and n_e are the ion and electron densities accordingly, m_i is the ion mass and Ze is the ion charge.

Neglecting the ion temperature in comparison with the electron temperature T_e, the plasma pressure P is given by

$$P = n_e k_B T_e. \tag{7.4}$$

In the electron momentum equation, the second equation of (7.3), the inertia term of the electrons ($m_e \, dv_e/dt$, where v_e is the electron fluid velocity) is neglected. This is justified when adding the two inertia terms of the electrons and the ions, since $m_e \ll m_i$, and neglecting the high-frequency oscillations (not relevant to this problem) one has $dv_e/dt \approx dv_i/dt$. Assuming charge neutrality $n_e = Zn_i$, adding the electron and ion momentum equations of (7.3), one gets

$$\frac{\partial v_i}{\partial t} + v_i \frac{\partial v_i}{\partial x} = -\frac{1}{m_i n_i} \frac{\partial P}{\partial x}. \tag{7.5}$$

Using the definition of the sound velocity, $n_e = Zn_i$, and equation (7.4), one gets

$$c_s^2 = \frac{1}{m_i} \frac{\partial P}{\partial n_i} = \frac{Z k_B T_e}{m_i} \tag{7.6}$$

where the electron temperature is assumed constant, a reasonable assumption for the plasma corona under investigation. Implying the identity $\partial P/\partial x = (\partial P/\partial n)(\partial n/\partial x)$ into the right-hand side of equation (7.5) and using (7.6), we obtain

$$\frac{\partial v_i}{\partial t} + v_i \frac{\partial v_i}{\partial x} + c_s^2 \left(\frac{1}{n_i} \frac{\partial n_i}{\partial x} \right) = 0. \tag{7.7}$$

One has to solve (7.7) together with the continuity equation (first of equations (7.3)). For this purpose we define the dimensionless variables

$$\begin{gathered} \xi = \frac{x}{c_s t}, \qquad v = \frac{v_i}{c_s}, \qquad n = \frac{n_i}{n_0} \\ \frac{\partial}{\partial x} = \frac{1}{c_s t} \frac{\partial}{\partial \xi}, \qquad \frac{\partial}{\partial t} = -\frac{\xi}{t} \frac{\partial}{\partial \xi} \end{gathered} \tag{7.8}$$

where n_0 is the background density. Substituting (7.8) into the first equation of (7.3) and (7.7), we get

$$\begin{pmatrix} v - \xi & 1 \\ 1 & v - \xi \end{pmatrix} \begin{pmatrix} d \ln n/d\xi \\ dv/d\xi \end{pmatrix} = \begin{pmatrix} 0 \\ 0 \end{pmatrix}. \tag{7.9}$$

The determinant of the 2×2 matrix should vanish in order to get a nonzero solution, yielding

$$v = \xi + 1 \;\Rightarrow\; v_i = \frac{x}{t} + c_s \tag{7.10}$$

where we choose the positive x axis in the direction of the plasma expansion. The density profile is obtained from one of the equations of (7.9) by using (7.10):

$$n_i = n_0 \exp(-\xi - 1) \tag{7.11}$$

where the boundary condition $n = n_0$ was taken for $\xi = -1$. The plasma is expanding in the $+x$ direction with a velocity v_i, but at the same time a disturbance (a rarefaction wave—see chapter 10) moving with the speed of sound c_s in the $-x$ direction is taking place. This rarefaction arrives at a position $x = -c_s t$ at time t, or equivalently at $\xi = -1$ in the dimensionless variable. For this reason one has to choose $n_i = n_0$ at $\xi = -1$.

The electric field is obtained from the second equation of (7.3) by using (7.6) and (7.11), yielding

$$E = -\frac{k_B T_e}{e n_e}\frac{\partial n_e}{\partial x} = -\frac{k_B T_e}{e c_s t}\frac{\partial \ln n}{\partial \xi} = \frac{k_B T_e}{e c_s t}. \tag{7.12}$$

From (7.12) one can see that the electric field is uniform (i.e. constant) in space: it goes to zero for $t \to \infty$, but has a singularity at $t = 0$. At $t = 0$ this solution is not relevant. The self-similar solution developed above (i.e. where the two variables x and t can be combined into one variable, x/t) is not permitted at very small t, small compared with the time scale defining the problem. In our case the time defining the laser–plasma interaction is the laser pulse duration; therefore, the above self-similar solution is relevant only for $t \gg \tau_L$ (the laser pulse duration). The electric field in the expanding plasma corona as given by (7.12) is about 10^4 V/cm at $t \approx 3\tau_L$, for a laser pulse duration of about 1 ns and a typical electron temperature (in energy units) of 1 keV ($c_s \approx 3 \times 10^7$ cm/s for $T_e = 1$ keV).

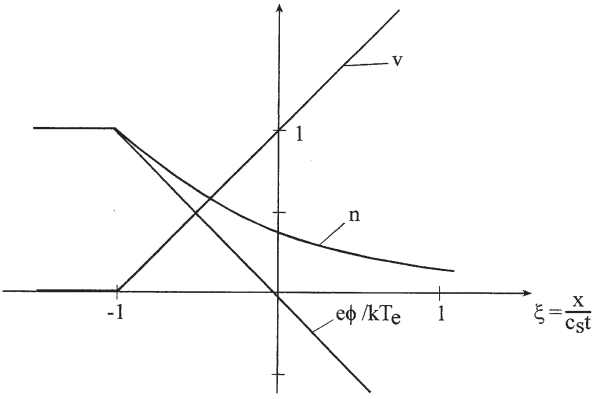

Figure 7.1. Self-similar solution—the plasma expansion into vacuum. v and n are the dimensionless ion velocity and density respectively and $x = \xi c_s t$, where c_s is the isothermal speed of sound. ϕ is the electric potential and T_e is the electron temperature.

The electric potential ϕ is given by

$$\phi = -\int E \, \mathrm{d}x = -\left(\frac{k_B T_e}{e}\right)\frac{x}{c_s t} = -\frac{k_B T_e}{e}\,\xi \tag{7.13}$$

where the boundary condition $\phi = 0$ for $\xi = 0$ was taken.

The self-similar solution, as developed in this section for v, n and $e\phi/k_B T_e$, is given in figure 7.1.

7.3 Double Layers

In a static model, the double layer (DL) consists of two adjacent regions of opposite electric charge, which induce a potential drop and an electric field. The plasma within the DL is not locally neutral, but over the entire DL region it maintains space charge neutrality (global neutrality). A characteristic distance of the order of Debye length separates these layers of positive and negative charges, although in many cases the distance may be many times the Debye length. The potential jump across these layers is of the order of magnitude of the electron thermal temperature (where both the potential and the temperature are in energy units).

In high-power laser–plasma interaction, the electric fields inside the DL are no longer static, and therefore the nomenclature 'dynamic electric fields' was introduced (Eliezer and Hora 1989). According to two-fluid simulations (Lalousis 1983, Hora *et al*. 1984) these fields act deep inside plasmas and are oscillating and damped.

The first research on DL was conducted by Langmuir (1929). A condition for DL formation was given by Bohm (1949). Although DLs have been studied since the early days of plasma physics, this phenomenon is still a subject of active research. The DL phenomenon is a highly nonlinear effect of great interest in basic plasma physics, as well as in many plasma applications. DL solutions have been obtained theoretically by using the Vlasov equation (Bernstein *et al*. 1957), by solving fluid models coupled by the Poisson equation where space charge quasi-neutrality is not assumed (Lalousis 1983, Lalousis and Hora 1983, Hora 2000), and by performing computer simulations (Smith 1987).

Electrostatic DLs are now a well-known phenomenon in laboratory plasmas (Saeki *et al*. 1980, Hatakeyama *et al*. 1983, Chan *et al*. 1984, Hershkowitz 1985). The experiments have shown the existence of various types of DLs that can arise under different plasma conditions, including both magnetized and non-magnetized plasmas. Dynamic DLs in laser–plasma interactions were also measured experimentally (Eliezer and Ludmirsky 1983, Ludmirsky *et al*. 1984).

A schematic potential $\phi(x)$, defining an electric field $E(x)$ and a space–charge density $\rho_e(x)$, are given in figure 7.2. The following three conditions

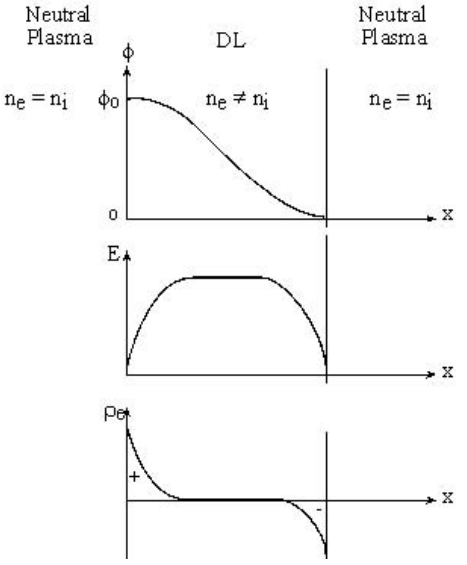

Figure 7.2. Schematic of the potential ϕ, the electric field E and the charge density ρ_e in a static DL.

must be fulfilled for the existence of a DL:

1. The potential drop ϕ_0 through the DL obeys the relation

$$\phi_0 \geq \frac{k_B T}{e} \tag{7.14}$$

   where T is the temperature of the coldest plasma bordering the layer, k_B is the Boltzmann constant and e is the electron charge.
2. Quasi-neutrality is locally violated in both space charge layers.
3. Global neutrality, i.e. zero net charge of the DL, is required.

The last constraint implies that the electric field is much stronger inside the DL than outside. The DL potential divides the plasma particles into four classes: free and trapped or reflected electrons and ions. The free electrons and ions have a kinetic energy larger than the potential barrier, and therefore they can move from one side of the DL to the other side. The particles with a kinetic energy smaller than the potential barrier are reflected or trapped at the DL borders and cannot move from one side of the DL to the other side. The charge separation in the DL is maintained by flux continuity of the free-streaming particles. The free particles are the streaming electrons from $\phi = 0$ towards $\phi = \phi_0$ and the ions are streaming in the opposite direction. Outside the DL, trapped or reflected ions on the low-potential side and trapped or reflected electrons on the high-potential end maintain charge neutrality.

In the next section it is shown how these DLs can accelerate electrons and ions.

7.4 Charged Particle Acceleration

7.4.1 A static model

Laser-produced plasma experiments have shown that high-energy ions are emitted and carry away a large fraction of the absorbed laser energy. X-ray emission measurements at laser intensities $I_L\lambda_L^2 > 10^{14}\,\mathrm{W\,\mu m^2/cm^2}$ (the laser irradiance I_L is measured in $\mathrm{W/cm^2}$ and the laser wavelength λ_L in μm) have shown non-Maxwellian electron velocity distribution (Haines 1979, Ahlstrom 1982). Two distinct electron temperatures, the so-called thermal (or cold) and supra-thermal (or hot) temperatures, usually characterize this distribution. These electron distributions are associated with the existence of fast ions. We shall now describe a very simple model showing how DLs accelerate ions.

A high-power laser irradiates a spherical pellet of radius R. The fast electrons emitted from the spherical plasma leave the sphere until an electrostatic potential is set up to stop the outgoing electrons. The thermal electrons then traverse this field (i.e. the DL), decelerate and accelerate back towards the sphere. The same field will accelerate positive ions from the outer surface of the plasma. The fast ions are field-extracted from the plasma and therefore they can be used to measure the electric field and the potential of the DL under consideration. For simplicity, monochromatic fast electrons and protons (the ions) species are assumed. The protons, with a mass M, are emitted from the DL with velocity v, so that

$$\tfrac{1}{2}Mv^2 = e\phi \tag{7.15}$$

where ϕ is the DL potential drop. Assuming that the fast protons have a total energy W and a total charge Q, one can write

$$W = Q\phi. \tag{7.16}$$

The charge of the proton q present at any moment inside the DL (defined by the potential drop ϕ and charge separation d) is given by

$$q = \frac{Qd}{v\tau_L} = \frac{Wd}{\phi v\tau_L} \tag{7.17}$$

where τ_L is the laser pulse duration. For the geometry under consideration, the DL can be modelled by a capacitor with a capacity C:

$$C = \frac{4\pi R^2}{d}. \tag{7.18}$$

The capacitor is charged with a charge greater than q (the momentary charge of the protons inside the DL) and with a voltage equal to ϕ; therefore

$$\phi > \frac{q}{C} = \frac{Wd^2}{4\pi R^2 \phi v \tau_L}. \tag{7.19}$$

This relation implies that the electric field created by the charge separation (i.e. the DL) is

$$E = \frac{\phi}{d} \geq \left(\frac{W}{4\pi R^2 v \tau_L} \right)^{1/2}. \tag{7.20}$$

The velocity of the ions is measured from the time of flight and the number of ions is measured with charge collectors, and from these their energy is deduced. Using a typical experiment where $W = 10\,\text{J}$, $v = 10^8\,\text{cm/s}$, $\tau_L = 1\,\text{ns}$, $R = 50\,\mu\text{m}$, one gets an electric field $E > 5 \times 10^8\,\text{V/cm}$.

From this simple model we can conclude that the fast electrons transfer their energy to the electrostatic field in order to create a DL, while the fast ions take their energy from the electric field of the DL. This mechanism can lead to very high electric fields, as is obtained above.

7.4.2 A dynamic model

DL solutions have been obtained theoretically by solving a two-fluid model coupled by the Poisson equation, where space-charge quasi-neutrality is not assumed. For example, in the simulation (Hora *et al.* 1984) of the interaction between a plasma with a highly bent parabolic initial density profile of 25 wavelengths thickness and a neodymium glass laser radiation of $10^{17}\,\text{W/cm}^2$ intensity, the following results were achieved:

(a) a caviton (i.e. a minimum in the density) is created,
(b) the plasma is accelerated towards the vacuum with a velocity of about $10^8\,\text{cm/s}$,
(c) a dynamic (time-dependent) DL is created with a maximum electric field about $10^9\,\text{V/cm}$ and
(d) electrons were accelerated to energies $\sim$140 keV.

The following simple dynamical model has been suggested in order to explain how dynamical DL accelerates electrons (Eliezer *et al.* 1995).

We assume that a DL is created at time $t = 0$ during a very short time interval, described by the Dirac delta function, $\delta(t)$. The Poisson equation gives

$$\frac{dE}{dx} = -4\pi e[n_e(x,t) - n_i(x,t)] = f(x)\delta(t). \tag{7.21}$$

Integrating this equation yields

$$E = \delta(t) \int f(x)\,\mathrm{d}x = F(x)\delta(t). \tag{7.22}$$

For example, from a 'quadrupole' type (two DL in a sequence) of interaction defined by a charge density

$$f(x) = K\left[\frac{2x}{\sigma^4}\left(1 - \frac{2x^2}{\sigma^2}\right)\right] \exp\left(-\frac{x^2}{\sigma^2}\right) \tag{7.23}$$

one gets a space-dependent electric field

$$F(x) = \frac{K}{\sigma^2}\left(1 + \frac{2x^2}{\sigma^2}\right) \exp\left(-\frac{x^2}{\sigma^2}\right). \tag{7.24}$$

The Newton equation for the electron

$$\frac{\mathrm{d}v}{\mathrm{d}t} = -\frac{eE}{m} = -\frac{e}{m} F(x)\delta(t) \tag{7.25}$$

has the solution

$$\begin{aligned} &\frac{\mathrm{d}x}{\mathrm{d}t} = v(t) = -\frac{e}{m} F(x)\theta(t) + v_0 = (v_1 - v_0)\theta(t) + v_0 \\ &\theta(t) = \begin{cases} 1 & \text{for } t > 0 \\ 0 & \text{for } t < 0 \end{cases} \end{aligned} \tag{7.26}$$

where v_0 is the initial velocity and v_1 the final velocity, after the acceleration. If the electron is at the position x when the force is applied (at $t = 0$ in this example), then the final velocity is achieved according to the value of $-eF(x)/m$.

The position of the electron is given by integrating (7.26):

$$x(t) = v_0 t + (v_1 - v_0)\theta(t)t \tag{7.27}$$

where the identity $\delta(t)t = 0$ was used.

Substituting (7.26) into (7.25), the electric field can be written

$$E(x,t) = F(x)\delta(t) = -\frac{m}{e}(v_1 - v_0)\delta(t). \tag{7.28}$$

The energy given to the particle by the electric field is given by using (7.26) and (7.28):

$$\begin{aligned} -e \int E(x,t)\,\mathrm{d}x = &-e \int_{-\infty}^{+\infty} E[x(t),t]\,\frac{\mathrm{d}x}{\mathrm{d}t}\,\mathrm{d}t \\ &= m(v_1 - v_0) \int_{-\infty}^{+\infty} \delta(t)[(v_1 - v_0)\theta(t) + v_0]\,\mathrm{d}t \\ &= \tfrac{1}{2} m(v_1^2 - v_0^2) \end{aligned} \tag{7.29}$$

where in the last stage we have used the identity

$$\int \theta(t)\delta(t)\,\mathrm{d}t = \tfrac{1}{2} \tag{7.30}$$

which can be easily proven by integrating by parts.

Equation (7.29) is the energy conservation, which shows that a particle can be accelerated or decelerated by E, depending on the value of the electric field at the particle position, at the time that the DL is created. It has been shown that under the right configuration a charged particle can be accelerated to high energies even when the electric field is changing very fast in time.

In summary, it has been demonstrated that a dynamic DL can accelerate charged particles, as was suggested in astrophysics (Fälthammer 1987, Alfvén 1988, Raadu 1989). The existence of DL in laser-produced plasma in the outer corona was detected directly by the deflection of a probing beam (Ehler 1975, Mendel and Olsen 1975) and by using Rogowski coils (Eliezer and Ludmirsky 1983). Therefore, similar to DL in astrophysics, the DL might play an important role in laser–plasma interactions.

Chapter 8

Laser-Induced Magnetic Fields in Plasma

When a laser irradiates a medium, the laser magnetic field $B_L \cos \omega_L t$ (together with the associated electric field) is propagating into the plasma, part of it is reflected and the other part is absorbed. The laser magnetic field amplitude and its frequency are given by

$$\begin{aligned} B_L(\text{Gauss}) &= 9.2 \times 10^6 \left(\frac{I_L}{10^{16}\ \text{W/cm}^2} \right)^{1/2} \\ \omega_L\ (\text{s}^{-1}) &= \frac{2\pi c}{\lambda_L} = 1.88 \times 10^{15} \left(\frac{\mu\text{m}}{\lambda_L} \right) \end{aligned} \tag{8.1}$$

where I_L is the laser energy flux and λ_L is the laser wavelength. ω_L sets the scale for high-frequency phenomena. The period of one laser oscillation ($2\pi/\omega_L$) is about 3.3 fs for a laser with a wavelength of 1 μm. The propagation of electromagnetic field in plasma was calculated in chapter 5. There are also high-frequency magnetic fields associated with the stimulated Brillouin and Raman scattering discussed in chapter 6.

In this chapter we are interested only in the slowly-varying (on the time scale of the laser pulse duration) magnetic fields, approximated as d.c. magnetic fields. The generation of d.c. mega-Gauss magnetic fields in laser-produced plasmas is well-documented (Stamper *et al.* 1971, Boyd and Cooke 1988, Horovitz *et al.* 1998). In this chapter we discuss the mechanisms proposed to explain the generation of the d.c. magnetic fields and some theoretical consequences.

In section 8.1, the $\nabla n \times \nabla T$ toroidal magnetic field (Raven *et al.* 1978, Bobin 1985, Stamper 1991) is derived. In section 8.2, the magneto-hydrodynamic equations are derived (Braginskii 1965, Nicholson 1983, Parks 1991). Using the generalized Ohm's law together with the Maxwell equations, a generalized equation for the d.c. magnetic field is obtained. In particular the magnetic Reynolds number is defined and the dynamo effect is described (Briand *et al.* 1983, Dragila 1987). Section 8.3 describes the Faraday effect

and the magnetic field created by the inverse Faraday effect (Steiger and Woods 1972, Eliezer *et al.* 1992, Lehner 1994, 2000, Sheng and Meyer-ter-Vehn 1996, Haines 2001). In section 8.4 we develop the dispersion relation for waves in the presence of the d.c. magnetic field. In particular, ordinary, extraordinary and Alfvén waves are analysed. We conclude this chapter with section 8.5, showing the effect of resonance absorption in the presence of the d.c. magnetic field (Woo *et al.* 1978, David and Pellat 1980).

8.1 The $\nabla n \times \nabla T$ Toroidal Magnetic Field

One can see from the Maxwell equation (in Gaussian units)

$$\nabla \times \mathbf{E} = -\frac{1}{c}\frac{\partial B}{\partial t} \tag{8.2}$$

that a magnetic field is generated if the electric field E does not have a vanishing curl, i.e. the electric field in the plasma is not derivable from a potential. As discussed in the previous chapter, the electric field in the plasma is required in order to keep quasi-neutrality on a large scale (compared with the Debye length) during long periods of time (compared with the inverse plasma frequency). From the electron momentum equation (see section 3.1), on the long time scale it is justifiable to neglect the inertia of the electrons, implying

$$0 = -\nabla P_{\mathrm{e}} - e n_{\mathrm{e}} \mathbf{E}. \tag{8.3}$$

This equation is equivalent to the assumption that the volume forces due to the free electrical charges balance the electron pressure gradient. In equation (8.3), the charge motion is neglected. Substituting the ideal gas equation of state

$$P_{\mathrm{e}} = n_{\mathrm{e}} k_{\mathrm{B}} T_{\mathrm{e}} \tag{8.4}$$

into equation (8.3), one gets the electric field E for equation (8.2), yielding

$$\frac{\partial \mathbf{B}}{\partial t} = \frac{c k_{\mathrm{B}}}{e n_{\mathrm{e}}} \nabla T_{\mathrm{e}} \times \nabla n_{\mathrm{e}}. \tag{8.5}$$

From this equation an estimate of the magnitude of the magnetic field B is obtained by the substitution of

$$\frac{\partial}{\partial t} \approx \frac{1}{\tau_{\mathrm{L}}}, \qquad \frac{\nabla n_{\mathrm{e}}}{n_{\mathrm{e}}} \approx \frac{1}{L_{\mathrm{n}}}, \qquad \nabla T_{\mathrm{e}} \approx \frac{T_{\mathrm{e}}}{L_{\mathrm{T}}} \tag{8.6}$$

into equation (8.5), implying

$$B\,(\mathrm{MGauss}) \approx 10 \left(\frac{\tau_{\mathrm{L}}}{1\,\mathrm{ns}}\right)\left(\frac{k_{\mathrm{B}} T_{\mathrm{e}}}{1\,\mathrm{keV}}\right)\left(\frac{30\,\mu\mathrm{m}}{L_{\mathrm{n}}}\right)\left(\frac{30\,\mu\mathrm{m}}{L_{\mathrm{T}}}\right) \tag{8.7}$$

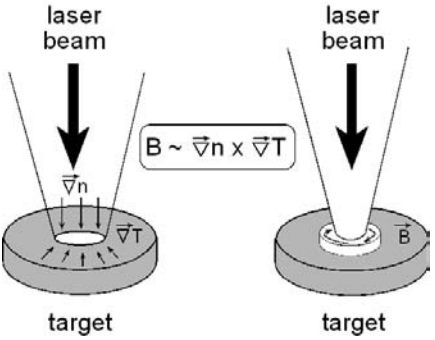

Figure 8.1. Magnetic field is generated from non-parallel density and temperature gradients.

where τ_L is the laser pulse duration or the characteristic loss time due to ablation and diffusion.

Thus a magnetic field is generated from non-parallel density and temperature gradients, as shown in figure 8.1. It turns out that this is the dominant phenomenon for the generation of a toroidal magnetic field, although there are other terms that contribute to the generation of d.c. toroidal magnetic fields, as proven in the following section.

8.2 Magneto-Hydrodynamics and the Evolution of the Magnetic Field

In this section the evolution equation of the magnetic field is developed. For this purpose the plasma is described as a magnetic fluid and the equations include the generalized Ohm's law, together with Maxwell equations. The following equations describe the mass conservation and the momentum conservation for the ion and electron fluids (in Gaussian units):

$$\begin{aligned}
&\frac{\partial n_i}{\partial t} + \nabla \cdot (n_i \mathbf{v}_i) = 0 \\
&\frac{\partial n_e}{\partial t} + \nabla \cdot (n_e \mathbf{v}_e) = 0 \\
&m_i n_i \frac{\partial \mathbf{v}_i}{\partial t} + m_i n_i (\mathbf{v}_i \cdot \nabla)\mathbf{v}_i = -\nabla P_i + Z e n_i \left(\mathbf{E} + \frac{\mathbf{v}_i \times \mathbf{B}}{c} \right) + \mathbf{R}_i \\
&m_e n_e \frac{\partial \mathbf{v}_e}{\partial t} + m_e n_e (\mathbf{v}_e \cdot \nabla)\mathbf{v}_e = -\nabla P_e - e n_e \left(\mathbf{E} + \frac{\mathbf{v}_e \times \mathbf{B}}{c} \right) + \mathbf{R}_e
\end{aligned} \tag{8.8}$$

where m_i, m_e and n_i, n_e are the ion and electron masses and densities, $\mathbf{v}_i$ and $\mathbf{v}_e$ are the ion and electron fluid velocities, P_i and P_e are the appropriate pressures, $\mathbf{E}$ and $\mathbf{B}$ are the electric and magnetic fields in the plasma

medium and c is the light velocity. $\mathbf{R}_e(\mathbf{r})$ represents the change in electron momentum at position $\mathbf{r}$ due to collisions with ions and $\mathbf{R}_i(\mathbf{r})$ is the change in ion momentum at $\mathbf{r}$ due to collisions with electrons. Therefore

$$\mathbf{R}_e = -\mathbf{R}_i. \tag{8.9}$$

We combine the ion and the electron equations to obtain the equations for one fluid. This fluid is described by the mass density $\rho(\mathbf{r})$, charge density $\rho_e(\mathbf{r})$, a centre of mass fluid flow $\mathbf{u}$ and an electrical current $\mathbf{J}$, defined by

$$\begin{aligned} \rho &= m_i n_i + m_e n_e \cong m_i n_i \\ \rho_e &= Z e n_i - e n_e \\ \mathbf{u} &= \frac{1}{\rho}(m_i n_i \mathbf{v}_i + m_e n_e \mathbf{v}_e) \\ J &= Z e n_i \mathbf{v}_i - e n_e \mathbf{v}_e \end{aligned} \tag{8.10}$$

and a total pressure

$$P = P_e + P_i\,. \tag{8.11}$$

Multiplying the first equation of (8.8) by m_i and the second equation by m_e and adding, one gets the one-fluid continuity equation (i.e. the mass conservation):

$$\frac{\partial \rho}{\partial t} + \nabla \cdot (\rho \mathbf{u}) = 0. \tag{8.12}$$

Multiplying the first equation of (8.8) by Ze and the second equation by $-e$ and adding, one gets the charge continuity, or the charge conservation law:

$$\frac{\partial \rho_e}{\partial t} + \nabla \cdot \mathbf{J} = 0. \tag{8.13}$$

It is assumed that $\mathbf{v}_e$, $\mathbf{v}_i$, $\partial n_e/\partial t$ and $\partial n_i/\partial t$ are small quantities and second-order terms, such as $(\mathbf{v} \cdot \nabla)\mathbf{v}$, are neglected. Adding the third equation of (8.8) with the fourth equation and using the definitions (8.10) and (8.11), one gets the one-fluid force equation (or the momentum conservation):

$$\rho \frac{\partial \mathbf{u}}{\partial t} = -\nabla P + \rho_e \mathbf{E} + \frac{1}{c}\,\mathbf{J} \times \mathbf{B}. \tag{8.14}$$

8.2.1 The generalized Ohm's law

We assume charge neutrality

$$n_e = Z n_i \tag{8.15}$$

and neglect the second-order terms (in $\mathbf{v}_e$, $\mathbf{v}_i$, $\partial n_e/\partial t$ and $\partial n_i/\partial t$) and $1/m_i \ll 1/m_e$. Adding the third equation of (8.8) multiplied by Ze/m_i with

the fourth equation multiplied by $-e/m_e$, and using the definitions (8.10), one gets

$$\frac{\partial \mathbf{J}}{\partial t} = \frac{e}{m_e}\nabla\left[\left(1+\frac{T_i}{ZT_e}\right)^{-1}P\right] + \frac{Ze^2\rho}{m_e m_i}\left(\mathbf{E}+\frac{1}{c}\,\mathbf{u}\times\mathbf{B}\right) - \frac{e}{m_e c}\,\mathbf{J}\times\mathbf{B} + \frac{e}{m_e}\,\mathbf{R}_i\,. \tag{8.16}$$

Algebraic relations such as the following were used in order to derive equation (8.16):

$$\frac{e^2 n_e}{m_e} = \frac{e^2 Z n_i}{m_e} = \frac{e^2 Z}{m_e m_i}(m_i n_i) \cong \frac{e^2 Z}{m_e m_i}(m_i n_i + m_e n_e) = \frac{e^2 Z\rho}{m_e m_i} \tag{8.17}$$

$$\frac{e^2 n_e \mathbf{v}_e}{m_e c} = \frac{e}{m_e c}(e n_e \mathbf{v}_e - Z e n_i \mathbf{v}_i) + \frac{Ze^2 n_i m_i \mathbf{v}_i}{m_e m_i c}$$

$$\cong -\frac{e}{m_e c}\mathbf{J} + \frac{Ze^2}{m_e m_i c}(n_i m_i \mathbf{v}_i + n_e m_e \mathbf{v}_e) = -\frac{e}{m_e c}\mathbf{J} + \frac{Ze^2}{m_e m_i c}\,\rho\mathbf{u} \tag{8.18}$$

$$\frac{Ze}{m_i}\,\mathbf{R}_i - \frac{e}{m_e}\,\mathbf{R}_e = \left(\frac{Ze}{m_i}+\frac{e}{m_e}\right)\mathbf{R}_i \cong \frac{e}{m_e}\,\mathbf{R}_i \tag{8.19}$$

$$\frac{P_e}{P} = \frac{n_e k_B T_e}{n_e k_B T_e + n_i k_B T_i} = \frac{Z n_i T_e}{Z n_i T_e + n_i T_i} = \left(1+\frac{T_i}{ZT_e}\right)^{-1} \tag{8.20}$$

where $\mathbf{R}_i$ in equation (8.16) is the change in the ion momentum due to collisions with electrons. Therefore, one can expand $\mathbf{R}_i$ as a Taylor series in the relative velocity between the ions and the electrons. Keeping only the first term in the Taylor expansion, one gets

$$\mathbf{R}_i = C_1(\mathbf{v}_i - \mathbf{v}_e). \tag{8.21}$$

Using charge neutrality and the definition of the electric current, equations (8.10) and (8.15), into equation (8.21) gives

$$\mathbf{R}_i = C_2\mathbf{J}. \tag{8.22}$$

Since the value of C_2 does not depend on the general structure of equation (8.16), one can consider this equation for the following special case: steady state, no pressure (or temperature) gradients and without magnetic field. Substituting (8.22) into (8.16) for this special case, one obtains

$$\frac{Ze\rho}{m_i}\,\mathbf{E} + C_2\mathbf{J} = 0. \tag{8.23}$$

Using now the simple Ohm's law for this case (see section 2.3), where σ_E is the electrical conductivity coefficient,

$$\mathbf{J} = \sigma_E\mathbf{E} \tag{8.24}$$

one gets the value of C_2, implying

$$\mathbf{R}_\mathrm{i} = C_2\mathbf{J} = -\frac{Ze\rho}{m_\mathrm{i}\sigma_\mathrm{E}}\,\mathbf{J}. \tag{8.25}$$

Substituting (8.25) into (8.16), we get the **generalized Ohm's law**:

$$\left(\frac{m_\mathrm{e}m_\mathrm{i}}{Ze^2\rho}\right)\frac{\partial\mathbf{J}}{\partial t} = \left(\frac{m_\mathrm{i}}{Ze\rho}\right)\nabla\left[\left(1+\frac{T_\mathrm{i}}{ZT_\mathrm{e}}\right)^{-1}P\right] + \mathbf{E} + \left(\frac{1}{c}\right)\mathbf{u}\times\mathbf{B} - \left(\frac{m_\mathrm{i}}{Zec\rho}\right)\mathbf{J}\times\mathbf{B} - \left(\frac{1}{\sigma_\mathrm{E}}\right)\mathbf{J}. \tag{8.26}$$

The magneto-hydrodynamic equations are (8.12), (8.13), (8.14) and (8.26), together with the following Maxwell equations:

$$\nabla\times\mathbf{E} = -\left(\frac{1}{c}\right)\frac{\partial\mathbf{B}}{\partial t}, \qquad \nabla\times\mathbf{B} = \left(\frac{4\pi}{c}\right)\mathbf{J} + \left(\frac{1}{c}\right)\frac{\partial\mathbf{E}}{\partial t}. \tag{8.27}$$

One therefore has 14 equations with 14 unknowns: ρ, ρ_E, $\mathbf{u}$, $\mathbf{J}$, $\mathbf{E}$ and $\mathbf{B}$. This is correct only if the temperatures T_e and T_i are known, otherwise the (electron and ion) energy conservation equations are also necessary. Moreover, knowledge of the equations of state, $P_\mathrm{e} = P_\mathrm{e}(\rho, T_\mathrm{e})$ and $P_\mathrm{i} = P_\mathrm{i}(\rho, T_\mathrm{i})$, is necessary. For not very dense plasmas ($\rho \ll \rho_\mathrm{solid}$), the ideal gas equations of state are suitable (such as those we have used in equation (8.20)).

In this chapter we are interested in calculating the steady-state magnetic field. Therefore, the generalized Ohm's law given in equation (8.26) is assumed, together with the assumption $\partial\mathbf{J}/\partial t = 0$, yielding an electric field

$$\mathbf{E} = \left(\frac{1}{\sigma_\mathrm{E}}\right)\mathbf{J} - \left(\frac{m_\mathrm{i}}{Ze\rho}\right)\nabla\left[\left(1+\frac{T_\mathrm{i}}{ZT_\mathrm{e}}\right)^{-1}P\right] - \left(\frac{1}{c}\right)\mathbf{u}\times\mathbf{B} + \left(\frac{m_\mathrm{i}}{Zec\rho}\right)\mathbf{J}\times\mathbf{B}. \tag{8.28}$$

From this equation we see that the electric field in the plasma has four contributions:

1. The $\mathbf{J}\times\mathbf{B}$ term, which is the Hall effect.
2. $\mathbf{u}\times\mathbf{B}$ is the convective (plasma flow) term.
3. ∇P is the pressure gradient contribution.
4. The $\mathbf{J}/\sigma_\mathrm{E}$ term is the (standard Ohm's law) voltage drop on plasma-active resistance.

Using for the electrical conductivity the value obtained in section 2.3 (Drude model),

$$\sigma_\mathrm{E} = \frac{e^2 n_\mathrm{e}}{m_\mathrm{e}\nu_\mathrm{ei}} \tag{8.29}$$

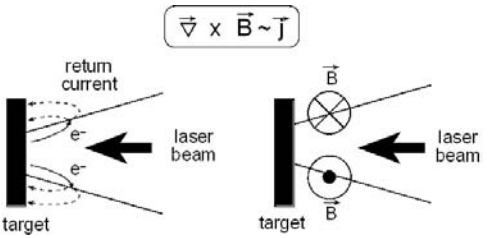

Figure 8.2. A toroidal magnetic field created by a return current.

and substituting (8.28) into the first equation of (8.27), one gets for $T_i \ll T_e$

$$\frac{\partial \mathbf{B}}{\partial t} = -\frac{m_e c \nu_{ei}}{e^2} \nabla \times \left(\frac{\mathbf{J}}{n_e} \right) + \frac{c k_B}{e n_e} \nabla T_e \times \nabla n_e + \nabla \times (\mathbf{u} \times \mathbf{B}) - \frac{1}{e} \nabla \times \left(\frac{\mathbf{J} \times \mathbf{B}}{n_e} \right). \tag{8.30}$$

The first term in (8.30) may contribute a toroidal magnetic field, as described in figure 8.2. The second term is the one given in the previous section and described schematically in figure 8.1.

The current **J** is substituted into (8.30) from the second equation of (8.27), and using the first equation of (8.27) one obtains a complex equation for the magnetic field generated in laser–plasma interaction. We consider now some special cases.

Case 1

It is assumed that the second and third terms of equation (8.30) are dominant. Looking for a d.c. solution ($\partial B/\partial t = 0$), one gets from equation (8.30):

$$\frac{c}{e n_e} \nabla P_e + \mathbf{u} \times \mathbf{B} = 0. \tag{8.31}$$

Taking $\nabla \approx 1/L$ and $u \approx c_s$, where L is the scale length of the electron pressure gradient and c_s is the speed of sound, and using the ideal gas equation of state for the electron pressure (equation (8.4)), one gets from equation (8.31):

$$B \approx \left(\frac{c}{c_s} \right) \frac{(k_B T_e / e)}{L} \approx \frac{(m_i c^2 k_B T_e)^{1/2}}{eL} \approx \left(\frac{m_i}{m_p} \right)^{1/2} \left(\frac{T_e}{\text{keV}} \right)^{1/2} \left(\frac{30\,\mu\text{m}}{L} \right) \quad [\text{MGauss}] \tag{8.32}$$

where m_i and m_p are the ion and the proton masses respectively. For an electron temperature of 1 keV and a pressure scale length of 30 μm one gets a d.c. magnetic field of 1 MG.

Case 2

It is now assumed that the first and third terms of equation (8.30) are dominant.

Moreover, a constant electrical conductivity is taken so that equation (8.30) can be rewritten as (after using equation (8.29))

$$\frac{\partial \mathbf{B}}{\partial t} = -\frac{c}{\sigma_{\mathrm{E}}} \nabla \times \mathbf{J} + \nabla \times (\mathbf{u} \times \mathbf{B}). \tag{8.33}$$

Substituting into this equation the second equation of (8.27) with $\partial E/\partial t = 0$, one obtains the equation for the magnetic field:

$$\frac{\partial \mathbf{B}}{\partial t} = -\frac{c^2}{4\pi\sigma_{\mathrm{E}}} \nabla \times (\nabla \times \mathbf{B}) + \nabla \times (u \times \mathbf{B}). \tag{8.34}$$

Using the identity

$$\nabla \times (\nabla \times \mathbf{B}) = -\nabla^2 \mathbf{B} + \nabla(\nabla \cdot \mathbf{B}) = -\nabla^2 \mathbf{B} \tag{8.35}$$

(where the Maxwell equation $\nabla \cdot \mathbf{B} = 0$ is used), one gets from equation (8.34):

$$\frac{\partial \mathbf{B}}{\partial t} = \left(\frac{c^2}{4\pi\sigma_{\mathrm{E}}}\right) \nabla^2 \mathbf{B} + \nabla \times (\mathbf{u} \times \mathbf{B}). \tag{8.36}$$

8.2.2 The magnetic Reynolds number

The first term on the right-hand side of (8.36) describes the diffusion of the magnetic field, while the second term is the convection of the plasma fluid moving with a velocity **u** (relative to a fixed observer, the laboratory frame of reference). The ratio between the convective and the diffusion terms defines the magnetic Reynolds number R_{m}:

$$R_{\mathrm{m}} = \left[\frac{uB/L}{(c^2 B)/(4\pi\sigma_{\mathrm{E}} L^2)}\right] = \left(\frac{4\pi}{c^2}\right) \sigma_{\mathrm{E}} L u \tag{8.37}$$

where L is the macroscopic scale length and u is the characteristic flow velocity. Note that R_{m} is dimensionless (in the Gaussian units used here the electrical conductivity coefficient σ_{E} has dimensions of s^{-1}). $c^2/(4\pi\sigma_{\mathrm{E}})$ is equivalent to the kinematic viscosity in defining the Reynolds number for a fluid flow (= inertial force/viscous force).

8.2.3 Magnetic Reynolds numbers $R_{\mathrm{m}} \ll 1$

For $R_{\mathrm{m}} \ll 1$ the convective term is negligible and equation (8.36) describes the diffusion of the magnetic field

$$\frac{\partial B}{\partial t} = \eta \nabla^2 B, \qquad \eta \equiv \frac{c^2}{4\pi\sigma_{\mathrm{E}}}. \tag{8.38}$$

This equation is similar to the heat diffusion equation

$$\frac{\partial T}{\partial t} = \kappa \nabla^2 T \tag{8.39}$$

where T is the temperature and κ is the coefficient of heat conduction. Similarly, in a viscous fluid flow the vorticity Ω satisfies a similar equation:

$$\frac{\partial \Omega}{\partial t} = \nu \nabla^2 \Omega, \qquad \Omega \equiv \nabla \times \mathbf{u} \tag{8.40}$$

where ν is the kinematic viscosity. Note that η, κ and ν have the dimension of cm^2/s in c.g.s. and m^2/s in m.k.s.

We now analyse equation (8.38). Assuming at $t = 0$ (initial condition) a magnetic field $B_{\mathrm{i}}(r, 0)$ in Cartesian coordinates ($i = x, y, z$), then at $t > 0$ the magnetic field is given by

$$B_i(\mathbf{r}, t) = \int \mathrm{d}^3 r' G(\mathbf{r} - \mathbf{r}', t) B_i(\mathbf{r}', 0) \tag{8.41}$$

where $G(\mathbf{r} - \mathbf{r}', t)$ is Green's function:

$$G(\mathbf{r} - \mathbf{r}', t) = \frac{1}{(4\pi\eta t)^{3/2}} \exp\left[-\frac{(\mathbf{r} - \mathbf{r}')^2}{4\eta t} \right]. \tag{8.42}$$

This solution shows that the magnetic field at an initial position $\mathbf{r}'$ diffuses in time with a Gaussian profile which has the width $(4\eta t)^{1/2}$, i.e. the width increases with the square root of time. An estimate of the magnetic field diffusion time is derived by taking $\nabla^2 \approx 1/L^2$ in equation (8.38), yielding

$$\frac{\partial \mathbf{B}}{\partial t} \approx \pm \frac{\eta}{L^2} B. \tag{8.43}$$

The solution of this equation is

$$B = B_0 \exp\left(\pm \frac{t}{\tau_{\mathrm{m}}} \right), \qquad \tau_{\mathrm{m}} = \frac{L^2}{\eta} = \frac{4\pi\sigma_{\mathrm{E}} L^2}{c^2} = \frac{R_{\mathrm{m}} L}{u}. \tag{8.44}$$

The + or − sign refer to 'gain' or 'loss' (with time) of the magnetic field.

For example, in a typical laser-produced plasma where diffusion is dominant, one has $L \approx 100\,\mu\mathrm{m}$ and $u \approx 10^6$ cm/s, implying a magnetic Reynolds number $R_{\mathrm{m}} \approx 0.1$ and a diffusion relaxation time $\tau_{\mathrm{m}} \approx 1$ ns.

8.2.4 Magnetic Reynolds numbers $R_{\mathrm{m}} \gg 1$

For $R_{\mathrm{m}} \gg 1$ the diffusion term is negligible and equation (8.36) describes the convection of the magnetic field:

$$\frac{\partial \mathbf{B}}{\partial t} = \nabla \times (\mathbf{u} \times \mathbf{B}). \tag{8.45}$$

In this case it is important to notice that if initially there is a magnetic field in the x–y plane, $\mathbf{B} = (B_x, B_y, B_z = 0)$, then equation (8.45) implies that for $t > 0$ a magnetic field perpendicular to the x–y plane is induced. For example,

$$\begin{aligned} t = 0: &\qquad \mathbf{B} = (B_x, B_y, 0), \qquad \mathbf{u} = (0, 0, u) \\ t > 0: &\qquad \frac{\partial B_z}{\partial t} = \frac{\partial (u B_y)}{\partial x} \;\Rightarrow\; B_z(t > 0) \approx \frac{tu}{L} B_y(t = 0). \end{aligned} \tag{8.46}$$

Assuming that in laser–plasma interactions ripples are created of the order of $L = 10\,\mu\text{m}$ and the plasma flow towards the laser is $u = 10^6\,\text{cm/s}$, then at a time $t \approx \tau_\text{L}$, where $\tau_\text{L} \approx 1\,\text{ns}$ is the laser pulse duration, one gets from (8.46)

$$B_z(t \approx \tau_\text{L}) \approx B_y(t = 0). \tag{8.47}$$

This phenomenon, where a magnetic field in the x–y plane develops into a magnetic field in the z direction, is called the **dynamo effect**. Therefore, we have seen that for a large magnetic Reynolds number the toroidal magnetic field may develop into a large axial magnetic field. However, for this phenomenon to happen fluctuations of small-scale L are necessary. Thus, this effect is a random process.

In the next section we shall see how an axial magnetic field (by definition, in the direction of the laser irradiation, or normal to the plane target) can be created in a controllable way for any magnetic Reynolds numbers.

8.3 Faraday and Inverse Faraday Effects

8.3.1 The Faraday effect

Michael Faraday discovered in 1845 that when plane-polarized light passed through lead glass in the direction of a magnetic field, the plane of polarization was rotated. The linear polarized electric field rotates when propagating along the magnetic field in a dielectric or a plasma medium. A linear polarized wave can be resolved into the sum of left- and right-circularly polarized waves, and the rotation arises due to the difference in the index of refraction between the two waves. The angle of rotation is proportional to the magnitude of the magnetic field.

We now calculate the angle of rotation for a linearly polarized light propagating in plasma or a dielectric media. Since there is an analogy between a dielectric medium and plasma, the Faraday effect is developed simultaneously for both media. The m.k.s. (SI) units are used in this section.

The equations of motion for the electrons in the presence of the laser electric field $\mathbf{E}_\mathrm{L}$ and the d.c. magnetic field $\mathbf{B}$ are (the $\mathbf{B}_\mathrm{L} \times \mathbf{v}$ force, where $\mathbf{B}_\mathrm{L}$ is the magnetic field of the laser that is negligible and therefore neglected)

$$\begin{aligned} \textbf{dielectric}: \quad & m_\mathrm{e}\frac{\mathrm{d}^2\mathbf{r}}{\mathrm{d}t^2} + m_\mathrm{e}\omega_0^2\mathbf{r} = -e\left(\mathbf{E}_\mathrm{L} + \frac{\mathrm{d}\mathbf{r}}{\mathrm{d}t}\times\mathbf{B}\right) \\ \textbf{plasma}: \quad & m_\mathrm{e}\frac{\mathrm{d}^2\mathbf{r}}{\mathrm{d}t^2} = -e\left(\mathbf{E}_\mathrm{L} + \frac{\mathrm{d}\mathbf{r}}{\mathrm{d}t}\times\mathbf{B}\right). \end{aligned} \tag{8.48}$$

$m_\mathrm{e}\omega_0^2\mathbf{r}$ is the restoring force of the center of charge of the electrons (q_e) of one atom in the dielectric medium. The dipole moment $\mathbf{p}$ of a single atom in the presence of a d.c. electric field $\mathbf{E}$ can be approximated by $\mathbf{p} = q_\mathrm{e} \simeq q_\mathrm{e}^2\mathbf{E}/(m_\mathrm{e}\omega_0^2)$. The laser electric field is in the x–y plane and propagates in the z direction, parallel to the d.c. magnetic field. Therefore, the electron motion is in the x–y plane and the following notation can be used in Cartesian coordinates:

$$\begin{aligned} \mathbf{B} &= (0,0,B), \qquad \mathbf{E} = (E_x, E_y, 0), \qquad \mathbf{r} = (x,y,0) \\ E_\pm &= E_x \pm \mathrm{i}E_y = E_0\exp[\mathrm{i}(k_\pm z - \omega t)] \\ E_x &= \frac{E_0}{2}\{\exp[\mathrm{i}(k_+ z - \omega t)] + \exp[\mathrm{i}(k_- z - \omega t)]\} \\ E_y &= -\mathrm{i}\frac{E_0}{2}\{\exp[\mathrm{i}(k_+ z - \omega t)] - \exp[\mathrm{i}(k_- z - \omega t)]\} \\ r_\pm &= x \pm \mathrm{i}y = r_0\exp[\mathrm{i}(k_\pm z - \omega t)] \end{aligned} \tag{8.49}$$

where r_0 and E_0 are real and $E_\pm$ describe circularly-polarized monochromatic lasers. One defines E_+ as right-handed circular polarization (RHCP) and E_- as left-handed circular polarization (LHCP). Using the notation of equations (8.49), one can write the solution of equations (8.48) in the following form:

$$\begin{aligned} \textbf{dielectric}: \quad & r_\pm = \frac{-(e/m_\mathrm{e})E_\pm}{\omega_0^2 \mp (eB/m_\mathrm{e})\omega - \omega^2} \\ \textbf{plasma}: \quad & r_\pm = \frac{-(e/m_\mathrm{e})E_\pm}{\mp\omega_\mathrm{c}\omega - \omega^2} \end{aligned} \tag{8.50}$$

where the electron cyclotron frequency is defined by

$$\omega_\mathrm{c} = \frac{eB}{m_\mathrm{e}}. \tag{8.51}$$

Using Maxwell equations, one obtains the following wave equations for the two appropriate media (see Appendix A):

$$\begin{aligned}
&\textbf{dielectric:} \quad \nabla^2\mathbf{E} - \frac{1}{c^2}\frac{\partial^2\mathbf{E}}{\partial t^2} - \mu_0\frac{\partial^2\mathbf{P}}{\partial t^2} = 0, \qquad \mathbf{P} = -en_e\mathbf{r} \\
&\textbf{plasma:} \quad \nabla^2\mathbf{E} - \frac{1}{c^2}\frac{\partial^2\mathbf{E}}{\partial t^2} - \mu_0\frac{\partial\mathbf{J}}{\partial t} = 0, \qquad \mathbf{J} = -en_e\frac{\mathrm{d}\mathbf{r}}{\mathrm{d}t}
\end{aligned} \tag{8.52}$$

where μ_0 is the magnetic permeability in vacuum, $\mathbf{P}$ is the polarization of the dielectric medium and $\mathbf{J}$ is the electric current in the plasma. Using equations (8.49) and (8.50) in (8.52), the following dispersion relations are derived:

$$\begin{aligned}
&\textbf{dielectric:} \quad k_\pm^2 = \frac{\omega^2}{c^2}\left[1 - \frac{\omega_{pe}^2}{\omega^2 \mp (eB/m_e)\omega - \omega_0^2}\right], \qquad \omega_{pe}^2 = \frac{e^2 n_e}{\varepsilon_0 m_e} \\
&\textbf{plasma:} \quad k_\pm^2 = \frac{\omega^2}{c^2}\left[1 - \frac{\omega_{pe}^2}{\omega^2 \mp \omega_c\omega}\right], \qquad \frac{1}{\varepsilon_0} = \mu_0 c^2
\end{aligned} \tag{8.53}$$

where ω_{pe} is the electron plasma frequency in the dielectric or the plasma medium.

The appropriate indices of refraction for the RHCP and LHCP are

$$n_\pm = \frac{ck_\pm}{\omega}. \tag{8.54}$$

At $z = 0$ one has a linearly polarized laser, given by

$$E_x(z=0) = E_0\cos\omega t = \frac{E_0}{2}[\exp(\mathrm{i}\omega t) + \exp(-\mathrm{i}\omega t)], \qquad E_y(z=0) = 0. \tag{8.55}$$

In order to obtain the values of $E_\pm$ at $z = l$ we define

$$\varphi(z) = \tfrac{1}{2}[z(k_+ + k_-)] - \omega t, \qquad \theta(z) = \tfrac{1}{2}[z(k_+ - k_-)]. \tag{8.56}$$

Using the identity

$$k_\pm = \tfrac{1}{2}(k_+ + k_-) \pm \tfrac{1}{2}(k_+ - k_-) \tag{8.57}$$

together with equations (8.49) and (8.56), one obtains the electric field (at $z = l$), after propagating along the d.c. magnetic field a distance l:

$$\begin{aligned}
E_\pm(z=l) &= E_0\exp[\mathrm{i}\varphi(l)]\exp[\pm\mathrm{i}\theta(l)] \\
E_x &= E_0\exp[\mathrm{i}\varphi(l)]\cos\theta(l) \\
E_y &= E_0\exp[\mathrm{i}\varphi(l)]\sin\theta(l).
\end{aligned} \tag{8.58}$$

From these equations one can see that φ is a phase of the amplitude and θ is the angle of rotation. At $z = 0$ the angle θ is zero (i.e. by definition of the linearly polarized light $E_y = 0$). From the definition of θ in (8.56) one gets at $z = l$:

$$\theta(l) = \frac{l}{2}(k_+ - k_-). \tag{8.59}$$

The values of $k_\pm$ are obtained from the dispersion relation (8.53). For constant electron density n_e and magnetic field B, and neglecting B^2 terms (i.e. $\omega_c/\omega \ll 1$), one gets

dielectric: $\theta = VlH, \qquad H = B/\mu_0$

$$V = \left(\frac{\mu_0 e}{2nm_e c}\right)\frac{\omega^2\omega_{pe}^2}{(\omega^2-\omega_0^2)^2}, \qquad n = \tfrac{1}{2}(n_+ + n_-) \tag{8.60}$$

plasma: $\theta = l\left(\frac{eB}{m_e c}\right)\left(\frac{\omega_{pe}^2}{\omega^2}\right) \approx 3.4\left(\frac{B}{\text{Tesla}}\right)\left(\frac{l}{100\,\mu\text{m}}\right)\left(\frac{\omega_{pe}^2}{\omega^2}\right)$ degrees.

For the dielectric medium case the coefficient V is called the Verdet constant.

For the plasma medium, one can see that close to the critical density ($\omega_{pe} \approx \omega$) the angle of rotation is 3.4° per Tesla for a laser propagating along $l = 100\,\mu$m. Equation (8.60) is valid if n_e = constant and B is small (we neglected B^2) on the scale defined by

$$\omega_c \ll \omega \;\Rightarrow\; \frac{B}{B_c} \ll 1, \qquad B_c \equiv \frac{m_e\omega}{e} \approx \frac{1.07\times 10^8}{\lambda_L\,(\mu\text{m})}\ \text{Gauss}. \tag{8.61}$$

For most experiments in laser–plasma interactions the constraint (8.61) is satisfied. However, the electron density is not constant in these experiments. For a non-constant electron density the angle θ in equation (8.59) is modified to

$$\theta = \frac{1}{2}\int_0^l \mathrm{d}z(k_+ - k_-). \tag{8.62}$$

Using the dispersion relation (8.53) in the plasma medium for $\omega_c \ll \omega$, one can use the approximations

$$\begin{aligned} k_+ - k_- = \frac{k_+^2 - k_-^2}{k_+ + k_-} &\approx \frac{(\omega_{pe}/\omega)^2(1+\omega_c/\omega) - (\omega_{pe}/\omega)^2(1-\omega_c/\omega)}{2(\omega/c)\sqrt{1-(\omega_{pe}/\omega)^2}} \\ &= \left(\frac{eBc}{m_e\omega^2}\right)\left(\frac{n_e}{n_{ec}}\right)\left[1-\left(\frac{n_e}{n_{ec}}\right)\right]^{-1/2} \end{aligned} \tag{8.63}$$

where n_{ec} is the electron critical density and ω is the angular frequency of the laser ('probe') beam:

$$\omega = \frac{2\pi c}{\lambda_p}. \tag{8.64}$$

Substituting (8.63) into (8.62), one obtains the angle of rotation (in practical units) for a plasma medium:

$$\theta(\text{deg}) = 3.02\left(\frac{\lambda_p}{\mu\text{m}}\right)^2\int_0^l\left(\frac{\mathrm{d}z}{\mu\text{m}}\right)\left(\frac{n_e}{10^{21}\,\text{cm}^{-3}}\right)\left(\frac{B}{\text{MGauss}}\right)\left(1-\frac{n_e}{n_{ec}}\right)^{-1/2}. \tag{8.65}$$

The Faraday effect is used in laser–plasma interactions to measure the magnetic field (Raven *et al.* 1978, Horovitz *et al.* 1997). For this purpose it is also necessary to know the electron density. At the critical density there is a singularity in equation (8.65), but this is not a problem since the laser cannot propagate along a critical density. Using this equation, megagauss (d.c.) magnetic fields were measured in laser–plasma interactions.

8.3.2 The inverse Faraday effect

The inverse Faraday effect is the phenomenon where a magnetic field is created in a medium due to the rotation of the electromagnetic field. In particular, a circularly-polarized laser can induce a magnetic field in the plasma. The magnetic field arises because the electrons quiver with the oscillating electric field of the incoming laser light, and if the laser is circularly polarized then the electrons describe a circular motion. The net effect of this is a circular current on the edge of the plasma, which generates the magnetic field (see figure 8.3).

A simple (order of magnitude) calculation for the magnetic field created by the inverse Faraday effect in cold plasma is now developed. The motion of the electrons in an applied electric field is, according to linearized law,

$$\frac{\partial \mathbf{v}}{\partial t} = -\frac{e}{m_e}\mathbf{E} \tag{8.66}$$

where $\mathbf{v}$ is the electron velocity and $\mathbf{E}$ is the applied electric field in the plasma, as a result of the absorbed laser energy. The ions are considered immobile. The electric field is incident in the z direction and is circularly polarized in the x–y plane:

$$\mathbf{E} = E_0\left(\frac{\hat{\mathbf{x}} + \mathrm{i}\hat{\mathbf{y}}}{\sqrt{2}}\right)\exp[-\mathrm{i}(\omega t - kz)] \tag{8.67}$$

where $\hat{\mathbf{x}}$ and $\hat{\mathbf{y}}$ are unit vectors in the x and y directions respectively.

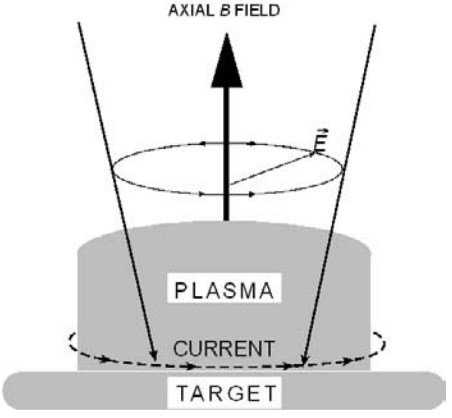

Figure 8.3. A schematic presentation of the inverse Faraday effect.

Substituting (8.67) into (8.66), one gets the solution for the electron (fluid) velocity:

$$\mathbf{v} = v_0 \left(\frac{-\mathrm{i}\hat{\mathbf{x}} + \hat{\mathbf{y}}}{\sqrt{2}} \right) \exp[-\mathrm{i}(\omega t - kz)], \qquad v_0 = \frac{eE_0}{m_\mathrm{e}\omega}. \tag{8.68}$$

The electrons also satisfy the continuity equation

$$\frac{\partial n_\mathrm{e}}{\partial t} = -\nabla \cdot (n_\mathrm{e}\mathbf{v}). \tag{8.69}$$

The density is assumed to consist of a background (n_0) and perturbed (n_1) components

$$n_\mathrm{e} = n_0 + n_1, \qquad n_0 \gg n_1 \tag{8.70}$$

where n_0 does not depend on time and $n_1 \approx \exp(-\mathrm{i}\omega t)$. Since $\nabla \cdot \mathbf{v} = 0$, the continuity equation (8.69) yields

$$\mathrm{i}\omega n_1 = \mathbf{v} \cdot (\nabla n_0). \tag{8.71}$$

The electric current, which in this approximation is a second-order perturbed value, is obtained by using (8.68) and (8.71):

$$\mathbf{J} = -e\langle n_1 \mathbf{v} \rangle = \left\langle \frac{\mathrm{i}e}{\omega} (\mathbf{v} \cdot \nabla n_0)\mathbf{v} \right\rangle = \frac{e^3 E_0^2}{2m_\mathrm{e}\omega^3} \nabla n_0 \times \hat{\mathbf{z}} \tag{8.72}$$

where $\langle\ \rangle$ is a time average over the fast oscillations and $\hat{\mathbf{z}}$ is the unit vector in the z direction. Note that the wave number vector $\mathbf{k}$ of the electromagnetic field is parallel to $\hat{\mathbf{z}}$. From equation (8.72) one can see that the electric current $\mathbf{J}$ has a contribution from the density gradient in the x–y plane (mainly from the edge of the plasma) and it points in the toroidal direction. This current produces an axial magnetic field (i.e. in the z direction) according to Maxwell's equation (we are using again Gaussian units):

$$\nabla \times \mathbf{B} = \frac{4\pi}{c} \mathbf{J}. \tag{8.73}$$

Substituting (8.72) into (8.73) yields the following order of magnitude estimate:

$$\mathbf{B} = B\hat{\mathbf{z}}, \qquad \frac{B}{B_\mathrm{c}} = \left(\frac{\omega_\mathrm{pe}^2}{2\omega^2} \right) \left(\frac{eE_0}{m_\mathrm{e}\omega c} \right)^2, \qquad B_\mathrm{c} \equiv \frac{m_\mathrm{e}\omega c}{e} = \frac{1.07 \times 10^8}{\lambda(\mu\mathrm{m})} \text{ Gauss}. \tag{8.74}$$

Assuming that all of the laser energy is absorbed,

$$I_\mathrm{L} = c\,\frac{E_0^2}{8\pi} \tag{8.75}$$

where I_L is the laser peak intensity (power/area). In this case the axial magnetic field given in (8.74) can be written, in practical units, as

$$B_z\,(\text{Gauss}) = 6.0 \times 10^4 \left(\frac{n_e}{n_{ec}}\right)\left(\frac{\lambda_L}{\mu m}\right)\left(\frac{I_L}{10^{14}\,\text{W/cm}^2}\right) \tag{8.76}$$

where λ_L is the laser wavelength and n_{ec} is the critical density.

Using ponderomotive forces (Lehner 1994), it was suggested that the induced magnetic field is not linear with I_L, as given by the classical inverse Faraday effect (equations (8.74) or (8.76)), but B is proportional to the square root of I_L. Moreover, the constant of proportionality is significantly larger than in the classical approach. In this formalism the electric current is a first-order effect rather than a second-order perturbation value. In the non-relativistic domain the axial magnetic field, as developed by Lehner, can be written as

$$B = B_c\left(\frac{\omega_{pe}}{\omega}\right)\left(\frac{eE_0}{m_e\omega c}\right) \approx 6.5 \times 10^5 \left(\frac{n_e}{n_{ec}}\right)^{1/2}\left(\frac{I_L}{10^{14}\,\text{W/cm}^2}\right)^{1/2}. \tag{8.77}$$

This formula fits some experiments (Horovitz *et al.* 1998) in the domain of $I_L \approx 10^{10}$ W/cm^2 to 10^{13} W/cm^2. However, for $\sim 10^{14}$ W/cm^2 the experimental values are larger than those estimated by equation (8.77).

8.3.3 Angular momentum considerations

In a circularly-polarized laser beam the spins of the photons are aligned (each photon has a spin $\hbar = h/(2\pi)$, where h is the Planck constant), so that the laser beam has an angular momentum. Denoting the number density of the photons by n_γ, and the angular momentum density parallel to the z axis for a laser beam moving in the z direction by L_z (Eliezer *et al.* 1992, Haines 2001), one has

$$L_z = n_\gamma \hbar. \tag{8.78}$$

Every photon has an energy $h\nu$ ($\omega = 2\pi\nu$); therefore, the laser pulse energy density W in the plasma medium is

$$W = n_\gamma \hbar\omega = \frac{|E|^2}{8\pi} = \frac{I}{c} \tag{8.79}$$

where I is the intensity of the electromagnetic field in the plasma. From (8.78) and (8.79) one can write for photons moving in the z direction:

$$I = n_\gamma \hbar\omega c = L_z \omega c. \tag{8.80}$$

This relation is globally correct for a uniform distribution of photons, or equivalently it is locally correct at any domain in space. For an axisymmetric

beam of a circularly polarized laser defined by

$$I = \begin{cases} I(r), & r < r_0 \\ 0, & r \geq 0 \end{cases} \tag{8.81}$$

one can write (Haines 2001)

$$L_z = -\frac{r}{2\omega c}\left(\frac{\partial I}{\partial z}\right). \tag{8.82}$$

One can easily check the validity of this equation by integrating it from $r = 0$ to $r = r_0$, where r_0 is the edge of the laser beam:

$$\int_0^{r_0} \mathrm{d}r\, 2\pi r L_z = -\frac{2\pi}{\omega c}\left\{\left[\frac{r^2 I(r)}{2}\right]_{r=0}^{r=r_0} - \int_0^{r_0} I(r) r\, \mathrm{d}r\right\} = \frac{2\pi}{\omega c}\int_0^{r_0} I(r) r\, \mathrm{d}r. \tag{8.83}$$

This is derived by using the laser beam profile defined by (8.81) and integrating by parts. Equation (8.83) shows that equation (8.80) is locally correct, thus justifying the classical equation (8.82).

Using cylindrical coordinates (r, θ, z), the angular momentum conservation equation for the electrons can be written by

$$\frac{\mathrm{d}L_z\,(\text{electrons})}{\mathrm{d}t} + \frac{\mathrm{d}L_z\,(\text{photons})}{\mathrm{d}t} = \left(\mathbf{r} \times \sum \mathbf{F}\right)_z. \tag{8.84}$$

The angular momentum of the absorbed photons is transferred to the electrons. The rate of change of the electron angular momentum is

$$\frac{\mathrm{d}L_z\,(\text{electrons})}{\mathrm{d}t} = n_\mathrm{e} m_\mathrm{e} r \frac{\mathrm{d}v_\theta}{\mathrm{d}t} + \nu_\mathrm{ei} n_\mathrm{e} m_\mathrm{e} r v_\theta \tag{8.85}$$

where v_θ is the toroidal electron velocity, $m_\mathrm{e} v_\theta$ is the linear momentum of one electron in the θ direction and $r m_\mathrm{e} v_\theta$ is the angular momentum of one electron in the z direction. The second term in the right-hand side of the last equation is due to electron–ion collisions, where ν_ei is the collision frequency.

The rate of change in the photon angular momentum is obtained using equation (8.82). The electromagnetic intensity I is equal to the laser absorption coefficient f_a times the laser intensity I_L. One can also write

$$\frac{\mathrm{d}I}{\mathrm{d}t} \approx \frac{cI}{l} \tag{8.86}$$

where l is the axial distance that the laser is absorbed by the fraction f_a. Therefore, one can approximate the second term of the left-hand side of equation (8.84) by

$$\frac{\mathrm{d}L_z\,(\text{photons})}{\mathrm{d}t} = \frac{f_\mathrm{a} r}{2l\omega}\left(\frac{\partial I_\mathrm{L}}{\partial r}\right). \tag{8.87}$$

The torque $(\mathbf{r} \times \sum \mathbf{F})_z$ applied on the electrons is

$$\left(\mathbf{r} \times \sum \mathbf{F}\right)_z = -en_e r\left[E_\theta + \frac{1}{c}(v_z B_r - v_r B_z)\right] \tag{8.88}$$

where E_θ is the toroidal electric field induced by the toroidal electron motion in such a way as to oppose the generation of the axial magnetic field. The electron velocity, electric field and magnetic field components are accordingly: $\mathbf{v} = (v_r, v_\theta, v_z)$, $\mathbf{E} = (E_r, E_\theta, E_z)$, $\mathbf{B} = (B_r, B_\theta, B_z)$. Substituting equations (8.85), (8.87) and (8.88) into (8.84), one gets the angular momentum conservation in the z direction (Haines 2001):

$$n_e m_e r\left(\frac{\mathrm{d}v_\theta}{\mathrm{d}t}\right) = -en_e r E_\theta - \frac{f_a r}{2l\omega}\left(\frac{\partial I_L}{\partial r}\right) - \frac{en_e r}{c}(v_z B_r - v_r B_z) - n_e m_e r \nu_{ei} v_\theta. \tag{8.89}$$

Assuming a steady state, $\mathrm{d}v_\theta/\mathrm{d}t = 0$ and, neglecting the last two terms on the right-hand side of equation (8.89), the following simplified equation is obtained:

$$E_\theta \approx -\frac{f_a}{en_e \omega l}\left(\frac{\partial I_L}{\partial r}\right). \tag{8.90}$$

Using now the Faraday–Maxwell equation (in cylindrical coordinates),

$$\frac{\partial B_z}{\partial t} = -\frac{c}{r}\frac{\partial}{\partial r}(rE_\theta) \tag{8.91}$$

and assuming a parabolic laser profile beam,

$$I_L = I_0\left(1 - \frac{r^2}{r_0^2}\right) \quad \text{for } r \le r_0 \text{ and zero otherwise} \tag{8.92}$$

one gets from (8.90), (8.91) and (8.92) the following solution for the axial magnetic field:

$$B_z = \frac{4c}{\omega l e r_0^2}\int \frac{f_a I_0}{n_e}\,\mathrm{d}t. \tag{8.93}$$

It is worth noting that this equation does not have a singularity at $n_e = 0$ since $f_a = 0$ in this case.

As one can see from this calculation of the inverse Faraday effect, the axial magnetic field apparently looks in complete disagreement with the previously derived equation (8.76). In particular, in (8.76) the magnetic field is proportional to the electron density, while in (8.93) B is inversely proportional to n_e. However, one has to be careful because the absorption coefficient f_a may be proportional to n_e^2. In section 5.1 we derived the inverse

bremsstrahlung absorption coefficient:

$$\frac{f_a}{l} \approx \kappa_{ib} = \frac{\nu_{ei}(n_{ec})}{c}\left(\frac{n_e}{n_{ec}}\right)^2\left(1-\frac{n_e}{n_{ec}}\right)^{-1/2}. \tag{8.94}$$

In summary of this section, we have derived two apparently different equations ((8.76) and (8.93)) for the axial magnetic field induced by the inverse Faraday effect (see also (8.77)). So far there are not enough experiments of the inverse Faraday effect in order to check the different theories. Furthermore, it seems that the theory of this phenomenon and the relevant numerical simulations have not yet been performed comprehensively in order to clarify this subject.

8.4 Waves in the Presence of the Steady-State Magnetic Field

In the previous sections of this chapter we have seen that non-negligible steady-state magnetic fields are created in laser–plasma interaction. These magnetic fields can be present only in configurations that do not possess an exact spherical symmetry. **No magnetic field can exist in a spherical symmetry.** However, most of the experiments done so far in laser–plasma interaction have a planar or cylindrical geometry rather than a spherical one. Even for the large laser systems with a 'perfect' spherical laser irradiance of spherical shells (with the purpose of achieving inertial confinement fusion), local spherical symmetry breaking can be induced by hydrodynamic instabilities. Therefore, large local magnetic fields might be created even in these cases. It seems that steady-state magnetic fields are always associated with laser–plasma interactions. In this section we analyse the dispersion relation for some plasma waves in the presence of a d.c. magnetic field.

8.4.1 Ordinary and Extraordinary Waves

We analyse now the behaviour of an electromagnetic wave that propagates in uniform and magnetized plasma. A constant magnetic field $\mathbf{B}_0$ in the z direction is present in the plasma medium considered here. For simplicity, a cold plasma is considered, i.e. $T_e = 0$. Since the electromagnetic waves have a high frequency, one can ignore the ion motion. The electromagnetic wave is described by the Maxwell equations, where the electric current is calculated from the electron momentum equation. Denoting the electromagnetic fields by $\mathbf{E}$ and $\mathbf{B}$, the linearized equations to be solved are (Gaussian units are used here)

$$\begin{aligned} \nabla\times\mathbf{E} &= -\frac{1}{c}\frac{\partial\mathbf{B}}{\partial t}, \qquad \nabla\times\mathbf{B} = \frac{1}{c}\frac{\partial\mathbf{E}}{\partial t}+\frac{4\pi}{c}\mathbf{J} \\ \mathbf{J} &= -en_e\mathbf{v}, \qquad m_e n_e\frac{\partial\mathbf{v}}{\partial t} = -en_e\mathbf{E}-\frac{en_e}{c}\mathbf{v}\times\mathbf{B}_0 \end{aligned} \tag{8.95}$$

where $\mathbf{v}$ is the electron (fluid) velocity, and $-e$, m_e and n_e are the charge, the mass and the density of the electrons respectively. Equations (8.95) are 12 equations with 12 unknowns: $\mathbf{E}$, $\mathbf{B}$, $\mathbf{v}$ and $\mathbf{J}$; so one has the same number of unknowns as equations (caution should be exercised not to add, during the algebra manipulations, new equations for these unknowns).

We now analyse waves that propagate perpendicularly to $\mathbf{B}_0$. Since $\mathbf{B}_0$ is parallel to $\hat{\mathbf{z}}$ (the unit vector in the z direction), the wave vector $\mathbf{k}$ is chosen in the x direction in Cartesian coordinates. In this case one has two possibilities:

(a) $\mathbf{E}$ parallel to $\mathbf{B}_0$, which is called **ordinary wave**, and
(b) $\mathbf{B}$ parallel to $\mathbf{B}_0$, which is called **extraordinary wave**.

$$\begin{aligned} &\mathbf{B}_0 = (0,0,B_0), \qquad \mathbf{k} = (0,0,k) \\ \textbf{ordinary wave}: \quad &\mathbf{E} = (0,0,E), \qquad \mathbf{B} = (0,B,0) \\ \textbf{extraordinary wave}: \quad &\mathbf{E} = (E_x,E_y,0), \qquad \mathbf{B} = (0,0,B). \end{aligned} \tag{8.96}$$

For an ordinary wave (defined also as O-mode) the electric field, in the z direction, induces an electron velocity in the z direction; therefore, the $\mathbf{v} \times \mathbf{B}_0$ term in the last of equations (8.95) vanishes. Therefore, equations (8.95) are identical to those obtained in the unmagnetized plasma (see section 2.7), where the following dispersion relation was obtained:

$$\omega^2 = \omega_{pe}^2 + k^2 c^2 \tag{8.97}$$

where ω_{pe} is the electron plasma frequency. This dispersion relation describes an electromagnetic wave that propagates in the plasma as if there is not a d.c. magnetic field (B_0). This may be the reason that it acquired the name of **ordinary wave**.

For **extraordinary wave** (defined also as **X-mode**) the electric field is perpendicular to $\mathbf{B}_0$, and therefore the electric field induces an electron velocity in the x–y plane. As a result the force $\mathbf{v} \times \mathbf{B}_0$ introduces another velocity term in this plane. Since in this case there is no velocity component in the z direction, one can write $\mathbf{v} = (v_x, v_y, 0)$. Assuming a uniform plasma, the following substitution can be made in the linear equations (8.95):

$$\nabla \Rightarrow \mathrm{i}\mathbf{k}, \qquad \frac{\partial}{\partial t} \Rightarrow -\mathrm{i}\omega. \tag{8.98}$$

(c) Using the geometry defined by (8.96) and the Fourier transform as expressed (for the linear equations) in (8.98), one gets from (8.95) the following five algebraic equations with five unknowns (v_x, v_y, E_x, E_y, B):

$$\begin{aligned} -\mathrm{i}\omega m_e v_x &= -eE_x - \frac{eB_0}{c} v_y, \qquad -\mathrm{i}\omega m_e v_y = -eE_y + \frac{eB_0}{c} v_x, \\ \mathrm{i}kE_y &= \frac{\mathrm{i}\omega}{c} B, \qquad -\mathrm{i}kB = -\frac{4\pi e n_e}{c} v_y - \frac{\mathrm{i}\omega}{c} E_y, \\ 0 &= -\frac{4\pi e n_e}{c} v_x - \frac{\mathrm{i}\omega}{c} E_x. \end{aligned} \tag{8.99}$$

Using the definitions of the plasma frequency $\omega_{\rm pe}$ and the cyclotron frequency $\omega_{\rm ce}$,

$$\omega_{\rm pe}^2 = \frac{4\pi e^2 n_{\rm e}}{m_{\rm e}}, \qquad \omega_{\rm ce}^2 = \frac{eB_0}{m_{\rm e}c} \tag{8.100}$$

we rewrite equations (8.99) in matrix form:

$$\begin{pmatrix} 1 & {\rm i}\Omega & 0 & 0 & {\rm i} \\ -{\rm i}\Omega & 1 & 0 & {\rm i} & 0 \\ 0 & 0 & 1 & -A & 0 \\ 0 & -{\rm i}C & -A & 1 & 0 \\ -{\rm i}C & 0 & 0 & 0 & 1 \end{pmatrix} \begin{pmatrix} (\omega m_{\rm e}/e)v_x \\ (\omega m_{\rm e}/e)v_y \\ B \\ E_y \\ E_x \end{pmatrix} = \begin{pmatrix} 0 \\ 0 \\ 0 \\ 0 \\ 0 \end{pmatrix} \tag{8.101}$$

$$\Omega \equiv (\omega_{\rm ce}/\omega), \qquad A \equiv (kc/\omega), \qquad C \equiv (\omega_{\rm pe}^2/\omega_{\rm ce}^2).$$

Note that all the variables have the same dimensional form (Gaussian units), so that all the elements of the matrix are dimensionless. In order to get a non-zero solution for the variables, it is necessary that the determinant of the matrix in (8.101) is zero. The vanishing determinant gives the following **dispersion relation** for the **extraordinary** electromagnetic wave:

$$n^2 = \frac{k^2c^2}{\omega^2} = 1 - \left(\frac{\omega_{\rm pe}^2}{\omega^2}\right)\left(\frac{\omega^2 - \omega_{\rm pe}^2}{\omega^2 - \omega_{\rm uh}^2}\right) \tag{8.102}$$

where n is the index of refraction and $\omega_{\rm uh}$ is called the **upper hybrid** frequency, given by

$$\omega_{\rm uh}^2 = \omega_{\rm pe}^2 + \omega_{\rm ce}^2. \tag{8.103}$$

It is worth mentioning that the extraordinary wave is a **superposition** of a **transverse wave** (electromagnetic), $\mathbf{k} = (k_x, 0, 0)$, $\mathbf{E} = (0, E_y, 0)$, $\mathbf{B} = (0, 0, B)$, and a **longitudinal wave**, $\mathbf{k} = (k_x, 0, 0)$, $\mathbf{E} = (E_x, 0, 0)$. Solving for E_x and E_y, one gets that at a given point in space the vector $\mathbf{E}$ rotates as a function of time ($E_x \approx \exp[{\rm i}(kx - \omega t)]$ and $E_y \approx \exp[{\rm i}(kx - \omega t)]$), and since E_x and E_y are not equal one gets an elliptical rotation of the electric field.

Analysing the dispersion relation (8.102), one can see that the index of refraction can attain zero values, called **cutoff**, and infinite values, called **resonance**. Since the phase velocity of the wave is

$$v_\phi = \frac{c}{n} = \frac{\omega}{k} \tag{8.104}$$

one defines

$$\begin{aligned} &\textbf{cutoff}: \quad n = 0,\ k = 0 \ \Rightarrow\ v_\phi(k = 0) = \infty \\ &\textbf{resonance}: \quad n = \infty,\ k = \pm\infty \ \Rightarrow\ v_\phi(k = \pm\infty) = 0. \end{aligned} \tag{8.105}$$

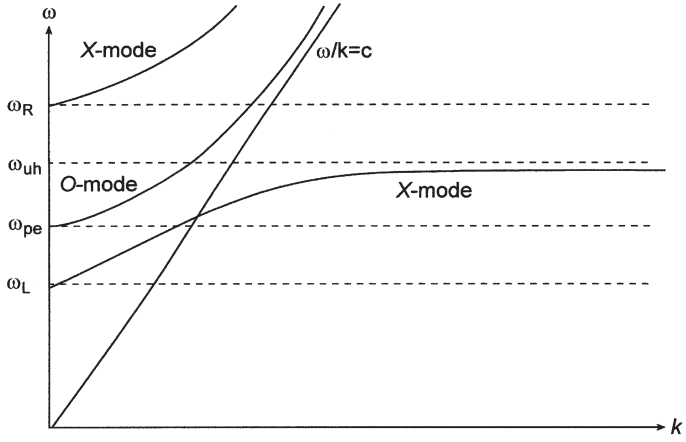

Figure 8.4. A schematic presentation of the dispersion relation $\omega = \omega(k)$ for extraordinary (X-mode) and ordinary (O-mode) waves.

From the dispersion relation, equation (8.102), the resonances for the X-mode (the extraordinary wave) are at

$$\textbf{X-mode resonances}: \quad \omega = 0, \quad \omega = \omega_{\mathrm{uh}} \tag{8.106}$$

and the cutoffs are the solution of the following quadratic equation:

$$\omega^4 - (\omega_{\mathrm{pe}}^2 + \omega_{\mathrm{uh}}^2)\omega^2 + \omega_{\mathrm{pe}}^4 = 0. \tag{8.107}$$

Denoting the two solutions of this quadratic equation by ω_{L} and ω_{R}, and using (8.103), one gets

$$\omega_{\pm} = \pm\frac{\omega_{\mathrm{ce}}}{2} + \sqrt{\omega_{\mathrm{pe}}^2 + \tfrac{1}{4}\omega_{\mathrm{ce}}^2}, \qquad \omega_{+} \equiv \omega_{\mathrm{R}}, \qquad \omega_{-} \equiv \omega_{\mathrm{L}}. \tag{8.108}$$

The notations R and L are used because these solutions describe right- and left-handed circular polarization. The right-hand rotation of the electric field is defined by the 'right-hand rule'. If the thumb is along k then the fingers of the right hand are in the direction of the rotation of the electric field for the R-wave. In the L-wave, E rotates in the opposite direction.

A schematic presentation of the dispersion relation $\omega = \omega(k)$ for extraordinary (X-mode) and ordinary (O-mode) waves, according to equations (8.102) and (8.97) respectively, is given in figure 8.4.

8.4.2 Electromagnetic waves propagating parallel to $\mathbf{B_0}$

In this case the following geometry is considered in Cartesian coordinates:

$$\begin{aligned} &\mathbf{B}_0 = (0, 0, B_0), \qquad \mathbf{k} = (0, 0, k), \qquad \mathbf{E} = (E_x, E_y, 0) \\ &\mathbf{B} = (B_x, B_y, 0), \qquad \mathbf{v} = (v_x, v_y, 0) \end{aligned} \tag{8.109}$$

Linearization and Fourier transform of equations (8.95) yields

$$\begin{aligned} \mathrm{i}\mathbf{k}\times\mathbf{E}-\frac{\mathrm{i}\omega}{c}B&=0\\ \mathrm{i}\mathbf{k}\times\mathbf{B}+\frac{\mathrm{i}\omega}{c}\mathbf{E}+\frac{4\pi e n_{\mathrm{e}}}{c}\mathbf{v}&=0\\ -\mathrm{i}\omega m_{\mathrm{e}}\mathbf{v}+e\mathbf{E}+\frac{e}{c}\mathbf{v}\times\mathbf{B}_0&=0. \end{aligned} \tag{8.110}$$

Writing this equation explicitly, for the configuration defined in (8.109), in matrix form we obtain

$$\begin{pmatrix} 1 & \mathrm{i}\Omega & 0 & 0 & \mathrm{i} & 0\\ \mathrm{i}\Omega & 1 & 0 & 0 & 0 & \mathrm{i}\\ 0 & 0 & 1 & 0 & 0 & A\\ 0 & 0 & 0 & 1 & -A & 0\\ -\mathrm{i}K & 0 & 0 & -A & 1 & 0\\ 0 & -\mathrm{i}K & A & 0 & 0 & 1 \end{pmatrix} \begin{pmatrix} (m_{\mathrm{e}}\omega/e)v_x\\ (m_{\mathrm{e}}\omega/e)v_y\\ B_x\\ B_y\\ E_x\\ E_y \end{pmatrix} = \begin{pmatrix} 0\\0\\0\\0\\0\\0 \end{pmatrix} \tag{8.111}$$

$$\Omega\equiv\frac{\omega_{\mathrm{ce}}}{\omega},\qquad A\equiv\frac{kc}{\omega},\qquad K\equiv\frac{\omega_{\mathrm{pe}}^2}{\omega^2}.$$

The dispersion relations are obtained by setting the determinant of this matrix equal to zero:

$$n_{\pm}^2=\frac{k^2c^2}{\omega_{\pm}^2}=1-\frac{\omega_{\mathrm{pe}}^2/\omega^2}{1\mp\omega_{\mathrm{ce}}/\omega} \tag{8.112}$$

where $+$ and $-$ denote right (R) and left (L) circular polarization, and n_+ and n_- are the indices of refraction for R and L waves propagating parallel to B_0 respectively. See equations (8.53) and (8.54).

From this dispersion relation we see that there is one resonance at $\omega=\omega_{\mathrm{ce}}$, and this is satisfied only for the R-wave. The cutoffs are derived by equating k to zero in (8.112), implying the same results as those of the X-mode in equation (8.108).

Figure 8.5 shows the schematic dispersion relation $\omega=\omega(k)$ of an electromagnetic wave propagating parallel to B_0 for two cases: (a) $\omega_{\mathrm{L}}<\omega_{\mathrm{pe}}<\omega_{\mathrm{ce}}$, (b) $\omega_{\mathrm{pe}}>\omega_{\mathrm{L}}>\omega_{\mathrm{ce}}$. As can be seen from these figures, there are two R-mode branches (as in the X-mode, figure 8.4) but only one L-mode, where $\omega>\omega_{\mathrm{L}}$ is satisfied. The low-frequency branch of the R-wave is also known as the electron–cyclotron wave.

The dispersion relation (8.112) shows that the index of refraction for the right-hand and left-hand polarization are not equal, as already derived in section 8.3 (equations (8.53) and (8.54)). Moreover, the index of refraction is complex (i.e. $n^2<0,\omega^2<0$) in the domain $\omega_{\mathrm{ce}}<\omega<\omega_{\mathrm{R}}$ for the R-wave

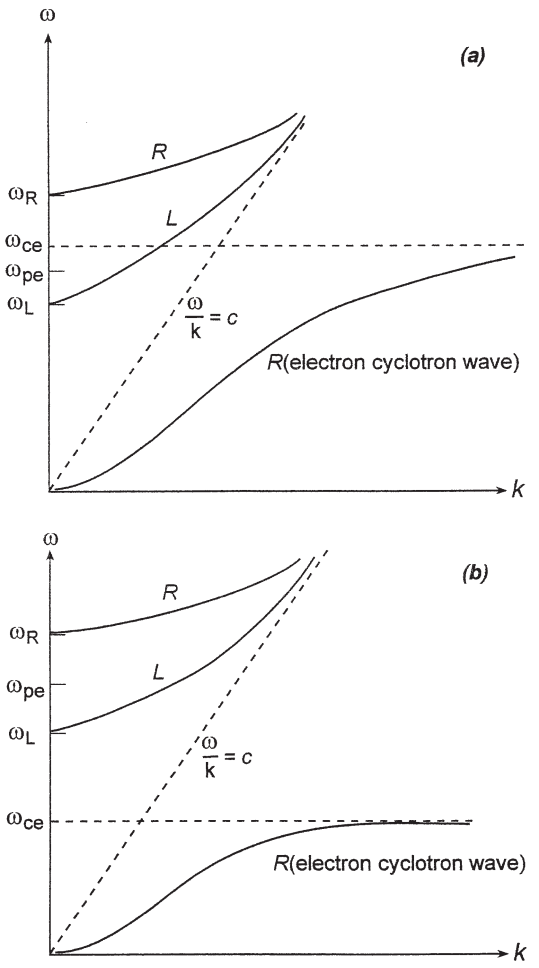

Figure 8.5. Schematic dispersion relation $\omega = \omega(k)$ for an electromagnetic wave propagating parallel to B_0: (a) $\omega_L < \omega_{pe} < \omega_{ce}$, (b) $\omega_{pe} > \omega_L > \omega_{ce}$.

and in the region $0 < \omega < \omega_L$ for the L-wave. Appropriate waves with these frequencies cannot propagate along B_0 in plasma.

The plasma and cyclotron frequencies can be expressed in practical units for typical laser-induced magnetic fields and densities:

$$\begin{aligned} \omega_{ce}\,[\mathrm{rad/s}] &= \frac{eB_0}{m_e c} = 1.76 \times 10^{13}\left(\frac{B_0}{\mathrm{MGauss}}\right) \\ \omega_{pe}\,[\mathrm{rad/s}] &= \left(\frac{4\pi e^2 n_e}{m_e}\right)^{1/2} = 5.64 \times 10^{14}\left(\frac{n_e}{10^{20}\,\mathrm{cm}^{-3}}\right)^{1/2}. \end{aligned} \tag{8.113}$$

Therefore, for figure 8.5(a) to be relevant for laser–plasma interactions, one requires

$$\omega_{ce} > \omega_{pe} \;\Rightarrow\; \left(\frac{B_0}{\text{MGauss}}\right) > 32.0\left(\frac{n_e}{10^{20}\,\text{cm}^{-3}}\right)^{1/2} \tag{8.114}$$

while for figure 8.5(b) it is necessary that the opposite inequality is satisfied, which in general is more realistic for laser–plasma interactions.

Last but not least, from figure 8.5 at high frequencies (for typical laser intensities and B_0, one usually has $\omega > \omega_{ce}$), one can see that the phase velocity ω/k is larger for an R-wave than for an L-wave. If a plane wave (i.e. linearly polarized) is propagating along B_0, then this wave can be described as a linear combination of an R-wave and an L-wave. These waves (R and L) propagate with different phase velocity; therefore, the plane of polarization of the wave rotates as it travels along B_0. This is the Faraday effect, as explained in section 8.3.

8.4.3 Alfvén waves

So far, in this section, the ion motion was ignored. Now we combine the ion motion with the electromagnetic equations (Maxwell equations). If an electromagnetic wave propagates along the d.c. magnetic field, i.e. the wave vector $\mathbf{k}$ is parallel to the magnetic field in the plasma B_0, one gets the famous Alfvén waves.

The following configuration is considered in Cartesian coordinates:

$$\begin{aligned} &\mathbf{k} = (0,0,k), \qquad \mathbf{B}_0 = (0,0,B_0), \qquad \mathbf{E} = (E,0,0) \\ &\mathbf{B} = (0,B,0), \qquad \mathbf{v}_e = (v_{ex}, v_{ey}, 0), \qquad \mathbf{v}_i = (v_{ix}, v_{iy}, 0) \end{aligned} \tag{8.115}$$

where $\mathbf{v}_e$ and $\mathbf{v}_i$ are the electron and ion velocities, and $\mathbf{E}$ and $\mathbf{B}$ are the electromagnetic fields propagating in the plasma. It is assumed that the plasma is neutral and cold (Z is the ion charge):

$$n_e = Zn_i = n_0, \qquad T_e = T_i = 0 \tag{8.116}$$

where n_e and n_i are the electron and ion densities, and T are appropriate temperatures. Moreover, it is assumed that the electron inertia can be neglected in the momentum equation. In this case the relevant linearized Fourier transform fluid equations, together with Maxwell's equations, are

$$\begin{aligned} 0 &= -e\mathbf{E} - (e/c)\mathbf{v}_e \times \mathbf{B}_0 \\ -\mathrm{i}\omega m_i v_i &= Ze\mathbf{E} + (Ze/c)\mathbf{v}_{ie} \times \mathbf{B}_0 \\ \mathrm{i}\mathbf{k} \times \mathbf{E} &= (\mathrm{i}\omega/c)\mathbf{B} \\ \mathrm{i}\mathbf{k} \times \mathbf{B} &= -(\mathrm{i}\omega/c)\mathbf{E} + (4\pi/c)n_0(\mathbf{v}_i - \mathbf{v}_e) \end{aligned} \tag{8.117}$$

where m_i is the ion mass. Using similar algebra as before, one gets from these equations the Alfvén dispersion relation

$$\omega^2 = \frac{k^2 v_A^2}{1 + (v_A^2/c^2)}$$
$$v_A = \left(\frac{B_0^2}{4\pi n_0 m_i}\right)^{1/2} \approx 2.18 \times 10^7 \left(\frac{m_p}{m_i}\right)\left(\frac{B_0}{\text{MGauss}}\right)\left(\frac{10^{20}\,\text{cm}^{-3}}{n_i}\right)^{1/2} \left[\frac{\text{cm}}{\text{s}}\right] \tag{8.118}$$

where v_A is the Alfvén wave velocity and m_p is the proton mass. In deriving this dispersion relation one must also assume that $\omega < \omega_{ci}$, where the ion cyclotron frequency is given by

$$\omega_{ci} = \frac{ZeB_0}{m_i c} \approx 9.58 \times 10^9 \left(\frac{Zm_p}{m_i}\right)\left(\frac{B_0}{\text{MGauss}}\right). \tag{8.119}$$

The condition $\omega < \omega_{ci}$ is nonrealistic for typical laser–plasma interactions. Moreover, using equation (8.118), one gets a time scale ($\sim 2\pi/\omega$) larger by many orders of magnitude than any high-power laser pulse duration. Therefore, it seems that the Alfvén waves do not play any important role in laser–plasma interactions.

8.5 Resonance Absorption in a Magnetized Plasma

Resonance absorption was considered in section 5.6. In this section we analyse how the absorption is modified due to the presence of a steady-state (d.c.) magnetic field. As in the previous section, we consider the electron momentum equation together with Maxwell equations for cold plasma. In this case one is interested in the effects of the density gradient, where the electric and magnetic fields in the plasma can be written for a monochromatic wave:

$$\mathbf{E}(\mathbf{r}, t) = \mathbf{E}(\mathbf{r}) \exp(-i\omega t), \qquad \mathbf{B}(\mathbf{r}, t) = \mathbf{B}(\mathbf{r}) \exp(-i\omega t). \tag{8.120}$$

Therefore, one cannot use the relation $\nabla \to i\mathbf{k}$ when taking the Fourier transform of the linear equations. However, the substitution $\partial/\partial t \to -i\omega$ is permitted for the class of solutions given by (8.120). The linearized equations to be solved are

$$\begin{aligned} \nabla \times \mathbf{E}(\mathbf{r}) &= \frac{i\omega}{c}\mathbf{B}(\mathbf{r}) \\ \nabla \times \mathbf{B}(\mathbf{r}) &= -\frac{i\omega}{c}\mathbf{E}(\mathbf{r}) - \frac{4\pi e n_e}{c}\mathbf{v} \\ -i\omega\mathbf{v} &= -\frac{e}{m_e}\left(\mathbf{E}(\mathbf{r}) + \frac{1}{c}\mathbf{v} \times \mathbf{B}_0(\mathbf{r})\right) \end{aligned} \tag{8.121}$$

where $\mathbf{v}$ is the average velocity of the electrons, and the d.c. magnetic field is taken parallel to the z axis but is not necessarily a constant in space. The third of these equations can be written in matrix form as

$$\begin{pmatrix} v_x \\ v_y \\ v_z \end{pmatrix} = \begin{pmatrix} -\mathrm{i}\omega\Delta & \omega_{\mathrm{ce}}\Delta & 0 \\ \omega_{\mathrm{ce}}\Delta & -\mathrm{i}\omega\Delta & 0 \\ 0 & 0 & -\mathrm{i}/\omega \end{pmatrix} \begin{pmatrix} (e/m_{\mathrm{e}})E_x \\ (e/m_{\mathrm{e}})E_y \\ (e/m_{\mathrm{e}})E_z \end{pmatrix} \qquad (8.122)$$

$$\Delta \equiv \frac{1}{\omega^2 - \omega_{\mathrm{ce}}^2}$$

where the electron cyclotron frequency is defined in (8.100). Substituting $\mathbf{v}$ from (8.122) into the second equation of (8.121), one gets

$$\nabla \times \mathbf{B}(\mathbf{r}) = -\frac{\mathrm{i}\omega}{c}\,\boldsymbol{\varepsilon} \cdot \mathbf{E}(\mathbf{r}) \qquad (8.123)$$

where this equation defines the **dielectric tensor** $\boldsymbol{\varepsilon}$, given by

$$\boldsymbol{\varepsilon} = \begin{pmatrix} \dfrac{\omega^2 - \omega_{\mathrm{uh}}^2}{\omega^2 - \omega_{\mathrm{ce}}^2} & \dfrac{\mathrm{i}\omega_{\mathrm{pe}}^2}{(\omega^2 - \omega_{\mathrm{ce}}^2)} & 0 \\ \dfrac{-\mathrm{i}\omega_{\mathrm{pe}}^2\omega_{\mathrm{ce}}}{\omega(\omega^2 - \omega_{\mathrm{ce}}^2)} & \dfrac{\omega^2 - \omega_{\mathrm{uh}}^2}{\omega^2 - \omega_{\mathrm{ce}}^2} & 0 \\ 0 & 0 & 1 - \dfrac{\omega_{\mathrm{pe}}^2}{\omega^2} \end{pmatrix} \qquad (8.124)$$

where the plasma frequency is given in (8.100) and the upper hybrid frequency ω_{uh} is defined in (8.103). Note that the elements of the dielectric tensor are dimensionless.

In order to get the electromagnetic field, one has to solve equation (8.123) and the first equation of (8.121). The equation for the electric field $\mathbf{E}$ is derived by taking $\nabla\times$[first equation of (8.121)] and using (8.123), yielding

$$\nabla^2\mathbf{E}(\mathbf{r}) + \frac{\omega^2}{c^2}\,\boldsymbol{\varepsilon} \cdot \mathbf{E}(\mathbf{r}) = 0 \qquad (8.125)$$

where the tensor $\boldsymbol{\varepsilon}$ is given in (8.124). In deriving this equation it was assumed that $\nabla \cdot \mathbf{E} = 0$, i.e. the plasma is neutral.

For the equation of the magnetic field $\mathbf{B}(\mathbf{r})$ it is convenient to use the inverse matrix $\boldsymbol{\varepsilon}^{-1}$ of the dielectric tensor $\boldsymbol{\varepsilon}$. The inverse matrix is defined by

$$\boldsymbol{\varepsilon}^{-1} \cdot \boldsymbol{\varepsilon} = \boldsymbol{\varepsilon} \cdot \boldsymbol{\varepsilon}^{-1} = \mathbf{1} \qquad (8.126)$$

where $\mathbf{1}$ is the unit matrix

$$\mathbf{1} = \begin{pmatrix} 1 & 0 & 0 \\ 0 & 1 & 0 \\ 0 & 0 & 1 \end{pmatrix}. \qquad (8.127)$$

Using the tensor $\boldsymbol{\varepsilon}^{-1}$, equation (8.123) can be rewritten by

$$\boldsymbol{\varepsilon}^{-1} \cdot \nabla \times \mathbf{B} = -\frac{\mathrm{i}\omega}{c}\,\mathbf{E}. \tag{8.128}$$

Using equations (8.124) and (8.126), one gets the inverse tensor of $\boldsymbol{\varepsilon}$ (David and Pellat 1980):

$$\begin{aligned}
\boldsymbol{\varepsilon}^{-1} &= \begin{pmatrix} \varepsilon_{\mathrm{e}}^{-1} & -\mathrm{i}\beta & 0 \\ \mathrm{i}\beta & \varepsilon_{\mathrm{e}}^{-1} & 0 \\ 0 & 0 & \varepsilon_0^{-1} \end{pmatrix} \\
\varepsilon_{\mathrm{e}} &= \left[\left(1 - \frac{\omega_{\mathrm{pe}}^2}{\omega^2}\right)^2 - \frac{\omega_{\mathrm{ce}}^2}{\omega^2}\right]\left(1 - \frac{\omega_{\mathrm{uh}}^2}{\omega^2}\right)^{-1} \\
\varepsilon_0 &= \left(1 - \frac{\omega_{\mathrm{pe}}^2}{\omega^2}\right)^2 \\
\beta &= \frac{\omega_{\mathrm{pe}}^2 \omega_{\mathrm{ce}}}{\omega^3}\left[\left(1 - \frac{\omega_{\mathrm{pe}}^2}{\omega^2}\right)^2 - \frac{\omega_{\mathrm{ce}}^2}{\omega^2}\right]^{-1}.
\end{aligned} \tag{8.129}$$

One can define ε_0 and ε_{e} as the square of the ordinary and extraordinary index of refraction respectively (see previous section).

The wave equation for the magnetic field $\mathbf{B}$ is derived by taking $\nabla \times$ (8.128) and using the first equation of (8.121), together with the Maxwell equation $\nabla \cdot \mathbf{B} = 0$, implying

$$\nabla \times (\boldsymbol{\varepsilon}^{-1} \cdot \nabla \times \mathbf{B}) - \frac{\omega^2}{c^2}\,\mathbf{B} = 0. \tag{8.130}$$

For the extraordinary mode the electric field $\mathbf{E}$ is perpendicular to the d.c. magnetic field $\mathbf{B}_0$. Choosing $\mathbf{B}_0$ to be in the z direction, the plane of the laser incidence is x–y, then the following configuration is defined (a p-polarization):

$$\begin{aligned}
\mathbf{B}_0 &= (0, 0, B_0), \qquad & \mathbf{k} &= (k\cos\theta, k\sin\theta, 0) \\
\mathbf{E} &= (E_x, E_y, 0), \qquad & \mathbf{B} &= (0, 0, B_z).
\end{aligned} \tag{8.131}$$

In this configuration the equation for B_z (the extraordinary mode) is derived from equation (8.130):

$$\nabla^2 B_z + \left(-\frac{\nabla\varepsilon_{\mathrm{e}}}{\varepsilon_{\mathrm{e}}} + i\varepsilon_{\mathrm{e}}\boldsymbol{\gamma}\right) \cdot \nabla B_z + k^2 \varepsilon_{\mathrm{e}} B_z = 0, \qquad \boldsymbol{\gamma} \equiv \hat{\mathbf{x}}\,\frac{\partial\beta}{\partial y} - \hat{\mathbf{y}}\,\frac{\partial\beta}{\partial x}. \tag{8.132}$$

For an ordinary wave the electric field $\mathbf{E}$ is parallel to the d.c. magnetic field $\mathbf{B}_0$ (chosen in the z direction) and equation (8.125) in this case is

$$\nabla^2 E_z + k^2 \varepsilon_0 E_z = 0. \tag{8.133}$$

The ordinary wave, i.e. the s-polarization wave in our case, is not modified by an external magnetic field $B_0\hat{\mathbf{z}}$, and this wave does not drive the resonance absorption mechanism.

The p-polarization wave described above describes an extraordinary wave and can drive the resonance absorption mechanism (see section 5.5). It is convenient to describe this case by the equation of the magnetic field (equation (8.132)). From this equation one gets a resonance for B_z, due to $\varepsilon_e = 0$, at

$$\textbf{resonance}: \quad \omega^2 = \omega_{uh}^2. \tag{8.134}$$

This resonance is responsible for the excitation of an electrostatic wave that is the origin of the resonant absorption phenomenon. Two other singularities of equation (8.132), where ε_e is zero and β becomes infinite, are derived from solving

$$1 - \frac{\omega_{pe}^2}{\omega^2} = \pm\frac{\omega_{ce}}{\omega}. \tag{8.135}$$

However, B_z is regular at these points and these two singularities describe the turning points of the WKB solution (see section 5.4).

It is assumed that the laser is incident at $x = -L$, in the x–y plane with a positive x component (the domain $x < -L$ is vacuum and $x > -L$ is plasma), and that the incident p-polarized wave is obliquely incident at an angle θ_0 with the density gradient. For a constant (in space and time) external magnetic field and a linear density profile, described by

$$\frac{n_e}{n_{ec}} = \left\{\begin{array}{ll} 0 & \text{for } x < -L \\ 1 + (x/L) & \text{for } x > -L \end{array}\right\} \Rightarrow \varepsilon_0 = \left\{\begin{array}{ll} 1 & \text{for } x < -L \\ -(x/L) & \text{for } x > -L \end{array}\right. \tag{8.136}$$

equation (8.132) takes the form (David and Pellat 1980)

$$\frac{d^2B}{d\xi^2} + \left(\frac{1}{\xi} - \frac{1}{\xi - \sigma} - \frac{1}{\xi + \sigma}\right)\frac{dB}{d\xi} + \left(\frac{\sigma^2}{\xi} - \xi - \tau^2 + \frac{\tau}{\xi - \sigma} - \frac{\tau}{\xi + \sigma}\right)B = 0. \tag{8.137}$$

The following change of variables is used in equation (8.132) in order to get equation (8.137):

$$\begin{aligned} B_z &= B(x)\exp(\mathrm{i}ky\sin\theta_0) \\ \xi &= x\left(\frac{k^2}{L}\right)^{1/3} \\ \tau &= (kL)^{1/3}\sin\theta_0 \\ \sigma &= (kL)^{2/3}\left(\frac{\omega_{ce}}{\omega}\right). \end{aligned} \tag{8.138}$$

Moreover, equation (8.137) is derived only for $\omega_{ce}/\omega \ll 1$ (i.e. we neglect $(\omega_{ce}/\omega)^2$ and higher-order terms), an assumption satisfied in most laser–plasma experiments.

As we have seen in chapter 5, without a dissipation mechanism such as electron ion–collisions or Landau damping, all of the laser light is reflected (or transferred, if the plasma density is smaller than the critical density everywhere) out of the plasma (i.e. no absorption). In order to obtain a laser absorption one requires an effective collision frequency ν_{eff}. If the mechanism of the damping of electrostatic waves is known then it is possible to include ν implicitly in the dielectric constant, e.g. changing equation (8.136) to

$$\varepsilon_0 = \begin{cases} 1 & \text{for } x < -l \\ -(x/L) + \mathrm{i}(\nu_{\text{eff}}/\omega) & \text{for } x > -L. \end{cases} \tag{8.139}$$

However, it turns out that in most cases the collision frequency determines the magnetic (or electric) field strength at resonance and its spatial structure there, but does not modify the qualitative values of the absorption coefficient. The amplitude ratio square between the outgoing and incoming wave (at $x = -L$ in our above example) gives the reflection coefficient R ($1 - R$ is the absorption coefficient). This value does not depend on ν_{eff} as long as it is not zero. In this case equation (8.137) is solved numerically by integrating

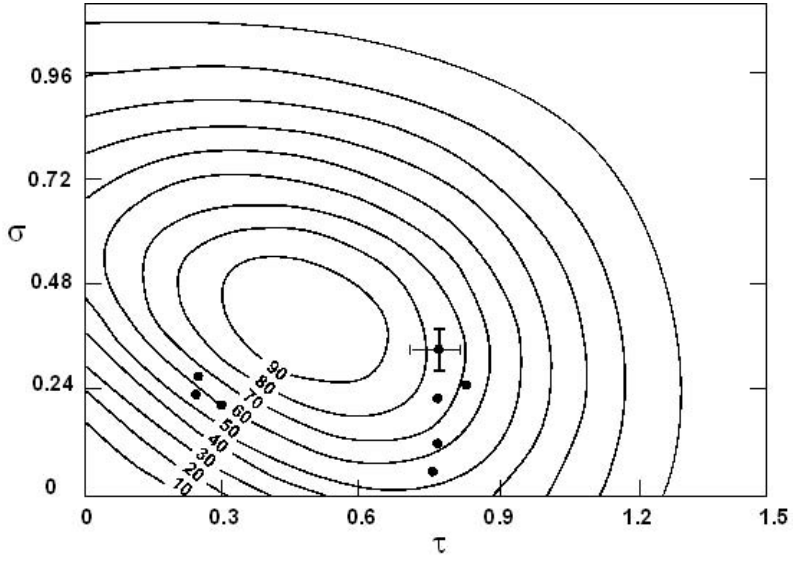

Figure 8.6. Absorption of p-polarized laser at oblique incidence in magnetized plasma. τ and σ are defined in equation (8.138). The dots are experimental points (Horovitz *et al.* 1998) of τ and σ. The measured absorption at these points fits within 10% of the theoretical values given in this figure.

it along a path in the complex plane (of ξ), where the singularities are avoided by taking a 'detour' from the x axis (i.e. the real ξ axis). The solution for the laser absorption, as given in figure 8.6 (Woo *et al*. 1978, David and Pellat 1980), shows that a p-polarized laser at oblique incidence in magnetized plasma can be almost 100% absorbed.

It turns out that the laser absorption depends only on two parameters, τ and σ, defined in equation (8.138). τ is related to the density gradient (scaling as L) and to the incidence angle θ_0, while σ is related both to the density gradient and the magnetic field. It is interesting to point out that even at normal incidence ($\theta_0 = 0$), the absorption can be as high as 50% for $\sigma \approx 0.5$. Using practical units for laser–plasma interactions, one can write

$$\sigma \approx 0.148 \left[\left(\frac{\lambda_L}{1\,\mu\text{m}} \right) \left(\frac{L}{10\,\mu\text{m}} \right)^2 \right]^{1/3} \left(\frac{B_0}{\text{MGauss}} \right) \tag{8.140}$$

so that $\sigma \approx 0.5$ for a magnetic field $\sim 3\,\text{MG}$ and a density scale length $\sim 10\,\mu\text{m}$, values measured experimentally in many plasmas created by lasers.

Chapter 9

Thermal Conduction and Heat Waves

9.1 The Scenario

Thermal conduction or, in more general terms, the energy transport in laser-produced plasma, is related to basic plasma physics in a wide range of parameters, such as density and temperature. This subject is of great interest because it plays a very important role in major applications, such as inertial confinement fusion (ICF), the production of x-ray sources and x-ray lasers. For example, the acceleration of shell targets for ICF relies not only on the energy absorbed by the plasma, but also on the efficient coupling between this energy and the solid shell. In section 9.2 we calculate this efficiency in a simple model.

A high intensity laser radiation ($>10^{11}\,\mathrm{W/cm^2}$), with pulse duration τ_L larger than 100 ps, is incident on a solid target. Plasma is created instantaneously (on a time scale shorter than τ_L by many orders of magnitude); it is heated to a high temperature and this plasma expands into the vacuum to create a low-density corona. Once the plasma corona is created, the laser radiation no longer reaches the solid since it cannot penetrate beyond the critical surface, with an electron density $n_{ec} = 10^{21}(\lambda_L/\mu m)^{-2}\,\mathrm{cm^{-3}}$, where λ_L is the laser wavelength. At the critical surface, part of the laser beam is absorbed and the other part is reflected into the corona. We have seen in chapter 5 that most of the absorption is done in the domain near the critical surface. Moreover, as has been shown in chapter 6, waves are created in the plasma-corona.

Figure 9.1 describes schematically the temperature and the electron density in laser-produced plasma. The temperature has a maximum in the region of the critical surface, where most of the laser energy is absorbed. The temperature decreases sharply towards the cold solid, and to a good approximation it is constant throughout the corona. The density is decreasing towards the vacuum and, for laser radiation intensities larger than about $10^{15}\,\mathrm{W/cm^2}$, there is a steep density gradient at the critical

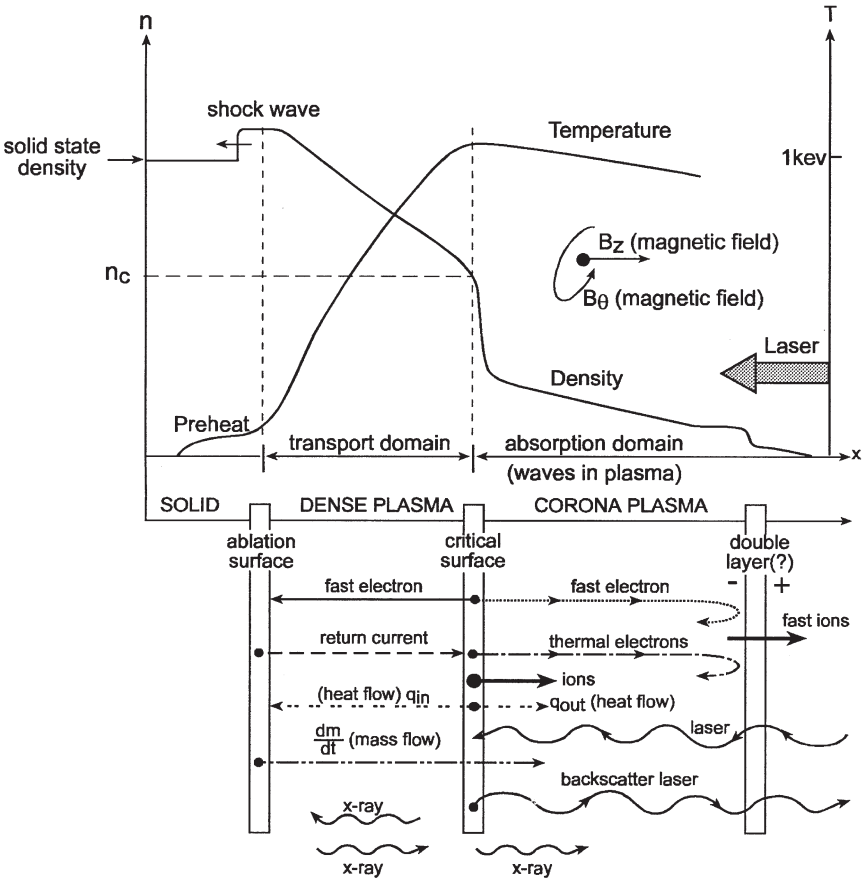

Figure 9.1. Schematic diagram of the temperature and density profile in a laser-induced plasma. A scenario is given for plasma particle streams, currents, heat flow, laser and laser-induced x-ray propagation, a possible double layer formation and the creation of axial and toroidal magnetic fields.

surface. The density and pressure rise towards the solid surface and the pressure (ablation pressure) reaches a maximum at the ablation surface, where plasma is created and the flow velocity is zero.

The energy absorbed at the critical surface domain is transported beyond the critical surface towards the solid target, either by (x-ray) radiation or by electron thermal conduction (figure 9.1). Most of the electrons in the plasma have a Maxwellian velocity distribution, with a temperature usually denoted by T_c (c stands for 'cold', which can be of the order of $k_B T_c \approx 1\,\mathrm{keV}$). For high laser intensities I_L, satisfying

$I_L\lambda_L^2 > 10^{14}\,(\mathrm{W/cm^2})\,\mu\mathrm{m}^2$, the electron velocity distribution may be described by two (or more) Maxwellian distributions with a second temperature T_h, much larger than T_c. In this case the fast electrons with a temperature T_h, which are created in the critical surface domain, transport part of their energy into the solid, causing preheating of the target. This is easily understood since the electron mean free path λ_e (for 90° deflection in multiple Coulomb collisions with ions, see section 9.3) is proportional to the square electron temperature,

$$\lambda_e(\mathrm{cm}) = 5.71 \times 10^4 \frac{T_e^2}{Zn_e \ln \Lambda} \tag{9.1}$$

where T_e, in degrees Kelvin, stands for the electron (cold or hot) temperature, Z is the charge of the ion, n_e is the electron density and $\ln \Lambda$ is the Coulomb logarithmic factor. For example, for $T_e = 10^7\,\mathrm{K} \approx 1\,\mathrm{keV}$, $Z = 10$, $\ln \Lambda = 10$ and $n_e = 10^{20}\,\mathrm{cm}^{-3}$, one gets $\lambda_e \approx 5.7\,\mu\mathrm{m}$. When $T_h/T_c \approx 10$, the energy of the hot electrons is deposited 100 times deeper into the target than the energy deposited by the cold electrons. Furthermore, if the cold electron mean free path is smaller than the temperature density gradient, then the thermal conduction is diffusive (see section 9.4) and the heat flux $\mathbf{q}$ (erg/(s·cm^2)) is given by (see section 2.3)

$$\mathbf{q} = -\tfrac{1}{3}\lambda_e v_e n_e k_B \nabla T_e = \kappa \nabla T_e \tag{9.2}$$

where v_e is the electron velocity and k_B is Boltzmann's constant. Substituting (9.1) into (9.2), one gets the classical result of Spitzer and Härm, denoted by SH theory (see section 9.5) for the conductivity κ:

$$\kappa(\mathrm{erg \cdot s^{-1} \cdot cm^{-1} \cdot K^{-1}}) = 1.77 \times 10^{-6} \frac{T_e^{5/2}}{Z \ln \Lambda}. \tag{9.3}$$

The heat flow is possible due to the distortion of the Maxwellian velocity distribution. For example, in one dimension the Gaussian form of the electron velocity distribution is changed in such a way that more electrons have a suitable velocity and energy to carry heat to the cold region. This effect creates an electric field $\mathbf{E}$. In order to keep charge neutrality, an electric current $\sigma_E\mathbf{E}$ (σ_E is the electrical conductivity coefficient), called 'return current', is created from the cold target towards the critical surface (see figure 9.1). The electrons in the return current have low energy. The thermal flux of electrons, from the critical surface towards the ablation surface, has a higher energy than the electrons in the return current, so the target is heated.

The temperature gradient between the critical surface and the ablation surface induces a thermoelectric effect. This phenomenon reduces the classical

heat flow according to the relation

$$\mathbf{J} = \sigma_E \mathbf{E} - \alpha \nabla T, \qquad \mathbf{q} = \beta \mathbf{E} - \kappa \nabla T \tag{9.4}$$

where $\mathbf{J}$ is the total electrical current, and the coefficients α, β, σ_E and κ are not independent (Onsager relations in irreversible thermodynamics). Assuming only a net heat flow transport, $\mathbf{J} = 0$, one gets from (9.4):

$$\mathbf{q} = -\kappa \left(1 - \frac{\alpha\beta}{\sigma_E \kappa}\right) \nabla T_e \tag{9.5}$$

where a reduction factor due to the thermoelectric effect shows up, which may reduce the heat transport by a factor of about 2.

Furthermore, the heat transport of the cold electrons for very steep temperature gradients does not satisfy the diffusion approach. The SH theory is valid only if the electron velocity distribution function f is slightly perturbed from its equilibrium distribution (f_0 is the Maxwell distribution), namely $f = f_0 + f_1$ where $f_0 \gg f_1$. The validity of the diffusion approximation (SH model) depends strongly on the ratio λ_e/L_T, where λ_e is the electron mean free path (see (9.1)) and L_T is the temperature density scale length:

$$L_T = \frac{T}{(\mathrm{d}T/\mathrm{d}x)}. \tag{9.6}$$

The diffusion approximation is valid for $\lambda_e \ll L_T$. It has been shown (Gray and Kilkenny 1980) that the diffusion approximation is valid only for $\lambda_e/L_T < 10^{-2}$. For $\lambda_e/L_T > 10^{-2}$ the energy transport is significantly reduced, and it is necessary to introduce an inhibition factor f in order to get agreement with experiments. The inhibition factor f is defined as the ratio between the actual heating flux q and the free streaming flux q_f, the maximum possible flux, defined by

$$q_f = n_e k_B T_e \left(\frac{k_B T_e}{m_e}\right)^{1/2}. \tag{9.7}$$

The free streaming is the heat flow carried by the electrons if they stream freely at their thermal velocity along the temperature gradient. For high laser irradiance, $I_L > 10^{15}\,\mathrm{W/cm^2}$, where $\lambda_e/L_T \approx 1$, the agreement with experiments are obtained when using an electron thermal flux

$$\mathbf{q} = f\mathbf{q}_f \approx 0.03\mathbf{q}_f \tag{9.8}$$

instead of the diffusion flux given by (9.2) (see, for example, Rosen 1984).

As we have seen in chapter 8, magnetic fields of the order of few megagauss are easily created in the corona of laser-produced plasma (see

figure 9.1). Magnetic fields significantly affect the electron transport if

$$\omega_{ce}\tau_e > 1, \qquad \omega_{ce} = \frac{eB}{m_e c} \tag{9.9}$$

where τ_e is the angular scattering time of the electron and ω_{ce} is the Larmor angular frequency. Assuming that the main contribution to τ_e is from electron–ion collisions, then (see section 2.2)

$$\tau_e[\mathrm{s}] \approx \tau_{ei} = 3.44 \times 10^{-16}\left[\left(\frac{10}{Z}\right)\left(\frac{10^{22}\,\mathrm{cm}^{-3}}{n_e}\right)\left(\frac{10}{\ln\Lambda}\right)\left(\frac{T_e}{100\,\mathrm{eV}}\right)^{3/2}\right] \tag{9.10}$$

and using

$$\omega_{ce}[\mathrm{s}^{-1}] = 1.76 \times 10^{13}\left(\frac{B}{\mathrm{MGauss}}\right) \tag{9.11}$$

one gets in practical units

$$\omega_{ce}\tau_e = 6.05 \times 10^{-3}\left(\frac{10}{Z}\right)\left(\frac{10^{22}\,\mathrm{cm}^{-3}}{n_e}\right)\left(\frac{10}{\ln\Lambda}\right)\left(\frac{T_e}{100\,\mathrm{eV}}\right)^{3/2}\left(\frac{B}{\mathrm{MGauss}}\right). \tag{9.12}$$

The megagauss magnetic fields were measured in the corona, where the electron density is much smaller than $10^{22}\,\mathrm{cm}^{-3}$ and the temperature can be much larger than 100 eV. In this case $\omega_{ce}\tau_e$ can be larger than one, and therefore in the corona the electron transport in a magnetized plasma might be relevant. However, in the more important domain of the energy transport, between the critical surface and the ablation surface, $\omega_{ce}\tau_e$ is in general smaller than one even if the large magnetic field penetrates from the corona into the solid. Thus the electron transport between the critical surface and the ablation surface seems not to be affected significantly by the magnetic field. We shall not further discuss in this chapter the transport in magnetized plasma.

Electron transport also plays an important role in spreading the absorbed laser energy uniformly around the solid target. It is well known that a high-laser-intensity beam does not have a uniform spatial distribution, and even for the same laser system the spatial intensity distribution changes from shot to shot. Therefore, a major difficulty in high-intensity laser–plasma experiments is the non-uniformity of the laser beams. This can cause irreproducible and uncontrollable experiments, and therefore is difficult to analyse and use in various applications (such as ICF). However, after a corona with a dimension much larger than the laser wavelength has been formed, the energy transport in the lateral direction (in the plasma) can redistribute the energy uniformly around the solid surface. Electron

conduction reduces the temperature within 'hot spots' and thus decreases the possible creation of hot and narrow filaments in the plasma.

Regarding the scenario in the corona, it is interesting to point out the possible existence of a double layer (DL) (see figure 9.1). The creation of hot electrons, also known as suprathermal electrons (see section 9.6), with a temperature higher by a factor of 10 or more than the cold temperature (the thermal electrons) may be associated with the formation of this DL in the expanding corona. The fastest particles, electrons and ions, in the low-density region lead the expansion of the plasma. The electric field in the expanding DL accelerates the ions and causes the fast electrons to turn back into the target. Such DLs were observed experimentally (Eliezer and Ludmirsky 1983) and suggested theoretically by the prediction of 'rarefaction shock waves' for $T_h/T_c > 9.9$ (Bezzerides *et al.* 1978, Wickens *et al.* 1978, Diebold *et al.* 1987). A rarefaction shock occurs (Zeldovich and Raizer 1966) when the following unusual condition is satisfied: $d^2P/dV^2 < 0$, $V = 1/\rho$, $\rho = m_i n_i$ in a plasma and P is the pressure. In this case P is composed of two components: $P = n_c k_B T_h + n_h k_B T_h$, where n_h and n_c are the electron densities of the hot and cold plasmas respectively.

Electron transport in plasmas has been a major issue since the beginning of modern plasma physics (Spitzer and Härm 1953, Rosenbluth *et al.* 1957, Spitzer 1962, Braginskii 1965, Trubnikov 1965, Hinton and Hezeltine 1976, Stacey 1980, Nicholson 1983, Horton 1989, Hazeltine and Meiss 1992). The electron transport phenomena in laser-produced plasma have been extensively discussed in the literature (Haines 1980, 1989, Key 1980, 1983, 1991, Bobin 1985, Shvarts 1986, Galeev and Natanzon 1991, Yamanaka 1991, Bell 1995). In this chapter we discuss electron transport phenomena relevant to laser-produced plasma.

9.2 The Rocket Model

We now consider a planar steady-state ablation from a target, as shown schematically in figure 9.1. In this section it is assumed that the fluxes of mass, momentum and energy are constant and the equation of state of an ideal gas is used:

$$\begin{aligned} \text{flux of mass} &= \rho u \\ \text{flux of momentum} &= P + \rho u^2 \\ \text{flux of energy} &= \frac{\gamma}{\gamma - 1} Pu + \frac{1}{2}\rho u^3 + q + I \end{aligned} \tag{9.13}$$

where u is the plasma flow velocity, ρ is the density, P is the pressure, q is the electron heat flux, I is the absorbed laser energy flux (erg s^{-1} cm^{-2}) and γ is the ratio of the heat capacity at constant pressure (C_P) to heat capacity at

constant volume C_V. The following **ideal gas equations of state** are also available:

$$\begin{aligned}
\text{internal energy:} \quad & \varepsilon = C_V T = \left(\frac{1}{\gamma - 1}\right)\frac{P}{\rho} \\
\text{enthalpy:} \quad & h = C_P T = \left(\frac{\gamma}{\gamma - 1}\right)\frac{P}{\rho} \\
& \gamma = \frac{C_P}{C_V} = \frac{g+2}{g} \\
\text{isothermal } (T = \text{const.}) \text{ speed sound:} \quad & c_T = \sqrt{\frac{P}{\rho}} \\
\text{isentropic } (S = \text{const.}) \text{ speed sound:} \quad & c_S = \sqrt{\frac{\gamma P}{\rho}}
\end{aligned} \tag{9.14}$$

where g is the number of degrees of freedom of one particle. For a monoatomic gas $g = 3$ and $\gamma = \frac{5}{3}$. For electrons in the plasma $\gamma = \frac{5}{3}$, so that $\gamma/(\gamma - 1) = \frac{5}{2}$.

We now write six equations describing the flux conservation for mass, momentum and energy, according to (9.13), at the critical surface and at the ablation surface:

at the critical surface:

$$\begin{aligned}
& \rho_c u_c = \rho u \equiv \dot{m} \\
& \rho_c u_c^2 + P_c = \rho u^2 + P \\
& \dot{m}\left[\left(\frac{5}{2}\right)\frac{P_c}{\rho_c} + \left(\frac{1}{2}\right)u_c^2\right] + q_{out} = \dot{m}\left[\left(\frac{5}{2}\right)\frac{P}{\rho} + \left(\frac{1}{2}\right)u^2\right] + q_{in} + I \\
& q_{out} = \rho u_c^3 = \dot{m} u_c^2 \quad \text{(free streaming plasma)}
\end{aligned} \tag{9.15}$$

at the ablation surface:

$$\begin{aligned}
& \dot{m} = \rho u = \text{const.} \quad \text{('source' of plasma)} \\
& P_a = \rho u^2 + P \quad \text{(ablation pressure)} \\
& \dot{m}\left[\left(\frac{5}{2}\right)\frac{P}{\rho} + \left(\frac{1}{2}\right)u^2\right] + q_{in} = 0
\end{aligned}$$

where the quantities with the index c denote the variables at the critical surface from the corona side, while those without the index c denote the values between the corona and the ablation surface. Note that at the ablation surface $u = 0$ and $P = P_a$. Since in the corona the temperature is constant to a good approximation, it is conceivable that the plasma expands with the

isothermal speed of sound in the corona c_T given by

$$u_c = c_T = \sqrt{\frac{P}{\rho}}. \tag{9.16}$$

Using this relation together with the first two relations of (9.15) and the value of the ablation pressure (the sixth relation of (9.15)), one gets

$$P_a = 2\dot{m}c_T. \tag{9.17}$$

The third, the fourth and the last of equations (9.15) yield

$$I = 4\dot{m}c_T^2. \tag{9.18}$$

Using now the rocket equation for a one-dimensional plane geometry,

$$m(t)\frac{dv(t)}{dt} = P_a. \tag{9.19}$$

The mass $m(t)$ (g/cm^2) is accelerated to a velocity $v(t)$ at a time t by an ablation pressure P_a. The accelerated mass is defined by

$$m(t) = m_0 - \int_0^t \left(\frac{dm}{dt}\right) dt = m_0 - \dot{m}t \tag{9.20}$$

where it is assumed that the rate of plasma production is constant, i.e. $dm/dt = \text{constant}$ and m_0 is the initial mass. Substituting (9.17) and (9.20) into (9.19),

$$(m_0 - \dot{m}t)\frac{dv}{dt} = 2\dot{m}c_T \tag{9.21}$$

and integrating, the plasma rocket equation is obtained:

$$v(t) = 2c_T \ln\left(\frac{m_0}{m(t)}\right). \tag{9.22}$$

The hydrodynamic efficiency η_h is defined by

$$\eta_h = \frac{\frac{1}{2}m(t)v(t)^2}{I\tau} \tag{9.23}$$

where $\tau \approx \tau_L$ is the absorption time of the laser energy which is of the order of the laser pulse duration τ_L, I is the (time) average absorbed laser flux and $I \cdot \tau$ is the absorbed energy (erg/cm^2). Using equations (9.18), (9.20) and (9.22) into (9.23), one gets the hydrodynamic efficiency:

$$\eta_h = \frac{X(\ln X)^2}{2(1-X)}, \qquad X \equiv \frac{m(\tau)}{m_0}. \tag{9.24}$$

Note that for $X = 0.3$ the hydrodynamic efficiency is 30%, while for $X = 0.9$ the efficiency drops to 5%.

We now generalize the above analysis in order to estimate the ablation pressure necessary to accelerate a thin spherical shell to high velocities. The initial mass of this shell can be written as

$$m_0 = \rho_0 \Delta R_0 \tag{9.25}$$

where ρ_0 and ΔR_0 are the initial density and shell thickness accordingly. If during the acceleration period τ, of the order of the laser pulse duration, the shell radius R is much larger than its thickness ΔR, then for each segment of the shell one can use the plane geometry formulas, as derived above. Using (9.25) together with (9.17), (9.18), (9.23) and (9.24), the ablation pressure is

$$P_a = \left(\frac{X}{\eta_h}\right)\left(\frac{R_0}{4c_T\tau}\right)\left(\frac{\Delta R_0}{R_0}\right)[\rho_0 v(\tau)^2] \tag{9.26}$$

where $v(\tau)$ is the final (maximum) velocity of the accelerated shell, c_T (the isothermal sound velocity in the corona) is the exhaust velocity of the plasma causing the acceleration and $R_0/\Delta R_0$ is called the aspect ratio, limited (the maximum value) by hydrodynamic instabilities. From this equation one can see that for a given final shell velocity the required ablation pressure is inversely proportional to the hydrodynamic efficiency, and the larger the aspect ratio the less ablation pressure is needed. As an example, relevant to ICF, assuming $X/\eta_h \approx 0.5$, $R_0/(4c_T\tau) \approx 1$, $R_0/(\Delta R_0) = 10$, $\rho_0 = 0.2\,\mathrm{g/cm^3}$, one requires an ablation pressure of $P_a \approx 100\,\mathrm{Mbar}$ in order to achieve a shell velocity of $v \approx 10^8\,\mathrm{cm/s}$.

9.3 Relaxation Rates

In analysing a test particle, denoted by an index 1, moving with velocity $\mathbf{v}_1$ and interacting with a background plasma composed of particles, labelled 2, there are four relaxation rates τ of interest: the momentum loss or slowing down, the energy loss and two relaxation times related to transverse and parallel diffusion. In this section we only discuss the momentum loss and energy loss relaxation rates.

The relevant interactions discussed here are the Coulomb interaction between two charged particles (charges q_1 and q_2), described by the Rutherford cross section σ_{12} (see section 2.2). As in section 2.2, the impact parameter is denoted by b, $\mathbf{v}$ is the relative velocity between the colliding two particles (with indices 1 and 2), and the reduced mass is defined by

$$m_r = \frac{m_1 m_2}{m_1 + m_2} \tag{9.27}$$

CM and L label the centre of mass and the laboratory coordinates accordingly and θ is the scattering angle in the collision (see figure 9.2).

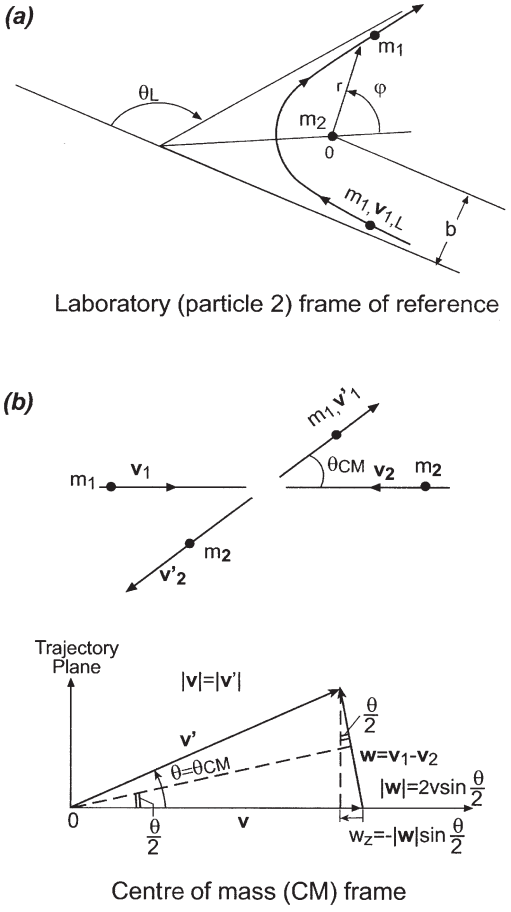

Figure 9.2. (a) Laboratory and (b) centre of mass (CM) frames of reference. In (a) the orbit is shown for a charged particle with mass m_1 scattered by a charged particle (with opposite charge) with mass m_2, positioned at O.

Conservation of momentum and energy of the Coulomb collision yields the scattering angle in the centre of mass (CM) system (in c.g.s. units):

$$\tan\left(\frac{\theta_{\mathrm{CM}}}{2}\right) = \frac{|q_1 q_2|}{m_{\mathrm{r}} v^2 b} \tag{9.28}$$

and the scattering angle of particle 1 in the laboratory frame is given by

$$\cot\theta_{\mathrm{L}} = \cot\theta_{\mathrm{CM}} + \frac{m_1}{m_2}\left(\frac{1}{\sin\theta_{\mathrm{CM}}}\right). \tag{9.29}$$

Since the collisions of interest are between the pairs electron–electron (ee), electron–ion (ei), ion–electron (ie) and ion–ion (ii), the following special cases are of interest:

$$\begin{aligned} m_1 \ll m_2: &\quad \theta_{\mathrm{L}} \approx \theta_{\mathrm{CM}} \\ m_1 = m_2: &\quad \theta_{\mathrm{L}} \approx \frac{\theta_{\mathrm{CM}}}{2} \\ m_1 \gg m_2: &\quad \theta_{\mathrm{L}} \approx \frac{m_2}{m_1}\sin\theta_{\mathrm{CM}}. \end{aligned} \tag{9.30}$$

All particles of type 1 incident into a ring between b and $b + \mathrm{d}b$ are scattered into angles θ_{CM} and $\theta_{\mathrm{CM}} + \mathrm{d}\theta_{\mathrm{CM}}$ in the CM frame of reference (or into angles θ_{L} and $\theta_{\mathrm{L}} + \mathrm{d}\theta_{\mathrm{L}}$ in the laboratory frame of reference). Therefore, the impact parameter b is related to the differential cross section $\mathrm{d}\sigma_{12}$ by

$$\mathrm{d}\sigma_{12}(\theta_{\mathrm{CM}}) = \sigma_{12}(\theta_{\mathrm{CM}})\,\mathrm{d}\Omega = \sigma_{12}(\theta_{\mathrm{CM}})2\pi\sin\theta_{\mathrm{CM}}\,\mathrm{d}\theta_{\mathrm{CM}} = 2\pi b\,\mathrm{d}b \tag{9.31}$$

where Ω is the solid angle and $\sigma(\theta_{\mathrm{CM}})$ is the Rutherford cross section (using (9.28)):

$$\sigma(\theta_{\mathrm{CM}}) = \frac{b\,\mathrm{d}b}{\sin\theta_{\mathrm{CM}}\,\mathrm{d}\theta_{\mathrm{CM}}} = \frac{(q_1 q_2)^2}{[2m_{\mathrm{r}}v^2\sin^2(\theta_{\mathrm{CM}}/2)]^2}. \tag{9.32}$$

Since the angle of deflection increases with the decrease of the impact parameter (see (9.28)), the cross section that a particle is scattered at any angle larger than 90° is given by the impact parameter for $\theta = 90^\circ$:

$$\sigma_{12}(\theta_{\mathrm{CM}} \geq 90^\circ) = \pi b(90^\circ)^2 = \frac{\pi q_1^2 q_2^2}{m_{\mathrm{r}}^2 v^4} \tag{9.33}$$

where equation (9.28) has been used.

Equation (9.33) gives the cross section for a scattering angle larger than or equal to 90° in one collision. Now we calculate small-angle scattering that adds up to a large angle, say 90° deflection. We denote the small-angle scattering in the centre of mass frame by θ ($\theta \ll 1$). From equation (9.28),

$$\theta = \frac{2|q_1 q_2|}{m_{\mathrm{r}}v^2 b}. \tag{9.34}$$

The mean square deflection of a particle (called the test particle) that goes along a distance L in a plasma with a density of particles n_2 (here we calculate the deflection caused by particles of type 2) is

$$\begin{aligned} \theta_{\mathrm{CM}}^2 &= \sum \theta^2 = n_2 L \int_{\theta_{\min}}^{\theta_{\max}} \theta^2 \sigma_{12}(\theta) 2\pi\sin\theta\,\mathrm{d}\theta \\ &= \frac{18\pi n_2 L q_1^2 q_2^2}{m_{\mathrm{r}}^2 v^4}\int_{b_{\min}}^{b_{\max}} \frac{\mathrm{d}b}{b} = \frac{18\pi n_2 L q_1^2 q_2^2 \ln\Lambda}{m_{\mathrm{r}}^2 v^4} \end{aligned} \tag{9.35}$$

where the Coulomb cutoff coefficient is defined by the ratio of Debye length to the distance of closest approach (see section 2.2):

$$\Lambda = \frac{b_{\max}}{b_{\min}} = \left(\frac{3}{2\sqrt{\pi}}\right)\left(\frac{1}{q_1 q_2^2}\right)\left[\frac{(k_B T)^3}{n_2}\right]^{1/2}. \tag{9.36}$$

The following relation has been used between the relative velocity v and the temperature T:

$$\tfrac{1}{2} m_r v^2 = \tfrac{3}{2} k_B T. \tag{9.37}$$

The mean free path for large angle deflection, L_{90}, is obtained from (9.35) by substituting there $\theta_{CM}^2 = 1$, yielding the cross section σ_{90} for a large-angle scattering due to many small-angle deflections,

$$\begin{aligned} L_{90} &= \frac{m_r^2 v^4}{18\pi q_1^2 q_2^2 n_2 \ln\Lambda} = \frac{(k_B T)^2}{2\pi q_1^2 q_2^2 n_2 \ln\Lambda} \\ \sigma_{90} &= \frac{1}{n_2 L_{90}} = \frac{18\pi q_1^2 q_2^2 \ln\Lambda}{m_r^2 v^4} = \frac{2\pi q_1^2 q_2^2 \ln\Lambda}{(k_B T)^2} \end{aligned} \tag{9.38}$$

where (9.37) has been used. Note that the first of equations (9.38) is the equation given in (9.1) ($q_1 = -e$, $q_2 = Z$ and $Z n_2 = n_e$).

It is important to note that the probability (which is proportional to the cross section) of a large-angle scattering due to a single collision (in most plasmas) is significantly smaller than the probability of a large deflection caused by many small-angle scatterings:

$$\frac{\sigma_{90}}{\sigma(\theta_{CM} \geq 90^\circ)} = 8 \ln\Lambda. \tag{9.39}$$

Equation (9.39) is derived from equations (9.33) and (9.38). The factor of $8 \ln\Lambda$ is in the domain of 10–10^2 for most plasma systems discussed in this book. This fact is very important in analysing collision phenomena in plasmas.

The time required for large-angle deflection, in the CM system, is obtained from (9.38) and (9.37):

$$\tau_{90} = \frac{L_{90}}{v} = \left(\frac{3\sqrt{3}}{8\pi}\right)\frac{\sqrt{m_r}(k_B T)^{3/2}}{q_1^2 q_2^2 n_2 \ln\Lambda}. \tag{9.40}$$

We are interested in the large-angle deflection times in the laboratory frame of reference. Therefore, from equation (9.30), one gets that if $m_2 \geq m_1$ then the deflection in the laboratory system is comparable with that in the CM system, so that the calculated value of L_{90} in the CM system is the same

as in the laboratory system. Therefore, one can use the above formulae for e–e, e–i and i–i collisions. However, for i–e collisions (the test particle is the ion which is scattered by electrons) it follows from equation (9.30) that $\theta_L \sim (m_e/m_i)\theta_{CM}$, i.e. since m_e/m_i is about 1/2000 (for the hydrogen plasma) the test particle (the ion) must travel a 2000 times larger distance in order to undergo a large deflection in the laboratory frame. For the identical particle collisions the reduced mass is half the particle mass, and a factor of 2 was introduced since $\theta_L \approx \frac{1}{2}\theta_{CM}$ (see equation (9.30)).

From the above formalism (equation (9.40)) the following collision times for large-angle scattering, or equivalently the **momentum loss relaxation times** τ, are obtained (we drop the subscript 90), as seen in the laboratory frame of reference (note that **the first particle in the superscript is the test particle**):

$$\begin{aligned}
\tau^{ee} &= \left(\frac{3\sqrt{6}}{8}\right)\frac{\sqrt{m_e}(k_B T)^{3/2}}{\pi e^4 n_e \ln\Lambda} \\
&\approx 1.07\times 10^{-11}\left(\frac{10^{20}\,\mathrm{cm}^{-3}}{n_e}\right)\left(\frac{10}{\ln\Lambda}\right)\left(\frac{T_e}{1\,\mathrm{keV}}\right)^{3/2} \quad [\mathrm{s}] \\
\tau^{ii} &= \left(\frac{3\sqrt{6}}{8}\right)\frac{\sqrt{m_i}(k_B T)^{3/2}}{\pi Z^4 e^4 n_i \ln\Lambda} \\
\tau^{ei} &= \left(\frac{3\sqrt{3}}{8}\right)\frac{\sqrt{m_e}(k_B T)^{3/2}}{\pi Z^4 e^4 n_i \ln\Lambda} \\
\tau^{ie} &\approx \left(\frac{m_i}{m_e}\right)\tau^{ei}.
\end{aligned} \tag{9.41}$$

Assuming a neutral plasma, $n_e = Zn_i$ and the same temperature, one can get from the last equation the following order of the large-angle deflection collision times:

$$\tau^{ee} : \tau^{ei} : \tau^{ii} : \tau^{ie} \approx 1 : \frac{1}{Z\sqrt{2}} : \frac{1}{Z^3}\left(\frac{m_i}{m_e}\right)^{1/2} : \frac{1}{Z^3\sqrt{2}}\left(\frac{m_i}{m_e}\right). \tag{9.42}$$

The large-angle scattering collision time calculated here is an approximation of the momentum loss of the test particle. If a particle has an initial momentum in some direction, after scattering to a large angle the momentum in the initial direction is lost.

We now estimate the time required for a test particle to lose its energy. From momentum and energy conservation during a collision, a test particle 1, with energy E_1, is releasing energy ΔE_1 in the laboratory

frame according to the equation

$$\frac{\Delta E_1}{E_1} = \frac{4m_1 m_2}{(m_1 + m_2)^2} \sin^2\left(\frac{\theta_{\mathrm{CM}}}{2}\right). \tag{9.43}$$

The energy lost in multiple-scattering small-angle collisions can be calculated by substituting $\theta_{\mathrm{CM}} = 90^\circ$ in the last equation, yielding

$$\frac{\Delta E_1}{E_1} = \frac{2m_1 m_2}{(m_1 + m_2)^2}. \tag{9.44}$$

Therefore, in 90° collisions between identical particles, half of the initial energy is transferred by the test particle to the background particles. However, for electron–ion scattering only the fraction $m_{\mathrm{e}}/m_{\mathrm{i}}$ of the initial energy of the test particle is transferred during 90° deflection. Denoting by τ_{E} **the energy relaxation time**, i.e. the time that $\Delta E_1/E_1 \approx 1$, one gets from equations (9.41), (9.42) and (9.44) (for $n_{\mathrm{e}} = Zn_{\mathrm{i}}$),

$$\begin{aligned}
\tau_{\mathrm{E}}^{\mathrm{ee}} &\approx \tau^{\mathrm{ee}} \\
\tau_{\mathrm{E}}^{\mathrm{ii}} &\approx \tau^{\mathrm{ii}} \approx \frac{1}{Z^3}\left(\frac{m_{\mathrm{i}}}{m_{\mathrm{e}}}\right)^{1/2} \tau^{\mathrm{ee}} \\
\tau_{\mathrm{E}}^{\mathrm{ei}} &\approx \frac{1}{Z}\left(\frac{m_{\mathrm{i}}}{m_{\mathrm{e}}}\right) \tau^{\mathrm{ee}} \\
\tau_{\mathrm{E}}^{\mathrm{ie}} &\approx \left(\frac{m_{\mathrm{i}}}{m_{\mathrm{e}}}\right) \tau^{\mathrm{ie}} \approx \left(\frac{m_{\mathrm{i}}}{m_{\mathrm{e}}}\right)^2 \tau^{\mathrm{ei}} \\
\tau^{\mathrm{ee}} : \tau_{\mathrm{E}}^{\mathrm{ee}} : \tau_{\mathrm{E}}^{\mathrm{ii}} : \tau_{\mathrm{E}}^{\mathrm{ei}} &\approx 1 : 1 : \frac{1}{Z^3}\left(\frac{m_{\mathrm{i}}}{m_{\mathrm{e}}}\right)^{1/2} : \frac{1}{Z}\left(\frac{m_{\mathrm{i}}}{m_{\mathrm{e}}}\right).
\end{aligned} \tag{9.45}$$

To conclude this analysis, it is important to note that the collision frequency ν^{12} for momentum loss and the collision frequency ν_{E}^{12} for the energy loss, where 1 denotes the test particle and 2 the background particles, are related to the relaxation times calculated above by

$$\nu^{12} = \frac{1}{\tau^{12}}, \qquad \nu_{\mathrm{E}}^{12} = \frac{1}{\tau_{\mathrm{E}}^{12}}. \tag{9.46}$$

The last of equations (9.45) show that electrons equilibrate, i.e. reach an equilibrium distribution (e.g. a Maxwell distribution of velocities), on a shorter time scale than the ions do by a factor of $Z^3(m_{\mathrm{e}}/m_{\mathrm{i}})^{1/2}$. Moreover, the electrons reach equilibrium with the ions on a time scale longer by a factor $(1/Z)(m_{\mathrm{i}}/m_{\mathrm{e}})$ than the electrons equilibrate with themselves. For example, in a typical corona of laser-produced plasma with an electron density $10^{20}\,\mathrm{cm}^{-3}$, an ion charge $Z = 10$, $m_{\mathrm{i}}/m_{\mathrm{e}} \approx 4 \times 10^4$ and an electron temperature 1 keV, $\ln\Lambda \approx 10$, one gets from equations (9.41) and (9.45)

that we can define an electron temperature after ~10 ps from the start of the laser–target interaction, an ion temperature after ~2 ps (note that for a hydrogen plasma this relaxation time changes to ~200 ps) and that the electron temperature is equal to the ion temperature after 40 ns. Thus, for most high-intensity laser pulses (0.1 ns to 10 ns) there is no equilibrium between the electrons and the ions in the corona. It is worth mentioning that for a solid state density plasma, $n_e \approx 10^{23}$, produced for example by a very short pulse duration (~100 fs), the above time scales are reduced by a factor of 1000 (assuming the same temperature). In this case the electrons will reach an equilibrium distribution with a temperature of 1 keV in about 10 fs.

The multiple small-angle scattering of the plasma introduces the **Coulomb logarithm ln Λ**, a factor included in the transport coefficients as well. $\ln \Lambda = b_{max}/b_{min}$ results from integration over the scattering angles θ, between large angles resulting from a small impact parameter b_{min} and small angles resulting from a large impact parameter b_{max}. The value of b_{max} is taken as the Debye shielding scale and is a function of electron velocity (i.e. temperature) and density. If the electrons move in a strong magnetic field, where the Larmor radius is smaller than the Debye length, then the Larmor radius should replace the value of b_{max}. However, this is seldom required in the laser-produced plasma. Last but not least, in dense and cold plasma the values of b_{max} and b_{min} are comparable and $\ln \Lambda$ may become negative, an unphysical result. This can happen when a large-angle deflection is more probable than the small-angle scattering. Such a plasma medium is the strongly-coupled plasma, where the electric potential energy is larger than the kinetic energy. In this case a value of $\ln \Lambda = 2$ is taken for practical calculations.

In conclusion, for plasmas where the small-angle scatterings are dominant, the Coulomb scattering of the plasma particles has a randomizing effect on the particle motion. Therefore, in this case, the electron drift motion may be described by diffusion or in the more general case by the Fokker–Planck equation.

9.4 The Fokker–Planck Equation

The electron energy transport can be described by the Boltzmann equation (see section 3.4):

$$\frac{\partial f}{\partial t} + \mathbf{v} \cdot \frac{\partial f}{\partial \mathbf{r}} + \frac{e\mathbf{E}}{m_e} \cdot \frac{\partial f}{\partial \mathbf{v}} = \left(\frac{\partial f}{\partial t}\right)_{coll} \tag{9.47}$$

where $f = f(\mathbf{r}, \mathbf{v}, t)$ is the electron density in phase space, $\mathbf{r} - \mathbf{v}$ space, $\mathbf{r}$ is the space coordinate and $\mathbf{v}$ is the particle velocity. $\mathbf{E}$ is the electrical field in the plasma and the magnetic field is neglected in (9.47). $(\partial f/\partial t)_{coll}$ is the collision term describing the scattering of electrons (by electrons and ions), as

described in the previous section. Assuming that the small-angle collisions are dominant, one can use the Fokker–Planck equation for the collision term.

The Fokker–Planck equation is derived in general by assuming a **Markov process**. If a measurable physical quantity develops in time in such a way that its 'future value' depends only on its 'present value', then the phenomenon describing this physical quantity is called a Markov process. In such a process the physical quantity changes in a random way. Let us take a physical variable X with measured values X_n, X_{n-1}, ..., X_1, X_0 at times $t_n > t_{n-1} > \cdots > t_1 > t_0$ respectively. The probability P to measure the value X_n, where the previous values were X_{n-1}, ..., X_1, X_0, in a Markov process is given by

$$P(X_n|X_{n-1}, \ldots, X_1, X_0) = P(X_n|X_{n-1}). \tag{9.48}$$

This equation describes the fact that the value X_n, measured at time t_n, depends only on its value X_{n-1} as measured at time t_{n-1}. A trivial example for a Markov process is the flipping of a coin. Then the number X_n of heads after n flips depends only on the number of heads X_{n-1} after $n-1$ flips, and not on all the history.

In analysing a continuous Markov process the situation is more complicated. If the physical phenomenon is described by a continuous function, then the existence of the derivatives contradicts the definition of the Markov process. For example, in this case X_{n+1} depends not only on X_n but also on the derivative $(\mathrm{d}X_n/\mathrm{d}t) = (X_n - X_{n-1})/\Delta t$, etc. Therefore, a Markov process may describe a continuous physical phenomenon only as an approximation. For example, in a Brownian motion the particle velocity undergoes a rapid variation due to each molecular collision, followed by a low-rate change due to the friction force. On a time scale of one collision the scattering is not Markovian. However, on a time scale of many collisions the Markov process is a very good approximation.

In plasma, due to the long-range Coulomb forces there are many small-angle scatterings causing large deflections (see previous section). The distribution function $f(v, t)$ is changing slowly on a time scale δt describing one (small-angle) collision. The Markov process may describe the changes on a time scale Δt, due to many small-angle collisions. In this case it is required that $\delta t \ll \Delta t$; however, Δt is small enough to define the variations and the derivatives of the physical quantities.

According to equation (9.48) for a Markov process the distribution function $f(v, t)$ is determined from the knowledge of $f(v - w, t)$, where $w = \Delta v$ is the change in velocity in the time interval Δt due to multiple small-angle collisions. It is assumed here that the distribution function in phase-space can be written $f(r, v, t) = n_0 f(v, t)$, where the spatial dependence is given by the constant n_0 (dimension cm^{-3}). The probability that a particle changes its velocity from v to $v + w$ is given by $P(v; w)$. If only

collisions are responsible to the change in $f(v,t)$, then one can write

$$\begin{aligned} f(\mathbf{v},t) &= \int P(\mathbf{v}-\mathbf{w};\mathbf{w}) f(\mathbf{v}-\mathbf{w}, t-\Delta t)\,\mathrm{d}^3 w \\ &\approx f(\mathbf{v},t)\int P(\mathbf{v};\mathbf{w})\,\mathrm{d}^3 w - \Delta t \frac{\partial f(\mathbf{v},t)}{\partial t}\int P(\mathbf{v};\mathbf{w})\,\mathrm{d}^3 w \\ &\quad - \int \sum_i w_i \frac{\partial}{\partial v_i}[P(\mathbf{v};\mathbf{w}) f(\mathbf{v},t)]\,\mathrm{d}^3 w \\ &\quad + \frac{1}{2}\int \sum_{i,j} w_i w_j \frac{\partial^2}{\partial v_i\,\partial v_j}[P(\mathbf{v};\mathbf{w}) f(\mathbf{v},t)] \end{aligned} \tag{9.49}$$

where a Taylor expansion has been made to second order, a good approximation for $\mathbf{w}$ small and Δt small. The indices i and j are the vector components in an orthogonal frame of reference. The integral of the probability function is one:

$$\int P(\mathbf{v};\mathbf{w})\,\mathrm{d}^3 w = 1 \tag{9.50}$$

and the rate of change of the first moment $\langle \mathbf{w} \rangle$ (dimension cm/s^2) and the second moments $\langle \mathbf{ww} \rangle$ (dimension cm^2/s^3) of $\mathbf{w}$ are

$$\begin{aligned} \langle w_i \rangle &= \frac{1}{\Delta t}\int P(\mathbf{v};\mathbf{w}) w_i\,\mathrm{d}^3 w \\ \langle w_i w_j \rangle &= \frac{1}{\Delta t}\int P(\mathbf{v};\mathbf{w}) w_i w_j\,\mathrm{d}^3 w. \end{aligned} \tag{9.51}$$

Substituting (9.50) and (9.51) into (9.49), one gets the **Fokker–Planck equation**

$$\left(\frac{\partial f}{\partial t}\right)_{\mathrm{coll}} = -\sum_i \frac{\partial}{\partial v_i}[\langle w_i \rangle f(\mathbf{v},t)] + \frac{1}{2}\sum_{i,j}\frac{\partial^2}{\partial v_i\,\partial v_j}[\langle w_i w_j \rangle f(\mathbf{v},t)]. \tag{9.52}$$

The first term on the right-hand side describes a 'drift', while the second term is the diffusion in the velocity space. In uniform plasma in thermal equilibrium the drift term 'pushes' the electrons to a zero velocity, but the electrons do not accumulate there because the diffusion term 'pushes' them away from the zero velocity.

The Fokker–Planck equation (9.52) can also be viewed as a continuity equation in the velocity space, with a density $f(\mathbf{v})$ and a current $\mathbf{J}(\mathbf{v})$:

$$\left(\frac{\partial f}{\partial t}\right)_{\mathrm{coll}} + \frac{\partial}{\partial \mathbf{v}} \cdot \mathbf{J}_{\mathrm{v}} = 0, \qquad \mathbf{J}_{\mathrm{v}} = \langle \mathbf{w} \rangle f - \frac{1}{2}\frac{\partial}{\partial \mathbf{v}} \cdot [\langle \mathbf{ww} \rangle f]. \tag{9.53}$$

As in the previous section, the test particles are denoted by index 1 and the background particles acquire index 2. The probability per unit time

($P\,\mathrm{d}^3v/\Delta t$) in equations (9.51) that a test particle, moving with relative velocity $\mathbf{v}_1 - \mathbf{v}_2$ relative to a background particle (moving with velocity $\mathbf{v}_2$), is scattered by the background particles, with a density $f_2\,\mathrm{d}^3v$, into the solid angle $\mathrm{d}\Omega$ is given by

$$\frac{P(\mathbf{v}_1;\mathbf{v}_2)\,\mathrm{d}^3\mathbf{v}_2}{\Delta t} = f_2(\mathbf{r}_2,\mathbf{v}_2,t)\sigma_{12}(v,\boldsymbol{\Omega})v\,\mathrm{d}^3\mathbf{v}_2\,\mathrm{d}\boldsymbol{\Omega}, \qquad v \equiv |\mathbf{v}_1 - \mathbf{v}_2| \tag{9.54}$$

where σ_{12} is the Rutherford cross section given in the CM frame by (9.32). The approximation $f(\mathbf{r},\mathbf{v},t) = n(\mathbf{r})f(\mathbf{v},t)$ is used, where $n(\mathbf{r})$ is the spatial density. $n(\mathbf{r})$ is omitted in the following analysis, since it cancels out in the Fokker–Planck equation (9.52). Note that the dimension of $f(\mathbf{r},\mathbf{v},t)$ is ($\mathrm{cm}^{-6}\,\mathrm{s}^3$), while the dimension of $f(\mathbf{v},t)$ is ($\mathrm{cm}^{-3}\,\mathrm{s}^3$).

Substituting (9.54) into (9.51), one has to calculate the averages

$$\begin{aligned}
\langle \mathbf{w}_1 \rangle &= \int \mathrm{d}^3v_2 \int \mathrm{d}\Omega\, \mathbf{w}_1 v\sigma(v,\boldsymbol{\Omega})f_2(\mathbf{v}_2) \\
\langle \mathbf{w}_1\mathbf{w}_1 \rangle &= \int \mathrm{d}^3v_2 \int \mathrm{d}\Omega\, \mathbf{w}_1\mathbf{w}_1 v\sigma(v,\boldsymbol{\Omega})f_2(\mathbf{v}_2) \\
\mathbf{w}_1 &= \mathbf{v}_1' - \mathbf{v}_1(\text{in lab. frame}) = \frac{m_2}{m_1+m_2}(\mathbf{v}' - \mathbf{v}) \equiv \frac{m_2}{m_1+m_2}\mathbf{w} \qquad (9.55) \\
&\left.\begin{aligned} \mathbf{v} &= \mathbf{v}_1 - \mathbf{v}_2 \\ \mathbf{v}' &= \mathbf{v}_1' - \mathbf{v}_2' \end{aligned}\right\}(\text{in CM frame}) \\
v &= |\mathbf{v}| = |\mathbf{v}'|
\end{aligned}$$

where primes denote the velocity value after the collision. The third equation of (9.55) is derived from the relation between the particle velocity in the laboratory frame and the particle velocity in the CM frame:

$$\begin{aligned}
\mathbf{v}_1(\text{lab}) &= \mathbf{v}_{\text{cm}} + \left(\frac{m_2}{m_1+m_2}\right)\mathbf{v} \\
\mathbf{v}_1'(\text{lab}) &= \mathbf{v}_{\text{cm}} + \left(\frac{m_2}{m_1+m_2}\right)\mathbf{v}' \\
\mathbf{v}_2(\text{lab}) &= \mathbf{v}_{\text{cm}} - \left(\frac{m_1}{m_1+m_2}\right)\mathbf{v} \\
\mathbf{v}_2'(\text{lab}) &= \mathbf{v}_{\text{cm}} - \left(\frac{m_1}{m_1+m_2}\right)\mathbf{v}'
\end{aligned} \tag{9.56}$$

where $\mathbf{v}_{\text{cm}}$ is the velocity of the centre of mass. The last equation of (9.55) is obtained by using in the centre of mass energy conservation ($\frac{1}{2}m_1v_1^2 + \frac{1}{2}m_2v_2^2 = \frac{1}{2}m_1v_1'^2 + \frac{1}{2}m_2v_2'^2$) and momentum conservation ($m_1\mathbf{v}_1 + m_2\mathbf{v}_2 = 0$; $m_1\mathbf{v}_1' + m_2\mathbf{v}_2' = 0$).

The change (in one collision) of the relative velocity **w** in the CM frame in Cartesian coordinates, where the z axis is chosen parallel to **v**, is (see figure 9.2)

$$\begin{aligned} w_z &= -2v\sin^2\left(\frac{\theta}{2}\right) \\ w_x &= 2v\sin\left(\frac{\theta}{2}\right)\cos\left(\frac{\theta}{2}\right)\cos\phi \\ w_y &= 2v\sin\left(\frac{\theta}{2}\right)\cos\left(\frac{\theta}{2}\right)\sin\phi \\ \mathrm{d}\Omega &= \sin\theta\,\mathrm{d}\theta\,\mathrm{d}\phi. \end{aligned} \tag{9.57}$$

Using (9.57) and the Rutherford cross section (9.32) in equations (9.55), one gets

$$\begin{aligned} \langle \mathbf{w}_1 \rangle &= -\Gamma_{12}\left(1+\frac{m_1}{m_2}\right)\int \mathrm{d}^3 v_2 f_2(\mathbf{v}_2)\frac{\mathbf{v}_1-\mathbf{v}_2}{|\mathbf{v}_1-\mathbf{v}_2|^3} \\ \Gamma_{12} &\equiv \frac{4\pi q_1^2 q_2^2 \ln\Lambda}{m_1^2}. \end{aligned} \tag{9.58}$$

In obtaining this result the integral on $\mathrm{d}\Omega$ has been done. Thus, integrals with w_x and w_y yield zero (for the choice of reference in (9.57)), while with w_z one has (using (9.34) and (9.36))

$$\begin{aligned} \int \frac{\mathrm{d}\Omega}{\sin^4\left(\frac{\theta}{2}\right)} &= 2\pi\int \frac{\mathrm{d}\theta\sin\theta}{\sin^4\left(\frac{\theta}{2}\right)} = 2\pi\int_{\theta_{\min}}^{\theta_{\max}} \frac{\mathrm{d}\left(\frac{\theta}{2}\right)\cos\left(\frac{\theta}{2}\right)}{\sin\left(\frac{\theta}{2}\right)} \\ &= 2\pi\left[\ln\sin\left(\frac{\theta}{2}\right)\right]_{\theta_{\min}}^{\theta_{\max}} \approx 2\pi\left[\ln\left(\frac{\theta}{2}\right)\right]_{\theta_{\min}}^{\theta_{\max}} \\ &= 2\pi\ln\left(\frac{\theta_{\max}}{\theta_{\min}}\right) = 2\pi\ln\Lambda. \end{aligned} \tag{9.59}$$

Equation (9.58) can be written in a more convenient form by introducing the Rosenbluth potential $H(\mathbf{v})$, which satisfies a Poisson equation in the velocity space:

$$\begin{aligned} H_2(\mathbf{v}_1) &= \left(1+\frac{m_1}{m_2}\right)\int \mathrm{d}^3 v_2 \frac{f_2(\mathbf{v}_2)}{|\mathbf{v}_1-\mathbf{v}_2|} \\ \nabla_{\mathrm{v}}^2 H_2(\mathbf{v}_1) &= -4\pi\left(1+\frac{m_1}{m_2}\right) f_2(\mathbf{v}_1) \\ \langle \mathbf{w}_1 \rangle &= \Gamma_{12}\frac{\partial H_2(\mathbf{v}_1)}{\partial \mathbf{v}_1}. \end{aligned} \tag{9.60}$$

Using the differentiation laws,

$$\frac{\partial^2|\mathbf{v}_1-\mathbf{v}_2|}{\partial v_{1i}\,\partial v_{1j}}=\frac{\partial}{\partial v_{1i}}\left(\frac{v_{1j}}{|\mathbf{v}_1-\mathbf{v}_2|}\right)=\frac{\delta_{ij}}{|\mathbf{v}_1-\mathbf{v}_2|}-\frac{v_{1i}v_{1j}}{|\mathbf{v}_1-\mathbf{v}_2|^3} \tag{9.61}$$

and neglecting the integral terms not containing $\mathrm{d}\theta/\theta$ (considered to be small), one gets (i and j are the three components of an orthogonal frame of reference)

$$\begin{aligned} G_2(\mathbf{v}_1)&=\int \mathrm{d}^3v_2 f(\mathbf{v}_2)|\mathbf{v}_1-\mathbf{v}_2| \\ \nabla_{\mathrm{v}}^4 G_2(\mathbf{v}_1)&=-8\pi f_2(\mathbf{v}_1) \\ \langle w_{1i}w_{1j}\rangle&=\Gamma_{12}\frac{\partial^2 G_2}{\partial v_{1i}\,\partial v_{2j}}. \end{aligned} \tag{9.62}$$

Substituting (9.60) and (9.62) into (9.52), one gets the Fokker–Planck equation

$$\left(\frac{\partial f_\alpha(\mathbf{r},\mathbf{v},t)}{\partial t}\right)_{\mathrm{coll}}=\sum_\beta \Gamma_{\alpha\beta}\left[-\sum_{i=1}^{3}\frac{\partial}{\partial v_i}\left(f_\alpha(\mathbf{v},t)\frac{\partial H_\beta}{\partial v_i}\right)+\frac{1}{2}\sum_{i,j=1}^{3}\frac{\partial^2}{\partial v_i\,\partial v_j}\left(f_\alpha(\mathbf{v},t)\frac{\partial^2 G_\beta}{\partial v_i\,\partial v_j}\right)\right] \tag{9.63}$$

where f_α is the distribution of the α-th species of particles and the sum β on the right-hand side of (9.63) is over the collisions with the background particles (for the test particle α). The Rosenbluth potentials in (9.63) are defined according to (9.60) and (9.62):

$$H_\beta(\mathbf{v})=\left(1+\frac{m_\alpha}{m_\beta}\right)\int \mathrm{d}^3u\frac{f_\beta(\mathbf{u})}{|\mathbf{v}-\mathbf{u}|},\qquad G_\beta(v)=\int \mathrm{d}^3u|\mathbf{v}-\mathbf{u}|f_\beta(\mathbf{u}) \tag{9.64}$$

and the coupling constants $\Gamma_{\alpha\beta}$ are given in the approximation of equation (9.58) by

$$\Gamma_{\alpha\beta}=\frac{4\pi q_1^2 q_2^2 n_\alpha \ln\Lambda}{m_\alpha^2}. \tag{9.65}$$

The density of the α particles n_α has been included in (9.65) (in comparison with (9.58)) since the left-hand side of (9.63) describes the full distribution in phase space. This is necessary in order to substitute (9.63) (together with (9.64) and (9.65)) into the Boltzmann equation (9.47). The Boltzmann equation with the collisional term given in (9.63) is occasionally called the Fokker–Planck equation.

9.5 The Spitzer–Härm Conductivity

Knowledge of the time development of a fully ionized plasma due to collisions requires the simultaneous solution of the collisions of electrons with electrons, electrons with ions, ions with electrons and ions with ions. The general solution of these nonlinear integral-differential equations is not an easy task and can be done only with large computer resources. It is therefore very useful to look for simpler but approximate solutions that enable us to generate simple models of transport. The analytical models are very useful to comprehend the complicated phenomena of heat transfer in laser–plasma interaction.

For a distribution function depending on one space–one velocity coordinates x and v, and on the angle θ between the velocity and the spatial coordinate, $f = f(x, v, \cos\theta, t)$, the Fokker–Planck equation (9.63) can also be written as (Shkarofsky *et al.* 1966)

$$\left(\frac{\partial f}{\partial t}\right)_{\text{coll}} = \frac{1}{v}\frac{\partial}{\partial v}\left[v^2\left(\frac{D_{\|}}{2}\frac{\partial f}{\partial v} + Cf\right)\right] + \frac{D_{\perp}}{2v^2\sin\theta}\frac{\partial}{\partial\theta}\left(\sin\theta\frac{\partial f}{\partial\theta}\right) \tag{9.66}$$

where C (dimension (s^{-1})), $D_{\|}$ (dimension ($cm\,s^{-2}$)) and $D_{\perp}$ (dimension ($cm^2\,s^{-3}$)) are the coefficients of slowing down, diffusion in velocity space and diffusion in angular space respectively. These coefficients depend on the distribution function of the plasma electrons and ions. The angular diffusion term is dominated by electron–ion collisions, while the velocity diffusion term and the slowing down are more affected by electron–electron collisions. Therefore, for plasma with ion charge Z, the second term on the right-hand side of equation (9.66) is about Z times larger than the first term on the right-hand side of this equation (see equation (9.42), where the collision frequencies are proportional as $\tau_{\text{ee}}^{-1} : \tau_{\text{ei}}^{-1} = 1 : Z$).

If a plasma has a temperature gradient scale L_{T} much larger than the electron mean free path λ_{e}, $\lambda_{\text{e}} \ll L_{\text{T}}$ (λ_{e} and L_{T} are defined in (9.1) and (9.6)) and the distribution function has a weak angular dependence, then the electron distribution function can be expressed by the first two terms in a $\cos\theta$ perturbation expansion

$$f(x, v, \theta, t) = f_0(x, v, t) + f_1(x, v, t)\cos\theta \tag{9.67}$$

where f_0 and f_1 are the isotropic and the anisotropic components respectively. Since the large electron–ion collision frequency tends to maintain the distribution function almost isotropically, it is possible to neglect the higher-order terms in $\cos\theta$ in the expansion (9.67).

The isotropic component is assumed to be equal to the equilibrium Maxwellian distribution f_{M}:

$$f_0 = f_{\text{M}} = \frac{n_{\text{e}}}{(\pi)^{3/2}v_{\text{T}}^3}\exp\left(-\frac{v^2}{v_{\text{T}}^2}\right), \qquad f_1 \ll f_{\text{M}}, \qquad v_{\text{T}} \equiv \sqrt{\frac{2k_{\text{B}}T}{m_{\text{e}}}}. \tag{9.68}$$

The Boltzmann equation with the Fokker–Planck collision term has an analytic solution for the **Lorenz plasma**, i.e. ions with large Z, where f_1, the electric field E, $\partial f_M/\partial x$ and $\partial f_M/\partial t$ are small quantities (i.e. second-order terms or higher are neglected). Moreover, it is assumed that $\partial f_M/\partial t = 0$ and $\partial f_1/\partial t = 0$. In the Fokker–Planck equation (9.66) only the second term on the right-hand side contributes to a Lorenz plasma. Therefore, within those approximations, the Boltzmann equation (9.47) simplifies to

$$v\frac{\partial f_M}{\partial x} + \frac{eE}{m_e}\frac{\partial f_M}{\partial v} = -\frac{A}{v^3}f_1$$
$$A \equiv vD_\perp = \frac{8\pi Z n_e e^4 \ln\Lambda}{m_e} = \frac{v_T^3}{\tau_{ei}} = \frac{v_T^4}{\lambda_e} \tag{9.69}$$

where τ_{ei} is given in equation (9.41) and the electron mean free path λ_e equals L_{90} (for e–i collisions) in equation (9.40).

An additional equation is needed for the electric field E. Assuming charge neutrality in the plasma, which means that there is no electric current along the density gradient, gives the equation

$$J = \frac{4\pi e}{3}\int_0^\infty f_1 v^3\,\mathrm{d}v = 0. \tag{9.70}$$

This model, the Lorentz model, is described mathematically by equations (9.68), (9.69) and (9.70). Substituting (9.68) into (9.69) and using

$$\frac{1}{n_e}\frac{\partial n_e}{\partial x} = \frac{1}{L_n}, \qquad \frac{1}{T}\frac{\partial T}{\partial x} = \frac{1}{L_T} \tag{9.71}$$

one gets

$$f_1 = -\frac{v^3}{A}\left(\frac{v}{L_n} - \frac{3v}{2L_T} + \frac{v^3}{v_T^2 L_T} - \frac{2eEv}{m_e v_T^2}\right)f_M. \tag{9.72}$$

Substituting f_1 from (9.72) into (9.70) and using

$$\int_0^\infty \mathrm{d}v\, v^{2k+1}\exp\left(-\frac{v^2}{2v_T^2}\right) = \frac{k!}{2}(2v_T^2)^{k+1}, \quad k = 0, 1, 2, 3, \ldots \tag{9.73}$$

one gets an expression for the electric field (that cancels the current induced by the temperature gradient, see (9.4)):

$$\frac{2eE}{m_e v_T^2} = \frac{eE}{k_B T} = \left(\frac{1}{L_n} + \frac{5}{2L_T}\right). \tag{9.74}$$

This electric field is inserted into (9.72) to give the anisotropic electron distribution function f_1:

$$f_1 = \frac{n_e}{(\pi)^{3/2} A L_T v_T^3}\left(4v^4 - \frac{v^6}{v_T^2}\right)\exp\left(-\frac{v^2}{v_T^2}\right). \tag{9.75}$$

The heat flow is calculated by integrating in the velocity space the drifting electron distribution. The number (per cm^3) of drifting electrons with velocities between zero and v is given by $\frac{4}{3}\pi v^3 f_1$, and each electron carries an energy $\frac{1}{2}m_e v^2$. Therefore, the heat flux q is given by

$$q = \frac{2\pi m_e}{3}\int_0^\infty f_1 v^5\,\mathrm{d}v = \frac{m_e n_e}{3(\pi)^{1/2}AL_T v_T^3}\int_0^\infty \mathrm{d}v\left(4v^9 - \frac{v^{11}}{v_T^2}\right)\exp\left(-\frac{v^2}{v_T^2}\right). \quad (9.76)$$

After integrating (9.76) the heat flux is

$$q = -\left(\frac{4}{\sqrt{\pi}}\right)\frac{m_e n_e v_T^7}{AL_T} = -\left(\frac{12}{\sqrt{\pi}}\right)\lambda_e v_T n_e k_B \frac{\mathrm{d}T}{\mathrm{d}x} \quad (9.77)$$

where A was taken from equation (9.69), the relation between v_T and T is given in (9.68) and L_T was substituted from (9.71). The heat flux in this equation is the Lorentz limit of the Spitzer–Härm conductivity. The classical Spitzer–Härm conductivity has been analytically derived in agreement, up to a constant, with the coefficient κ in (9.2). Substituting the free-streaming flux from (9.7) into the flux (9.77), one gets

$$q \propto \left(\frac{\lambda_e}{L_T}\right)q_f \quad (9.78)$$

and for $\lambda_e/L_T \ll 1$ this is a reasonable result.

For $\lambda_e/L_T > 1$ (even for $\lambda_e/L_T > 0.1$ using the above numerical coefficients) the diffusion flux q is becoming larger than the free-streaming flux, which is absurd. In typical high-power laser-produced plasmas, between the critical surface and the ablation surface, the criterion $\lambda_e/L_T \ll 1$ is not satisfied. Therefore, the heat transport between the critical surface and the ablation surface cannot be described by the diffusion approximation, or by approximating the collision term in the Boltzmann equation by the Fokker–Planck equation. Another approach is needed in laser–plasma interactions in order to calculate how the energy is transported into the target. For this purpose the heat inhibition factor was introduced.

Another way to come to the same conclusion is to analyse f_1/f_M. Using equations (9.75), (9.68) and (9.69), this ratio is

$$\frac{f_1}{f_M} = \left(\frac{\lambda_e}{L_T}\right)\left(\frac{v}{v_T}\right)^4\left(4 - \left(\frac{v}{v_T}\right)^2\right). \quad (9.79)$$

This equation shows that f_1/f_M increases with λ_e/L_T and is equal to one for some value of the electron velocity v. However, the Spitzer–Härm approximation is valid only for $f_1/f_M \ll 1$. Between the ablation surface and the critical surface, L_T is chosen positive (i.e. $\mathrm{d}T/\mathrm{d}x > 0$); therefore, the positive x axis is pointing towards the laser radiation source (i.e. towards the vacuum) (see figure 9.1). The differential heat flux $q(v)$, which is is proportional to

$f_1 v^5$ (the integrand in (9.76)), is positive (flow towards the vacuum) if $f_1 > 0$ and negative when $f_1 < 0$. Since $f_1/f_M < 0$ for $v > 2v_T$ (f_M is always positive), all electrons with a velocity higher than $2v_T$ are transporting heat inside the target, while those electrons with $v < 2v_T$ are carrying energy from the ablation surface towards the corona. The reverse flow at low velocities is caused by the electric field and it is referred to in the literature as the 'return current'. The return current carries an equal but opposite current to that transported by the high-velocity electrons heating the target. This phenomenon ensures quasi-neutrality. The total heat flow is negative (see (9.77)); therefore, a net energy is transported into the target, so that the heat is predominantly carried by electrons with velocities between $2v_T$ and $3v_T$.

The total distribution function (9.67) can be written

$$f = f_M + f_1 \cos\theta = f_M \left[1 + \left(\frac{f_1}{f_M}\right)\frac{v_x}{v}\right]. \tag{9.80}$$

For particles moving into the target, $v_x/v = 1$, and therefore f becomes negative (an impossible situation) at $f_1/f_M < -1$. Analysing equation (9.79), one gets the unphysical situation, negative f, even for apparently a large temperature scale length such as $L_T/\lambda_e = 150$ if $v/v_T \approx 2.65$, a non-negligible region of energy transport into the target. It turns out that $L_T/\lambda_e > 10^3$ is required for the Spitzer–Härm approximation to be valid. Between the corona and the ablation surface this constraint is not usually satisfied. The steep temperature gradient in laser-produced plasmas requires, in general, a different formalism in order to explain the energy transport.

If there is a steep temperature gradient the electrons which have a long mean free path modify the local distribution function. This phenomenon is called non-local transport, since a large domain affects the heat transport. Because of the difficult problems of heat transport, between the corona and the ablation surface, a phenomenological approach is taken by using an effective inhibition factor in front of the free-streaming flow of electrons (see equation (9.8)).

In the next section a short discussion is given on the existence of hot electrons. In this case the physical phenomena are explained by two temperatures (or more), which in turn are derived from two (or more) Maxwellian electron distribution functions.

9.6 Hot Electrons

In laser-produced plasma the energy is absorbed by the electrons. When these electrons collide with the ions they are decelerated and emit x-ray radiation due to the bremsstrahlung effect. The logarithm of the energy spectrum of an x-ray when plotted as a function of the photon energy is a straight line if the electron distribution is Maxwellian. From the slope of this line the electron

temperature is deduced. This phenomenon is explained in the following paragraphs.

If there are two species of electrons then attempts are made to describe the electrons by two temperatures. Two temperatures imply two Maxwellian electron distributions, and the logarithm of the energy spectrum of x-ray when plotted as a function of the photon energy is described by a 'broken line'. From the slopes of the two lines the two temperatures can be deduced. It has been found experimentally that at laser intensities larger than $10^{15}\,\mathrm{W/cm^2}$, the x-ray emission from the laser-irradiated targets have an energy spectrum induced by a double Maxwellian electron distribution (Haines 1980).

The acceleration $a(t)$ of an electron while colliding with an ion, with charge Ze at a distance r, is given by the Coulomb force (c.g.s. units):

$$a(t) = \frac{Ze^2}{m_e r(t)^2}. \tag{9.81}$$

Classical electrodynamics shows that the accelerated electron radiates a power P:

$$P(t) = \frac{2e^2a^2}{3c^3} = \left(\frac{2Z^2e^6}{3m_e^2c^3}\right)\frac{1}{r^4} \tag{9.82}$$

where c is the speed of light and equation (9.81) has been used. Integrating over r and multiplying by the density numbers of the electron and the ion gives the total density power Q_b (erg/cm^3 s), emitted by bremsstrahlung:

$$Q_b = \frac{2Z^2e^6n_en_i}{3c^3m_e^2}\int_{r_{min}}^{\infty}\frac{4\pi r^2\,dr}{r^4} = \frac{8\pi Z^2e^6n_en_i}{3c^3m_e^2r_{min}}. \tag{9.83}$$

At r_{min} the classical approximation is no longer valid, since the uncertainty principle does not permit localization of the electron to a zero volume. As occasionally done in plasma physics, one takes the de Broglie scale length for r_{min} and relates the electron velocity to the temperature

$$r_{min} = \frac{\hbar}{m_e v}, \qquad v = \sqrt{\frac{k_B T}{m_e}}. \tag{9.84}$$

Substituting (9.84) into (9.83), the total power emitted per unit volume by the electrons, due to bremsstrahlung, is

$$Q_b = \left(\frac{16\pi^2Z^2e^6n_en_ik_B^{1/2}}{3c^3hm_e^{3/2}}\right)T_e^{1/2}. \tag{9.85}$$

In order to measure the electron temperature, a knowledge of the photon energy spectrum is required, rather than the total density power given in

this equation. For this purpose we analyse the energy ε emitted by one electron during the time it interacts with one ion. Equation (9.82) yields

$$\varepsilon = \int_{-\infty}^{+\infty} P \,\mathrm{d}t = \frac{2e^2}{3c^3} \int_{-\infty}^{+\infty} a(t)^2 \,\mathrm{d}t \equiv \int_0^{\infty} P_\nu \,\mathrm{d}\nu \tag{9.86}$$

where P_ν is the radiated energy per unit frequency emitted (by one electron passing an ion) with a frequency ν. In classical mechanics the electron trajectory and its acceleration are calculated for the electron passing an ion, assuming that the energy loss of the electron is neglected (this approximation is correct for weak radiation). In a Coulomb interaction between two charges q_1 and q_2 with a reduced mass m_r, the trajectory $r(t)$ and the acceleration $a(t)$ are conveniently given as a function of a parameter α, the impact parameter b and the relative velocity v (see figure 9.2(a)):

$$\begin{aligned}
t &= \frac{1}{2}\left(\alpha + \frac{\alpha^3}{3}\right)\left[\frac{m_\mathrm{r}^2 b^3 v^3}{q_1^2 q_2^2}\right], \qquad r = \frac{1}{2}(1+\alpha^2)\left[\frac{m_\mathrm{r} b^2 v^2}{|q_1 q_2|}\right] \\
\cos\varphi &\equiv -\frac{1-\alpha^2}{1+\alpha^2}, \qquad \sin\varphi \equiv \frac{2\alpha}{1+\alpha^2} \\
a_\perp &= \frac{\mathrm{d}^2}{\mathrm{d}t^2}(r\sin\varphi) = \left[\frac{q_1 q_2}{m_\mathrm{r} b v^2}\right]^3 \left(\frac{v^2}{b}\right) \frac{8\alpha}{(1+\alpha^2)^3} \\
a_{\|} &= \frac{\mathrm{d}^2}{\mathrm{d}t^2}(r\cos\varphi) = -\left[\frac{q_1 q_2}{m_\mathrm{r} b v^2}\right]^3 \left(\frac{v^2}{b}\right) \frac{4(1-\alpha^2)}{(1+\alpha^2)^3} \\
a^2 &= a_\perp^2 + a_{\|}^2.
\end{aligned} \tag{9.87}$$

The solution $a(t)$ is substituted into (9.86) so that ε is calculated exactly (Miyamoto 1980). Here an estimate is given (Zeldovich and Raizer 1966, Haines 1980), which is correct within a constant of about 2, and the exact solution is quoted at the end of this calculation.

The time of interaction between the electron and the ion is of the order $\tau \approx b/v$. The dominant frequency in the Fourier transport is $2\pi\nu \approx 1/\tau \approx v/b$ (the dominant Fourier transport frequency usually satisfies $\omega\tau \approx 1$, where $\omega = 2\pi\nu$). Therefore, we can use these relations and (9.81) to obtain

$$\nu = \frac{v}{2\pi b}, \qquad \mathrm{d}\nu = -\frac{v\,\mathrm{d}b}{2\pi b^2} \tag{9.88}$$

$$\varepsilon = \left(\frac{2e^2 a^2}{3c^3}\right)\tau = \left(\frac{2Z^2 e^6}{3c^3 m_\mathrm{e}^2}\right)\frac{1}{b^3 v}. \tag{9.89}$$

The electron with energy ε undergoes $n_\mathrm{i}\sigma(b)v$ collisions per unit time with ions in the impact parameter range b to $b + \mathrm{d}b$, where the cross section is

$\sigma_{ei}(b) = 2\pi b\,\mathrm{d}b$. Therefore, the energy radiated per unit time by an electron is

$$\begin{aligned}
\frac{\mathrm{d}E}{\mathrm{d}t} &= \int_{b_{\min}}^{\infty} \varepsilon n_i v 2\pi b\,\mathrm{d}b = \frac{4\pi Z^2 e^6 n_i}{3m_e^2 c^3}\int_{b_{\min}}^{\infty}\frac{\mathrm{d}b}{b^2} = \frac{8\pi^2 Z^2 e^6 n_i}{3m_e^2 c^3 v}\int_0^{\nu_{\max}}\mathrm{d}\nu \\
\frac{\mathrm{d}E}{\mathrm{d}t} &= \int_0^{\nu_{\max}} q_\nu\,\mathrm{d}\nu \\
q_\nu &\equiv \frac{8\pi^2 Z^2 e^6 n_i}{3m_e^2 c^3 v} \\
h\nu_{\max} &= \tfrac{1}{2}m_e v^2
\end{aligned} \tag{9.90}$$

where (9.88) is used and the photon energy ($h\nu$) cannot be larger than the kinetic energy of the electron. The power radiated per unit volume by the electrons is obtained by using (9.90):

$$\begin{aligned}
Q_b &\equiv \int \mathrm{d}\nu\, Q_\nu = \int \mathrm{d}\nu \int_{\sqrt{2h\nu/m_e}}^{\infty} q_\nu n_e f_M(v) 4\pi v^2\,\mathrm{d}v \\
f_M(v) &= \left(\frac{1}{\pi v_T^2}\right)^{3/2}\exp\left(-\frac{v^2}{v_T^2}\right) \\
v_T^2 &= \frac{2k_B T_e}{m_e} \\
Q_\nu &= \left(\frac{8\sqrt{2}}{3}\right)\frac{\pi^{3/2}Z^2 e^6 n_i n_e}{m_e^{3/2}c^3(k_B T_e)^{1/2}}\exp\left(-\frac{h\nu}{k_B T_e}\right).
\end{aligned} \tag{9.91}$$

An exact calculation yields $4/\sqrt{3} \approx 2.3$ times Q_ν of equation (9.91). The integral of (9.91) gives (9.85).

From equation (9.91) it is evident that a plot of $\ln[\mathrm{d}Q_b/\mathrm{d}(h\nu)]$ versus $h\nu$ yields a straight line, and from the slope it is easy to deduce the electron temperature. If the electron velocity distribution can be described not by one Maxwellian (as in the proof of (9.91)), but as a superposition of two Maxwellian distributions with two temperatures, then the integral of (9.91) yields

$$Q_\nu \propto \frac{n_c}{T_c^{1/2}}\exp\left(-\frac{h\nu}{k_B T_c}\right) + \frac{n_h}{T_h^{1/2}}\exp\left(-\frac{h\nu}{k_B T_h}\right) \tag{9.92}$$

where n_c and n_h are the spatial densities of the cold and hot electron species, while T_c and T_h are their respective temperatures. Such a spectrum was measured (Haines 1980) for neodymium laser pulses of the order of 1 ns and with intensity larger than $10^{15}\,\mathrm{W/cm^2}$ (see figure 9.3).

Energy transfer from electron plasma waves, nonlinear wave phenomena and resonance absorption can create the hot electrons. It appears that the

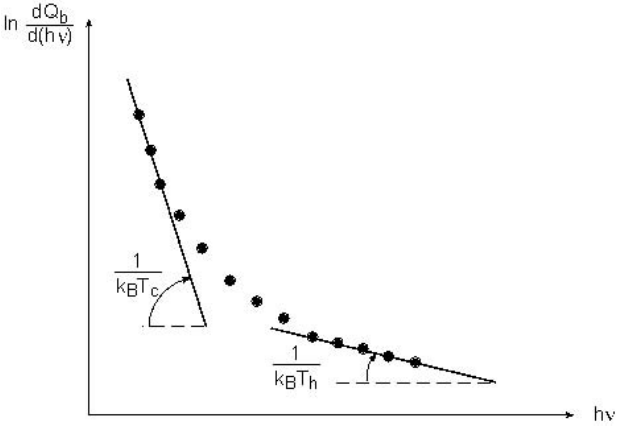

Figure 9.3. A typical x-ray spectrum induced by two electron temperatures.

dominant source of hot electrons is resonance absorption. It was found experimentally that the following scaling laws are satisfied for the hot electron temperature T_h:

$$T_h(\text{keV}) = 10\left(\frac{I_L\lambda_L^2}{10^{15}\,\text{W}\cdot\text{cm}^{-2}\,\mu\text{m}^2}\right)^{0.30\pm0.05} \quad \text{for } I_L\lambda_L^2 \geq 10^{15}\,\text{W}\cdot\text{cm}^{-2}\,\mu\text{m}^2$$

$$T_h(\text{keV}) = 10\left(\frac{I_L\lambda_L^2}{10^{15}\,\text{W}\cdot\text{cm}^{-2}\,\mu\text{m}^2}\right)^{2/3} \quad \text{for } I_L\lambda_L^2 \leq 10^{15}\,\text{W}\cdot\text{cm}^{-2}\,\mu\text{m}^2. \tag{9.93}$$

It is important to mention that with the femtosecond lasers, MeV electrons (and ions) have been measured for $I_L > 10^{19}\,\text{W/cm}^2$.

We conclude this section by showing that a very strange phenomenon can occur in thermodynamics for plasma with two temperatures. For a cold ion ($T_i = 0$) the ideal equation of state is

$$P = n_h k_B T_h + n_c k_B T_c. \tag{9.94}$$

For $T_h/T_c > 10$ one can obtain a (plasma) fluid which can satisfy

$$\left(\frac{\partial^2 P}{\partial V^2}\right)_S < 0, \qquad V = \frac{1}{\rho} = \frac{1}{m_i n_i} \tag{9.95}$$

where S is the entropy. A normal fluid cannot satisfy equation (9.95). However, two phase mixtures such as liquid and vapour can obey this equation. If (9.95) is satisfied then an unusual wave, called rarefaction shock wave, can exist (Zeldovich and Raizer 1966). As we shall see in the next chapter, in a shock wave the medium is compressed, while in a rarefaction wave the density of the medium is reduced. From this point of

view the rarefaction shock wave behaves like a rarefaction wave. However, while in a rarefaction wave the entropy S is conserved, in a shock wave the entropy increases, and in the rarefaction wave the entropy is decreasing: an unstable process.

In the following, we write the fluid equations for the plasma expanding into vacuum, where the plasma has two components of electrons (Bezzerides *et al.* 1978, Wickens *et al.* 1978). The continuity and the momentum equation for the ions moving without collisions in the electrostatic potential ϕ are

$$\frac{\partial n_\mathrm{i}}{\partial t}+\frac{\partial}{\partial x}(n_\mathrm{i}v_\mathrm{i})=0, \qquad m_\mathrm{i}\left(\frac{\partial v_\mathrm{i}}{\partial t}+v_\mathrm{i}\frac{\partial v_\mathrm{i}}{\partial x}\right)=-Ze\frac{\partial \phi}{\partial x}. \tag{9.96}$$

Neglecting the inertial term in both electronic fluids, the pressure of the hot and cold electrons are balanced by the potential force

$$\begin{aligned} en_\mathrm{c}\frac{\partial \phi}{\partial x}-k_\mathrm{B}T_\mathrm{c}\frac{\partial n_\mathrm{c}}{\partial x}=0 \Rightarrow n_\mathrm{c}=n_{\mathrm{c}0}\exp\left(\frac{e\phi}{k_\mathrm{B}T_\mathrm{c}}\right) \\ en_\mathrm{h}\frac{\partial \phi}{\partial x}-k_\mathrm{B}T_\mathrm{h}\frac{\partial n_\mathrm{h}}{\partial x}=0 \Rightarrow n_\mathrm{h}=n_{\mathrm{h}0}\exp\left(\frac{e\phi}{k_\mathrm{B}T_\mathrm{h}}\right). \end{aligned} \tag{9.97}$$

The temperatures T_c and T_h are assumed constants. Equations (9.96) and (9.97) are solved, together with the requirement of charge neutrality:

$$Zn_\mathrm{i}=n_\mathrm{c}+n_\mathrm{h}. \tag{9.98}$$

Using (9.94), (9.97) and (9.98), one can write the second equation of (9.96) in the following ways:

$$\begin{aligned} &\frac{\partial v_\mathrm{i}}{\partial t}+v_\mathrm{i}\frac{\partial v_\mathrm{i}}{\partial x}=-\frac{1}{n_\mathrm{i}m_\mathrm{i}}\frac{\partial P}{\partial x}=-\frac{1}{n_\mathrm{i}m_\mathrm{i}}\frac{\partial P}{\partial n_\mathrm{i}}\frac{\partial n_\mathrm{i}}{\partial x}=-c_\mathrm{S}(\phi)^2\frac{1}{n_\mathrm{i}}\frac{\partial n_\mathrm{i}}{\partial x} \\ &c_\mathrm{S}(\phi)^2=\frac{1}{m_\mathrm{i}}\frac{\partial P}{\partial n_\mathrm{i}}=\frac{1}{m_\mathrm{i}}\frac{\partial P}{\partial \phi}\left(\frac{\partial n_\mathrm{i}}{\partial \phi}\right)^{-1}=\frac{Z}{m_\mathrm{i}}\left[\frac{n_\mathrm{h}+n_\mathrm{c}}{(n_\mathrm{h}/k_\mathrm{B}T_\mathrm{h})+(n_\mathrm{c}/k_\mathrm{B}T_\mathrm{c})}\right]. \end{aligned} \tag{9.99}$$

We now look for a **self-similar solution**, like the one obtained in section 7.2, in analysing the plasma expansion into vacuum. The variables n_c, n_h, n_i, v_i and ϕ are functions of only one variable ξ:

$$\xi=\frac{x}{t}, \qquad \frac{\partial}{\partial x}=\frac{1}{t}\frac{\partial}{\partial \xi}, \qquad \frac{\partial}{\partial t}=-\frac{\xi}{t}\frac{\partial}{\partial \xi}. \tag{9.100}$$

Using these relations in the two equations of (9.96), where the second equation is taken from (9.99), one gets

$$\begin{pmatrix} v_\mathrm{i}-\xi & n_\mathrm{i} \\ c_\mathrm{s}^2/n_\mathrm{i} & v_\mathrm{i}-\xi \end{pmatrix}\begin{pmatrix} \mathrm{d}n_\mathrm{i}/\mathrm{d}\xi \\ \mathrm{d}v_\mathrm{i}/\mathrm{d}\xi \end{pmatrix}=\begin{pmatrix} 0 \\ 0 \end{pmatrix}. \tag{9.101}$$

Equations (9.101) have a solution only if the determinant of the matrix vanishes, implying

$$v_{\mathrm{i}} = c_{\mathrm{s}}(\phi) + \xi. \tag{9.102}$$

Substituting this relation into one of the equations of (9.101), one gets

$$n_{\mathrm{i}} \frac{\mathrm{d}v_{\mathrm{i}}}{\mathrm{d}\xi} + c_{\mathrm{s}}(\phi) \frac{\mathrm{d}n_{\mathrm{i}}}{\mathrm{d}\xi} = 0. \tag{9.103}$$

Using (9.97) and (9.98), with the boundary condition $\phi = 0$, $v = 0$ and $c_{\mathrm{s}} = c_0$ in the undisturbed plasma, one obtains after integrating (9.103) the following solution:

$$\begin{aligned} v_{\mathrm{i}} &= \left(\frac{1}{T_{\mathrm{c}}} - \frac{1}{T_{\mathrm{h}}}\right)^{-1} \left\{ \frac{c_{\mathrm{c}}}{T_{\mathrm{c}}} \ln \left[\left(\frac{c_{\mathrm{s}} - c_{\mathrm{c}}}{c_0 - c_{\mathrm{c}}} \right) \left(\frac{c_0 + c_{\mathrm{c}}}{c_{\mathrm{s}} + c_{\mathrm{c}}} \right) \right] \right. \\ &\qquad \left. + \frac{c_{\mathrm{h}}}{T_{\mathrm{h}}} \ln \left[\left(\frac{c_{\mathrm{h}} - c_0}{c_{\mathrm{h}} - c_{\mathrm{s}}} \right) \left(\frac{c_{\mathrm{h}} + c_{\mathrm{s}}}{c_{\mathrm{h}} + c_0} \right) \right] \right\} \\ c_{\mathrm{c}}^2 &\equiv \frac{Z k_{\mathrm{B}} T_{\mathrm{c}}}{m_{\mathrm{i}}}, \qquad c_{\mathrm{h}}^2 \equiv \frac{Z k_{\mathrm{B}} T_{\mathrm{h}}}{m_{\mathrm{i}}} \\ c_0^2 &= \left(\frac{Z}{m_{\mathrm{i}} k_{\mathrm{B}}} \right) \frac{n_{\mathrm{c}0} + n_{\mathrm{h}0}}{(n_{\mathrm{c}0}/T_{\mathrm{c}}) + (n_{\mathrm{h}0}/T_{\mathrm{h}})}. \end{aligned} \tag{9.104}$$

From (9.102) and (9.104) the solution of the potential $\phi(\xi)$ is obtained, implying for $T_{\mathrm{h}}/T_{\mathrm{c}} > 10$ a jump in the potential as shown schematically in figure 9.1 (the double layer).

The jump in the potential and the rarefaction shock wave are obtained if

$$\frac{\mathrm{d}^2 P}{\mathrm{d}V^2} = n_{\mathrm{i}}^3 m_{\mathrm{i}}^3 c_{\mathrm{s}}^2 \left(2 + \frac{\mathrm{d}c_{\mathrm{s}}^2}{\mathrm{d}\phi} \right) \leq 0. \tag{9.105}$$

Using (9.97) and (9.99) in this inequality, we get

$$\begin{aligned} &2 + \frac{\mathrm{d}c_{\mathrm{s}}^2}{\mathrm{d}\phi} \leq 0 \Rightarrow 2\beta^2 + \beta(6\alpha - 1 - \alpha^2) + 2\alpha^2 \leq 0 \\ &\alpha \equiv \frac{T_{\mathrm{h}}}{T_{\mathrm{c}}}, \qquad \beta \equiv \frac{n_{\mathrm{h}}}{n_{\mathrm{c}}}. \end{aligned} \tag{9.106}$$

This equation has a real solution for β only if

$$(6\alpha - 1 - \alpha^2)^2 - 16\alpha^2 \geq 0 \Rightarrow \alpha \equiv \frac{T_{\mathrm{h}}}{T_{\mathrm{c}}} \geq 5 + \sqrt{24} \approx 9.9. \tag{9.107}$$

In this domain of parameters the function $\phi(\xi)$ is not well defined, i.e. ϕ has three values for the same ξ, therefore the jump of ϕ (the singularity) is settled in this domain and a rarefaction wave is obtained.

Hot electrons is a peculiar and interesting phenomenon associated with high-power laser-produced plasmas. Sometimes this phenomenon is disturbing, like the preheating of solid targets for applications of shock waves, and sometimes it is a desirable effect, like in the creation of sources of high-energy x-rays.

9.7 Heat Waves

The local absorption of the laser energy is associated with the creation of a temperature gradient and a thermal flux to transport the absorbed energy. With the temperature gradient there are also pressure gradients that set the plasma into a 'fluid' motion. In most laser-produced plasmas the hydrodynamic energy transport substantially exceeds the heat conduction. However, in the interaction of very short laser pulses (of the order of 1 ps or less) with matter, the hydrodynamic motion does not have time to develop, and therefore in these cases the heat transport is dominant. Electrons or x-rays may serve as heat carriers (Ditmire *et al.* 1996, Fraenkel *et al.* 2000). For nonlinear transport coefficients, like the electron conductivity discussed in section 9.5, we expect that the energy transport is caused by a heat wave. Heat waves may also play an important role in inertial confinement fusion during the ignition process. In this section we shall formally show the solution for a one-dimensional geometry heat wave (Zeldovich and Raizer 1966, Krokhin 1971).

Let us consider the energy conservation equation:

$$\rho C_{\mathrm{V}} \frac{\partial T}{\partial t} = -\nabla \cdot (\mathbf{q}_{\mathrm{H}} - \mathbf{I}), \qquad \mathbf{q}_{\mathrm{H}} = -\kappa \nabla T, \qquad \kappa = BT^{\mathrm{n}}, \qquad \nabla \cdot \mathbf{I} \equiv W \tag{9.108}$$

where ρ is the density (g/cm^3), T is the temperature in Kelvin, $\mathbf{I}$ is the absorbed laser flux [erg/(time $\cdot$ cm^2)], $\mathbf{q}_{\mathrm{H}}$ is the heat flux [erg/(time $\cdot$ cm^2)], κ is the coefficient of thermal conductivity [erg/(cm $\cdot$ s $\cdot$ K)], W is the power density deposited by the laser [erg/(s $\cdot$ cm^3)], C_{V} is the specific heat at constant volume [erg/(g $\cdot$ K)], and B and n are constants. In one space dimension, chosen as x, and assuming a constant density ρ (a reasonable assumption for short laser pulse duration) and a constant C_{V}, equation (9.108) takes the form

$$\frac{\partial T}{\partial t} = \frac{\partial}{\partial x}\left(\chi \frac{\partial T}{\partial x}\right) + w, \qquad \chi = \frac{\kappa}{\rho C_{\mathrm{V}}}, \qquad w = \frac{W}{\rho C_{\mathrm{V}}}. \tag{9.109}$$

The coefficient χ is called the thermal diffusivity (cm^2/s) and can be expressed as

$$\chi = aT^n \tag{9.110}$$

where a is a constant.

If $n = 0$, i.e. a constant thermal diffusivity, then equation (9.109) is the simple diffusion equation. Assuming that the laser energy is deposited at $x = 0$ (e.g. all the energy is deposited at the critical surface located at $x = 0$) and at time $t = 0$ (i.e. a very short pulse duration), then

$$\frac{\partial T}{\partial t} = a\left(\frac{\partial^2 T}{\partial x^2}\right) + w, \qquad w = T_0 L\delta(x)\delta(t), \qquad T(x,0) = T_0 L\delta(x) \tag{9.111}$$

where $\delta(x)$ and $\delta(t)$ are the Dirac delta function

$$\int_{-L/2}^{L/2} \delta(x)\,\mathrm{d}x = 1, \qquad \int_{-\tau/2}^{\tau/2} \delta(t)\,\mathrm{d}t = 1 \tag{9.112}$$

and L is a scale length factor for the energy deposition and τ is the laser pulse duration. The solution of equation (9.111) is

$$T(x,t) = \frac{T_0 L}{(4\pi a t)^{1/2}} \exp\left(-\frac{x^2}{4at}\right). \tag{9.113}$$

Equation (9.113) is the solution of the linear heat transport equation (9.111). The nonlinear heat transport equation is

$$\frac{\partial T}{\partial t} = a\frac{\partial}{\partial x}\left(T^n \frac{\partial T}{\partial x}\right) + w. \tag{9.114}$$

For example, for electrons in plasma one can use equation (9.2) (proven in section 2.3), together with the C_V value of $\frac{3}{2}k_B$ per particle, to get

$$\left.\begin{aligned} \kappa &= \tfrac{1}{3}\lambda_e v_e n_e k_B \\ C_V &= \tfrac{3}{2}k_B\left(\frac{n_e}{\rho}\right) \end{aligned}\right\} \Rightarrow \chi = \frac{\kappa}{\rho C_V} = \frac{2}{9}\lambda_e v_e \propto T^{5/2} \tag{9.115}$$

where we have used equation (9.1), the electron mean free path $\lambda_e \approx T^2$, and the thermal speed of the electron $v_e \approx T^{1/2}$. Therefore, for the nonlinear electron heat transport in the plasma, $n = \frac{5}{2}$ in equation (9.114). In comparison, for radiation (x-rays) transport in a multiply-ionized plasma the power of T in this equation is in the domain ~4.5–5.5.

In some cases, like in a solid medium, C_V depends on temperature (C_V/particle equals $3k_B/2$ only for an ideal gas with three degrees of freedom). In this case equation (9.114) is not satisfied. When the specific heat is a function of the temperature, one can write for the energy E (erg/g),

$$E = \alpha T^k \Rightarrow T = \left(\frac{E}{\alpha}\right)^{1/k}, \qquad C_V = \left(\frac{\partial E}{\partial T}\right)_V = \alpha k T^{k-1} \tag{9.116}$$

where α is a constant (it can be a function of density ρ, but $V = 1/\rho$ is constant). In metals (see section 5.7), the electronic contribution to the equation of state is described by $k = 2$ to a good approximation (Eliezer *et al.* 1986). The coefficient α is given by the equation of state of the medium under consideration. Substituting (9.116) into (9.108) and using

$$\frac{\partial T}{\partial t} = \left(\frac{\partial E}{\partial T}\right)^{-1} \frac{\partial E}{\partial t} = \frac{1}{C_V} \frac{\partial E}{\partial t} \tag{9.117}$$

one gets the equation for the energy/mass E:

$$\frac{\partial E}{\partial t} = A \frac{\partial}{\partial t}\left(E^N \frac{\partial E}{\partial x}\right) + W, \qquad A \equiv \frac{B}{\rho k \alpha^{(n+1)/k}}, \qquad N \equiv \frac{n-k+1}{k}. \tag{9.118}$$

Equations (9.114) and (9.118) are identical from the mathematical point of view. If C_V is temperature-independent one has to solve equation (9.114), while if C_V depends on temperature then (9.118) has to be solved.

We now obtain an analytic solution (Zeldovich and Raizer 1966) of equation (9.114). The energy is deposited instantaneously at $t = 0$, at a plane positioned at $x = 0$. For $t > 0$ the heat propagates away from the $x = 0$ plane. The energy conservation is obtained by integrating equation (9.114) in space ($\int \mathrm{d}x$ from $-\infty$ to $+\infty$) and in time ($\int \mathrm{d}t$ from 0 to t). The first term on the right-hand side of the space integral of (9.114) vanishes, because $T(x = -\infty) = 0$ and $T(x = +\infty) = 0$. Therefore, the energy conservation implies the following equation:

$$\int_{-\infty}^{+\infty} T(x,t)\,\mathrm{d}x = \frac{1}{\rho C_V} \int I(t)\,\mathrm{d}t = \frac{\varepsilon}{\rho C_V} \equiv Q \tag{9.119}$$

where ε (erg/cm^2) is the deposited laser energy per unit area. The energy conservation (9.119) is satisfied, together with the heat conduction equation (9.114) for $t > 0$:

$$\frac{\partial T}{\partial t} = a \frac{\partial}{\partial x}\left(T^n \frac{\partial T}{\partial x}\right). \tag{9.120}$$

The energy deposition of the laser is instantaneous if the laser pulse duration is τ, if we are analysing times t much larger than τ ($t \gg \tau$). In this case the problem is defined only by two parameters: a [cm^2/(K^n · s)] and Q (K · cm), where K is Kelvin. There is only one way to describe the dimensions of temperature T and position x:

$$(x) = (aQ^n t)^{1/(n+2)}, \qquad (T) = \left(\frac{Q^2}{at}\right)^{1/(n+2)}. \tag{9.121}$$

Therefore, the measurable solution $T(x,t)$ cannot be a function of two variables x and t, but only of one dimensionless variable ξ that can be constructed from a, Q, x and t,

$$\xi = \frac{x}{(aQ^n t)^{1/(n+2)}} \tag{9.122}$$

and a coefficient which has the dimension of T. The general solution of equation (9.120) can be presented as

$$T(x,t) = \left(\frac{Q^2}{at}\right)^{1/(n+2)} f(\xi). \tag{9.123}$$

Substituting (9.123) into (9.120) and using (9.121) in order to take the derivatives

$$\frac{\partial f}{\partial t} = -\left(\frac{1}{n+2}\right)\left(\frac{\xi}{t}\right)\frac{\mathrm{d}f}{\mathrm{d}\xi}, \qquad \frac{\partial f}{\partial x} = \left(\frac{1}{aQ^n t}\right)^{1/(n+2)}\frac{\mathrm{d}f}{\mathrm{d}\xi} \tag{9.124}$$

one gets the ordinary differential equation for $f(\xi)$:

$$(n+2)\frac{\mathrm{d}}{\mathrm{d}\xi}\left(f^n\frac{\mathrm{d}f}{\mathrm{d}\xi}\right) + \xi\frac{\mathrm{d}f}{\mathrm{d}\xi} + f = 0. \tag{9.125}$$

This equation has to be solved subject to the boundary conditions

$$f(\xi = \infty) = 0, \qquad \frac{\mathrm{d}f}{\mathrm{d}\xi}(\xi = 0) = 0. \tag{9.126}$$

These boundary values are derived from $T(x = -\infty) = 0$ and $T(x = +\infty) = 0$, which are equivalent to $T(x = +\infty) = 0$ and $\partial T/\partial x(x = 0) = 0$. The second relation is the manifestation of the mirror symmetry $(x \leftrightarrow -x)$ about the plane $x = 0$.

A solution of equation (9.125) with the boundary condition (9.126) is

$$f(\xi) = \begin{cases} \left[\dfrac{n\xi_0^2}{2(n+2)}\right]^{1/n}\left[1 - \left(\dfrac{\xi}{\xi_0}\right)^2\right]^{1/n} & \text{for } \xi < \xi_0 \\ 0 & \text{for } \xi > \xi_0. \end{cases} \tag{9.127}$$

The constant ξ_0 is obtained by using the energy conservation (9.119), yielding

$$\int_{-\xi_0}^{+\xi_0} f(\xi)\,\mathrm{d}\xi = 1 \Rightarrow \xi_0 = \left[\frac{(n+2)}{n2^{n-1}\pi^{n/2}}\right]^{1/(n+2)}\left[\frac{\Gamma(1/2+1/n)}{\Gamma(1/n)}\right]^{n/(n+2)} \tag{9.128}$$

where Γ is the gamma function. Defining $x_f(t)$ as the front coordinate of the heat wave and $T_0(t)$ as the temperature at $x = 0$, the temperature $T(x, t)$ from (9.123) is given from (9.127) and (9.122):

$$\begin{aligned} T(x,t) &= T_0(t)\left(1 - \frac{x^2}{x_f(t)^2}\right)^{1/n} \\ x_f(t) &= \xi_0 (aQ^n t)^{1/(n+2)} \\ T_0(t) &= \left[\frac{n\xi_0^2}{2(n+2)}\right]^{1/n} \left(\frac{Q^2}{at}\right)^{1/(n+2)}. \end{aligned} \tag{9.129}$$

A typical temperature T as a function of x at a given time t is shown in figure 9.4.

The speed of propagation u_{hw} of the heat wave is defined by

$$u_{hw} = \frac{dx_f}{dt} = \left(\frac{\xi_0}{n+2}\right)(aQ^n)^{1/(n+2)} t^{-[(n+1)/(n+2)]}. \tag{9.130}$$

From equations (9.129) and (9.130), it appears that at $t = 0$ both the temperature and the heat wave velocity are singular ($\to \infty$). However, as was previously explained, the self-similar solution derived here is relevant only for times $t \gg \tau$, where τ is the laser pulse duration. Therefore, it might be convenient to write the solutions for T_0 and u in the form

$$\left.\begin{aligned} \frac{T_0(t)}{T_0(\tau)} &= \left(\frac{\tau}{t}\right)^{1/(n+2)} \\ \frac{u_{hw}(t)}{u_{hw}(\tau)} &= \left(\frac{\tau}{t}\right)^{(n+1)/(n+2)} \end{aligned}\right\} \quad \text{for } t \gg \tau. \tag{9.131}$$

In figure 9.4 the heat wave temperature space profile (at a time t), the flux and the cooling and heating domains are shown. Using the solution (9.129), one gets

$$\begin{aligned} T(x,t) &= T_0(t)\left(1 - \frac{x^2}{x_f^2}\right)^{1/n} \\ q_H(x,t) &= -BT^n \frac{dT}{dx} = \left(\frac{2BT_0^{n+1}}{x_f^2}\right)\left(1 - \frac{x^2}{x_f^2}\right)^{1/n} x \\ \rho C_V \frac{\partial T}{\partial t} &= -\frac{\partial q_H}{\partial x} = \left(\frac{2BT_0^{n+1}}{x_f^2}\right)\left(1 - \frac{x^2}{x_f^2}\right)^{-[(n-1)/n]} \left[\left(\frac{2+n}{n}\right)\frac{x^2}{x_f^2} - 1\right]. \end{aligned} \tag{9.132}$$

The heat flux q_H increases linearly, to a good approximation, from $x = 0$ to almost the front of the wave and drops very fast to zero at $x = x_f$. From the

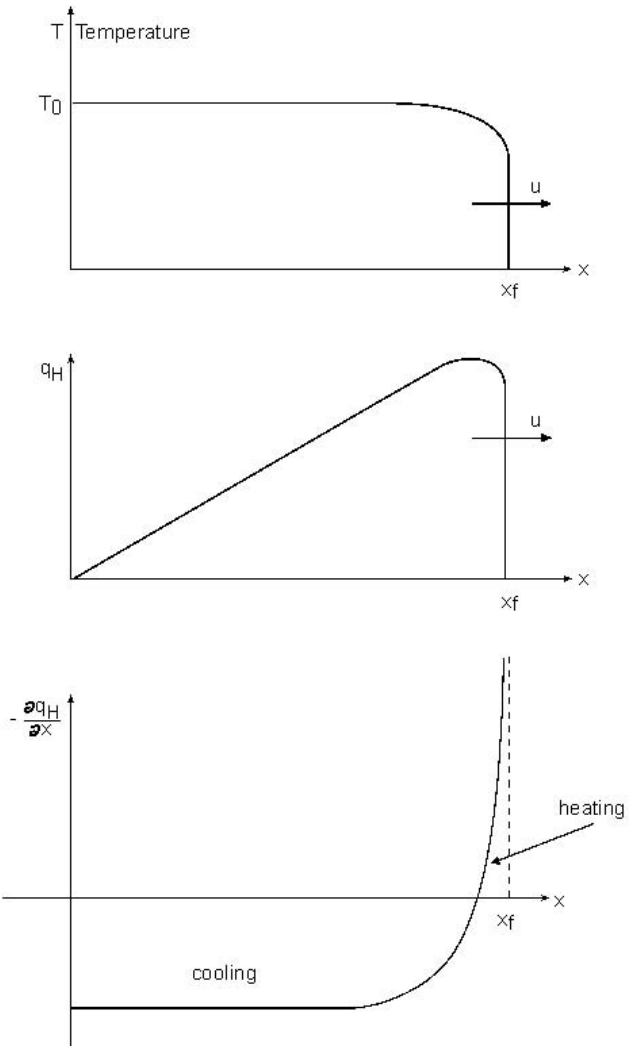

Figure 9.4. A schematic solution for a nonlinear heat wave.

last of equations (9.132), one notes that for $x/x_f < [n/(n+2)]^{1/2}$ the medium is cooled (i.e. the temperature decreases with time), while for $x/x_f > [n/(n+2)]^{1/2}$ the medium is heated. At $x/x_f = 1$ there is a singularity in the increase (in time) in temperature. However, the energy conservation ($\int T\,dx = \text{constant}$) is not violated, as required by this formalism. The main hot region is cooled almost uniformly and only the domain with the edge of the wave is heated very fast. The temperature near the wave front

can be described by the following approximation:

$$T(x,t) = T_0\left(1 - \frac{x^2}{x_f^2}\right)^{1/n} \approx T_0 2^{1/n}\left(1 - \frac{x}{x_f}\right)^{1/n} \quad \text{for } \frac{x}{x_f} \approx 1. \tag{9.133}$$

In laser–plasma interactions with very short laser pulses, the heat wave induced by the transport of x-rays may become more important than the heat wave created by electron transport (Ditmire *et al.* 1996, Fraenkel *et al.* 2000). We now give a short summary of the heat conduction by photons in a medium of thermal equilibrium between the electrons and the radiation.

The radiation heat flux is given by (see section 2.4)

$$\begin{aligned} \mathbf{q}_R &= -\frac{\lambda_R c}{3}\nabla U_p = -\kappa_R \nabla T \\ U_p &= \frac{4\sigma_{SB} T^4}{c} \\ \kappa_R &= \frac{16\sigma_{SB} T^3 \lambda_R}{3} \\ \lambda_R &= AT^j \quad \text{for } \rho = \text{const.} \end{aligned} \tag{9.134}$$

where T is the temperature of the electrons and the radiation; they are equal in thermal equilibrium. U_p is the radiation energy density (erg/cm^3), c is the speed of light, σ_{SB} is the Stefan–Boltzmann constant, ρ is the medium density and A and j are positive constants. λ_R is the radiation mean free path (the Rosseland mean free path) and for the equilibrium condition it is necessary that λ_R is smaller than the dimension of the medium. If the plasma is multiply ionized then j is in the domain of 1.5–2.5 (in λ_R given in equation (9.134)). In a fully ionized plasma the absorption and emission of the photons is by bremsstrahlung (i.e. electron–photon interaction in the presence of the ions) and in this case $j = \frac{7}{2}$ (Zeldovich and Raizer 1966):

$$\lambda_R(\text{bremsstrahlung}) = 4.8 \times 10^{24}\frac{T^{7/2}}{Z^2 n_i n_e} \quad [\text{cm}]. \tag{9.135}$$

Z is the charge of the ions, and n_i and n_e are the ion and electron densities respectively. For example, $Z = 1$, $Zn_i = n_e = 5 \times 10^{22}$ (appropriate for a femtosecond laser interacting with a deuterium plasma with solid density) and a temperature of 10^5 (about 10 eV), one gets a mean free path of about 6.1 μm.

The (Rosseland) mean free path for hydrogen-like plasma with a charge Z is given by

$$\lambda_R(\text{H-like}) \approx 8.7 \times 10^6 \frac{T^2}{Z^2 n_i} \quad [\text{cm}]. \tag{9.136}$$

In this case a comparison between the electron thermal conductivity (Spitzer–Härm conductivity κ_e—see sections 9.1 and 9.5) and the radiation

conductivity yields (Ditmire *et al*. 1996)

$$\frac{\kappa_{\mathrm{R}}}{\kappa_{\mathrm{e}}} \approx 5 \times 10^{18} \left(\frac{k_{\mathrm{B}} T}{\mathrm{eV}}\right)^{5/2} \left(\frac{\mathrm{cm}^{-3}}{n_{\mathrm{e}}}\right). \tag{9.137}$$

This relation implies that for a solid state density plasma $n_{\mathrm{e}} = Z n_{\mathrm{i}} = 10^{23}\,\mathrm{cm}^{-3}$, the radiation transport is more important than the electron heat transport for $k_{\mathrm{B}} T > 100\,\mathrm{eV}$.

Chapter 10

Shock Waves and Rarefaction Waves

10.1 A Perspective

The science of high pressure (Eliezer *et al.* 1986, Eliezer and Ricci 1991) is studied experimentally in the laboratory by using static and dynamic techniques. In static experiments the sample is squeezed between pistons or anvils. The conditions in these static experiments are limited by the strength of the construction materials. In the dynamic exdepends periments shock waves are created. Since the passage time of the shock is short in comparison with the disassembly time of the shocked sample, one can do shock wave research for any pressure that can be supplied by a driver, assuming that a proper diagnostic is available. In the scientific literature, the following shock-wave generators are discussed: a variety of guns (such as rail guns and a two-stage light–gas gun) that accelerate a foil to collide with a target, exploding foils, magnetic compression, chemical explosives, nuclear explosions and high-power lasers. The conventional high explosive and gun drivers can achieve pressures up to a few megabars.

The **dimension of pressure** is given by the scale defined by the pressure of one atmosphere at standard conditions $\approx$ **bar** $=$ **10^6 dyne/cm^2** (in c.g.s. units) $=$ **10^5 Pascal** (in m.k.s. units, Pascal $= \mathrm{N/m^2}$).

In 1974 the first direct observation of a laser-driven shock wave was reported (van Kessel and Sigel 1974). A planar solid hydrogen target (taken from a liquid-helium-cooled cryostat and inserted into an evacuated interaction chamber) was irradiated with a 10 J, 5 ns, Nd laser (1.06 μm wavelength) and the spatial development of the laser-driven shock wave was measured using high-speed photography. The estimated pressure in this pioneer experiment was 2 Mbar.

Twenty years after the first published experiment, the Nova laser from Livermore laboratories in the USA created a pressure of 750 ± 200 Mbar (Cauble *et al.* 1994). This was achieved in a collision between two gold foils, where the flyer (Au foil) was accelerated by a high-intensity x-ray flux created by the laser–plasma interaction.

The science of high pressure is usually analysed in a medium that has been compressed by a one-dimensional shock wave. For a one-dimensional shock wave traversing a known medium (density and temperature are known before the shock wave passes through), the density, pressure and energy of the shocked material are uniquely determined from the conservation of mass, momentum and energy, and the measurement of the shock and particle flow velocities.

The starting points in analysing the one-dimensional shock waves are the conservation laws of mass, momentum and energy in a fluid flow:

$$\begin{aligned} \frac{\partial \rho}{\partial t} &= -\frac{\partial}{\partial x}(\rho u) \\ \frac{\partial}{\partial t}(\rho u) &= -\frac{\partial}{\partial x}(P + \rho u^2) \\ \frac{\partial}{\partial t}\left(\rho E + \frac{1}{2}\rho u^2\right) &= -\frac{\partial}{\partial x}\left(\rho E u + P u + \frac{1}{2}\rho u^3\right). \end{aligned} \tag{10.1}$$

The usual notation is used, where x–t is space–time, ρ is the density, u is the flow velocity, P is the pressure and E is the internal energy per unit mass. In the previous chapter (section 9.7), in the discussion of heat waves, the fluid flow was neglected in favour of the heat flow. In this chapter we analyse a medium dominated by its flow and the disturbances that propagate with a speed of the order of the velocity of sound. In this case (unlike in section 9.7), the time of interest is in the domain where the heat wave velocity u_{hw} is much smaller than the sound velocity c_{s}. Furthermore, the laser pulse duration is not negligible. Therefore, to a good approximation one may assume that during the laser pulse duration a constant flux (the laser absorbed flux I) is supplied by the laser to the fluid at the boundary $x = 0$:

$$I = -\kappa\left(\frac{\partial T}{\partial x}\right)_{x=0} = -c_{\mathrm{V}}\rho a T^n\left(\frac{\partial T}{\partial x}\right)_{x=0} = \text{const.}, \qquad I \approx \frac{c_{\mathrm{V}}\rho a T_0^{n+1}}{x_{\mathrm{f}}} \tag{10.2}$$

where a is a constant, c_{V} is the heat capacity at constant volume and ρ is the density of the medium. x_{f} is the front position of the heat wave (see section 9.7) and T_0 is the temperature at the origin ($x = 0$), i.e. how far the heat wave front is from the origin $x = 0$ and how much the temperature increases there during the laser pulse duration.

The heat wave equation (energy conservation) can be approximated by

$$\rho c_{\mathrm{V}}\frac{\partial T}{\partial t} \approx \rho c_{\mathrm{V}}\frac{T_0}{t} \approx \frac{I}{x_{\mathrm{f}}}. \tag{10.3}$$

Solving equations (10.2) and (10.3) yields the order of magnitude solutions:

$$T_0 \approx \left(\frac{I}{\rho c_V}\right)^{2/(n+2)} a^{-1/(n+2)} t^{1/(n+2)}$$
$$x_f \approx \left(\frac{I}{\rho c_V}\right)^{n/(n+2)} a^{1/(n+2)} t^{(n+1)/(n+2)}. \tag{10.4}$$

These scaling laws can be derived by dimensional analysis. The problem under consideration is defined by two parameters: $[I/(\rho \cdot c_V)]$ with dimension [cm · K/s] and the diffusivity of the medium $\chi = aT^n$, defined by the coefficient a with dimension $[\mathrm{cm}^2/(\mathrm{K}^n \cdot \mathrm{s})]$. Therefore, the solution x_f scales as $[I/(\rho \cdot c_V)]^\alpha [a]^\beta [t]^\gamma = [\mathrm{cm}]$, yielding

$$\left(\frac{\mathrm{cm} \cdot \mathrm{K}}{\mathrm{s}}\right)^\alpha \left(\frac{\mathrm{cm}^2}{\mathrm{K}^n \cdot \mathrm{s}}\right)^\beta \mathrm{s}^\gamma = \mathrm{cm}^1$$
$$\Rightarrow \alpha + 2\beta = 1, \qquad \alpha - n\beta = 0, \qquad -\alpha - \beta + \gamma = 0$$
$$\Rightarrow \alpha = \frac{n}{n+2}, \qquad \beta = \frac{1}{n+2}, \qquad \gamma = \frac{n+1}{n+2}$$
$$\Rightarrow x_f \approx \left(\frac{I}{\rho c_V}\right)^{n/(n+2)} a^{1/(n+2)} t^{(n+1)/(n+2)}. \tag{10.5}$$

A similar procedure gives $T_0 = [I/(\rho \cdot c_V)]^\alpha [a]^\beta [t]^\gamma$, with $\alpha = 2/(n+2)$, $\beta = -1/(n+2)$ and $\gamma = 1/(n+2)$. This procedure justifies equations (10.4) as an order of magnitude solution, and implies that the exact solution is given by this equation up to a dimensionless constant, usually of the order 1.

According to equations (10.4), the heat wave velocity u_{hw} and the sound velocity c_s have a time dependence

$$u_{hw} = \frac{\mathrm{d}x_f}{\mathrm{d}t} \propto t^{-1/(n+2)}, \qquad c_s \propto T_0^{1/2} \propto t^{1/[2(n+2)]}. \tag{10.6}$$

From these equations one can see that the heat wave speed decreases with time, while the acoustic wave increases with time, so that the acoustic disturbance overtakes the thermal wave (see figure 10.1). An exact calculation of this problem (Babuel-Peyrissac *et al.* 1969) shows that for solid deuterium, with a density 0.2 g/cm^3, and for an absorbed laser flux of 10^{15} W/cm^2, the sound wave overtakes the heat wave at 10 ps. From the above scaling laws it is evident that this time decreases for higher densities and lower absorbed laser intensity. Moreover, the inhibited thermal transport, as discussed in section 9.6, also reduces the time of heat-wave dominance. Therefore, in laser interaction with a solid target, the hydrodynamics effects predominate over the heat wave for laser pulse duration larger than 100 ps.

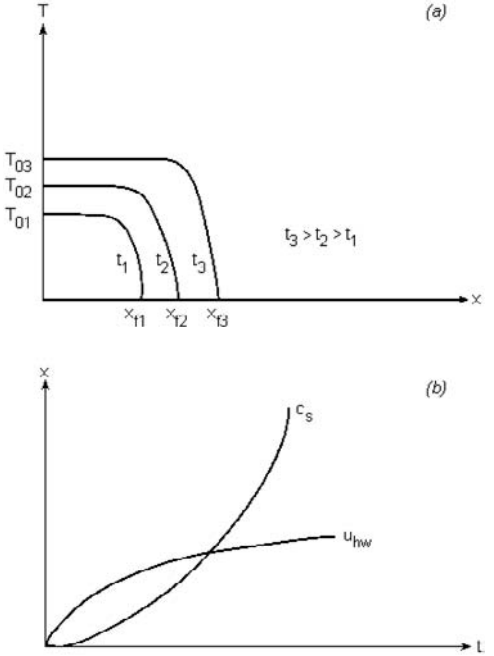

Figure 10.1. (a) Propagation of a heat wave during the laser pulse duration, where the laser absorbed flux is deposited at $x = 0$. (b) The positions of the heat wave front and the acoustic wave disturbance.

In sections 10.2 and 10.3 the sound wave and the rarefaction wave equations are given. The shock wave is discussed in sections 10.4 and 10.5. Section 10.6 analyses the constraints of a laser-induced shock wave for application in high-pressure physics. In sections 10.7 and 10.8 two possible applications of laser-induced shock waves and rarefaction waves are discussed.

In this chapter we consider only waves in one dimension with planar symmetry. In this case the variables describing the wave phenomena are functions only of the displacement x and the time t. The pressure P, the density ρ and the flow velocity u are, in general, functions of x and t.

10.2 Sound Waves

The physics of sound waves (Courant and Friedrichs 1976) is described by the motion of the fluid and the changes of density of the medium, caused by a pressure change. For an equilibrium pressure P_0 and density ρ_0, the

changes in pressure ΔP and density $\Delta\rho$ due to the existence of a sound wave are extremely small:

$$\begin{aligned} \rho &= \rho_0 + \Delta\rho, \qquad \frac{\Delta\rho}{\rho_0} \ll 1 \\ P &= P_0 + \Delta P, \qquad \frac{\Delta P}{P_0} \ll 1. \end{aligned} \tag{10.7}$$

It is now assumed that the undisturbed flow velocity is zero and the flow speed caused by the pressure disturbance is Δu, so that

$$u = u_0 + \Delta u, \qquad u_0 = 0, \qquad \frac{\Delta u}{c_s} \ll 1 \tag{10.8}$$

where c_s is the speed of sound. Using the small perturbations of (10.7) and (10.8), and neglecting second-order quantities in $\Delta\rho$, ΔP and u, the mass and momentum equations of (10.1) can be written in the form

$$\frac{\partial(\Delta\rho)}{\partial t} = -\rho_0 \frac{\partial u}{\partial x}, \qquad \rho_0 \frac{\partial u}{\partial t} = -\frac{\partial P}{\partial x}. \tag{10.9}$$

The motion in a sound wave is isentropic, $S(x) = \text{const.}$, therefore the change in the pressure is given by

$$\Delta P = \left(\frac{\partial P}{\partial \rho}\right)_S \Delta\rho \equiv c_s^2 \Delta\rho. \tag{10.10}$$

Differentiating the first equation of (10.9) with respect to time and the second equation with respect to space, adding the equations and using (10.10), one gets the wave equation

$$\frac{\partial^2(\Delta\rho)}{\partial t^2} - c_s^2 \frac{\partial^2(\Delta\rho)}{\partial x^2} = 0. \tag{10.11}$$

From this equation it is evident that c_s is the velocity of the $\Delta\rho$ disturbance, which is defined as the velocity of the sound wave. The pressure change ΔP and the flow velocity u satisfy a similar wave equation. Equation (10.11) has two families of solutions f and g:

$$\left.\begin{matrix} \Delta\rho \\ \Delta P \\ \Delta u \end{matrix}\right\} \approx f(x - c_s t) \quad \text{and} \quad g(x + c_s t) \tag{10.12}$$

where the speed of sound is

$$c_s = +\sqrt{\left(\frac{\partial P}{\partial \rho}\right)_S}. \tag{10.13}$$

The disturbances $f(x - c_s t)$ are moving in the positive x direction, while $g(x + c_s t)$ propagates in the negative x direction.

For a plasma satisfying an ideal equation of state, where the electron density $n_e = Zn_i$, Z is the ion charge and n_i is the ion density, and $T_e = T_i = T$ are the electron and ion temperatures, the pressure is given by

$$P = n_e k_B T_e + n_i k_B T_i = n_i (Z+1) k_B T = \frac{\rho}{m_i}(Z+1)k_B T \tag{10.14}$$

where m_i is the ion mass. An adiabatic process is described by

$$P = P_0 \left(\frac{\rho}{\rho_0}\right)^{\gamma}, \qquad \gamma = \frac{C_P}{C_V} \tag{10.15}$$

where C_P and C_V are the heat capacities at constant pressure and constant volume accordingly, and in a fully ionized plasma $\gamma = \frac{5}{3}$. The speed of sound for the ideal gas is

$$c_s = \left(\frac{\gamma P}{\rho}\right)^{1/2} = \left(\frac{\gamma(Z+1)k_B T}{m_i}\right)^{1/2}. \tag{10.16}$$

If the undisturbed gas is not stationary, then the flow stream carries the waves. A transformation from the coordinates moving with the flow (velocity u in the $+x$ direction) to the laboratory coordinates means that the sound wave is travelling with a velocity $u + c_s$ in the $+x$ direction and $u - c_s$ in the $-x$ direction. The curves in the x–t plane in the direction of propagation of small disturbances are called **characteristic curves**. For isentropic flow there are two families of characteristics described by

$$C_+: \quad \frac{dx}{dt} = u + c_s, \qquad C_-: \quad \frac{dx}{dt} = u - c_s \tag{10.17}$$

so that the physical quantities P and ρ do not change along these stream lines. There is also a characteristic curve C_0, where $dx/dt = u$, not discussed here. The $C_\pm$ characteristics are curved lines in the x–t plane because u and c_s are, in general, functions of x and t.

The equations of state describe any thermodynamic variable as a function of two other variables (assuming that the number of particles do not change). For example, the density $\rho = \rho(P, S)$ is a function of the pressure P and entropy S; therefore, for $S = \text{const.}$ one gets

$$\rho = \rho(P), \qquad \frac{\partial \rho}{\partial t} = \left(\frac{\partial \rho}{\partial P}\right)_S \frac{\partial P}{\partial t} = \frac{1}{c_s^2}\frac{\partial P}{\partial t}, \qquad \frac{\partial \rho}{\partial x} = \frac{1}{c_s^2}\frac{\partial P}{\partial x}. \tag{10.18}$$

Using these relations into the mass conservation and the momentum conservation given in (10.1), we get

$$\frac{1}{\rho c_s}\frac{\partial P}{\partial t} + \frac{u}{\rho c_s}\frac{\partial P}{\partial x} + c_s \frac{\partial u}{\partial x} = 0, \qquad \frac{\partial u}{\partial t} + u\frac{\partial u}{\partial x} + \frac{1}{\rho}\frac{\partial P}{\partial x} = 0. \tag{10.19}$$

Adding and subtracting these two relations yields

$$\begin{aligned}\left[\frac{\partial u}{\partial t}+(u+c_\mathrm{s})\frac{\partial u}{\partial x}\right]+\frac{1}{\rho c_\mathrm{s}}\left[\frac{\partial P}{\partial t}+(u+c_\mathrm{s})\frac{\partial P}{\partial x}\right]&=0\\ \left[\frac{\partial u}{\partial t}+(u-c_\mathrm{s})\frac{\partial u}{\partial x}\right]-\frac{1}{\rho c_\mathrm{s}}\left[\frac{\partial P}{\partial t}+(u-c_\mathrm{s})\frac{\partial P}{\partial x}\right]&=0.\end{aligned} \tag{10.20}$$

The brackets [ ] in these equations are derivatives along the characteristics $C_\pm$. In order to comprehend this statement, we define a curve $x=y(t)$. The derivative of a function $F(x,t)$ along the curve $y(t)$ is given by

$$\begin{aligned}\left(\frac{\mathrm{d}F}{\mathrm{d}t}\right)_y&=\frac{\partial F}{\partial t}+\frac{\partial F}{\partial x}\frac{\mathrm{d}x}{\mathrm{d}t}=\frac{\partial F}{\partial t}+y'\frac{\partial F}{\partial x}\\ \mathrm{d}F&=\int\left(\frac{\mathrm{d}F}{\mathrm{d}t}\right)_y\mathrm{d}t,\qquad x=y(t),\qquad y'\equiv\frac{\mathrm{d}x}{\mathrm{d}t}.\end{aligned} \tag{10.21}$$

For example, for the derivative of F along $x=$ constant one has $y'=0$, along a **stream line** $y'=u$, along the **characteristic** C_+ we have $y'=u+c_\mathrm{s}$, etc. Therefore, equations (10.20) and (10.21) can be rewritten as

$$\begin{aligned}\mathrm{d}J_+&\equiv\mathrm{d}u+\frac{1}{\rho c_\mathrm{s}}\mathrm{d}P=0\quad\text{along } C_+\left(\frac{\mathrm{d}x}{\mathrm{d}t}=u+c_\mathrm{s}\right)\\ \mathrm{d}J_-&\equiv\mathrm{d}u-\frac{1}{\rho c_\mathrm{s}}\mathrm{d}P=0\quad\text{along } C_-\left(\frac{\mathrm{d}x}{\mathrm{d}t}=u-c_\mathrm{s}\right).\end{aligned} \tag{10.22}$$

These equations describe an isentropic flow in one dimension with planar symmetry. $\mathrm{d}J_\pm$ are total differentials and can be integrated:

$$J_+=u+\int\frac{\mathrm{d}P}{\rho c_\mathrm{s}}=u+\int\frac{c_\mathrm{s}\,\mathrm{d}\rho}{\rho},\qquad J_-=u-\int\frac{\mathrm{d}P}{\rho c_\mathrm{s}}=u-\int\frac{c_\mathrm{s}\,\mathrm{d}\rho}{\rho} \tag{10.23}$$

for the second relation on the right-hand side of these equations (10.10) has been used. J_+ and J_- are called **Riemann invariants** and are occasionally used to solve numerically the flow equations for (and only for) an isentropic process, since J_+ and J_- are constants along the characteristics C_+ and C_- respectively. For a non-isentropic flow the density and the speed of sound are functions of two variables, $\mathrm{d}J_+$ and $\mathrm{d}J_-$ are not total differentials, and therefore J_+ and J_- have no physical (or mathematical) meaning.

10.3 Rarefaction Waves

We now analyse the case where the pressure is suddenly dropped in an isentropic process, e.g. after the high-power laser is switched off and the ablation pressure drops. Another interesting case is after the laser-induced high-pressure wave has reached the back of a target and at the interface

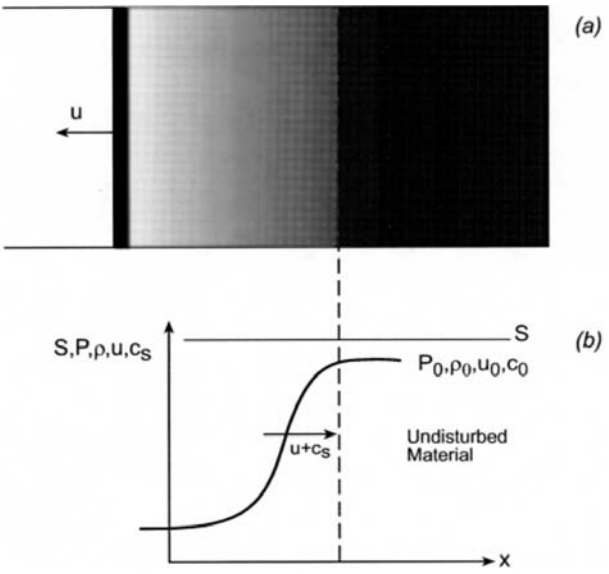

Figure 10.2. A forward moving rarefaction wave. The propagation velocity of the rarefaction wave at each point is $u + c_s$.

with the vacuum there is a sudden drop in pressure. In these cases, if one follows the variation in time for a given fluid element, one gets

$$\frac{D\rho}{Dt} < 0, \qquad \frac{DP}{Dt} < 0, \qquad \frac{D}{Dt} \equiv \frac{\partial}{\partial t} + u\frac{\partial}{\partial x}. \tag{10.24}$$

We consider the behaviour of a gas caused by a receding piston (figure 10.2a) in order to visualize the phenomenon of a rarefaction wave. In this figure the piston is moving in the $-x$ direction so that the gas is continually rarefied as it flows (in the $-x$ direction). The disturbance, called a rarefaction wave, is moving forward, in the $+x$ direction. One can consider the rarefaction wave to be represented by a sequence of jumps $\mathrm{d}\rho$, $\mathrm{d}P$, $\mathrm{d}u$, etc., so that we can use the Riemann invariant in order to solve the problem. The forward rarefaction wave moves into an undisturbed material defined by pressure P_0, density ρ_0, flow u_0 and the speed of sound c_{s_0}. Using (10.23) we get

$$u - u_0 = \int_{P_0}^{P} \frac{\mathrm{d}P}{\rho c_s} = \int_{\rho_0}^{\rho} \frac{c_s\,\mathrm{d}\rho}{\rho} \quad \text{rarefaction moving in } +x \text{ direction}$$

$$u - u_0 = -\int_{P_0}^{P} \frac{\mathrm{d}P}{\rho c_s} = -\int_{\rho_0}^{\rho} \frac{c_s\,\mathrm{d}\rho}{\rho} \quad \text{rarefaction moving in } -x \text{ direction.} \tag{10.25}$$

As an example we calculate some physical quantities for a rarefaction wave in an ideal gas. Since in a rarefaction wave the entropy is constant, one has the

following relation between the pressure, the density and the speed of sound (see equations (10.15) and (10.16)):

$$\frac{P}{P_0} = \left(\frac{\rho}{\rho_0}\right)^{\gamma}, \qquad \frac{c_s}{c_{s_0}} = \left(\frac{\rho}{\rho_0}\right)^{(\gamma-1)/2}. \tag{10.26}$$

Substituting (10.26) into (10.25) and doing the integral, one gets

$$u - u_0 = \int_{\rho_0}^{\rho} \frac{c_s \, d\rho}{\rho} = \int_{c_{s_0}}^{c_s} \frac{2 \, dc_s}{(\gamma - 1)} = \frac{2}{(\gamma - 1)}(c_s - c_{s_0})$$

$$\Rightarrow c_s = c_{s_0} + \tfrac{1}{2}(\gamma - 1)(u - u_0). \tag{10.27}$$

In this example the piston is moving in the $-x$ direction and at the gas–piston interface, and the gas velocity is the same as the piston velocity which has a negative value. The absolute value of the negative gas flow velocity is limited since the speed of sound is positive, i.e.

$$c_{s_0} + \tfrac{1}{2}(\gamma - 1)(u - u_0) \geq 0 \Rightarrow \frac{2c_{s_0}}{(\gamma - 1)} \geq -u + u_0 \geq -u = |u|. \tag{10.28}$$

From equation (10.27) it is evident that the speed of sound is decreased since u is negative. This implies, according to equations (10.26), that the density and the pressure are decreasing, as expressed mathematically in (10.24) and shown schematically in figure 10.2(b).

10.4 Shock Waves

The development of singularities, in the form of shock waves, in a wave profile due to the nonlinear nature of the conservation equations (10.1) has already been discussed by B. Riemann, W. J. M. Rankine and H. Hugoniot in the second half of the 19th century (1860–1890).

A shock wave is created in a medium that suffers a sudden impact (e.g. a collision between an accelerated foil and a target) or in a medium that releases large amounts of energy in a short period of time (e.g. high explosives). When a pulsed high-power laser interacts with matter, very hot plasma is created. This plasma exerts a high pressure on the surrounding material, leading to the formation of an intense shock wave, moving into the interior of the target. The momentum of the out-flowing plasma balances the momentum imparted to the compressed medium behind the shock front. The thermal pressure together with the momentum of the ablated material drives the shock wave.

It is convenient to analyse a shock wave by inspecting a gas compressed by a piston, moving into it with a constant velocity u. The medium has initially (the undisturbed medium) a density ρ_0 and a pressure P_0, and it is at rest, $u_0 = 0$. A shock wave starts moving into the material with a velocity

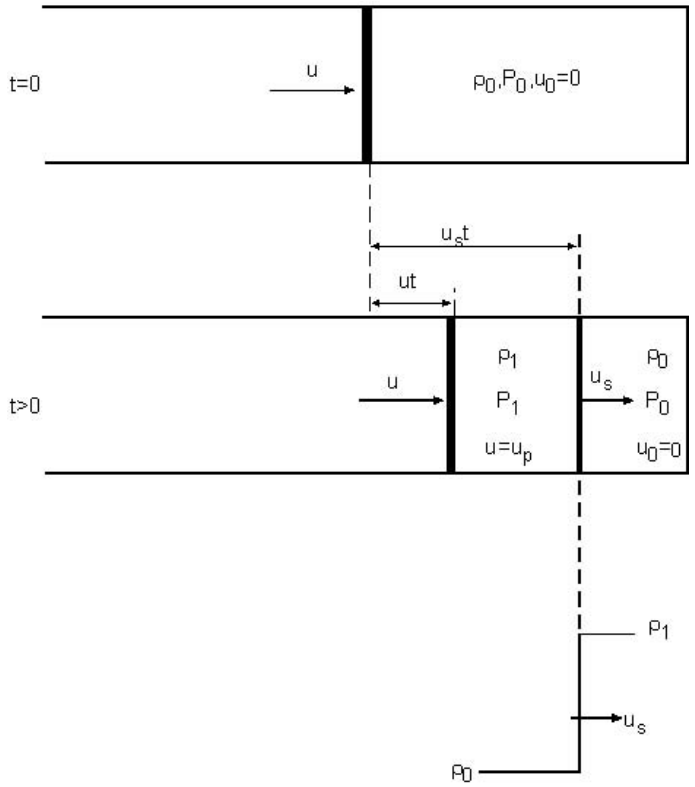

Figure 10.3. Shock wave created by the motion of a piston (the velocities are in the laboratory frame of reference). The subscript one denotes the unknown downstream variables, while the **upstream** variables (known initial condition) have a subscript zero.

denoted by u_s. Behind the shock front, the medium is compressed to a density ρ_1 and a pressure P_1. The gas flow velocity, denoted by u_p and usually called the particle velocity, in the compressed region is equal to the piston velocity, $u = u_p$. This case is schematically illustrated in figure 10.3. The initial mass before it is compressed, $\rho_0 A u_s t$ (A is the cross-sectional area of the tube), equals the mass after compression, $\rho_1 A(u_s - u_p t)$, implying the mass conservation law:

$$\rho_0 u_s = \rho_1 (u_s - u_p). \tag{10.29}$$

The momentum of the gas put into motion, $(\rho_0 A u_s t)u_p$, equals the impulse due to the pressure forces, $(P_1 - P_0)At$, yielding the momentum conservation law (or Newton's second law):

$$\rho_0 u_s u_p = P_1 - P_0. \tag{10.30}$$

The increase of internal energy E (energy/mass) and of kinetic energy per unit mass due to the piston-induced motion is $(\rho_0 A u_s t)(E_1 - E_0 + u_p^2/2)$. This increase in energy is supplied by the piston work, thus the energy conservation implies

$$\rho_0 u_s (E_1 - E_0 + \tfrac{1}{2} u_p^2) = P_1 u_p. \tag{10.31}$$

In the shock wave frame of reference, the undisturbed gas flows into the shock discontinuity with a velocity $v_0 = -u_s$ and leaves this discontinuity with a velocity $v_1 = -(u_s - u_p)$:

$$v_0 = -u_s, \qquad v_1 = -(u_s - u_p). \tag{10.32}$$

Substituting (10.32) into (10.29), (10.30) and (10.31), one gets the conservation laws of mass, momentum and energy, as seen from the shock-wave-front frame of reference:

$$\textbf{shock wave frame} \begin{cases} \rho_1 v_1 = \rho_0 v_0 \\ P_1 + \rho_1 v_1^2 = P_0 + \rho_0 v_0^2 \\ E_1 + \dfrac{P_1}{\rho_1} + \dfrac{v_1^2}{2} = E_0 + \dfrac{P_0}{\rho_0} + \dfrac{v_0^2}{2}. \end{cases} \tag{10.33}$$

These equations can be obtained more rigorously from the fluid equation (10.1) by integrating these equations over the shock wave layer. Assuming that the thickness of the shock wave front tends to zero, then for two points x_0 and x_1 lying on both sides of the shock discontinuity, one can write

$$\lim_{x_1 \to x_0} \int_{x_0}^{x_1} \frac{\partial}{\partial t} [\cdots] \, \mathrm{d}x = 0, \qquad \lim_{x_1 \to x_0} \int_{x_0}^{x_1} \frac{\partial}{\partial x} [\cdots] \, \mathrm{d}x = [\cdots]_{x_1} - [\cdots]_{x_0} \tag{10.34}$$

where $[\cdots]$ represent the different terms of equations (10.1). The procedure described in (10.34) yields the **jump conditions** in the shock wave frame of reference, as given by equations (10.33).

The jump conditions in the laboratory frame of reference are given in (10.29), (10.30) and (10.31) for a fluid initially at rest. In the more general case, the material is set in motion before the arrival of the shock wave (for example, by another shock wave). If the initial flow velocity is $u_0 \neq 0$, then the conservation laws (mass, momentum and energy) in the laboratory frame of reference (see figure 10.3) can be written

$$\textbf{laboratory frame} \begin{cases} \rho_0 (u_s - u_0) = \rho_1 (u_s - u_p) \\ \rho_0 (u_s - u_0)(u_p - u_0) = P_1 - P_0 \\ \rho_0 (u_s - u_0)(E_1 - E_0 + \tfrac{1}{2} u_p^2 - \tfrac{1}{2} u_0^2) = P_1 u_p - P_0 u_0. \end{cases} \tag{10.35}$$

Equations (10.34) or (10.35) are occasionally called the Rankine–Hugoniot relations. The Hugoniot relations are used to determine the state of the compressed solid behind the shock front. Assuming that the initial state is well defined and the quantities E_0, u_0, P_0 and ρ_0 are known, one has five unknowns E_1, u_p, P_1, ρ_1 and u_s with three equations (10.35). Usually the shock-wave velocity is measured experimentally, and if the equation of state is known (in this case one has four equations), $E = E(P, \rho)$, then the quantities of the compressed state can be calculated. If the equation of state is not known, then one has to measure experimentally two quantities of the shocked material, for example u_s and u_p, in order to solve the problem.

From the first two equations of (10.33) and using (10.32), the following general relations can be written:

$$\begin{aligned} &\frac{v_0}{v_1} = \frac{\rho_1}{\rho_0} \equiv \frac{V_0}{V_1}, \qquad V \equiv \frac{1}{\rho} \\ &v_0 = V_0 \left(\frac{P_1 - P_0}{V_0 - V_1} \right)^{1/2} = |u_s| \\ &v_1 = V_1 \left(\frac{P_1 - P_0}{V_0 - V_1} \right)^{1/2} \\ &v_0 - v_1 = [(P_1 - P_0)(V_0 - V_1)]^{1/2} = |u_p|. \end{aligned} \tag{10.36}$$

Substituting v_0 and v_1 from these relations into the third relation of (10.33), one gets

$$E_1(V_1, P_1) - E_0(V_0, P_0) = \tfrac{1}{2}(P_1 + P_0)(V_0 - V_1). \tag{10.37}$$

The thermodynamic relation $E(V, P)$ is the equation of state of the material under consideration, and assuming knowledge of this function, then equation (10.37), yields a graph (the notation of P_1 is changed to P_H and V_1 is V):

$$P_H = P_H(V; V_0, P_0). \tag{10.38}$$

This curve is known in literature as the Hugoniot curve. The Hugoniot curve, shown schematically in figure 10.4(a), is a two-parameter (V_0, P_0) family of curves, so that for each initial condition (V_0, P_0) there is a different curve. The Hugoniot curve is not a thermodynamic function, it does not show the pressure–volume (or density) trajectory of a shock wave development, but it is a plot of all possible final shocked (compressed) states for a given initial state (V_0, P_0). For example, the Hugoniot curve is different from the isentropic curves of the pressure $P_S(V, S)$, which describe the thermodynamic trajectory of pressure–volume (or density) for any given entropy S. In figure 10.4(a) two isentropes and one isotherm are also plotted schematically. It is interesting to note that for a given final pressure the compression is higher for an isentrope relative to the Hugoniot, and the isothermal compression is the highest.

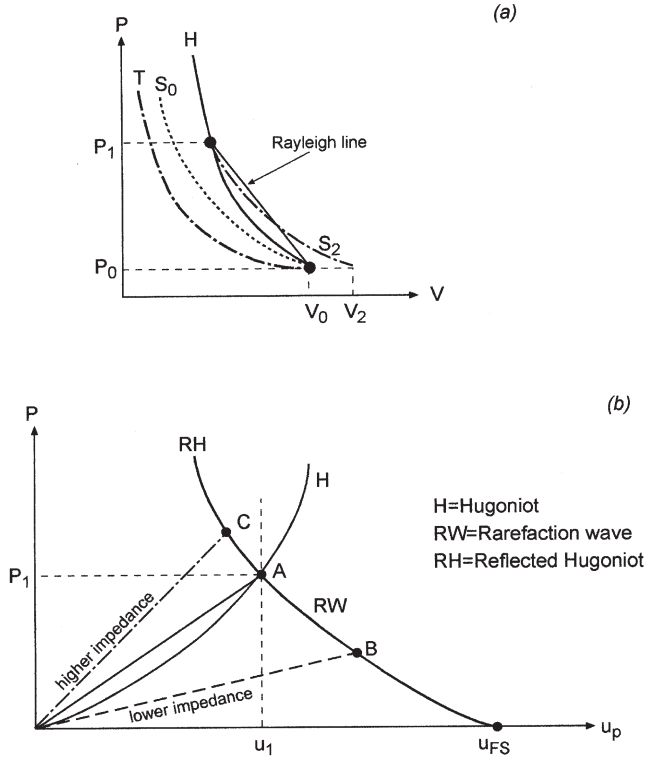

Figure 10.4. (a) The Hugoniot P–V curve, denoted by H, an isentrope S_0 and an isotherm, denoted by T, both starting like the Hugoniot at V_0, and an isentrope S_2 starting at the final shock pressure P_1. (b) The Hugoniot P–u_p curve. RW is the release wave (rarefaction wave), while RH is the reflected Hugoniot.

It is useful to consider the shock wave relations for an ideal gas with constant specific heats. In this case the equations of state are

$$E = C_V T = \frac{PV}{\gamma - 1}, \qquad S = C_V \ln(PV^\gamma) \tag{10.39}$$

where γ is defined in (10.15). Substituting (10.39) into (10.37), the Hugoniot curve for an ideal gas equation of state is obtained:

$$\frac{P_1}{P_0} = \frac{(\gamma+1)V_0 - (\gamma-1)V_1}{(\gamma+1)V_1 - (\gamma-1)V_0}. \tag{10.40}$$

From this equation it follows that the compression ratio $\rho_1/\rho_0 = V_0/V_1$ cannot increase above a certain value determined by γ. The pressure in the shocked ideal gas tends to infinity for the maximum possible compression,

given by

$$\frac{P_1}{P_0} \to \infty \Rightarrow \left(\frac{\rho_1}{\rho_0}\right)_{\max} = \left(\frac{V_0}{V_1}\right)_{\max} = \frac{\gamma+1}{\gamma-1}. \tag{10.41}$$

For example, the maximum compression caused by a planar shock wave in a medium with $\gamma = \frac{5}{3}$ is $4\rho_0$.

Using equation (10.16), for the speed of sound c_s, and equation (10.40), both for the ideal equation of state fluid, one obtains from (10.36):

$$\begin{aligned} M_0^2 &\equiv \left(\frac{u_s}{c_{s_0}}\right)^2 = \left(\frac{v_0}{c_{s_0}}\right)^2 = \frac{1}{2\gamma}\left[(\gamma-1)+(\gamma+1)\frac{P_1}{P_0}\right] > 1 \\ M_1^2 &\equiv \left(\frac{v_1}{c_{s_1}}\right)^2 = \frac{1}{2\gamma}\left[(\gamma-1)+(\gamma+1)\frac{P_0}{P_1}\right] < 1. \end{aligned} \tag{10.42}$$

The ratio M of the flow velocity to the sound velocity is known as the **Mach number**. In the limit of a weak shock wave, defined by $P_1 \approx P_0$, one has $M_1 \approx M_0 \approx 1$. However, equations (10.42) yield in general $M_1 < 1$ and $M_0 > 1$. The meaning of these relations is that in the shock frame of reference, the fluid flows into the shock front at a **supersonic velocity** ($M_0 > 1$) and flows out at a **subsonic velocity** ($M_1 < 1$). In the laboratory frame of reference, one has the well-known result that the shock wave propagates at a supersonic speed (with respect to the undisturbed medium), and at a subsonic speed with respect to the compressed material behind the shock. Although this phenomenon has been proven here for an ideal gas equation of state, this result is true for any medium, independent of the equation of state (Landau and Lifshitz 1987).

In a shock wave the entropy always increases. For example, in an ideal gas, equations (10.39) and (10.40) give the increase in entropy during a shock wave process:

$$\begin{aligned} S_1 - S_0 &= C_v \ln\left(\frac{P_1 V_1^\gamma}{P_0 V_0^\gamma}\right) \\ &= \left[\frac{P_0 V_0}{(\gamma-1)T_0}\right] \ln\left\{\left(\frac{P_1}{P_0}\right)\left[\frac{(\gamma-1)(P_1/P_0)+(\gamma+1)}{(\gamma+1)(P_1/P_0)+(\gamma-1)}\right]^\gamma\right\} > 0. \end{aligned} \tag{10.43}$$

The increase in entropy indicates that a shock wave is not a reversible process, but a dissipative phenomenon. The entropy jump of a medium compressed by shock wave increases with the strength of the shock wave (defined by the ratio P_1/P_0). The larger P_1/P_0, the larger is $S_1 - S_0 = \Delta S$. The value of ΔS is determined by the conservation laws (mass, momentum and energy) and by the equation of state. However, the mechanism of this change is described by viscosity and thermal conductivity (Zeldovich and Raizer 1966), not discussed in this book.

So far we have discussed a one-dimensional, steady-state shock wave passing through a gas or a fluid medium, with a thermal equilibrium ahead of and behind the shock wave front. When a shock wave is created in a solid material, one has to take into account the elastic–plastic properties of the target (Asay and Shahinpoor 1993). For shock waves with a pressure larger than 20 kbar, all the material strength properties are negligible and the solid target may be considered a liquid. Since we are interested in high pressures, larger than 20 kbar, the fluid jump equations (10.33) and (10.35) are relevant.

It was found experimentally (McQueen 1991) that for many solid materials, initially at rest, the following linear relation between the shock velocity u_s and the particle velocity u_p is valid to a very good approximation:

$$u_s = c_0 + \alpha u_p \tag{10.44}$$

where c_0 and α are constants. c_0 is the bulk sound speed at standard conditions. In table 10.1 the experimental values of c_0 and α are given (Steinberg 1996) for some elements that fit equation (10.44). ρ_0 is the initial density of the elements (with an atomic number Z). Equation (10.44) is occasionally called the (Hugoniot) equation of state.

Table 10.1. The experimental fit to $u_s = c_0 + \alpha u_p$ on the Hugoniot curve. u_s is the shock wave velocity, u_p is the particle flow velocity and ρ_0 is the initial density of the element with an atomic number Z.

	Element	Z	ρ_0 (g/cm^3)	c_0 (cm/μs)	α
Li	Lithium	3	0.534	0.477	1.066
Be	Beryllium (S200)	4	1.85	0.800	1.124
Mg	Magnesium	12	1.78	0.452	1.242
Al	Aluminium (6061-T6)	13	2.703	0.524	1.40
V	Vanadium	23	6.10	0.5077	1.201
Ni	Nickel	28	8.90	0.465	1.445
Cu	Copper	29	8.93	0.394	1.489
Zn	Zinc	30	7.139	0.303	1.55
Nb	Niobium	41	8.59	0.444	1.207
Mo	Molybdenum	42	10.2	0.5143	1.255
Ag	Silver	47	10.49	0.327	1.55
Cd	Cadmium	48	8.639	0.248	1.64
Sn	Tin	50	7.287	0.259	1.49
Ta	Tantalum	73	16.69	0.341	1.2
W	Tungsten	74	19.3	0.403	1.237
Pt	Platinum	78	21.44	0.364	1.54
Au	Gold	79	19.3	0.308	1.56
Th	Thorium	90	11.7	0.213	1.278
U	Uranium	92	19.05	0.248	1.53

It is convenient to describe the Hugoniot curve in the pressure–particle speed space, $P - u_p$. In particular, for the (10.44) equation of state, the Hugoniot is a parabola in this space (see figure 10.4(b)). When the shock wave reaches the back surface of the solid target, the free surface starts moving (into the vacuum or the surrounding atmosphere) with a velocity u_{FS} and a release wave, in the form of a rarefaction wave, is backscattered into the medium. Note that if the target is positioned in vacuum, then the pressure of the back surface (denoted in the literature as the **free surface**) is zero, a boundary value fixed by the vacuum. If an atmosphere surrounds the target, then a shock wave will run into this atmosphere. In our analysis we do not consider this effect and take $P = 0$ at the free surface. This approximation is justified for analysing the high-pressure shocked targets that are considered here.

If the target A is bounded by another solid target B (see figure 10.5(a)), then a shock wave passes from A into B and a wave is backscattered (into A). The **impedances** $Z = \rho_0 u_s$ of A and B are responsible for the character of this reflected wave. If $Z_A > Z_B$ then a rarefaction wave is backscattered (into A), while in the $Z_A < Z_B$ case a shock wave is backscattered at the interface between A and B. Note that in both cases a shock wave goes through (into medium B). These possibilities are shown schematically in figure 10.4(b). The main laser beam creates a shock wave. The Hugoniot of A is denoted by H, and point A describes the pressure and particle flow velocity of the shock wave (just) before reaching the interface between the targets. If $Z_A > Z_B$ then the lower impedance line (the line $P = Zu_p$) meets the rarefaction wave (RW) curve at point B, while point C describes the case $Z_A < Z_B$ (a higher impedance) where at the interface a shock wave is backscattered. The final pressure and final flow velocity (just) after the wave passes the interface is determined by point C for the higher impedance ($Z_B > Z_A$) and by point B for the lower impedance ($Z_B < Z_A$). This latter case is shown in detail in figure 10.5(b).

If the impedances of A and B are not very different, **impedance matching**, then to a very good approximation the RW curve in figure 10.5(b) and RH–RW curve in figure 10.4 are the mirror reflection (with respect to the vertical line at $u_1 = \text{constant}$) of the Hugoniot H curve. In this case, from figure 10.5(b), one has

$$\begin{aligned} Z &\equiv \rho_0 u_s \\ P_1 &= Z_A u_1 = \rho_{0A} u_{sA} u_1 \\ u_{sA} &= c_{0A} + \alpha_A u_1 \\ P_2 &= Z_B u_2 \\ \tan\theta = \frac{u_2 - u_1}{P_1 - P_2} &= \frac{u_1}{P_1} \Rightarrow \frac{P_2}{P_1} = \frac{2Z_B}{Z_A + Z_B} \approx \frac{2\rho_{0B} c_{0B}}{\rho_{0A} c_{0A} + \rho_{0B} c_{0B}} \end{aligned} \tag{10.45}$$

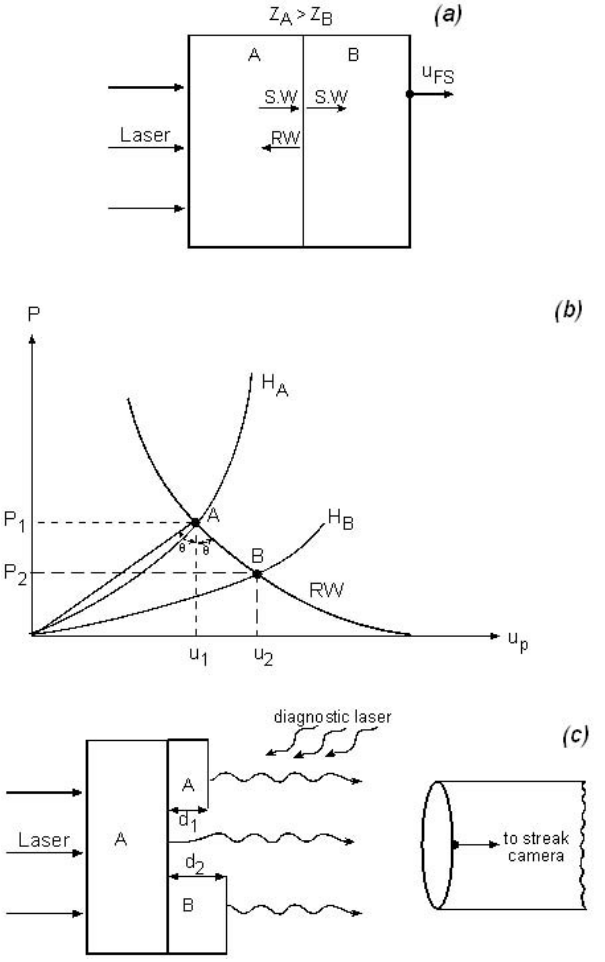

Figure 10.5. (a) A laser induces a shock wave into target A with impedance smaller than target B. A rarefaction wave (RW) is reflected at the interface A–B. (b) The Hugoniot curves H_A and H_B for shock waves in A and B. The reflected rarefaction wave (RW) is also shown. (c) A schematic setup for an impedance-matching experiment.

where the last approximate equality is for weak shock waves. A similar result is obtained in the case with higher impedance ($Z_B > Z_A$).

In figure 10.5(c) a schematic setup of an impedance-matching experiment is given. When a shock wave reaches the interface with the vacuum (or the surrounding atmosphere), it irradiates according to the temperature of the shock wave heated medium. Note that it is a very difficult task to calculate the temperature of the shocked medium from the measurement of this irradiation. If the shock wave temperature is high (about a few thousand

K), then the self-illumination may be large enough to be detected by a streak camera (or other appropriate optical collecting device with a fast information recording). If the detecting devices are not sensitive to the self-illumination then the measurement of a reflected (diagnostic) laser may be more useful, since the reflection changes significantly with the arrival of the shock wave. The shock wave velocities in A and B are directly measured in this way by recording the signal of shock breakthrough from the base of A, and from the external surfaces of the stepped targets. The time t_1 that the shock wave travels through a distance d_1 in A, and the time t_2 that the shock wave travels through a distance d_2 in B, yields the appropriate shock velocities in both targets. Since the initial densities are known, the impedances of A and B are directly measured. The equation of state of A is known and the Hugoniot of A is plotted. Using equations (10.45), P_1 is known (from the measurement of u_{sA}) and P_2 is directly calculated from the measurements of both impedances. In this way, the difficult task of measuring two parameters in the unknown (equation of state) material B is avoided.

As has been shown, it is quite straightforward to measure the shock-wave velocity (assuming that the shock wave is steady, one-dimensional and the measurement device is very accurate). It is also possible to measure indirectly the particle flow velocity by measuring the free-surface velocity. Accurate optical devices, called VISAR (velocity interferometer system for any reflector) and ORVIS (optically recording velocity interferometer system) (practically, very fast recording 'radar' devices in the optical spectrum), have been developed to measure accurately the free-surface velocity. After the shock wave reaches the back surface of the target, a release wave with the characteristics of a rarefaction wave is backscattered into the target. Since this isentrope is almost the mirror image of the Hugoniot (see figure 10.4(b); the 'mirror' is at $u_1 =$ constant), one gets

$$u_1 = \tfrac{1}{2} u_{FS}. \tag{10.46}$$

Therefore, the measurement of u_s and u_{FS} determines all the parameters in the compressed medium (assuming the initial state is accurately known).

The highest laser-induced pressures, $\sim 10^8$–10^9 atm, have been obtained during the collision of a target with an accelerating foil. This acceleration was achieved by laser-produced plasma, or by x-rays from a cavity produced by laser–plasma interactions. It is therefore now shown how the pressure is calculated in a planar collision between a flyer and a target.

The flyer has a known (i.e. measured experimentally) initial velocity before impact, u_f. The initial state before collision is for the target (B), $u_p = 0$ and $P = 0$, while for the flyer (A), $u_p = u_f$ and $P = 0$. Upon impact, a shock wave moves forward into B, and another shock wave goes into the flyer in the opposite direction. The pressure and the particle velocity are continuous at the target–flyer interface. Therefore, the particle velocity of the target changes from zero to u, while the particle velocity in the flyer

changes from u_f to u. Moreover, the pressure in the flyer plate A equals the pressure in the target plate B, and if the equations of state are known and given by (10.44), and the second equation of (10.35) is used to calculate the pressure, one gets

$$P_H = \rho_{0B} u(c_{0B} + \alpha_B u) = \rho_{0A}(u_f - u)[c_{0A} + \alpha_A(u_f - u)]. \tag{10.47}$$

This is a quadratic equation in u, with the following solution:

$$\begin{aligned} u &= \frac{-b - \sqrt{b^2 - 4ac}}{2a} \\ a &\equiv \rho_{0A}\alpha_A - \rho_{0B}\alpha_B \\ b &\equiv -(c_{0A}\rho_{0A} + c_{0B}\rho_{0B} + 2\rho_{0A}\alpha_A u_f) \\ c &\equiv (c_{0A}\rho_{0A} + \rho_{0A}\alpha_A u_f)u_f. \end{aligned} \tag{10.48}$$

Once the flow velocity is known, it is substituted into (10.47) to derive the pressure. If the equation of state of the target is not known, then it is necessary to measure the shock-wave velocity u_{sB} as explained above. In this case, the pressure equality in the flyer and the target yields

$$P_H = \rho_{0B} u_{sB} u = \rho_{0A}[c_{0A} + \alpha_A(u_f - u)](u_f - u). \tag{10.49}$$

Note that in this equation u_{sB} is known. The solution of this equation is

$$\begin{aligned} u &= u_f + w - \left[w^2 + \left(\frac{\rho_{0B}}{\rho_{0A}\alpha_A}\right) u_{sB} u_f\right]^{1/2} \\ w &\equiv \frac{1}{2\alpha_A}\left(c_{0A} + \frac{\rho_{0B} u_{sB}}{\rho_{0A}}\right). \end{aligned} \tag{10.50}$$

In these types of experiment it is occasionally convenient to measure the free-surface velocity of the target and to also study the dynamic strength of materials, as explained in section 10.8.

We end this section with a short comment on shock-wave stability. One can see from (10.26) that different disturbances of density travel with different velocities, so that the larger the density ρ the faster the wave travels. Therefore, an initial profile $\rho(x, 0)$ becomes distorted with time. This is true not only for the density but also for the pressure $P(x, 0)$, for the flow velocity $u(x, 0)$, etc. In this way a smooth function of these parameters will steepen in time due to the nonlinear effect of the wave propagation (higher amplitudes move faster). Therefore, a compression wave is steepened into a shock wave because in most solids the sound velocity is an increasing function of the pressure. In the laboratory frame of reference, the speed of a disturbance is the sum of the flow velocity and the sound velocity $(c_s + u)$. Therefore, a higher-pressure disturbance will catch up with the lower-pressure disturbance, causing a sharpening profile of the wave. In

reality there are also dissipative mechanisms such as viscosity and thermal transport. Therefore, the sharpening profile mechanism can only increase until the dissipative forces become significant, and they begin to cancel out the effect of increasing sound speed with pressure. When the sum of these opposing mechanisms cancels out, the wave profile no longer changes in time and it becomes a steady shock wave.

The dissipative phenomena are nonlinear functions of the strain rate (strain is the relative distortion of a solid $\sim \mathrm{d}l/l$ and the strain rate is the time derivative of the strain). Therefore, for very fast laser-induced phenomena, the rise-time of a shock wave is very small and it can be significantly less than 1 ns.

As already stated above, a disturbance moves at the speed $c_\mathrm{s} + u$ in a compression wave. Therefore, a disturbance behind the shock front cannot be slower than the shock velocity, because in this case it will not be able to catch the wave front, and the shock would decay (i.e. the shock is unstable to small disturbances behind it). Similarly, a small compressive disturbance ahead of the shock must move slower than the shock front in order not to create another shock wave. Thus the conditions for a stable shock wave can be summarized as

$$\frac{\mathrm{d}c_\mathrm{s}}{\mathrm{d}P} > 0, \qquad c_\mathrm{s} + u_\mathrm{p} \geq u_\mathrm{s}, \qquad u_\mathrm{s} > c_{\mathrm{s}_0}. \tag{10.51}$$

The first of these equations states that the speed of sound increases with increasing pressure. The second equation describes the fact that the shock wave is subsonic (Mach number smaller than one) with respect to the shocked medium. The last equation of (10.51) is the well-known phenomenon that a shock wave is supersonic (Mach number larger than one) with respect to the unshocked medium. Using equations (10.13) and (10.36),

$$c_\mathrm{s} = \sqrt{\left(\frac{\partial P}{\partial \rho}\right)_\mathrm{S}} = V\sqrt{-\left(\frac{\partial P}{\partial V}\right)_\mathrm{S}}, \qquad u_\mathrm{s} = V_0\sqrt{\frac{P_1 - P_0}{V_0 - V_1}} \tag{10.52}$$

one gets from the last of equations (10.51) the following shock stability criterion:

$$\frac{P_1 - P_0}{V_0 - V_1} > -\left(\frac{\partial P}{\partial V}\right)_{\mathrm{S},0}. \tag{10.53}$$

This inequality states that the slope of the Rayleigh line (figure 10.4(a)) is larger than the slope of the isentrope at the initial state. Similarly, one can show that the second of equations (10.51) yields the criterion that the Hugoniot at the final state (denoted by 1) must be steeper than the Rayleigh line:

$$\frac{P_1 - P_0}{V_0 - V_1} \leq -\left(\frac{\mathrm{d}P}{\mathrm{d}V}\right)_{\mathrm{H},1}. \tag{10.54}$$

It is important to point out that these criteria are not always satisfied. For example, the speed of sound of fused silica decreases with pressure in a domain of low pressures, so that in this case the shock wave is not stable. Moreover, in the regime of phase transitions (solid–solid due to change in symmetry or solid–liquid), the shock wave can split into two or more shock waves. However, in these cases the stability criteria can be satisfied for each individual shock wave.

10.5 Shock Waves in the Presence of Magnetic Fields

Megagauss magnetic fields are easily achieved in laser plasma interactions (see chapter 8). These large magnetic fields, which are created in the corona, have a large pressure:

$$P_{\mathrm{B}}(\mathrm{Mbar}) \approx 0.04[B(\mathrm{Mgauss})]^2. \tag{10.55}$$

The magnetic fields do not penetrate into the solid on the time scale of the shock-wave transient. Since we are mainly interested in the high pressures ($\sim$Mbar) achieved in the solid target, it appears that the high magnetic fields in the corona do not play any important role. However, if shock waves are created in the corona, or between the critical surface and the ablation surface, then the magnetic pressure, the thermal pressure and the shock-wave pressure might be comparable:

$$\beta \equiv \frac{P_{\mathrm{T}}}{P_{\mathrm{B}}} \approx 4\left(\frac{n_{\mathrm{e}}}{10^{20}\,\mathrm{cm}^{-3}}\right)\left(\frac{T_{\mathrm{e}}}{\mathrm{keV}}\right)\left(\frac{\mathrm{MGauss}}{B}\right)^2. \tag{10.56}$$

For small magnetic fields, $\beta \gg 1$, the magnetic fields are not important. However, for $\beta \approx 1$ or smaller, a state that is possible to achieve with a few megagauss magnetic field, the creation of a shock wave requires the analysis of shock waves in the presence of a magnetic field.

Since the magnetic field has in general a direction not parallel to the shock-wave velocity, it is necessary to consider the directions normal and parallel to the shock-wave front (the discontinuity). In the following the shock-wave (front) frame of reference is used. The normal components to the shock front are denoted by a subscript 'n', while the tangential components (i.e. the components parallel to the shock-wave surface) have the subscript 't'. As in the previous section, the variables before the shock (upstream) and after the shock (downstream) get the subscript 0 and 1 respectively. In this case one has the following jump equations (across the shock-wave discontinuity):

(a) mass conservation;
(b) momentum conservation normal and parallel to the shock front;

(c) energy conservation; and
(d) continuity (over the shock front) of the normal magnetic induction field B_n and of the parallel electric field E_t.

We use the magneto-hydrodynamic equations (in Gaussian units) to derive conservation laws in the form

$$\begin{aligned}
&\frac{\partial}{\partial t}[X] + \nabla \cdot \Gamma = 0 \\
&\lim_{V \to 0} \iiint_V \frac{\partial}{\partial t}[X] = 0 \Rightarrow \iiint_V \nabla \cdot \Gamma \, \mathrm{d}V = \oiint_A \boldsymbol{\Gamma} \cdot \mathbf{n} \, \mathrm{d}A = 0 \\
&\Rightarrow (\boldsymbol{\Gamma}_0 - \boldsymbol{\Gamma}_1) \cdot \mathbf{n} \equiv [\boldsymbol{\Gamma} \cdot \mathbf{n}] = 0
\end{aligned} \tag{10.57}$$

where V is a volume containing the shock wave singularity, A is the area enclosing the volume V (Gauss divergence theorem) and $\mathbf{n}$ is a unit vector perpendicular to the area under consideration. The area A is taken as a small box surrounding the shock front, where the thickness of the box tends to zero (therefore V goes to zero). In this case only the two faces with directions $\mathbf{n}$ and $-\mathbf{n}$, on either side of the shock front, contribute to the integral. Γ_0 and Γ_1 are the values of Γ on either side of the shock surface (the discontinuity). The end result of the class of equations (10.57) is the jump conditions across the shock wave front.

The Maxwell equation, which describes the fact that there are no magnetic poles, gives immediately a jump condition:

$$\nabla \cdot \mathbf{B} = 0 \Rightarrow (\mathbf{B}_0 - \mathbf{B}_1) \cdot \mathbf{n} = 0 \Rightarrow B_{0n} = B_{1n}. \tag{10.58}$$

Another Maxwell equation, together with the zero Lorentz force ($\mathbf{E} + \mathbf{v} \times \mathbf{B}/c = 0$), yields

$$\begin{aligned}
&\frac{\partial \mathbf{B}}{\partial t} = -c\nabla \times \mathbf{E} = \nabla \times (\mathbf{v} \times \mathbf{B}) = \nabla \cdot (\mathbf{B}\mathbf{v} - \mathbf{v}\mathbf{B}) = 0 \\
&\Rightarrow [(\mathbf{B}\mathbf{v} - \mathbf{v}\mathbf{B}) \cdot \mathbf{n}] = 0 \Rightarrow [B_t v_n - v_t B_n] = 0 \\
&\Rightarrow B_{0t} v_{0n} - v_{0t} B_{0n} = B_{1t} v_{1n} - v_{1t} B_{1n}
\end{aligned} \tag{10.59}$$

a new jump condition. This equation is the continuity of the tangential component of the electric field (note that $\mathbf{E} = \mathbf{B} \times \mathbf{v}/c$ in the present approximation).

The mass conservation is directly derived in the usual form:

$$\frac{\partial \rho}{\partial t} + \nabla \cdot (\rho \mathbf{v}) = 0 \Rightarrow [\rho \mathbf{v} \cdot \mathbf{n}] = 0 \Rightarrow \rho_0 v_{0n} = \rho_1 v_{1n}. \tag{10.60}$$

The momentum jump conditions (two equations) are obtained from the following combined momentum and Maxwell equations:

$$\begin{aligned} &\rho\frac{\mathrm{d}\mathbf{v}}{\mathrm{d}t} = -\nabla P + \frac{1}{c}\mathbf{J}\times\mathbf{B} \\ &\nabla\times\mathbf{B} = \frac{4\pi}{c}\mathbf{J} \\ &\Rightarrow \rho\frac{\mathrm{d}\mathbf{v}}{\mathrm{d}t} = -\nabla P + \frac{1}{4\pi}(-\tfrac{1}{2}\nabla B^2 + \mathbf{B}\cdot\nabla\mathbf{B}). \end{aligned} \tag{10.61}$$

The following identities, derived by using (10.58) and (10.60),

$$\nabla\cdot(\rho\mathbf{v}\mathbf{v}) = \rho\mathbf{v}\cdot\nabla\mathbf{v} - \mathbf{v}\frac{\partial\rho}{\partial t} = \rho\frac{\mathrm{d}\mathbf{v}}{\mathrm{d}t} - \frac{\partial}{\partial t}(\rho\mathbf{v}), \qquad \nabla\cdot(\mathbf{B}\mathbf{B}) = \mathbf{B}\cdot\nabla\mathbf{B} \tag{10.62}$$

are used in (10.61) in order to derive the momentum equation in the following form (it is more convenient to use these identities in this new equation in order to derive (10.61)):

$$\frac{\partial}{\partial t}(\rho\mathbf{v}) + \nabla\cdot\left[\rho\mathbf{v}\mathbf{v} - \frac{1}{4\pi}\mathbf{B}\mathbf{B} + \mathbf{I}\left(P + \frac{B^2}{8\pi}\right)\right] = 0 \tag{10.63}$$

where $\mathbf{v}\mathbf{v}$ and $\mathbf{B}\mathbf{B}$ are tensors of the second rank (i.e. matrices with components $v_i v_j$, $B_i B_j$, $i,j = 1,2,3$ in Cartesian coordinates), and $\mathbf{I}$ is the unit matrix (with components $\delta_{ij} = 1$ for $i = j$ and zero for $i \neq j$, so that $\nabla\cdot(\mathbf{I}\psi) = \nabla\psi$). This equation is in the desired form of (10.57), yielding the momentum jump conditions:

$$\begin{aligned} &\left[\left(\rho\mathbf{v}\mathbf{v} - \frac{1}{4\pi}\mathbf{B}\mathbf{B}\right)\cdot\mathbf{n}\right] + \left[\left(P + \frac{B^2}{8\pi}\right)\mathbf{n}\right] = 0 \\ &\Rightarrow \begin{cases} \left[\rho v_{\mathrm{n}}^2 + P + \dfrac{B_{\mathrm{t}}^2}{8\pi}\right] = 0 \\ \left[\rho v_{\mathrm{t}} v_{\mathrm{n}} - \dfrac{B_{\mathrm{t}} B_{\mathrm{n}}}{4\pi}\right] = 0. \end{cases} \end{aligned} \tag{10.64}$$

The two relations were obtained for the normal and tangential components (the jump condition for B_{n} has been used in the first relation).

The last equation to be obtained is the energy relation. In section 3.1 (equation 3.19), the following energy conservation is derived:

$$\frac{\partial}{\partial t}\left[\rho\left(\varepsilon + \frac{1}{2}v^2\right)\right] + \nabla\cdot\left[\rho\mathbf{v}\left(\varepsilon + \frac{P}{\rho} + \frac{1}{2}v^2\right)\right] - \mathbf{E}\cdot\mathbf{J} = 0 \tag{10.65}$$

where the transport term and the external forces are neglected. The problem now is to write the Joule heating term in a format required by a conservation law (like the first two terms of (10.65)). Using $\mathbf{E}$ and $\mathbf{J}$ from equations (10.59)

and (10.61). the Joule heating term can be written in the following way:

$$-\mathbf{E}\cdot\mathbf{J} = \frac{1}{4\pi}[(\mathbf{v}\times\mathbf{B})\cdot\nabla\times\mathbf{B}]$$
$$= \frac{1}{4\pi}[\mathbf{B}\cdot(\mathbf{v}\cdot\nabla)\mathbf{B} - \mathbf{v}\cdot(\mathbf{B}\cdot\nabla)\mathbf{B}]. \tag{10.66}$$

Using (10.59) (multiplied by **B**) and vector algebra, the following identity is derived:

$$\frac{\mathrm{d}}{\mathrm{d}t}\left(\frac{B^2}{2}\right) = B^2\nabla\cdot\mathbf{v} - \mathbf{B}(\mathbf{B}\cdot\nabla)\mathbf{v}$$
$$\Rightarrow \frac{\partial}{\partial t}\left(\frac{B^2}{2}\right) = B^2\nabla\cdot\mathbf{v} - \mathbf{B}(\mathbf{B}\cdot\nabla)\mathbf{v} - \mathbf{v}\cdot\nabla\left(\frac{B^2}{2}\right). \tag{10.67}$$

Using the identity (10.67) in (10.66), we can write

$$-\mathbf{E}\cdot\mathbf{J} = \frac{\partial}{\partial t}\left(\frac{B^2}{8\pi}\right) + \frac{1}{4\pi}\nabla\cdot[B^2\mathbf{v} - (\mathbf{B}\cdot\mathbf{v})\mathbf{B}]. \tag{10.68}$$

We confirm this identity by an alternative derivation. The energy conservation of the electromagnetic field in a medium is (see Appendix A, equations (A.10) and (A.14), in Gaussian units)

$$\frac{\partial}{\partial t}\left(\frac{B^2}{8\pi}\right) + \nabla\cdot\left(\frac{c}{4\pi}\mathbf{E}\times\mathbf{B}\right) = -\mathbf{J}\cdot\mathbf{E} \tag{10.69}$$

where the $\mathbf{D}\cdot\mathbf{E} = \varepsilon E^2$ (ε is the dielectric coefficient) is neglected. This equation together with

$$\mathbf{E} + \frac{\mathbf{v}\times\mathbf{B}}{c} = 0, \qquad (\mathbf{B}\times\mathbf{v})\times\mathbf{B} = B^2\mathbf{v} - (\mathbf{B}\cdot\mathbf{v})\mathbf{B} \tag{10.70}$$

yields equation (10.68).

Substituting (10.68) into (10.65) gives the energy equation in the desired form for the jump condition across the shock wave:

$$\frac{\partial}{\partial t}\left[\rho\left(\varepsilon + \frac{1}{2}v^2 + \frac{B^2}{8\pi}\right)\right] + \nabla\cdot\left\{\rho\mathbf{v}\left(\varepsilon + \frac{P}{\rho} + \frac{1}{2}v^2\right) + \frac{1}{4\pi}[B^2\mathbf{v} - (\mathbf{B}\cdot\mathbf{v})\mathbf{B}]\right\} = 0$$
$$\Rightarrow \left[\left\{\rho\mathbf{v}\left(\varepsilon + \frac{P}{\rho} + \frac{1}{2}v^2\right) + \frac{1}{4\pi}[B^2\mathbf{v} - (\mathbf{B}\cdot\mathbf{v})\mathbf{B}]\right\}\cdot\mathbf{n}\right] = 0$$
$$\Rightarrow \left[\varepsilon + \frac{P}{\rho} + \frac{1}{2}(v_\mathrm{n}^2 + v_\mathrm{t}^2) + \frac{B_\mathrm{t}^2}{4\pi\rho} - \frac{v_\mathrm{t}B_\mathrm{t}B_\mathrm{n}}{4\pi}\right] = 0. \tag{10.71}$$

In summary, the jump equations derived above are: (10.58), (10.59), (10.60), (10.64) and (10.71). The shock-wave surface is at an angle θ relative to the magnetic induction **B**, i.e. the shock front propagates with an angle θ relative

to the magnetic induction **B**. The variables before the shock and after the shock in the shock-wave frame of reference are

$$\begin{aligned} &\textbf{upstream}: \quad \rho_0, P_0, E_0; v_{0\mathrm{n}}, v_{0\mathrm{t}}; B_{0\mathrm{n}} = B\cos\theta, B_{0\mathrm{t}} = B\sin\theta \\ &\textbf{downstream}: \quad \rho_1, P_1, E_1; v_{1\mathrm{n}}, v_{1\mathrm{t}}; B_{1\mathrm{n}}, B_{1\mathrm{t}} \end{aligned} \tag{10.72}$$

where $\rho = 1/V$ is the density, P is the pressure, E is the internal energy connected to the entropy and the density by the thermodynamic relation

$$\mathrm{d}E = T\,\mathrm{d}S - P\,\mathrm{d}V \tag{10.73}$$

and **v** is the medium velocity in the shock-wave frame of reference. As shown above, one has the following six jump conditions (Thompson 1962, Shkarofsky *et al*. 1966):

$$\begin{aligned} &(1) \quad \rho_0 v_{0\mathrm{n}} = \rho_1 v_{1\mathrm{n}} \\ &(2) \quad P_0 + \rho_0 v_{0\mathrm{n}}^2 + \frac{B_{0\mathrm{t}}^2}{8\pi} = P_1 + \rho_1 v_{1\mathrm{n}}^2 + \frac{B_{1\mathrm{t}}^2}{8\pi} \\ &(3) \quad \rho_0 v_{0\mathrm{n}} v_{0\mathrm{t}} - \frac{B_{0\mathrm{n}} B_{0\mathrm{t}}}{4\pi} = \rho_1 v_{1\mathrm{n}} v_{1\mathrm{t}} - \frac{B_{1\mathrm{n}} B_{1\mathrm{t}}}{4\pi} \\ &(4) \quad \frac{1}{2}(v_{0\mathrm{n}}^2 + v_{0\mathrm{t}}^2) + \varepsilon_0 + \frac{P_0}{\rho_0} + \frac{v_{0\mathrm{n}} B_{0\mathrm{t}}^2 - v_{0\mathrm{t}} B_{0\mathrm{n}} B_{0\mathrm{t}}}{4\pi\rho_0 v_{0\mathrm{n}}} \\ &\qquad = \frac{1}{2}(v_{1\mathrm{n}}^2 + v_{1\mathrm{t}}^2) + \varepsilon_1 + \frac{P_1}{\rho_1} + \frac{v_{1\mathrm{n}} B_{1\mathrm{t}}^2 - v_{1\mathrm{t}} B_{1\mathrm{n}} B_{1\mathrm{t}}}{4\pi\rho_1 v_{1\mathrm{n}}} \\ &(5) \quad B_{0\mathrm{n}} = B_{1\mathrm{n}} \\ &(6) \quad v_{0\mathrm{n}} B_{0\mathrm{t}} - v_{0\mathrm{t}} B_{0\mathrm{n}} = v_{1\mathrm{n}} B_{1\mathrm{t}} - v_{1\mathrm{t}} B_{1\mathrm{n}}. \end{aligned} \tag{10.74}$$

The first equation is the mass conservation, the second and third equations are the momentum conservation and the fourth equation is the energy conservation. The fifth equation is the continuity of the normal component of **B**, while the last equation is the continuity of the tangential component of the electric field (note that $\mathbf{E} = \mathbf{B} \times \mathbf{v}/c$). Assuming that the initial conditions are known, one has in (10.74) six equations with seven unknowns (see the downstream variables of (10.72)). Therefore, it is necessary to measure one parameter. For example, if the plasma satisfies the ideal gas equation of state, then a measurement of the temperature behind the shock wave gives the pressure.

10.6 The Study of High-Pressure Physics

The problems with laser-induced shock waves are the small size of the targets ($\sim$100 μm), the short laser pulse duration ($\sim$1 ns), the poor spatial uniformity

of a coherent electromagnetic pulse (the laser), and therefore the non-uniformity of the created pressure. All these difficulties have been addressed in the literature and the subject of laser-induced shock wave research has been developed significantly. The critical problems are summarized below and their possible solutions are discussed.

(a) The planarity (one-dimensional) of the shock wave regardless of the laser irradiance non-uniformity.
(b) Steady shock wave during the diagnostic measurements in spite of the laser short-pulse duration.
(c) Well-known initial conditions of the shocked medium. This is required to control (i.e. to avoid) the fast electron and x-ray preheating.
(d) Good accuracy ($\sim$1%) of the measurements.

The planarity of the shock wave is achieved by using optical smoothing techniques (Lehmberg and Obenschain 1983, Kato *et al.* 1984, Skupsky *et al.* 1989, Koenig *et al.* 1994, Batani *et al.* 1996). With these devices the laser is deposited in the target uniformly, within $\sim$2% of energy deposition. For example (Lehmberg and Obenschain 1983), one technique denoted as 'induced spatial incoherence' (ISI) consists of breaking each laser beam into a large number of beamlets by reflecting the beam off a large number of echelons. The size of each beamlet is chosen in such a way that its diffraction-limited spot size is about the target diameter. All of the beamlets are independently focused and overlapped on the target. Another technique (Kato *et al.* 1984) divides the beam into many elements that have a random phase shift. This is achieved by passing the laser beam through a phase plate with a randomly phase-shifted mask.

The focal spot of the laser beam on target has to be much larger than the target thickness in order to achieve a one-dimensional steady-state shock wave. In figure 10.6 one can see a schematic profile of a planar target with thickness d, irradiated by a laser with a focal spot area $= \pi R_L^2$. A lateral rarefaction wave enters the shocked area and reduces the pressure and density of the shocked area. This effect distorts the one-dimensional character of the wave, since the shock front is bent in such a way that for very large distances ($\gg d$) the shock-wave front becomes spherical. The rarefaction wave propagates toward the symmetry axis with the speed of sound c_s (in the shock-compressed area), which is larger than the shock-wave velocity u_s. Therefore, the good (i.e. undisturbed by the rarefaction wave) one-dimensional shock area $= \pi R_g^2$ is limited by

$$R_g = R_L - \left(\frac{d}{u_s}\right) c_s = R_L - d\tan\theta \leq R_L - d, \qquad A \equiv \pi R_L^2 \geq 10d^2 \quad (10.75)$$

where d/u_s is the time that the shock wave reaches the back surface. Therefore, in order to have a one-dimensional shock wave one requires that $R_g \approx d$, implying an $R_L \approx 2d$ at least, so that the laser focal spot area

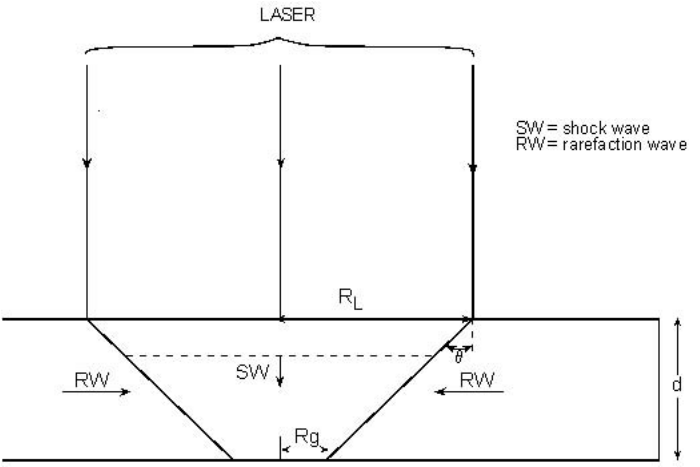

Figure 10.6. A planar target profile irradiated by a laser (the target thickness is d). The one-dimensional spot area $= \pi R_g^2$ (g for 'good') in comparison with the laser irradiation area $= \pi R_L^2$. RW and SW stand for rarefaction wave and shock wave respectively.

$A \approx 10d^2$. This constraint implies very large laser focal spots for thick targets.

The second constraint requires a steady shock wave, i.e. the shock velocity has to be constant as it traverses the target. In figure 10.7 one can see a schematic x–t (space–time) diagram of a laser-induced shock wave. A rarefaction wave (RW), initiated at a time $\Delta t \approx \tau_L$ (the laser pulse duration) after the end of the laser pulse, follows a shock wave (SW) into the target. It is necessary that the rarefaction wave does not overtake the shock wave at position $x = d$ (the back surface) during the measurement of the shock-wave velocity, implying $\tau_L > d/u_s$. For strong shocks, the shock velocity is of the order of the square root of the pressure (see (10.36) or (10.52)), therefore

$$\tau_L > \frac{d}{u_s} \propto \frac{d}{\sqrt{P}}. \tag{10.76}$$

Hot electrons can appear during the laser–plasma interaction (see section 9.6), causing preheating of the target. This preheats the target before the shock wave arrives, therefore 'spoiling' the initial conditions for the high-pressure experiment. Since it is not easy to measure accurately the temperature of the target due to this preheating, it is necessary to avoid preheating. By using shorter wavelengths (0.5 μm or less), the fast electron preheat is significantly reduced. It is therefore required that the target thickness d is larger than the hot electron mean free path λ_e. Using the scaling law for

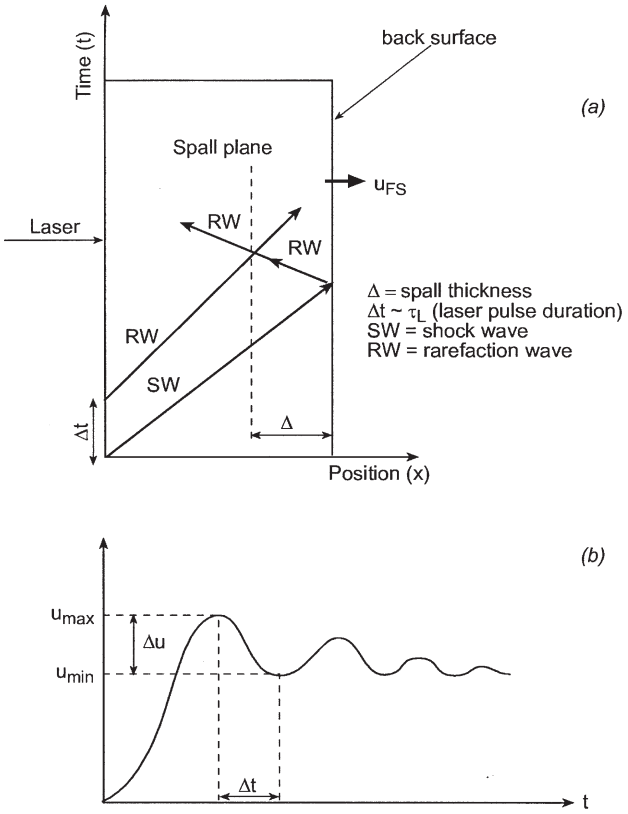

Figure 10.7. (a) *x–t* (space–time) diagram of a laser-induced shock wave. A rarefaction (RW), initiated after the end of the laser pulse, follows a shock wave (SW) into the target. After the shock wave reaches the back surface a rarefaction is reflected. A spall may be created at the intersection of the two rarefaction waves. (b) Typical free-surface velocity when a spall is created.

the hot electron temperature T_h (see equation (9.94)), one has

$$d \gg \lambda_e \propto T_h^2 \propto (I_L \lambda_L)^{0.6}. \tag{10.77}$$

Taking into account all of the constraints given by the relations (10.75), (10.76) and (10.77), and using the experimental scaling law

$$P \propto I_L^{0.8} \tag{10.78}$$

one gets the scaling of the laser energy W_L

$$W_L = I_L A \tau_L \propto I_L^{2.4} \propto P^3. \tag{10.79}$$

Therefore, in order to increase the one-dimensional shock-wave pressure by a factor two, it is necessary to increase the laser energy by an order of magnitude.

A more elegant and efficient way to overcome this problem is to accelerate a thin foil. The foil absorbs the laser, plasma is created (ablation) and the foil is accelerated as in a rocket. In this way, the flyer stores kinetic energy from the laser during the laser pulse duration (the acceleration time) and delivers it, in a shorter time during the collision with a target, in the form of thermal energy. The flyer is effectively shielding the target so that the target initial conditions are not changed by fast electrons or by laser-produced x-rays. For these reasons the laser-driven flyer can achieve much higher pressures on impact than the directly-laser-induced shock wave (Fabbro *et al.* 1986, Cauble *et al.* 1994).

The accuracy of measurements in the study of laser-induced high-pressure physics require diagnostics with a time resolution better than 100 ps, and occasionally better than 1 ps, and a spatial resolution of the order of few microns. The accurate measurements of shock-wave speed and particle-flow velocity are usually obtained with optical devices, including streak camera (Veeser *et al.* 1979, Cottet *et al.* 1985, Ng *et al.* 1987, Evans *et al.* 1996) and velocity interferometers (Moshe *et al.* 1996, Celliers *et al.* 1998).

10.7 Studies of Equations of State

The phenomena of shock-wave propagation through condensed matter are strongly related to the physics of the equations of state (Altshuler 1965, Eliezer *et al.* 1986, Eliezer and Ricci 1991, Bushman *et al.* 1993, Eliezer *et al.* 2002). Atoms in a solid state are attracted to each other at large distances and repel each other at short distances. At zero temperature and zero pressure the equilibrium is obtained at a specific volume V_{0c}, reached at the minimum of the (potential) energy. The atoms can be separated to a large distance by supplying the binding energy (also known as the cohesion energy) of the order of a few eV/atom, while compressing a condensed matter requires energy to overcome the repulsive forces.

Small pressures, of the order of 10^2 atm, can compress a gas to a few times its initial density. However, the compression of a metal by only 10% requires an external pressure (static or shock wave) of the order of 10^5 atm. This is evident from the values of the **compressibility** at standard conditions $\sim 10^{-6}$ atm^{-1}, where κ is defined by

$$\kappa_S = -\frac{1}{V}\left(\frac{\partial V}{\partial P}\right)_S. \tag{10.80}$$

Note that the **bulk modulus** B_S is the inverse of the compressibility, $B_S = 1/\kappa_S$.

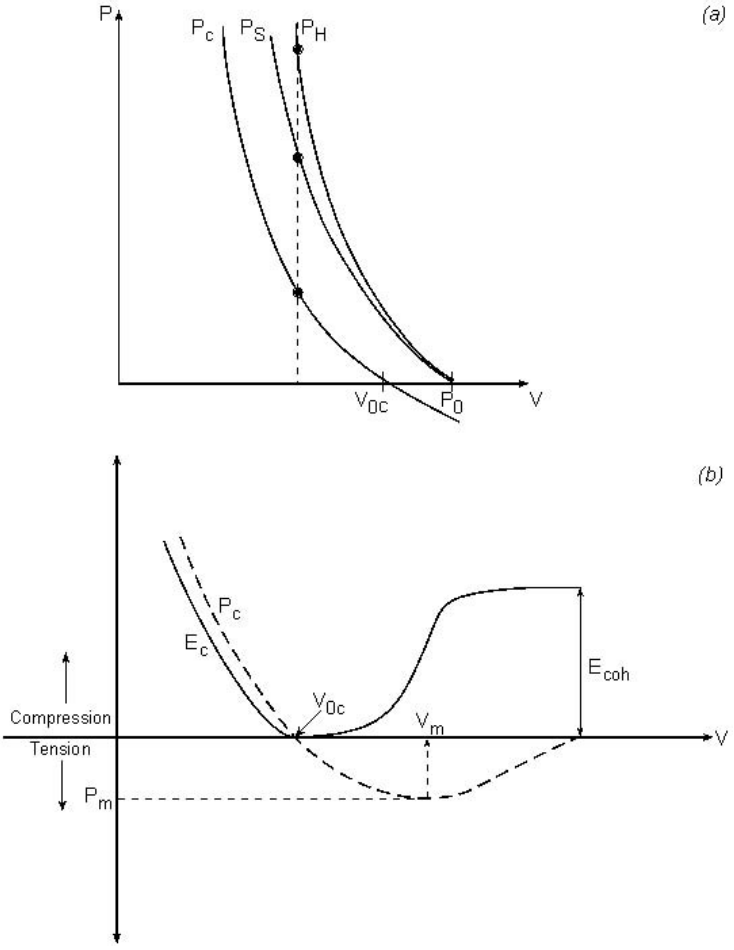

Figure 10.8. (a) The cold pressure P_c, the Hugoniot pressure P_H and the isentrope P_s. The initial conditions for P_H and P_s are $V_0 = 1/\rho_0$, $P_0 = 0$ and T_0 (room temperature). (b) A schematic presentation is given for the cold energy E_c and pressure P_c. The cohesion energy E_{coh} and the minimum pressure P_m, both at $T = 0$, are also shown. For $P_c > 0$ the solid is compressed, while for $P_c < 0$ a tension is applied on the medium.

The P–V diagram in figure 10.8(a) describes the Hugoniot curve $P_H(V)$ for the initial conditions V_0, T_0 and $P_0 = 0$. Note that the atmospheric pressure is negligibly small in comparison with the shock-wave pressures under consideration, so that $P_0 = 0$ or 1 atm are equivalent initial conditions for shock-wave experiments in solids. The difference in figure 10.8(a) at any particular value of V between the cold pressure P_c and the Hugoniot pressure P_H, is equal to the thermal pressure P_T that is caused by the shock wave.

Since P_T is positive, the cold pressure at room temperature is negative, $P_c(V_0) < 0$. In this figure the isentrope P_S that passes through the beginning of the Hugoniot is also shown, so that the mutual positions of P_H, P_S and P_c are illustrated.

The pressure and the internal energy of a material can be divided into two contributions:

(a) The temperature-independent term caused by the interaction forces between the atoms of the material. The appropriate pressure P_c and energy E_c are defined as 'cold pressure' and 'cold energy' respectively.
(b) The thermal term is usually divided into two parts: one part describes the motion of the atoms in the lattice, while the second part is due to the electron thermal motion.

P_a and E_a denote the thermal lattice pressure and energy respectively, and the appropriate electron contributions are P_e and E_e. Therefore, the equation of state is usually written in the following form:

$$\begin{aligned} P(V,T) &= P_c(V) + P_T(V,T) \\ P_T(V,T) &= P_a(V,T) + P_e(V,T) \\ E(V,T) &= E_c(V) + E_T(V,T) \\ E_T(V,T) &= E_a(V,T) + E_e(V,T). \end{aligned} \tag{10.81}$$

The thermodynamic relation relates the cold pressure and energy:

$$E_c(V) = -\int_{V_{0c}}^{V} P_c(V)\,\mathrm{d}V. \tag{10.82}$$

As usual, the potential energy is fixed up to a constant, and this constant has been chosen in such a way that $E_c(V_{0c}) = 0$. Note that $P_c(V_{0c}) = 0$ is the definition of V_{0c}. It has been found that to a good approximation, near the Hugoniot curve, the lattice thermal energy and pressure are related through the Gruneisen equation of state, and the energy is described by the Debye solid-state theory:

$$E_a = C_V(T - T_0) + E_0, \qquad P_a(V,T) = \frac{\gamma_a(V)}{V} E_a \tag{10.83}$$

where γ_a is the Gruneisen coefficient (assumed to be a function of V), C_V is the lattice specific heat at constant volume, T_0 is the initial temperature in the shock wave experiment, usually the room temperature, and E_0 is the internal energy at T_0, defined by

$$E_0 = \int_0^{T_0} C_V(T)\,\mathrm{d}T. \tag{10.84}$$

At room temperature and for slightly lower and higher temperatures, the specific heat C_V has the Dulong–Petit value

$$\begin{aligned} C_V &= \frac{3R}{\langle A\rangle}\left[\frac{\text{erg}}{\text{g}\cdot\text{deg}}\right] \\ R &= 8.314\times 10^7\left[\frac{\text{erg}}{\text{mol}\cdot\text{deg}}\right] \\ \langle A\rangle &= \text{average atomic weight}\left[\frac{\text{g}}{\text{mol}}\right]. \end{aligned} \tag{10.85}$$

For example, $\langle A\rangle$ for aluminium and copper is 27 and 63.55 respectively.

Assuming for the electron thermal part an equation of state similar to the Gruneisen equation of state for the lattice, one has

$$P_e = \frac{\gamma_e}{V}E_e. \tag{10.86}$$

To the first approximation, the thermal electron energy is taken from the free electron model,

$$E_e = \tfrac{1}{2}\beta T^2 \tag{10.87}$$

and β is related to the specific volume V by the thermodynamic relation,

$$\left(\frac{\partial E}{\partial V}\right)_T = T\left(\frac{\partial P}{\partial T}\right)_V - P. \tag{10.88}$$

Substituting (10.86) and (10.87) into (10.88) yields

$$\begin{aligned} \frac{\partial\beta}{\partial V} = \frac{\gamma_e\beta}{V} &\Rightarrow \beta = \gamma_e \exp\left(\int_{V_0}^{V}\frac{\gamma_e\,\mathrm{d}V}{V}\right) \\ \beta &= \beta_0\left(\frac{V}{V_0}\right)^{1/2} \quad \text{for } \gamma_e = 0.5. \end{aligned} \tag{10.89}$$

The value of $\gamma_e = 0.5$ is a good approximation for many metals up to shock-wave data of a few megabars pressure.

Combining equations (10.81), (10.82), (10.83), (10.86) and (10.89), one gets

$$\begin{aligned} P &= P_c + \frac{\gamma_a}{V}[C_V(T-T_0)+E_0] + \frac{1}{4}\left(\frac{\beta_0}{V_0}\right)\left(\frac{V_0}{V}\right)^{1/2}T^2 \\ E &= -\int^V P_c\,\mathrm{d}V + C_V(T-T_0) + E_0 + \frac{\beta_0}{2}\left(\frac{V}{V_0}\right)^{1/2}T^2. \end{aligned} \tag{10.90}$$

The cold pressure can be described by a polynomial in $(V_{0c}/V)^{1/3}$ in such a way that it fits the experimental values of the bulk modulus, the derivative of the bulk modulus at zero pressure, the cohesion energy and the Thomas–Fermi model (or modified models) at very high compressions.

Although the equations of state described in equations (10.90) have 10 parameters, they do not describe phase transitions, such as solid to solid with different symmetry or melting and evaporation. In order to describe these phenomena, many more parameters based on theoretical models and experimental data are required.

As explained in section 10.4, in a shock-wave experiment one can measure the shock-wave velocity (u_s) and the particle velocity (u_p). It has also been attempted to measure the temperature associated with a shock wave; however, the experimental data so far are not very accurate.

The shock-wave velocity is directly measured in a stepped target (velocity = measured step length/measured time difference) using an optical streak camera. The particle velocity is more difficult to measure, and u_p is deduced, for example, from impedance-matching experiments (see section 10.4) or by the optical measuring of the free-surface (i.e. back surface) velocity. The measured equation of state is given in the form of the linear u_s–u_p equation (10.44). The velocity measurements should have an accuracy of about 1%, in order to give good accuracy (~10%) in other variables such as pressure, energy, etc. It is important to point out that the linear u_s–u_p relation (equation (10.44) and table 10.1), is not always correct for all solid elements.

Sometimes a higher polynomial in u_p is necessary to fit the experimental data. For example (Steinberg 1996),

$$\begin{aligned}
\textbf{hafnium}: \quad & u_s(\mathrm{cm}/\mu\mathrm{s}) = 0.298 + 1.448u_p - 3.852\left(\frac{u_p}{u_s}\right)u_p + 7.0\left(\frac{u_p}{u_s}\right)^2 u_p \\
\textbf{lead}: \quad & u_s(\mathrm{cm}/\mu\mathrm{s}) = 0.2006 + 1.429u_p + 0.8506\left(\frac{u_p}{u_s}\right)u_p - 1.64\left(\frac{u_p}{u_s}\right)^2 u_p \\
\textbf{titanium}: \quad & u_s(\mathrm{cm}/\mu\mathrm{s}) = 0.502 + 1.536u_p - 5.138\left(\frac{u_p}{u_s}\right)u_p + 10.82\left(\frac{u_p}{u_s}\right)^2 u_p.
\end{aligned} \tag{10.91}$$

In the following part of this section, it is shown how one can study the thermodynamic equations of state in the neighbourhood of the Hugoniot from the measurements of the shock velocity and the particle velocity. For simplicity, the further discussion assumes the linear u_s–u_p relation (equation (10.44)), valid for many metals.

It is convenient to define the parameter η related to the compression ρ/ρ_0, in such a way that $\eta = 0$ for no compression and $\eta = 1$ for an

infinite ρ/ρ_0:

$$\eta \equiv 1 - \frac{V}{V_0} = 1 - \frac{\rho_0}{\rho}. \tag{10.92}$$

Using equations (10.36) and (10.44), the particle velocity and the shock velocity can be presented in the following way:

$$\left.\begin{aligned} \frac{u_\mathrm{p}}{u_\mathrm{s}} &= \frac{V_0 - V}{V_0} = \eta \\ u_\mathrm{s} &= c_0 + \alpha u_\mathrm{p} \end{aligned}\right\} \Rightarrow \begin{cases} u_\mathrm{p} = \dfrac{\eta c_0}{1 - \alpha\eta} \\ u_\mathrm{s} = \dfrac{c_0}{1 - \alpha\eta} \end{cases}. \tag{10.93}$$

Substituting these results into the Hugoniot pressure, one gets P_H as a function of V (or η), the experimentally measured quantities c_0 and α, and the initial condition V_0:

$$P_\mathrm{H} = \rho_0 u_\mathrm{s} u_\mathrm{p} = \frac{\eta c_0^2}{V_0(1 - \alpha\eta)^2} = \frac{c_0^2(V_0 - V)}{[V_0 - \alpha(V_0 - V)]^2}. \tag{10.94}$$

It is interesting to point out that from this equation the maximum possible compression is obtained for an infinite P_H, implying

$$\frac{\rho_\mathrm{max}}{\rho_0} = \frac{\alpha}{\alpha - 1}. \tag{10.95}$$

For example (see table 10.1), α of aluminium equals 1.4, implying that in a shock wave the compression ρ/ρ_0 is smaller than 2.5.

The derivative of this pressure with respect to the specific volume V is

$$\begin{aligned} P'_\mathrm{H} \equiv \left(\frac{\mathrm{d}P}{\mathrm{d}V}\right)_\mathrm{H} &= \frac{\mathrm{d}P_\mathrm{H}}{\mathrm{d}V} = -\left(\frac{c_0}{V_0}\right)^2 \frac{1 + \alpha\eta}{(1 - \alpha\eta)^3} \\ &= -c_0^2 \left\{ \frac{V_0 + \alpha(V_0 - V)}{[V_0 - \alpha(V_0 - V)]^3} \right\}. \end{aligned} \tag{10.96}$$

Using this relation, the bulk modulus on the Hugoniot, B_H, is obtained:

$$B_\mathrm{H} = -V\left(\frac{\mathrm{d}P}{\mathrm{d}V}\right)_\mathrm{H} \tag{10.97}$$

and its derivative with respect to the pressure can also be derived:

$$\begin{aligned} \left(\frac{\mathrm{d}B_\mathrm{H}}{\mathrm{d}P}\right)_\mathrm{H} &= \left(\frac{\mathrm{d}B_\mathrm{H}}{\mathrm{d}V}\right)_\mathrm{H} \left(\frac{\mathrm{d}V}{\mathrm{d}P}\right)_\mathrm{H} \\ &= -\left[\left(\frac{\mathrm{d}P}{\mathrm{d}V}\right)_\mathrm{H} + V\left(\frac{\mathrm{d}^2P}{\mathrm{d}V^2}\right)_\mathrm{H}\right] \frac{1}{(\mathrm{d}P/\mathrm{d}V)_\mathrm{H}} \\ &= -\left[1 + \frac{V(\mathrm{d}^2P/\mathrm{d}V^2)_\mathrm{H}}{(\mathrm{d}P/\mathrm{d}V)_\mathrm{H}}\right]. \end{aligned} \tag{10.98}$$

Experimentally one measures the bulk modulus at constant entropy and its derivative at $V = V_0$, $P = P_0 = 0$ (the shock wave initial condition). For the Hugoniot pressure and the isentrope P_S starting at $V = V_0$, $P = P_0 = 0$, the following relations are valid:

$$\left(\frac{dP_H}{dV}\right)_{P_0,V_0} = \left(\frac{dP_S}{dV}\right)_{P_0,V_0}, \qquad \left(\frac{d^2P_H}{dV^2}\right)_{P_0,V_0} = \left(\frac{d^2P_S}{dV^2}\right)_{P_0,V_0}. \tag{10.99}$$

From equations (10.96), (10.97), (10.98) and (10.99), the following important relations are derived:

$$\begin{aligned} B_H(P_0,V_0) &= B_S(P_0,V_0) = \frac{c_0^2}{V_0} = \rho_0 c_0^2 \\ B'_H(P_0,V_0) &= B'_S(P_0,V_0) = 4\alpha - 1. \end{aligned} \tag{10.100}$$

From shock-wave data (equation of state), one knows c_0 and α and therefore the bulk modulus and its pressure derivative. The last two physical quantities, B_S and $dB_S/dP = B'_S$, are very important in calculating the cold pressure P_c and energy E_c. B_S, of the order of 1 Mbar, can also be measured in static experiments thanks to the technological advances in reaching high pressures (up to a few megabars). However, it is difficult to measure B'_S in static experiments to a good accuracy since this quantity measures the curvature of the P–V curve. On the other hand, the shock-wave experiments in this domain of pressure are easily and accurately performed.

We now calculate the speed of sound:

$$c_s = \sqrt{\left(\frac{\partial P}{\partial \rho}\right)_S} = V\sqrt{-\left(\frac{\partial P}{\partial V}\right)_S} \equiv V\sqrt{-\frac{dP_S(V)}{dV}}. \tag{10.101}$$

For this purpose one needs the isentrope pressure curve $P_S(V)$, which can be calculated from the knowledge of the Hugoniot pressure $P_H(V)$ using the (ion) Gruneisen equation of state. In order to do so, the electron thermal contribution P_e should be neglected. For most of the solid materials, $P_e \ll P_a$ for pressures less than a few hundred kilobars. For example, we demonstrate this for aluminium at a shock-wave pressure of 580 kbar. At this Hugoniot point, the compression is 1.40 and the temperature is 1480 K. Using the following experimental data at standard conditions

aluminium:
$$\begin{aligned} V_0^{-1} &= \rho_0 = 2.70\ [\mathrm{g/cm^3}] \\ C_V &= 8.96 \times 10^6\ [\mathrm{erg/(g \cdot deg)}] \\ B_S &= 1.36 \times 10^{12}\ [\mathrm{dyne/cm^2}] = 1.36\ \mathrm{Mbar} \\ E_0 &= 10^7\ [\mathrm{erg/g}] \\ \gamma_a &= 2.09 \\ \beta_0 &= 500\ [\mathrm{erg/(g \cdot deg^2)}] \end{aligned} \tag{10.102}$$

we get from the equations of state (10.90):

$$\textbf{aluminium}: \quad \frac{V_0}{V} = \frac{\rho}{\rho_0} = 1.40, \quad T_{\mathrm{H}} = 1480\,\mathrm{K}, \quad P_{\mathrm{H}} = 580\,\mathrm{kbar}$$
$$\Rightarrow P_{\mathrm{c}} = 495.6\,\mathrm{kbar}, \quad P_{\mathrm{a}} = 83.5\,\mathrm{kbar}, \quad P_{\mathrm{e}} = 0.9\,\mathrm{kbar}. \tag{10.103}$$

From this example one can see that even in a shock wave with 580 kbar of pressure in aluminium, the electronic thermal part contributes about 0.15% to the total pressure. Therefore, in the following analysis the electronic thermal part is neglected.

The Gruneisen equation of state (see (10.83)) can be written in the form

$$P(V, E) = P_{\mathrm{c}}(V) + \frac{\gamma_{\mathrm{a}}(V)}{V}[E - E_{\mathrm{c}}(V)]. \tag{10.104}$$

Substituting $P = P_{\mathrm{H}}$ in this equation and subtracting it from P, one gets

$$P - P_{\mathrm{H}} = \frac{\gamma_{\mathrm{a}}}{V}(E - E_{\mathrm{H}}). \tag{10.105}$$

For $P = P_{\mathrm{S}}$, the derivative of (10.105) yields (after using $\mathrm{d}E_{\mathrm{S}}/\mathrm{d}V = -P_{\mathrm{S}}$)

$$P_{\mathrm{S}} = -\frac{\mathrm{d}E_{\mathrm{H}}}{\mathrm{d}V} + (P_{\mathrm{H}} - P_{\mathrm{S}})\frac{d}{\mathrm{d}V}\left(\frac{V}{\gamma_{\mathrm{a}}}\right) + \frac{V}{\gamma_{\mathrm{a}}}\left(\frac{\mathrm{d}P_{\mathrm{H}}}{\mathrm{d}V} - \frac{\mathrm{d}P_{\mathrm{S}}}{\mathrm{d}V}\right). \tag{10.106}$$

Taking the derivative of the Hugoniot energy relation (10.37) gives

$$\frac{\mathrm{d}E_{\mathrm{H}}}{\mathrm{d}V} = \left(\frac{V_0 - V}{2}\right)\frac{\mathrm{d}P_{\mathrm{H}}}{\mathrm{d}V} - \left(\frac{P_0 + P_{\mathrm{H}}}{2}\right). \tag{10.107}$$

Substituting (10.107) into (10.106) yields

$$\frac{\mathrm{d}P_{\mathrm{S}}}{\mathrm{d}V} = \left[1 - \frac{\gamma_{\mathrm{a}}}{2V}(V_0 - V)\right]\frac{\mathrm{d}P_{\mathrm{H}}}{\mathrm{d}V} + \frac{\gamma_{\mathrm{a}}}{2V}(P_0 + P_{\mathrm{H}}) + \frac{\gamma_{\mathrm{a}}}{V}(P_{\mathrm{H}} - P_{\mathrm{S}})\frac{\mathrm{d}}{\mathrm{d}V}\left(\frac{V}{\gamma_{\mathrm{a}}}\right) - P_{\mathrm{S}}\left(\frac{\gamma_{\mathrm{a}}}{V}\right). \tag{10.108}$$

Using equations (10.101) and (10.108) and defining the sound speed on the Hugoniot points, i.e. c_{H} is equal to c_{S} for $P_{\mathrm{S}} = P_{\mathrm{H}}$, one gets

$$c_{\mathrm{H}}^2 = \left(\frac{\gamma_{\mathrm{a}}V}{2}\right)P_{\mathrm{H}} + \left[\left(\frac{\gamma_{\mathrm{a}}V}{2}\right)(V_0 - V) - V^2\right]\frac{\mathrm{d}P_{\mathrm{H}}}{\mathrm{d}V}$$
$$c_{\mathrm{S}}^2 = c_{\mathrm{H}}^2 + \gamma_{\mathrm{a}}V(P_{\mathrm{S}} - P_{\mathrm{H}})\left[1 + \frac{\mathrm{d}}{\mathrm{d}V}\left(\frac{V}{\gamma_{\mathrm{a}}}\right)\right]. \tag{10.109}$$

In the second equation of (10.109), the speed of sound c_{S} is along the release isentrope off the Hugoniot (i.e. an isentrope starting after the shock-wave point with pressure P_{H}). See curve S_2 in figure 10.4(a). It was

found experimentally that the Gruneisen coefficient satisfies the relation

$$\frac{\gamma_a(V)}{V} = \frac{\gamma_0}{V_0} = \text{const.} \tag{10.110}$$

Using this relation in (10.109) yields the approximate relation

$$c_S^2 \approx c_H^2 + \gamma_0 \left(\frac{V^2}{V_0}\right)(P_S - P_H). \tag{10.111}$$

Substituting into (10.109) the equations (10.93), (10.94) and (10.96), one gets the sound speed on the Hugoniot points as a function of measured quantities, $\eta = u_p/u_s$, c_0 and α:

$$c_H = c_0 \frac{1-\eta}{(1-\alpha\eta)^{3/2}} \sqrt{\frac{\gamma_0 \eta}{2}} (1 + \alpha\eta - \gamma_0 \alpha \eta^2)^{1/2}. \tag{10.112}$$

From equation (10.111), or more accurately from (10.109), the Gruneisen parameter may be determined if the Hugoniot pressure and the speed of sound are measured experimentally. By placing a transparent material coupled to the target under consideration, the rarefaction overtakes the shock wave and reduces significantly the shock pressure. By measuring this phenomenon, the change in light radiance caused by the decrease in the shock pressure, the speed of sound in the shocked material can be measured.

10.8 Studies of Dynamic Strength of Materials

Spall is a dynamic fracture of materials, extensively studied in ballistic research (Rosenberg *et al*. 1983, Bushman *et al*. 1993). The term spall, as used in shock wave research, is defined as planar separation of material, parallel to the wave front as a result of dynamic tension perpendicular to this plane. The reflection of a shock-wave pulse from the rear surface (the free surface) of a target causes the appearance of a rarefaction wave into the target. Tension (i.e. negative pressure) is induced within the target by the crossing of two opposite rarefaction waves, one coming from the front surface due to the fall of the input pressure and the second due to reflection of the shock wave from the back surface (see figure 10.7(a)). If the magnitude and duration of this tension are sufficient then internal rupture, called spall, occurs. In this section we point out that this type of research can also be done with laser beams (Gilath *et al*. 1988, Eliezer *et al*. 1990, Boustie and Cottet 1991, Fortov *et al*. 1991, De Resseguier and Cottet 1995, Eliaz *et al*. 2000, Moshe *et al*. 2000).

Spall in ductile materials is controlled by localized plastic deformation around small voids that grow and coalesce to form the spall plane. In very fast phenomena and very high tension, as in high-power pulsed laser

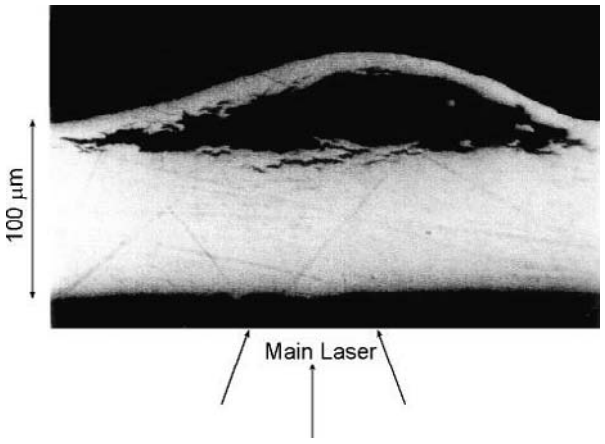

Figure 10.9. Cross section in an Al 6061 target after the spall creation.

interaction with a target, new voids are created due to fluctuations and also contribute to the spall formation. Spall in brittle materials takes place by dynamic crack propagation without large-scale plastic deformation. In this section we do not describe the physics of dynamic failure (Grady 1988, Dekel *et al*. 1998).

In figure 10.9 a cross section with a spall of an aluminium (6061) target, 100 μm thick, is shown. A laser-created shock wave in the aluminium target induced the spall. This typical metallurgical cross section was taken after the experiment was finished. The strain ε that has been formed at the spall area is defined by

$$\varepsilon(1\mathrm{D}) = \frac{\Delta l}{l}, \qquad \varepsilon(3\mathrm{D}) = \frac{\Delta V}{V} = -\frac{\Delta \rho}{\rho} \tag{10.113}$$

where Δl is the difference between the final and original lengths of the target in one dimension and l is the original length, while in three dimensions the strain is defined by the relative change in the volume. From the cross section of figure 10.9 one can measure directly the dynamic strain. One of the important parameters, for the different models describing the spall creation, is the strain rate

$$\dot{\varepsilon} = \frac{\mathrm{d}\varepsilon}{\mathrm{d}t}. \tag{10.114}$$

High-power short-pulse lasers have been used to create strain rates as high as $5 \times 10^8\ \mathrm{s}^{-1}$. When the shock wave reaches the back surface of the solid target, bounded by the vacuum (or the atmosphere), the free surface develops a velocity $u_{\mathrm{FS}}(t)$. This velocity is given by the sum of the particle flow velocity u_{p} and the rarefaction wave velocity U_{r}. The material velocity increase U_{r} is given by the Riemann integral along an isentrope from some point on the

Hugoniot (pressure P_H) to zero pressure (see equations (10.25) and (10.101)):

$$u_{FS} = u_p + U_r, \qquad U_r = \int_0^{P_H} \frac{dP}{\rho c_s} = \int_{\rho_0}^{\rho} \frac{c_s\, d\rho}{\rho} = \int_{V(P_H)}^{V(P=0)} \left(-\frac{dP_S}{dV}\right)^{1/2} dV. \tag{10.115}$$

The derivative dP_S/dV is given in equation (10.108), so that knowledge of P_S gives the value of U_r. Layers of the target adjacent to the free surface go into motion under the influence of the shock-wave transition from V_0, $P_0 = 0$ to V, P_H, and subsequent isentropic expansion in the reflected rarefaction wave from P_H, V to $P_0 = 0$, V_2 (see figure 10.4(a)), where $V_2 > V_0$. Although these two processes are not the same, it turns out that for $u_p \ll u_s$ one has, to a very good approximation,

$$u_p \approx U_r \Rightarrow u_{FS} \approx 2u_p. \tag{10.116}$$

It was found experimentally, for many materials, that this relation is very good (within 1%) up to shock-wave pressures of about 1 Mbar. Therefore, from the free-surface velocity measurements, one can calculate the particle flow velocity of the shock-wave compressed material. This free-surface velocity, together with the experimental measurement of the shock-wave velocity, might serve as the two necessary quantities, out of five (P_H, $V = 1/\rho$, E_H, u_s, u_p), to fix a point on the Hugoniot.

A typical free-surface velocity measurement, in the case of the creation of a spall, is given in figure 10.7(b). u_{max} (related to u_p in the above discussion) in this figure is the maximum free-surface velocity. At later times the free-surface velocity decreases to u_{min} until a second shock arrives from the spall, 'the new free surface'. When a rarefaction wave reaches the internal rupture of the target (the spall) a shock wave is reflected towards the free surface, causing an increase in the free-surface velocity. These reverberation phenomena are repeated until the free surface reaches an asymptotic constant velocity. The spall strength Σ, i.e. the negative pressure (tension) that a spall occurs, can be calculated using the Riemann invariants

$$\left.\begin{aligned} u(P=0, u=u_{min}) \equiv u_{min} &= u_0' - \int_{\Sigma}^{0} \frac{dP}{\rho c_s} \\ u(P=0, u=u_{max}) \equiv u_{max} &= u_0' + \int_{\Sigma}^{0} \frac{dP}{\rho c_s} \end{aligned}\right\} \Rightarrow \Delta u \equiv u_{max} - u_{min} = 2\int_{\Sigma}^{0} \frac{dP}{\rho c_s}. \tag{10.117}$$

Assuming that the negative pressure is not too large, then to a good approximation $\rho = \rho_0$ and $c_s = c_0$, implying that the spall strength is

$$\Sigma = -\frac{\rho_0 c_0 (u_{max} - u_{min})}{2} \equiv -\sigma_{spall}. \tag{10.118}$$

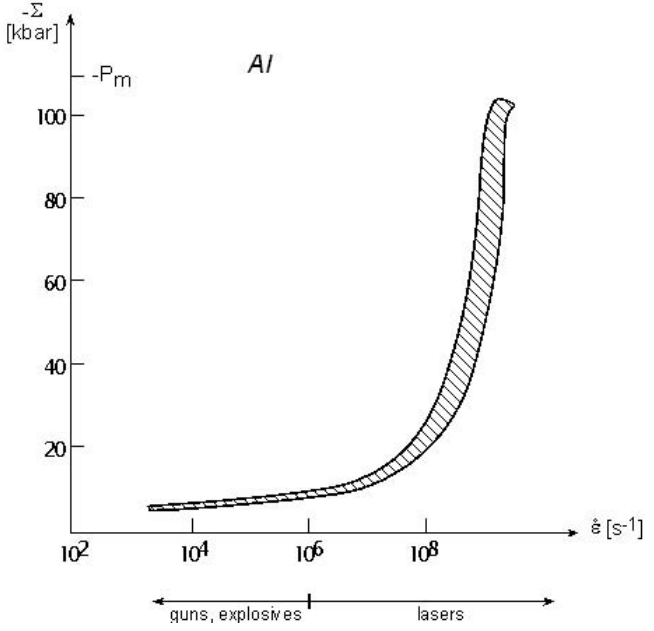

Figure 10.10. Experimental values of spall strength σ_{spall} as a function of the strain rate for aluminium. $-P_{\text{m}}$ is the maximum theoretical value of the spall strength (see figure 10.8(b)).

The minimum (i.e. the maximum absolute value) possible Σ is given by the equation of state, as shown in figure 10.8 by the value P_{m}.

The strain ε and the strain rate $\mathrm{d}\varepsilon/\mathrm{d}t$ can be approximated by

$$\varepsilon = \frac{u_{\text{p}}}{c_0}, \qquad \dot{\varepsilon} = \frac{\mathrm{d}\varepsilon}{\mathrm{d}t} = \frac{1}{2c_0}\frac{\mathrm{d}u_{\text{FS}}}{\mathrm{d}t} \approx \frac{1}{2c_0}\frac{\Delta u}{\Delta t} \tag{10.119}$$

where Δt is the time difference (see figure 10.7(b)) between the time measurements of $u_{\max}$ and $u_{\min}$. The experimental data of σ_{spall} as a function of the strain rate are summarized in figure 10.10 for aluminium targets. Up to about a strain rate of $10^6\,\text{s}^{-1}$, the strain creation methods are gun drivers of plates or high explosives, while the higher strain rates are achieved with high-power pulsed laser drivers. The minimum pressure, in the pressure-specific volume curve, gives the equation of state theoretical spall strength. As already mentioned above, in reality the theoretical value of spall is not achieved due to material defects. However, for extremely high strain rates, the theoretical values from the equations of state are expected, since the material defects do not have enough time to 'combine' and induce a spall, so that the inter-atomic forces dominate the strength of the material in this case. As can be seen from the isotherms of aluminium in figure 10.11, calculated with a semi-empirical wide range equation of state, the spall strength also depends on the temperature of the shocked target.

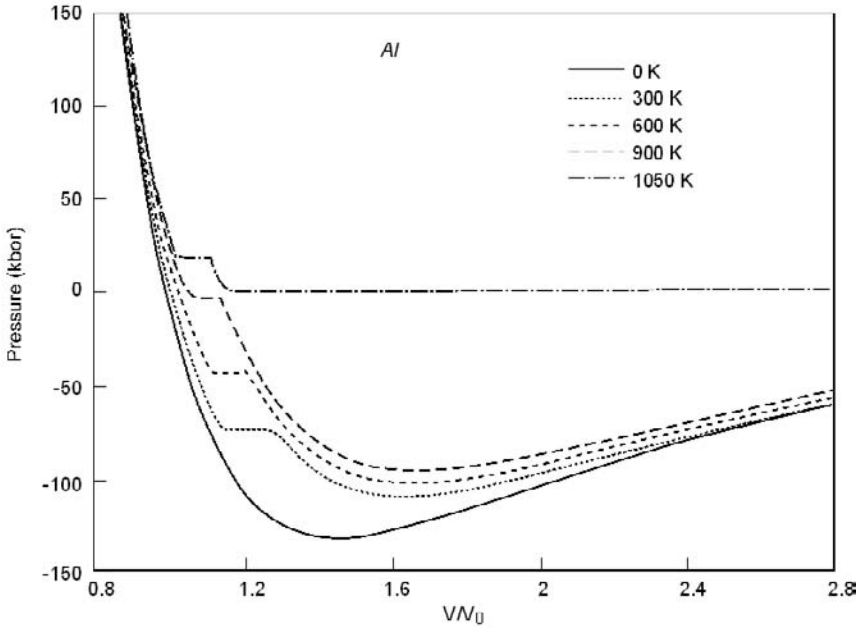

Figure 10.11. Isotherm of aluminium, calculated with a semi-empirical wide range equations of state.

Last, but not least, from the free-surface measurements the shock-wave pressure is known if the equation of state is available (equation (10.44)):

$$P_{\mathrm{H}} = \rho_0 u_{\mathrm{s}} u_{\mathrm{p}} \approx \rho_0 \left(c_0 + \alpha \frac{u_{\max}}{2} \right) \frac{u_{\max}}{2}. \tag{10.120}$$

From the analysis in this chapter, one can see that the high-power laser devices are successfully 'joining' the club of high-pressure physics.

Chapter 11

Hydrodynamic Instabilities

11.1 Background

The Rayleigh–Taylor (RT) instability occurs if a heavy fluid is supported by a light fluid in a gravitational field (Rayleigh 1883). Equivalently, one gets RT instability when a light fluid pushes and accelerates a heavy fluid (Taylor 1950) (see figure 11.1). In general, the RT instability occurs whenever a pressure gradient opposes a density gradient (∇P is in an opposite direction to $\nabla\rho$).

The hydrodynamic instabilities, and in particular the RT instability, have been reviewed in the literature (Chandrasekhar 1961, Drazin and Reid 1981, Kull 1991). Reviews on RT instabilities in laser–plasma interactions, with an emphasis on inertial confinement fusion (ICF), are also available (Bodner 1991, Gamaly 1993, Hoffman 1995).

A sinusoidal wave, with amplitude ξ, on the surface between the two RT unstable fluids will grow exponentially:

$$\xi = \xi_0 \exp(\gamma_0 t), \qquad \gamma_0 = \sqrt{Aka}, \qquad A \equiv \frac{\rho_H - \rho_L}{\rho_H + \rho_L}, \qquad k = \frac{2\pi}{\lambda} \tag{11.1}$$

where λ is the wavelength of the sinusoidal wave, a is the acceleration of the two fluids (or $a = g$ in the gravitational field, without acceleration), ρ_H and ρ_L are the densities of the heavier and the lighter fluids and A is the Atwood number. γ_0 is the classical value obtained by Rayleigh, more than a hundred years ago, for two fluids in contact in the gravitational field ($a = g$ in (11.1)).

For example, when a high-power laser interacts with a thin foil, plasma is created and accelerates the foil. In this case one has a low-density medium (the plasma) accelerating a high-density medium (the solid target); therefore, the acceleration is subject to RT instabilities. For a typical high-power laser acceleration of the order of $10^{15}\,\mathrm{cm/s^2}$ and a wavelength of the order of the foil thickness $\sim 100\,\mu\mathrm{m}$, one gets $\gamma_0 \approx 10^9\,\mathrm{s^{-1}}$, implying that the classical e-folding time is $1/\gamma_0 \approx 1\,\mathrm{ns}$.

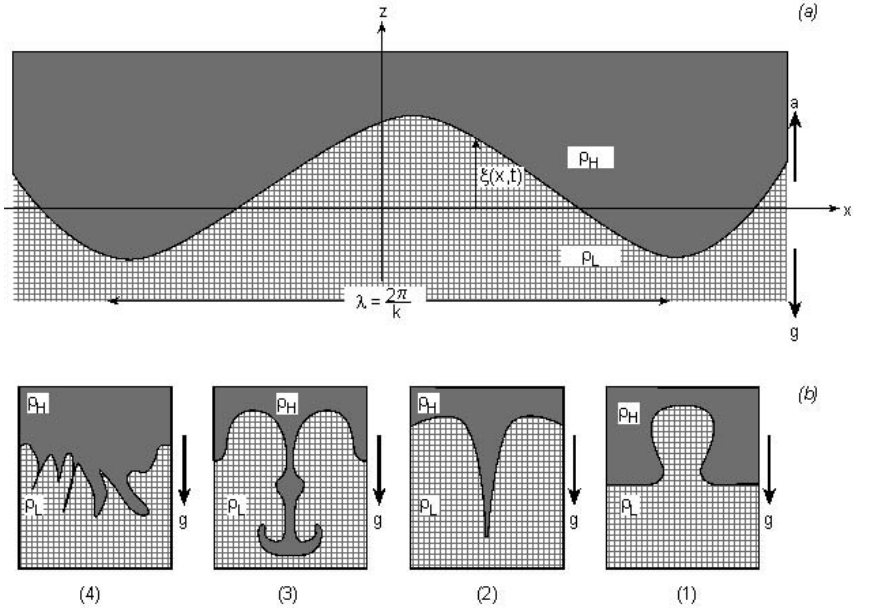

Figure 11.1. Rayleigh–Taylor (RT) instability in the presence of gravitation g (down) or acceleration a (up). The upper fluid density ρ_H is larger than the lower fluid density ρ_L. (a) A normal mode is shown. (b) Characteristic flow patterns in the evolution of RT instability: (1) a bubble formation penetrating the heavy fluid, (2) a spike entering a medium with very low density, (3) a spike formation with vortex motion, (4) intermixing between the fluids.

Another very important example is the acceleration of thin shells, subject to RT instabilities, in ICF. The use of shells in ICF, in comparison with solid spheres, has reduced significantly the peak laser power (and energy) required to ignite a target of a given mass. The following order of magnitude calculations demonstrate the importance of RT instabilities in ICF. The ablation pressure P_a, that accelerates the shell, is a function of the irradiating laser intensity I, which scales like $P_a \sim I^{2/3}$. For a shell with an initial radius R_0 and thickness ΔR_0, the implosion velocity v_f scales as $v_f^2 \sim P_a(R_0/\Delta R_0)$. The resulting stagnation pressure is $P_f \approx P_a(R_0/\Delta R_0)G$, where G is a radial convergence factor of the order of 100. The minimum energy for ignition scales as $1/P_f^2$. The ablation pressure for ICF pellets, expected to be about $P_a \approx 30\,\text{Mbar}$, has to increase to about $P_f \approx 100\,\text{Gbar}$, i.e. by a factor of 3000, implying an aspect ratio $R_0/\Delta R_0 \approx 30$. The larger the aspect ratio the higher the implosion pressure (P_f), implying a smaller laser energy ($\sim 1/P_f^2$). However, the magnitude of $R_0/\Delta R_0$ is limited by RT instabilities.

Since the beginning of the ICF programme, the RT instability has been a subject of uncertainties and controversies. Some scientists believe that an initial aspect ratio $R_0/\Delta R_0$ as high as 100 is 'safe' against RT instabilities, while others

were predicting that even an aspect ratio of 4 is going to 'destroy' the shell (before the desired high compression is achieved) by RT instabilities. The aspect ratio is a very important parameter for ICF since thicker pellets require a higher laser intensity to achieve the desired high pressure, and very high laser intensity could drive unacceptable plasma instabilities (see chapter 6). In addition, thicker shells require a larger amount of laser energy.

The RT instability can cause a disturbance to grow from extremely small amplitude to a level that can disrupt the flow completely. In the above examples it can break the accelerated foil or the shell before it reaches the desired final velocity.

The initial disturbance, called the 'seed', arises from limitations to fabricate a perfect plane (for foil acceleration) or a perfect spherical shell for ICF. Small perturbations caused by the roughness of the material structures, or by machining marks during the preparation of the target, are sources of instability seeds. Furthermore, the pattern of the laser intensity on the target can imprint a disturbance on an initially perfect smooth target. Since these types of disturbance are facts of reality, one has to calculate the constraints on the target smoothness and on the laser uniformity from the hydrodynamic instability theory.

Any initial perturbation can be described as an infinite series (e.g. a Fourier series) of normal modes (with wavelength $\lambda = L/j$, $j = 1, 2, 3, \ldots$). Any given mode is not growing to infinity by the RT instability, but is expected to saturate at a finite amplitude ($\sim\lambda/2$). On their route to saturation, perturbations with wavelength greater than the fluid thickness would destroy the flow (break the foil or the shell).

The shorter wavelength modes reach saturation before the longer wavelength modes (see equation (11.1), $\gamma_0 \sim (a/\lambda)^{1/2}$). After the shorter wavelength modes stop growing, they transfer their acquired energy to the longer wavelength disturbances, and the small disturbances are converted into larger structures. It turns out that these structures have the topology of bubbles and spikes. The lighter fluid penetrates the heavier fluid in the form of bubbles, and spikes of the heavier fluid enter the lighter fluid. Characteristic flow patterns in the evolution of RT instability are shown in figure 11.1(b), where a bubble formation penetrating the heavy fluid is shown together with possible spikes entering the lighter medium. A schematic spike formation with vortex motion and late intermixing between the fluids are also shown in this figure.

The saturation mechanism can be understood (Shvarts *et al.* 1995) by the existence of a nonlinear drag force:

$$F_{\mathrm{d}} \approx -\rho_{\mathrm{d}} S u^2. \tag{11.2}$$

The ambient fluid for bubbles is the heavy liquid and the ambient fluid for spikes is the light fluid; therefore, $\rho_{\mathrm{d}} = \rho_{\mathrm{H}}$ for bubbles and $\rho_{\mathrm{d}} = \rho_{\mathrm{L}}$ for spikes. S is the area and u the velocity of the bubbles or the spikes. Equating

the drag force with the buoyancy force for a disturbance with volume V,

$$F_{\mathrm{b}} \approx (\rho_{\mathrm{H}} - \rho_{\mathrm{L}})aV \tag{11.3}$$

one gets

$$u \approx \sqrt{a\lambda}, \qquad \text{amplitude} \approx \frac{u^2}{2a} = \frac{\lambda}{2}. \tag{11.4}$$

In order to get a feeling of the size of RT instability according to equation (11.1), we consider the shell uniformity requirement in ICF. According to this equation the shorter wavelengths have higher growth rates; therefore, one has to consider the shortest wavelength that will destroy the shell, about $\lambda \approx 3\Delta R_0$. The shell is first accelerated, then it expands at a constant velocity and finally it decelerates during the compression stages. The RT instabilities occur during the acceleration and during the deceleration phases, since in both cases ∇P is in an opposite direction to $\nabla\rho$. In this example we are interested in the RT instability during the acceleration phase. As an order of magnitude estimate, one can assume that the shell acceleration is constant until the shell is at a distance $R_0/2$ from the centre, $R_0/2 \approx \frac{1}{2}at^2$. Using this relation and $\lambda \approx 3\Delta R_0$, the growth of an initial amplitude ξ_0 for Atwood number ≈ 1 is, according to equation (11.1),

$$\frac{\xi}{\xi_0} = \exp\sqrt{\frac{2R_0}{\Delta R_0}}$$

$$\xi = \frac{\Delta R_0}{2} \approx 50\,\mu\mathrm{m} \Rightarrow \begin{cases} \xi_0 \approx 3.6 \times 10^{-9}\,\mathrm{cm} & \text{for } \dfrac{R_0}{\Delta R_0} = 100 \\ \xi_0 \approx 2.2 \times 10^{-6}\,\mathrm{cm} & \text{for } \dfrac{R_0}{\Delta R_0} = 30. \end{cases} \tag{11.5}$$

Taking into account the pellet fabrication and the laser initial imprint on the shell surface, it seems that such initial smoothness is technologically impossible. Therefore, there must be some mechanism that reduces the RT instabilities significantly or all ICF schemes would fail.

Following the Landau–Lifshitz analysis (Landau and Lifshitz 1987) of a chemical burn front of a weak deflagration, it was suggested (Bodner 1974, Takabe *et al*. 1985) that the plasma ablation stabilizes the RT instability. The ablated material flows away from the target interface, creating the low-density corona that accelerates the target. The pressure increase from the target towards the corona gives the acceleration force. The ablation flow through the unstable region and the smoothing of temperature perturbations by the radiation flux can act to reduce the growth rate in the RT instability at the ablation surface. The ablation stabilization is explained by the fact that the disturbance is convected away from the interface before it grows. According to this stabilization, the growth rate of the RT instability is

effectively reduced to

$$\gamma = \alpha\sqrt{ka} - \beta k u_a, \qquad u_a = \frac{1}{\rho_{max}}\left(\frac{dm}{dt}\right), \qquad \alpha \approx 0.9, \quad \beta \approx 3 \tag{11.6}$$

where ρ_{max} is the peak density at the interface and dm/dt is the mass (per unit area) ablation rate. The ratio between the u_a term and the classical RT term for ICF plasmas is about 25% only, therefore this stabilization is not sufficient.

In analysing the RT instability it is required to consider the evolution of multimode perturbation. In spherical geometry the perturbation wave number is given by the angular momentum number l:

$$l = \frac{2\pi R}{\lambda}. \tag{11.7}$$

The growth rate for each mode is $\gamma_l = (al/R_0)^{1/2}$ and using the approximation $at^2 \sim R_0$, one gets

$$\gamma_l t \approx \sqrt{l}. \tag{11.8}$$

The nonlinear evolution of the RT instability, starting with a multimode initial perturbation (Gardner *et al*. 1988, Haan 1989, Dahlburg *et al*. 1995, Shvarts *et al*. 1995, Oron *et al*. 1998), was comprehensively studied using numerical simulations in two and three dimensions.

Other hydrodynamic instabilities of importance in laser–target interaction are the Richtmyer–Meshkov (RM) instability and the Kelvin–Helmholtz (KH) instability. The RM instability (Richtmyer 1960, Meshkov 1969) occurs when a shock wave passes through a corrugated interface between two fluids of different densities (see figure 11.2). This phenomenon is a limiting case of the RT instability, where the shock wave imparts an impulsive acceleration to the interface, so that the acceleration acts on the fluid during an infinitesimally short duration. As in the RT case under unstable conditions, small perturbations on the interface can grow into bubbles of light fluid penetrating the heavy fluid and spikes of heavy fluid entering into the light fluid.

The KH instability (Kelvin 1910, Chandrasekhar 1961, Brown and Roshko 1974, Melrose 1986) occurs when two fluids in contact have different flow velocities (in the direction parallel to the interface) across the interface. The classical example is the generation of water waves by wind blowing over the surface of the water. The gradient in the parallel velocity, referred to in the literature as 'velocity shear', can be unstable and produce vortices and turbulence, creating a mixing zone between the fluids. The KH instability can develop along the interface of 'climbing' bubbles and 'declining' spikes at the late stage of RT instability, when the shear velocity is large. A shear velocity is also generated in RM instability if the shock wave is crossing the interface not in a normal direction to the interface between the fluids.

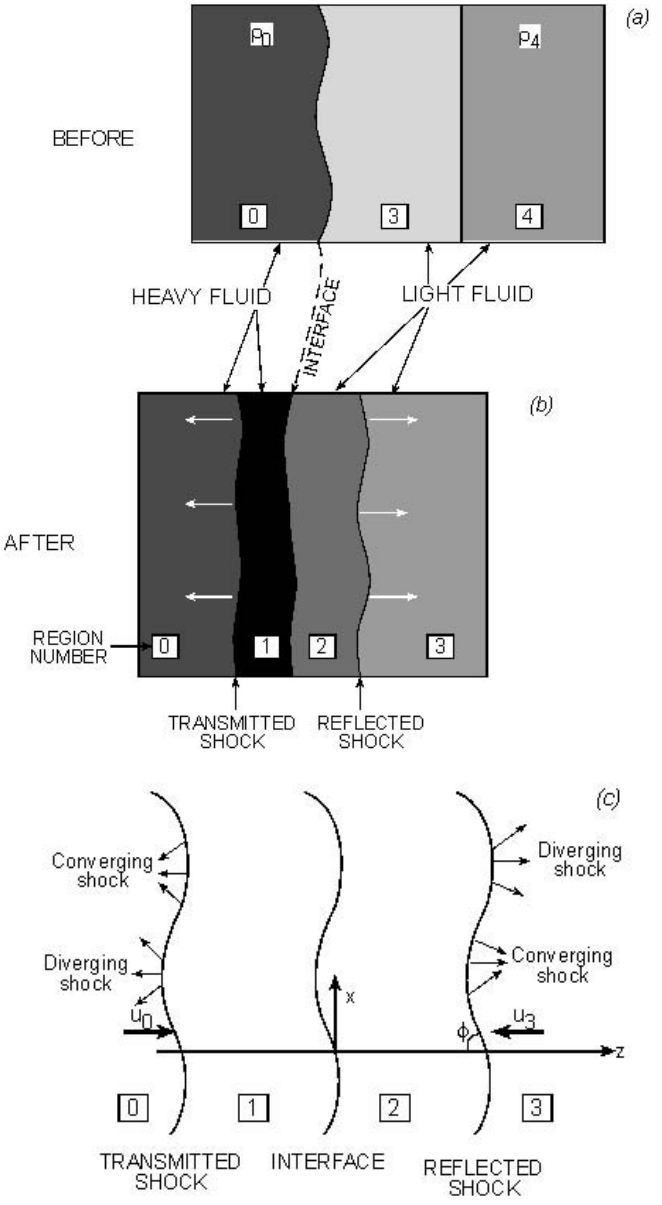

Figure 11.2. A presentation of the Richtmyer–Meshkov instability. A shock wave passes through a perturbed interface between two fluids, from the light to the heavy fluid. (a) Before the shock crosses the interface, (b) after the shock crosses the interface and (c) converging and diverging shocks at the shock wave surfaces.

In the following sections the RT, RM and KH instabilities are analysed. The RT instability is discussed in greater detail (the next four sections) than the other instabilities.

11.2 Rayleigh–Taylor Instability, Linear Analysis

The hydrodynamic equations describing the motion under consideration are the following mass and the momentum conservation equations:

$$\frac{\partial \rho}{\partial t} + \nabla \cdot (\rho \mathbf{v}) = 0, \qquad \rho \frac{\partial \mathbf{v}}{\partial t} + \rho(\mathbf{v} \cdot \nabla)\mathbf{v} = -\nabla P + \rho \mathbf{g} \tag{11.9}$$

where ρ is the fluid density, $\mathbf{v}$ is the flow velocity, P is the pressure and $\rho\mathbf{g}$ is the external force acting on the fluid (if there is an acceleration, then $\mathbf{a} = -\mathbf{g}$). The Cartesian coordinates with unit vectors $\hat{\mathbf{x}}$, $\hat{\mathbf{y}}$ and $\hat{\mathbf{z}}$ are used, and the gravitational field (or the acceleration) is perpendicular to the interface between the fluids

$$\mathbf{g} = -g\hat{\mathbf{z}}. \tag{11.10}$$

The instability is investigated here in the linear approximation (Chandrasekhar 1961, Hoffman 1995):

$$\begin{aligned} \rho &= \rho_0 + \rho_1, & \rho_0 &\gg \rho_1 \\ \mathbf{v} &= \mathbf{v}_0 + \mathbf{v}_1, & \mathbf{v}_0 &\gg \mathbf{v}_1 \\ P &= P_0 + P_1, & P_0 &\gg P_1. \end{aligned} \tag{11.11}$$

The variables with subscript 1 describe how a small perturbation grows in time. If the amplitude of the perturbation never returns to its initial value, then it is said that the flow is unstable with respect to the initial perturbation. Substituting (11.11) into equations (11.9), and neglecting higher orders than one (see section 2.5), yields the following equations to the zeroth order and the first order respectively:

$$\frac{\partial \rho_0}{\partial t} + \nabla \cdot (\rho_0 \mathbf{v}_0) = 0, \qquad \rho_0 \frac{\partial \mathbf{v}_0}{\partial t} + \rho_0(\mathbf{v}_0 \cdot \nabla)\mathbf{v}_0 = -\nabla P_0 + \rho_0 \mathbf{g} \tag{11.12}$$

$$\begin{gathered} \frac{\partial \rho_1}{\partial t} + \nabla \cdot (\rho_0 \mathbf{v}_1 + \rho_1 \mathbf{v}_0) = 0 \\ \rho_1 \frac{\partial \mathbf{v}_0}{\partial t} + \rho_0 \frac{\partial \mathbf{v}_1}{\partial t} + \rho_0[(\mathbf{v}_1 \cdot \nabla)\mathbf{v}_0 + (\mathbf{v}_0 \cdot \nabla)\mathbf{v}_1] + \rho_1(\mathbf{v}_0 \cdot \nabla)\mathbf{v}_0 = -\nabla P_1 + \rho_1 \mathbf{g} \end{gathered} \tag{11.13}$$

For the analysis of RT instability it is assumed that $\mathbf{v}_0 = 0$, so that the equations (11.13) for the perturbations are simplified to

$$\frac{\partial \rho_1}{\partial t} + \nabla \cdot (\rho_0 \mathbf{v}_1) = 0, \qquad \rho_0 \frac{\partial \mathbf{v}_1}{\partial t} + \nabla P_1 - \rho_1 \mathbf{g} = 0\,. \tag{11.14}$$

For an incompressible fluid the speed of sound equals infinity, so that communications by sound signal are instantaneous. Therefore, it is assumed that an incompressible flow is a reasonable assumption for flow velocities much smaller than the local speed of sound. In Lagrangian coordinates (see section 3.2) the density in this case does not change with time:

$$\frac{\mathrm{d}\rho}{\mathrm{d}t} = \frac{\partial \rho}{\partial t} + \mathbf{v} \cdot \nabla \rho = 0. \tag{11.15}$$

Using the linearization procedure in this equation, together with the first of equations (11.14), one gets the following two equations:

$$\nabla \cdot \mathbf{v}_1 = 0 \tag{11.16}$$

$$\frac{\partial \rho_1}{\partial t} + \mathbf{v}_1 \cdot \nabla \rho_0 = 0. \tag{11.17}$$

Instead of equations (11.14) we have to solve for the incompressible fluid the second equation of (11.14), together with equations (11.16) and (11.17). In our problem ρ_0 is constant in both fluids, and therefore the initial density changes only in the z direction, normal to the interface between the two fluids. This implies that $\partial\rho_0/\partial x = 0$, $\partial\rho_0/\partial y = 0$ and only at the interface $\partial\rho_0/\partial z \neq 0$. Writing these equations explicitly in Cartesian coordinates, one gets

$$\begin{aligned}
\rho_0 \frac{\partial v_{1x}}{\partial t} + \frac{\partial P_1}{\partial x} &= 0 \\
\rho_0 \frac{\partial v_{1y}}{\partial t} + \frac{\partial P_1}{\partial y} &= 0 \\
\rho_0 \frac{\partial v_{1z}}{\partial t} + \frac{\partial P_1}{\partial z} + \rho_1 g &= 0 \\
\frac{\partial \rho_1}{\partial t} + v_{1z} \frac{\partial \rho_0}{\partial z} &= 0 \\
\frac{\partial v_{1x}}{\partial x} + \frac{\partial v_{1y}}{\partial y} + \frac{\partial v_{1z}}{\partial z} &= 0
\end{aligned} \tag{11.18}$$

We have five equations with five unknowns, v_{1x}, v_{1y}, v_{1z}, P_1 and ρ_1. It is convenient to solve these equations after a Fourier transform in x–y, or equivalently the disturbance is analysed by its normal modes, with solutions depending on x, y and t in the following way:

$$\left.\begin{aligned}
\mathbf{v}_1(x, y, z, t) &= \mathbf{u}(z) \\
P_1(x, y, z, t) &= \delta P(z) \\
\rho_1(x, y, z, t) &= \delta\rho(z)
\end{aligned}\right\} \times \exp(\mathrm{i}k_x x + \mathrm{i}k_y y + \gamma t) \tag{11.19}$$

where k_x, k_y and γ are constants. Substituting (11.19) into equations (11.18) gives

$$\begin{aligned}
\gamma\rho_0 u_x + \mathrm{i}k_x \delta P &= 0 \\
\gamma\rho_0 u_y + \mathrm{i}k_y \delta P &= 0 \\
\gamma\rho_0 u_z + \frac{\partial \delta P}{\partial z} + g\delta\rho &= 0 \\
u_z \frac{\mathrm{d}\rho_0}{\mathrm{d}z} + \gamma\delta\rho &= 0 \\
\mathrm{i}k_x u_x + \mathrm{i}k_y u_y + \frac{\partial u_z}{\partial z} &= 0.
\end{aligned} \tag{11.20}$$

Multiplying the first equation by $\mathrm{i}k_x$, the second equation by $\mathrm{i}k_y$, adding these two new equations and solving with the last equation, one gets

$$\delta P(z) = -\left(\frac{\gamma\rho_0}{k^2}\right)\frac{\mathrm{d}u_z}{\mathrm{d}z} \tag{11.21}$$

where k is defined by

$$k^2 = k_x^2 + k_y^2. \tag{11.22}$$

Substituting $\delta\rho(z)$ from the fourth equation of (11.20), together with $\delta P(z)$ from (11.21) into the third equation of (11.20), one gets the following equation for u_z:

$$\frac{d}{\mathrm{d}z}\left(\rho_0 \frac{\mathrm{d}u_z}{\mathrm{d}z}\right) - \left[k^2\rho_0 - \left(\frac{k^2 g}{\gamma^2}\right)\frac{\mathrm{d}\rho_0}{\mathrm{d}z}\right]u_z = 0. \tag{11.23}$$

If the fluid is confined between two rigid planes at $+z_\mathrm{B}$ and $-z_\mathrm{B}$, then the boundary conditions are

$$u_z(\pm z_\mathrm{B}) = 0, \qquad \left(\frac{\mathrm{d}u_z}{\mathrm{d}z}\right)_{\pm z_\mathrm{B}} = 0. \tag{11.24}$$

We take in our following analysis $z_\mathrm{B} \to \infty$. Equation (11.23) is an eigenvalue equation, with u_z the eigenfunction and the term in $[\cdots]$ is the eigenvalue. Therefore, γ is fixed for any given values of $\rho_0(z)$, k and g.

The interface is the surface $z = 0$, and the density is assumed constant anywhere except between the fluids at $z = 0$. Therefore, for $z \neq 0$, equation (11.23) is given by

$$z \neq 0: \quad \frac{\partial^2 u_z(z)}{\partial z^2} - k^2 u_z(z) = 0 \tag{11.25}$$

and its general solution is

$$z \neq 0: \quad u_z(z) = \alpha\exp(kz) + \beta\exp(-kz). \tag{11.26}$$

Since u_z vanishes at the boundary, and the velocity is continuous at the interface (otherwise an infinite acceleration is needed for the fluid to cross the interface), one has the solution

$$u_z(z) = \begin{cases} w\exp(+kz) & \text{for } z < 0 \\ w\exp(-kz) & \text{for } z > 0. \end{cases} \tag{11.27}$$

Equation (11.23) is now integrated across the interface from $-\varepsilon$ to $+\varepsilon$, where ε is an infinitesimal element of z. Using (11.27) and denoting the density of the fluid above and below the interface by ρ_{up} and ρ_{down} accordingly (the direction up and down is determined by the direction of **g**), the integral gives

$$\begin{aligned} &\int_{-\varepsilon}^{+\varepsilon} \frac{\mathrm{d}}{\mathrm{d}z}\left(\rho_0 \frac{\partial u_z}{\partial z}\right)\mathrm{d}z - \int_{-\varepsilon}^{+\varepsilon} k^2\rho_0 u_z\,\mathrm{d}z + \int_{-\varepsilon}^{+\varepsilon} \frac{gk^2 u_z}{\gamma^2}\frac{\mathrm{d}\rho_0}{\mathrm{d}z}\,\mathrm{d}z = 0 \\ &\lim_{\varepsilon\to 0}\int_{-\varepsilon}^{+\varepsilon} \frac{\mathrm{d}}{\mathrm{d}z}F(z)\,\mathrm{d}z = \lim_{\varepsilon\to 0}\left[F(+\varepsilon) - F(-\varepsilon)\right] \equiv \Delta_0 F; \\ &\lim_{\varepsilon\to 0}\int_{-\varepsilon}^{+\varepsilon} G(z)\,\mathrm{d}z = 0, \qquad G(z) \text{ continuous at } z = 0 \\ &\Rightarrow kw\left[-(\rho_{\text{up}} + \rho_{\text{down}}) + \frac{gk}{\gamma^2}(\rho_{\text{up}} - \rho_{\text{down}})\right] = 0. \end{aligned} \tag{11.28}$$

The first integral gives the first term, the second integral vanishes and the third integral gives the second term. Using the solution of the last equation for the instability parameter γ and equation (11.19), the following result is obtained:

$$\begin{aligned} \gamma^2 &= Akg \\ A &\equiv \frac{\rho_{\text{up}} - \rho_{\text{down}}}{\rho_{\text{up}} + \rho_{\text{down}}} \\ v_z(x,y,z,t) &= \begin{cases} w\exp[\mathrm{i}(k_x x + k_y y)]\exp(+kz)\exp(\gamma t) & \text{for } z < 0 \\ w\exp[\mathrm{i}(k_x x + k_y y)]\exp(-kz)\exp(\gamma t) & \text{for } z > 0. \end{cases} \end{aligned} \tag{11.29}$$

The dimensionless parameter A is called the Atwood number. If $\rho_{\text{up}} > \rho_{\text{down}}$, then A is positive and therefore γ is a real number. In this case the perturbation grows exponentially and the interface is unstable. On the other hand, if $\rho_{\text{up}} < \rho_{\text{down}}$, then A is negative and therefore γ is an imaginary number, causing the interface and the physical quantities (e.g. pressure, v_z) to oscillate with a frequency of $(|A|kg)^{1/2}$. From the solutions (11.19) (see in particular (11.29)), one has that the physical variables oscillate in the x–y plane with a wavelength λ, related to the wave number k by

$$\lambda = \frac{2\pi}{k}, \qquad k = \sqrt{k_x^2 + k_y^2} \tag{11.30}$$

and the time dependence is given by $\exp(\gamma t)$.

11.3 Ablation-Surface Instability

The ablation-surface instability occurs when a laser is accelerating a solid foil or shell. In this case a high-pressure low-density plasma region is created from the ablated material that accelerates the foil, due to the expanding plasma (the rocket effect). During the acceleration the foil is subject to Rayleigh–Taylor instabilities since a low-density medium accelerates a high-density medium (for the high accelerations obtained here, the gravitation is not relevant).

Because energy is deposited at the interface between the foil (with a density ρ_{foil}) and the adjacent plasma (with a density ρ_{pl}), a velocity discontinuity is permitted at the interface together with the density jump. It is assumed that there is a sharp density jump, so that the density is described by a θ function:

$$\rho_0(z) = \rho_{\text{pl}}\theta(-z) + \rho_{\text{foil}}\theta(z), \qquad \theta(z) = \begin{cases} 1 & \text{for } z > 0 \\ 0 & \text{for } z < 0. \end{cases} \tag{11.31}$$

In the foil reference frame of coordinates (the foil is at rest in this frame), the ablated material moves in the $-\hat{\mathbf{z}}$ direction ($\hat{\mathbf{z}}$ is a unit vector in the z direction) with velocity v_{pl}:

$$\mathbf{v}_0 = -v_{\text{pl}}\theta(-z)\hat{\mathbf{z}} = \begin{cases} -v_{\text{pl}}\hat{\mathbf{z}} & \text{for } z < 0 \\ 0 & \text{for } z > 0. \end{cases} \tag{11.32}$$

The second equations of (11.12) and (11.13), without the gravitational term, can be combined in the following way:

$$\rho_0\left(\frac{\partial \mathbf{v}_1}{\partial t} + \mathbf{v}_1 \cdot \nabla \mathbf{v}_0 + \mathbf{v}_0 \cdot \nabla \mathbf{v}_1\right) = \frac{\rho_1}{\rho_0}\nabla P_0 - \nabla P_1. \tag{11.33}$$

These three equations, together with the last two equations of (11.20) (the incompressibility assumption), are the five equations with the five unknowns to be solved. Substituting (11.19) into these equations leads, in a similar way that equation (11.23) was obtained, to the following equation for the velocity $u_z(z)$:

$$\frac{\partial}{\partial z}\left(\rho_0 \frac{\partial u_z}{\partial z}\right) - \frac{k^2 \rho_0 v_{0z}}{\gamma}\frac{\partial u_z}{\partial z} - \left(k^2\rho_0 - \frac{ak^2}{\gamma^2}\frac{\partial \rho_0}{\partial z} + \frac{k^2\rho_0}{\gamma}\frac{\partial v_{0z}}{\partial z}\right)u_z = 0 \tag{11.34}$$

where the acceleration a is defined by

$$a \equiv -\left(\frac{1}{\rho_0}\right)\frac{\partial P_0}{\partial z}. \tag{11.35}$$

Equation (11.34) is now integrated across the interface from $-\varepsilon$ to $+\varepsilon$, where ε is an infinitesimal element of z. The density and the initial velocity are described by a θ function, and the derivative of these terms gives the Dirac

δ function since

$$\frac{\mathrm{d}\theta(z)}{\mathrm{d}z} = \delta(z). \tag{11.36}$$

The integral of the Dirac function over the segment, including the zero of the argument, is equal to one, while the integral of regular functions and the θ function from $-\varepsilon$ to $+\varepsilon$, where $\varepsilon \to 0$, is equal to zero. Therefore, the integrals of the second and third terms of (11.34) vanish, the integrals of the first and fourth terms (using (11.27)) are similar to the integrals of (11.28), and only the integral of the fifth term in (11.34) is new and is equal to

$$\int_{-\varepsilon}^{+\varepsilon} \frac{k^2\rho_0 u_z}{\gamma}\frac{\partial v_{0z}}{\partial z}\,\mathrm{d}z = \frac{k^2 w}{\gamma}\int_{-\varepsilon}^{+\varepsilon}\rho_0\frac{\partial v_{0z}}{\partial z}\,\mathrm{d}z = \frac{k^2 w}{\gamma}\left[\left(\frac{\rho_{\mathrm{pl}}+\rho_{\mathrm{foil}}}{2}\right)v_{\mathrm{pl}}\right]. \tag{11.37}$$

At the last step we have used the symmetry of δ ($\delta(z) = \delta(-z)$) and the identity

$$\int_{-\varepsilon}^{+\varepsilon}\theta(z)\delta(z)\,\mathrm{d}z = \frac{1}{2} \tag{11.38}$$

that can be easily verified from integrating by parts.

Therefore, the integral of (11.34) over the interface yields (using (11.38) and the integrals in (11.28))

$$kw\left[(\rho_{\mathrm{foil}}+\rho_{\mathrm{pl}}) - \frac{ak}{\gamma^2}(\rho_{\mathrm{foil}}-\rho_{\mathrm{pl}}) + \frac{k}{2\gamma}(\rho_{\mathrm{foil}}+\rho_{\mathrm{pl}})v_{\mathrm{pl}}\right] = 0. \tag{11.39}$$

Simplifying this equation gives

$$\gamma^2 + \left(\frac{kv_{\mathrm{pl}}}{2}\right)\gamma - akA = 0, \qquad A \equiv \frac{\rho_{\mathrm{foil}}-\rho_{\mathrm{pl}}}{\rho_{\mathrm{foil}}+\rho_{\mathrm{pl}}}. \tag{11.40}$$

The solution of this quadratic equation is

$$\begin{gathered}\gamma = -\frac{kv_{\mathrm{pl}}}{4} \pm \sqrt{\left(\frac{kv_{\mathrm{pl}}}{4}\right)^2 + Aka} \\ v_{\mathrm{pl}} \ll 4\sqrt{\frac{Aa}{k}} \Rightarrow \gamma \approx \sqrt{Aka} - \frac{kv_{\mathrm{pl}}}{4} + \cdots.\end{gathered} \tag{11.41}$$

From this result one can see that the ablation reduces (compare with equation (11.29) for $g = a$) the growth rate of the RT instability.

In deriving equation (11.41), many simplifying assumptions have been made. For example, the incompressibility assumption, the spatial extent and the density gradient of the plasma were neglected, the plasma heating was not taken into account, etc.

It is interesting to point out that a detailed numerical simulation of the ablation instability, taking all the above-mentioned effects into account

(Takabe *et al.* 1985) gives a fit described by equation (11.6). In comparison between this fit and equation (11.41): there are two main differences the constant $\frac{1}{4}$ is changed to about 3 and u_a is changed to v_{pl} ($(A)^{1/2} \approx 0.9$ is a good approximation for the plasma–solid interface). While v_{pl} is the plasma velocity far from the ablation surface, the u_a represents the mass ablation rate per unit area divided by the density of the ablation surface. Since $v_{pl} \gg u_a$, the numerical fit (11.6) and equation (11.41) seem not to be inconsistent. There is, however, a difference between the numerical fit (11.6) and equation (11.41), since in the above value of γ the approximation $kv_{pl}/4 \ll (Aka)^{1/2}$ has been made, while the numerical fit does not require this perturbation. Therefore, in analysing equation (11.6) it is permitted to introduce a cutoff wavenumber k_c, defined by

$$\gamma(k_c) = 0 \Rightarrow k_c = \left(\frac{\alpha}{\beta}\right)^2 \left(\frac{a}{u_a^2}\right), \qquad \lambda_c \equiv \frac{2\pi}{k_c}. \tag{11.42}$$

Equation (11.6) shows that for wavelength $\lambda < \lambda_c$ (i.e. $k > k_c$) the ablation is stable, and only the wavelengths higher than λ_c contribute to the ablation RT instability.

11.4 The Magnetic Field Effect

In high-power laser–plasma interactions very strong magnetic fields are created (see chapter 8). Megagauss magnetic fields (d.c.) were measured for moderate laser intensities. In this section it is shown that the magnetic field parallel to the accelerated interface between two fluids, where the heavier fluid is above the lighter fluid, stabilizes the RT instability.

The acceleration is assumed to be in the z direction, the interface between the fluids are in the x–y plane $z = 0$ and the fluids are incompressible plasmas with zero resistivity (= 1/electrical conductivity = $1/\sigma_E$). The linearization procedure, as in equation (11.11), is used in this analysis with a magnetic field (Gaussian units are used):

$$\mathbf{B} = \mathbf{B}_0 + \mathbf{B}_1, \qquad \mathbf{B}_0 = \textbf{const.}, \qquad \frac{|\mathbf{B}_1|}{|\mathbf{B}_0|} \ll 1. \tag{11.43}$$

The momentum equation is (see equations (3.10) and (3.11), where the electric field **E** is neglected relative to the **B** field)

$$\rho \frac{\partial \mathbf{v}}{\partial t} = -\nabla P + \frac{1}{c}(\mathbf{J} \times \mathbf{B}) \tag{11.44}$$

where **v** is the fluid velocity, ρ and P are density and pressure respectively, **J** is the electric current and c is the speed of light. Using the Maxwell equation,

$$\mathbf{J} = \left(\frac{c}{4\pi}\right) \nabla \times \mathbf{B}. \tag{11.45}$$

The linearized momentum equation can be written

$$\rho_0 \frac{\partial \mathbf{v}}{\partial t} = -\nabla P_1 - \frac{\mathbf{B}_0}{4\pi} \times (\nabla \times \mathbf{B}_1) - g\rho_1 \hat{\mathbf{z}}. \tag{11.46}$$

This equation has to be solved, together with the following linearized Maxwell equation for zero resistivity (see equation (8.33), with $1/\sigma_E = 0$):

$$\frac{\partial \mathbf{B}}{\partial t} = -c\nabla \times \mathbf{E} = \nabla \times (\mathbf{v} \times \mathbf{B}_0) \tag{11.47}$$

the mass conservation and the incompressibility requirement (equations (11.16) and (11.17)). In these approximations, the zero divergence of the magnetic field

$$\nabla \cdot \mathbf{B}_1 = 0 \tag{11.48}$$

is not an independent equation, since it is derived from equation (11.47).

In this problem there are eight independent equations, (11.46), (11.47), (11.16) and (11.17), with eight unknowns, ρ_1, P_1, $\mathbf{v}$ and $\mathbf{B}_1$. We shall write explicitly these equations for two cases:

1. The initial magnetic field is perpendicular (vertical) to the interface between the fluids, $\mathbf{B}_0 = B_0\hat{\mathbf{z}}$.
2. The initial magnetic field is parallel (horizontal) to the interface between the fluids, $\mathbf{B}_0 = B_0\hat{\mathbf{x}}$:

$$\begin{aligned}
\mathbf{B}_0 = B_0\hat{\mathbf{z}}: \quad & \rho_0 \frac{\partial v_x}{\partial t} = -\frac{\partial P_1}{\partial x} + \frac{B_0}{4\pi}\left(\frac{\partial B_{1x}}{\partial z} - \frac{\partial B_{1z}}{\partial x}\right) \\
& \rho_0 \frac{\partial v_y}{\partial t} = -\frac{\partial P_1}{\partial y} + \frac{B_0}{4\pi}\left(\frac{\partial B_{1y}}{\partial z} - \frac{\partial B_{1z}}{\partial y}\right) \\
& \rho_0 \frac{\partial v_z}{\partial t} = -\frac{\partial P_1}{\partial z} - g\rho_1 \\
& \frac{\partial \mathbf{B}_1}{\partial t} = B_0 \frac{\partial \mathbf{v}}{\partial z}, \qquad \nabla \cdot \mathbf{v} = 0, \qquad \frac{\partial \rho_1}{\partial t} + v_z \frac{\partial \rho_0}{\partial z} = 0
\end{aligned} \tag{11.49}$$

$$\begin{aligned}
\mathbf{B}_0 = B_0\hat{\mathbf{x}}: \quad & \rho_0 \frac{\partial v_x}{\partial t} = -\frac{\partial P_1}{\partial x} \\
& \rho_0 \frac{\partial v_y}{\partial t} = -\frac{\partial P_1}{\partial y} + \frac{B_0}{4\pi}\left(\frac{\partial B_{1y}}{\partial x} - \frac{\partial B_{1x}}{\partial y}\right) \\
& \rho_0 \frac{\partial v_z}{\partial t} = -\frac{\partial P_1}{\partial z} + \frac{B_0}{4\pi}\left(\frac{\partial B_{1z}}{\partial x} - \frac{\partial B_{1x}}{\partial z}\right) - g\rho_1 \\
& \frac{\partial \mathbf{B}_1}{\partial t} = B_0 \frac{\partial \mathbf{v}}{\partial x}, \qquad \nabla \cdot \mathbf{v} = 0, \qquad \frac{\partial \rho_1}{\partial t} + v_z \frac{\partial \rho_0}{\partial z} = 0.
\end{aligned} \tag{11.50}$$

As in the previous two sections, the following x–y–t dependence of the variables is assumed:

$$\left.\begin{aligned} \mathbf{v} &= \mathbf{u}(z) \\ \mathbf{B}_1 &= \delta\mathbf{B}(z) \\ P_1 &= \delta P(z) \\ \rho_1 &= \delta\rho(z) \end{aligned}\right\} \times \exp(\mathrm{i}k_x + \mathrm{i}k_y + \gamma t). \tag{11.51}$$

Substituting (11.51) into equations (11.49) and (11.50) yields, after algebraic manipulations, the following differential equations for the two cases under consideration:

$\mathbf{B} = B_0\hat{\mathbf{z}}$:

$$\left[\frac{\mathrm{d}}{\mathrm{d}z}\left(\rho_0\frac{\mathrm{d}}{\mathrm{d}z}\right) - \frac{B_0^2}{4\pi\gamma^2}\left(\frac{\mathrm{d}^2}{\mathrm{d}z^2} - k^2\right)\frac{\mathrm{d}^2}{\mathrm{d}z^2}\right]u_z(z) = \left[\rho_0 k^2 - \frac{gk^2}{\gamma^2}\left(\frac{\mathrm{d}\rho_0}{\mathrm{d}z}\right)\right]u_z(z). \tag{11.52}$$

$\mathbf{B} = B_0\hat{\mathbf{x}}$:

$$\left[\frac{\mathrm{d}}{\mathrm{d}z}\left(\rho_0\frac{\mathrm{d}}{\mathrm{d}z}\right) + \frac{B_0^2k_x^2}{4\pi\gamma^2}\left(\frac{\mathrm{d}^2}{\mathrm{d}z^2} - k^2\right)\right]u_z(z) = \left[\rho_0 k^2 - \frac{gk^2}{\gamma^2}\left(\frac{\mathrm{d}\rho_0}{\mathrm{d}z}\right)\right]u_z(z). \tag{11.53}$$

In laser–plasma interaction the horizontal magnetic field might play an important role in stabilizing the RT instabilities. In particular, if the large d.c. magnetic field (e.g. the vector product of the density gradient and the temperature gradient; see chapter 8), created in the corona, penetrates into the ablation surface then the ablation surface instability is significantly modified. Therefore, only equation (11.53) is further analysed in the following part of this section.

For $k_x = 0$, equation (11.53) is identical to equation (11.23), where no magnetic field is applied. Therefore, the disturbances that are independent of the coordinate along the direction of $\mathbf{B}_0$ (perpendicular to $\mathbf{g}$) are not affected by the existence of the magnetic field. In this case, $\mathbf{B}_0$ does not contribute to the development of the RT instability. In other words, the magnetic field in the x direction, which can stabilize the RT instabilities for wavelengths shorter than a critical value λ_c, does not stabilize any RT instability that develops along the y direction.

For $k_x \neq 0$. the RT instabilities in the hydromagnetic problem (equation (11.53)) are not identical to the RT instabilities in the hydrodynamic problem (equation (11.23)). We solve equation (11.53) for two uniform fluids separated at the surface $z = 0$, with a density distribution given by

$$\rho(z) = \rho_{\mathrm{up}}\theta(z) + \rho_{\mathrm{down}}\theta(-z). \tag{11.54}$$

At the horizontal boundary $z = 0$, the following continuity conditions must be satisfied:

$$\begin{aligned} &\lim_{\varepsilon \to 0} \{u_z(+\varepsilon) = u_z(-\varepsilon)\} \\ &\lim_{\varepsilon \to 0} \{B_z(+\varepsilon) = B_z(-\varepsilon)\}. \end{aligned} \tag{11.55}$$

The second equation follows from the first equation (or vice versa) by the use of (11.51) in the fourth equation of (11.50). The physical meaning of the first equation (11.55) is that there is not an infinite acceleration when a fluid element crosses the interface, while the second equation describes the fact that monopoles do not exist ($\nabla \cdot \mathbf{B} = 0$). Using the solution (11.27), which is also valid in this problem, one gets by integrating equation (11.53) along the interface (similar to the integrals in the previous two sections):

$$\gamma^2 = gk \left[\frac{\rho_{\text{up}} - \rho_{\text{down}}}{\rho_{\text{up}} + \rho_{\text{down}}} - \frac{B_0^2 k_x^2}{2\pi(\rho_{\text{up}} + \rho_{\text{down}})gk} \right]. \tag{11.56}$$

The angle ϕ between the k vector and the initial magnetic field (x axis), and the wavelength of a sinusoidal disturbance (a normal mode), are defined by

$$\cos\phi = \frac{k_x}{k} = \frac{k_x}{\sqrt{k_x^2 + k_y^2}}, \qquad \lambda = \frac{2\pi}{k}. \tag{11.57}$$

The stable modes, $\gamma^2 < 0$, are therefore satisfying

$$\lambda < \frac{B_0^2 \cos^2\phi}{g\Delta\rho} \equiv \lambda_{\text{c}}, \qquad \Delta\rho \equiv \rho_{\text{up}} - \rho_{\text{down}}. \tag{11.58}$$

For example, in laser plasma acceleration with $g \approx 10^{15}\,\text{cm/s}^2$, magnetic fields of the order of 10 MG, $\Delta\rho \approx 1\,\text{g/cm}^3$ and $\cos\phi \approx 0.5$, one gets stable modes for wavelengths smaller than 0.05 cm, a non-negligible dimension for high-intensity laser–plasma interactions.

It is interesting to see that if $\cos\phi \to 0$, then the hydromagnetic result (11.56) goes to the hydrodynamic result (11.29).

We end this section by pointing out that surface tension σ_{st} (dimension $\text{erg/cm}^2 = \text{dyne/cm}$) also stabilizes the RT instability (Chandrasekhar 1961). The hydrodynamic instability in this case gives a similar result to equation (11.56) with the substitution

$$\sigma_{\text{st}} \to \frac{B_0^2 \cos^2\phi}{2\pi k}, \qquad \gamma^2 = gk \left[\frac{\rho_{\text{up}} - \rho_{\text{down}}}{\rho_{\text{up}} + \rho_{\text{down}}} - \frac{k^2 \sigma_{\text{st}}}{g(\rho_{\text{up}} + \rho_{\text{down}})} \right]. \tag{11.59}$$

11.5 Bubbles from Rayleigh–Taylor Instability

It has been shown in section 11.2 that the amplitude of a sinusoidal perturbation increases exponentially with time in the RT instability. When the

amplitude becomes of the order of the wavelength ($>0.1\lambda$), then higher harmonics of the original perturbation appear in the disturbance. The interaction between the different modes results in the formation of bubbles, with the light fluid penetrating into the heavy fluid and spikes of heavy fluid falling into the light fluid. The full-time development of the RT instability has been discussed in the literature (Davies and Taylor 1950, Layzer 1955). In this section the asymptotic steady state of the bubble motion is considered (Hoffman 1995) using the potential flow theory.

For an incompressible irrotational fluid the flow velocity $\mathbf{v}(\mathbf{r}, t)$ satisfies the following equations:

$$\nabla \cdot \mathbf{v} = 0, \qquad \nabla \times \mathbf{v} = 0 \tag{11.60}$$

Using these equations and the identity $\nabla \times (\nabla\varphi) = 0$, one can define a velocity potential ϕ which obeys the Laplace equation:

$$\nabla^2\varphi = 0. \tag{11.61}$$

The Cartesian coordinates are chosen in such a way that the bubble moves in the z direction and the vector $\mathbf{k}$ ($k_x = k, k_y = 0$) is chosen in the x direction so that the y direction can be neglected. The bubble surface motion is analysed in the bubble centre of mass coordinates, where the Laplace equation takes the form

$$\frac{\partial^2\varphi}{\partial x^2} + \frac{\partial^2\varphi}{\partial z^2} = 0. \tag{11.62}$$

The following boundary conditions are appropriate for this problem:

$$v_x\left(x = \pm\frac{\lambda}{2}\right) = 0, \qquad v_z(z = +\infty) = -u\,. \tag{11.63}$$

The first equation describes an array of identical moving bubbles with a period of $\lambda = 2\pi/k$, or equivalently one bubble with a radius λ moving between two parallel frictionless walls at $x = \pm\lambda/2$. The second boundary condition is equivalent to the motion of a bubble with an asymptotic constant velocity u, or equivalently in the frame of reference of the bubble the flow is moving at $z =$ infinity with a velocity $-u$.

The solution of equation (11.62), subject to the boundary conditions (11.63), is

$$\begin{aligned} \varphi(x, z) &= -zu - \frac{\lambda}{2\pi}\sum_{n=1}^{\infty}\left(\frac{a_n}{n}\right)\exp\left(-\frac{2\pi n z}{\lambda}\right)\cos\left(\frac{2\pi n x}{\lambda}\right) \\ v_x &= \frac{\partial\varphi}{\partial x}, \qquad v_y = \frac{\partial\varphi}{\partial y}. \end{aligned} \tag{11.64}$$

It is convenient at this stage to introduce the concept of **streamlines** (Courant and Friedrichs 1948, Landau and Lifshitz 1987). The tangent to a streamline at any point on this line gives the direction of the velocity at that point as

determined by the differential equations $\mathrm{d}x/v_x = \mathrm{d}y/v_y = \mathrm{d}z/v_z$. In steady flow the streamlines are constant in time and coincide with the trajectories of the fluid particles. In this case a particle trajectory is given by a constant value of the stream function ψ, associated with the velocity potential by

$$\frac{\partial\psi}{\partial x} = \frac{\partial\varphi}{\partial z}, \qquad \frac{\partial\psi}{\partial z} = -\frac{\partial\varphi}{\partial x}. \tag{11.65}$$

The stream function that satisfies equations (11.64) and (11.65) is given by

$$\psi(x,z) = -xu - \frac{\lambda}{2\pi}\sum_{n=1}^{\infty}\left(\frac{a_n}{n}\right)\exp\left(-\frac{2\pi nz}{\lambda}\right)\sin\left(\frac{2\pi nx}{\lambda}\right). \tag{11.66}$$

At $z = +\infty$ the stream function equals $-xu$. Since in this model all the bubbles are identical, it is convenient to choose a trajectory

$$\psi(x,z) = 0. \tag{11.67}$$

Substituting (11.67) into (11.66) yields the equation that describes the surface of a bubble:

$$1 = \frac{\lambda}{2\pi xu}\sum_{n=1}^{\infty}\left(\frac{a_n}{n}\right)\exp\left(-\frac{2\pi nz}{\lambda}\right)\sin\left(\frac{2\pi nx}{\lambda}\right). \tag{11.68}$$

This equation has been solved (Davies and Taylor 1950) by using only the first term in the potential and in the streaming functions, i.e. $a_n \neq 0$ only for $n = 1$. Under this assumption the fluid flow velocity is

$$\begin{aligned} v_x &= a_1\exp\left(-\frac{2\pi z}{\lambda}\right)\sin\left(\frac{2\pi x}{\lambda}\right) \\ v_z &= -u + a_1\exp\left(-\frac{2\pi z}{\lambda}\right)\cos\left(\frac{2\pi x}{\lambda}\right) \end{aligned} \tag{11.69}$$

and the surface of the bubble is described by

$$a_1\exp\left(-\frac{2\pi z}{\lambda}\right)\sin\left(\frac{2\pi x}{\lambda}\right) = \frac{2\pi xu}{\lambda}. \tag{11.70}$$

Choosing the coordinates in such a way that for $x = 0$ the peak of the bubble is at $z = 0$, then one has to solve equations (11.69) and (11.70) for

$$a_1 = u \tag{11.71}$$

in order to find the asymptotic velocity u.

For a steady flow ($\partial\mathbf{v}/\partial t = 0$), like the case under consideration, the momentum equation yields the famous **Bernoulli law** along a streamline:

$$\frac{1}{2}v^2 + \frac{P}{\rho} + gz = \text{const.} \tag{11.72}$$

In the present model it is assumed that the Atwood number $A \approx 1$, i.e. the upper fluid has a density much larger than the lower fluid. Therefore, it is

conceivable to assume a constant pressure within the lower density bubble at its border with the heavy fluid. On the other hand, the high-density fluid is in equilibrium with the bubble, and combining this with the assumption of constant density (incompressible fluid), one can rewrite Bernoulli's equation:

$$0 = \tfrac{1}{2}(v_x^2 + v_y^2) + gz \tag{11.73}$$

where the constant has been taken at zero since the peak at $z = 0$ of the bubble is a stagnation point with $v_x = v_y = 0$. Substituting (11.69) and (11.71), into (11.73) one gets

$$1 + \exp\left(-\frac{4\pi z}{\lambda}\right) - 2\exp\left(-\frac{2\pi z}{\lambda}\right)\cos\left(\frac{2\pi x}{\lambda}\right) + \frac{2gz}{u^2} = 0. \tag{11.74}$$

One has to solve the momentum equation, as expressed in equation (11.74), together with the bubble surface equation (11.70) (with $a_1 = u$), yielding the following equation for x:

$$\xi^2 \tan\xi - 2\xi\sin^2\xi + \tan\xi\sin^2\xi + \left(\frac{g\lambda}{\pi u^2}\right)\tan\xi\sin^2\xi\ln\left(\frac{\sin\xi}{\xi}\right) = 0 \tag{11.75}$$

$$\xi \equiv \frac{2\pi x}{\lambda}.$$

Except for $\xi = 0$ (i.e. $x = 0$), this equation has only one solution for a given value of $g\lambda/u^2$. In order to get the more general solution for all points on the bubble surface, one has to take into account the full expansions (or more terms) of equations (11.64) and (11.68). However, u can be obtained to a good approximation by solving equation (11.75) in the neighbourhood of $x = 0$ for different values of g, λ and u. For this purpose this equation is expanded in a series of ξ, yielding the following equation to the lowest relevant order (ξ^5):

$$\xi^5\left(1 - \frac{g\lambda}{6\pi u^2}\right) = 0 \tag{11.76}$$

with the following solution, for the asymptotic velocity of the bubble:

$$u = \sqrt{\frac{g\lambda}{6\pi}} \approx 0.2304\sqrt{g\lambda}. \tag{11.77}$$

As explained in section 11.1, equations (11.2), (11.3) and (11.4), this result is consistent with balancing the buoyancy force and the drag force acting on a rising bubble.

11.6 Richtmyer–Meshkov Instability

The Richtmyer–Meshkov (RM) instability is named after Robert D. Richtmyer, who suggested and also developed the theory of the instability,

and E. E. Meshkov, who proved experimentally the existence of this instability. The RM instability describes the behaviour of the interface between two fluids or gases, traversed by a shock wave. This interface is unstable when the shock wave crosses from the lighter to the heavier media and it is also unstable when the shock wave passes in the opposite direction. A schematic presentation of RM instability is given in figure 11.2. The shock wave imparts an impulsive acceleration to the interface, and as a result an interface disturbance grows initially linearly with time, it saturates, and it can develop into bubbles and spikes like in the RT instability.

We analyse two incompressible fluids with a disturbance of the interface given by

$$z(x,t) = \zeta(t)\exp(\mathrm{i}kx), \qquad k\zeta \ll 1 \tag{11.78}$$

where the real part of the right-hand side (i.e. $\cos kx$) is taken to describe the real z values. If the system is accelerated in the z direction with an acceleration $g(t)$, then the amplitude of the interface disturbance satisfies the equation:

$$\frac{\mathrm{d}^2\zeta(t)}{\mathrm{d}t^2} = kg(t)A\zeta(t), \qquad A \equiv \frac{\rho_{\mathrm{up}} - \rho_{\mathrm{down}}}{\rho_{\mathrm{up}} + \rho_{\mathrm{down}}}. \tag{11.79}$$

This equation is easily obtained from equations (11.29) in the two-dimensional space x–z. The fluid flow velocity solution derived in (11.29) satisfies

$$\frac{\partial^2 v_z}{\partial t^2} = \gamma^2 v_z, \qquad \gamma^2 = kgA \tag{11.80}$$

and therefore, if the displacement $\zeta(t)$ is defined by

$$\frac{\partial \zeta}{\partial t} = v_z \tag{11.81}$$

then equation (11.80) implies the validity of equation (11.79).

Denoting by U the increment of the velocity of an instantaneous impulse at $t = 0$,

$$g(t) = U\,\delta(t) \Rightarrow \int g(t)\,\mathrm{d}t = U \tag{11.82}$$

where $\delta(t)$ is the Dirac delta function, then equation (11.79) can be integrated to give

$$\begin{aligned} &\textbf{before impulse } (t<0): \quad \zeta = \zeta_0, \qquad \frac{\mathrm{d}\zeta}{\mathrm{d}t} = 0 \\ &\textbf{immediately after impulse}: \quad \zeta = \zeta_0, \qquad \frac{\mathrm{d}\zeta}{\mathrm{d}t} = kUA\zeta_0. \end{aligned} \tag{11.83}$$

As can be seen from this equation, after the impulse the amplitude ζ grows at a constant rate.

Table 11.1. The notation for the variables described in figure 11.2, in the case of weak shock waves: velocity $\mathbf{v} = (v_x, v_z)$, specific volume $V = 1/\rho$ where ρ is the fluid density, and pressure P. Note that $P_1 = P_2$.

The variable	Region 0 (heavy fluid)	Region 1 (heavy fluid)	Region 2 (light fluid)	Region 3 (light fluid)
Velocity $v_x(x,z,t)$	0	$u_{1,x}(z,t)\exp(\mathrm{i}kx)$	$u_{1,x}(z,t)\exp(\mathrm{i}kx)$	
Velocity $v_z(x,z,t)$	$u_0 > 0$	$u_{1,z}(z,t)\exp(\mathrm{i}kx)$	$u_{1,z}(z,t)\exp(\mathrm{i}kx)$	$u_3 < 0$
Specific volume $V(x,z,t) = 1/\rho$	V_0	$V_1 + \delta V(z,t)\exp(\mathrm{i}kx)$	$V_2 + \delta V(z,t)\exp(\mathrm{i}kx)$	V_3
Pressure $P(x,z,t)$	P_0	$P_1 + \delta P(z,t)\exp(\mathrm{i}kx)$	$P_2 + \delta P(z,t)\exp(\mathrm{i}kx)$	P_3

One of the basic assumptions for the correctness of (11.79) is that the medium is incompressible. For an impulsive acceleration, such as induced by a shock wave, this assumption is no longer valid and equation (11.79) cannot be used.

Following Richtmyer, we analyse the interface between two fluids (or gases) when a shock wave passes across a disturbed interface from the less dense to a denser medium. As described in figure 11.2, before and after the impulse, a planar shock wave passes a corrugated interface that causes the transmitted and the reflected shocks to also have corrugated surfaces. Before the arrival of the shock the medium is assumed to be at rest. Furthermore, the shock pressure behind the incident shock is assumed constant. In table 11.1 the notation is summarized for the fluid variables, described in figure 11.2. The notation of table 11.1 is given for weak shock waves, where

$$\frac{\delta V}{V_j} \ll 1, \quad j = 1,2, \qquad \frac{\delta P}{P_j} \ll 1, \quad j = 1,2 \tag{11.84}$$

and terms of the second order and higher in δP and δV are neglected. The fluid velocities are given in the frame of reference of the moving interface (after the shock wave has crossed the interface). In this system the mean position of the interface is $z = 0$, and the coordinates of the surfaces (1) between the fluids (the interface), (2) the transmitted shock wave and (3) the reflected shock wave are

$$\begin{aligned} \textbf{interface}: &\quad z = \zeta_0(t)\exp(\mathrm{i}kx) \\ \textbf{transmitted shock}: &\quad z = -w_1 t + \zeta_1(t)\exp(\mathrm{i}kx) \\ \textbf{reflected shock}: &\quad z = w_2 t + \zeta_2(t)\exp(\mathrm{i}kx) \end{aligned} \tag{11.85}$$

where w_1 and w_2 are the shock wave velocities in the interface frame of reference.

Since we are using the linear theory, one can take $\exp(\mathrm{i}kx)$ and $-\mathrm{i}\exp(\mathrm{i}kx)$ for $\cos kx$ and $\sin kx$ respectively. In general, complex functions are used with the meaning that at the last step the real values should be taken.

11.6.1 The differential equation for the pressure in regions 1 and 2

This analysis is a first-order perturbation theory with the small variables as given by (11.84) and also $u_{1,z} \ll w_1$ and w_2, and $\zeta_j k$ (for $j = 0, 1, 2) \ll 1$. For a weak shock wave (Zeldovich and Raizer 1966), the first-order perturbation theory gives the following relation between the pressure increase δP and the specific volume change δV (note that the notation of table 11.1 is used):

$$\delta P(z,t) = \left(\frac{\partial P}{\partial V}\right)_{\mathrm{S}} \delta V(z,t) = -\left(\frac{c_1^2}{V_1^2}\right)\delta V(z,t) \tag{11.86}$$

where c_1 is the speed of sound in the undisturbed medium of region 1 (the heavy fluid). This equation can be considered as the **equation of state** in our approximation.

The **mass conservation**, the first of equations (11.14), can be written as

$$\begin{aligned} &\frac{\partial}{\partial t}\left(\frac{1}{V_1+\delta V}\right) + \left(\frac{1}{V_1+\delta V}\right)\nabla\cdot\mathbf{v}(x,z,t) = 0 \\ &\Rightarrow V_1\left(iku_{1,x} + \frac{\partial u_{1,z}}{\partial z}\right) = \frac{\partial(\delta V)}{\partial t} = -\left(\frac{V_1^2}{c_1^2}\right)\frac{\partial(\delta P)}{\partial t} \end{aligned} \tag{11.87}$$

where at the last step equation (11.86) has been used.

The following two equations are obtained from the **momentum conservation**:

$$\begin{aligned} &\left(\frac{1}{V_1+\delta V}\right)\frac{\partial \mathbf{v}(x,z,t)}{\partial t} = -\nabla[P_1 + \delta P(z,t)\exp(\mathrm{i}kx)] \\ &\Rightarrow \begin{cases} \dfrac{1}{V_1}\dfrac{\partial u_{1,z}}{\partial t} = -\dfrac{\partial(\delta P)}{\partial z} \\ \dfrac{1}{V_1}\dfrac{\partial u_{1,x}}{\partial t} = -\mathrm{i}k\delta P. \end{cases} \end{aligned} \tag{11.88}$$

From equations (11.87) (one equation) and (11.88) (two equations), the following wave equation is derived for $\delta P(z,t)$ in region 1 (see figure 11.2), and similarly the second wave equation is obtained in region 2 with the substitution $c_1 \to c_2$:

$$\begin{aligned} &\frac{\partial^2}{\partial t^2}(\delta P) - c_1^2\left(\frac{\partial^2}{\partial z^2} - k^2\right)(\delta P) = 0 \\ &\frac{\partial^2}{\partial t^2}(\delta P) - c_2^2\left(\frac{\partial^2}{\partial z^2} - k^2\right)(\delta P) = 0. \end{aligned} \tag{11.89}$$

11.6.2 The boundary conditions on the interface

In order to solve equations (11.89) in regions 1 and 2, the equations at the boundaries of these domains have to be defined. Region 1 is defined between the interface (between the fluids) and the transmitted shock surfaces, while region 2 is between the interface and the reflected shock. The normal fluid velocities from both regions are equal at the interface, and therefore one can also write the acceleration continuity on the interface. Using the interface equation (11.85) and the momentum equation (11.88), the following boundary equations are derived by the requirement that the accelerations in the z direction, $\partial u_{1,z}/\partial t$ and $\partial u_{2,z}/\partial t$ are continuous:

$$\begin{aligned} \frac{\mathrm{d}^2\zeta_0(t)}{\mathrm{d}t^2} &= \left[-V_1\left(\frac{\partial(\delta P)}{\partial z}\right)\right]_{z=-0} \\ \left[V_1\left(\frac{\partial(\delta P)}{\partial z}\right)\right]_{z=-0} &= \left[V_2\left(\frac{\partial(\delta P)}{\partial z}\right)\right]_{z=+0}. \end{aligned} \tag{11.90}$$

The second equation is the needed boundary (at the interface) for the partial differential equation (11.89). The main objective of this problem is the study of the RM instability, and for this purpose the first of equations (11.90) gives the required information, i.e. the calculation of ζ_0(t).

In order to complete this problem the boundary conditions at the shock-wave surfaces are also needed.

11.6.3 The boundary conditions at the shock-wave surfaces

First, we use the Hugoniot relations (equations (10.36)) on the boundary of regions 2 and 3, at the reflected shock wave. One has to note that the initial conditions for the Hugoniot equations are those obtained at the final stage after the crossing of the first shock wave. In other words, the reflected shock enters a shocked medium. Moreover, area 3 has also been shocked before the present analysis is considered. However, for this domain the simple Hugoniot relations can be used, and P_3 and V_3 are easily calculated from the initial conditions of region 4, as shown in figure 11.2(a).

Therefore, the first and the fourth equations of (10.36) on the boundary of regions 2 and 3 can be written in the following way:

$$\begin{aligned} \frac{w_2 + \dot{\zeta}_2(t)\exp(\mathrm{i}kx) - u_{1,z}(w_2t,t)\exp(\mathrm{i}kx)}{V_2 + \delta V(w_2t,t)\exp(\mathrm{i}kx)} \\ = \frac{w_2 + \dot{\zeta}_2(t)\exp(\mathrm{i}kx) - u_3}{V_3} \\ \frac{w_2 + \dot{\zeta}_2(t)\exp(\mathrm{i}kx) - u_3}{V_3} = \sqrt{\frac{P_2 + \delta P(w_2t,t)\exp(\mathrm{i}kx) - P_3}{V_3 - V_2 - \delta V(w_2t,t)\exp(\mathrm{i}kx)}} \end{aligned} \tag{11.91}$$

where the dot means time derivative and $P_2 = P_1$. The Hugoniot relations in the form of equations (10.36) are correct only for the velocity components perpendicular to the shock surface. Since the shock front is not a plane, one has to multiply the fluid velocities in these equations with the cosines of the angle between the velocity and the normal to the surface. However, since the angles are first-order variables, these cosines differ from unity by second-order quantities. Therefore, equations (11.91) are correct only to first order in perturbation theory, and by expanding these equations the following zeroth- and first-order equations are obtained respectively:

$$\frac{w_2}{V_2} = \frac{w_2 - u_3}{V_3}, \qquad \frac{w_2}{V_2} = \sqrt{\frac{P_2 - P_3}{V_3 - V_2}} \quad (\text{note: } P_2 = P_1) \tag{11.92}$$

$$\begin{aligned} &\frac{1}{V_2}\left[\frac{d\zeta_2}{\mathrm{d}t} - u_{1,z}(w_2 t, t)\right] - \frac{w_2}{V_2^2}\delta V(w_2 t, t) \\ &\qquad = \frac{1}{2}\sqrt{\frac{P_2 - P_3}{V_3 - V_2}}\left[\frac{\delta P(w_2 t, t)}{P_2 - P_3} + \frac{\delta V(w_2 t, t)}{V_3 - V_2}\right] \end{aligned} \tag{11.93}$$

$$\frac{1}{V_3}\frac{\mathrm{d}\zeta_2}{\mathrm{d}t} = \frac{1}{2}\sqrt{\frac{P_2 - P_3}{V_3 - V_2}}\left[\frac{\delta P(w_2 t, t)}{P_2 - P_3} + \frac{\delta V(w_2 t, t)}{V_3 - V_2}\right].$$

Inspecting the zeroth-order equations (11.92), one can easily recognize the Hugoniot jump conditions for planar one-dimensional waves. It turns out that our problem to zeroth order can be described by planar waves. The corrugation of the surfaces (interface and the shock waves) are described in this analysis by the first-order terms. Using the property that the Hugoniot pressure derivative with respect to the specific volume equals the isentrope derivative at the initial point on the Hugoniot (equation (10.99)), the first-order expansion of the Hugoniot pressure can be described by

$$\begin{aligned} \delta P(w_2 t, t) \equiv \delta P_2(t) &= \left(\frac{\mathrm{d}\delta P_2}{\mathrm{d}V}\right)_{V_2}\delta V = \left(\frac{\mathrm{d}P_\mathrm{S}}{\mathrm{d}V}\right)_{V_2}\delta V \\ &= -\frac{c_2^2 \delta V}{(V_2 + \delta V)^2} \approx \frac{c_2^2 \delta V}{V_2^2} \end{aligned} \tag{11.94}$$

where P_S is the isentropic pressure. Substituting this result into the second equation of (11.93) yields the following boundary condition:

$$\begin{aligned} &\frac{\mathrm{d}\zeta_2(t)}{\mathrm{d}t} = \frac{1}{2}\left(\frac{V_3 V_2}{V_3 - V_2}\right)\left(\frac{c_2^2 - w_2^2}{c_2^2 w_2}\right)\delta P_2(t) \\ &\delta P_2(t) \equiv \delta P(z = w_2 t, t). \end{aligned} \tag{11.95}$$

A similar procedure at the transmitted shock-wave surface yields a similar boundary relation:

$$\frac{\mathrm{d}\zeta_1(t)}{\mathrm{d}t} = \frac{1}{2}\left(\frac{V_0 V_1}{V_0 - V_1}\right)\left(\frac{c_1^2 - w_1^2}{c_1^2 w_1}\right)\delta P_1(t)$$
$$\delta P_1(t) \equiv \delta P(z = -w_1 t, t). \tag{11.96}$$

A second boundary value equation for the reflected shock-wave surface is obtained by the use of the first equation of (11.93). Substituting into this equation the relation between δP and δV at the shock front (equation (11.94)), and comparing the obtained value of $\mathrm{d}\zeta_2/\mathrm{d}t$ with that derived in (11.95), gives

$$u_{1,z}(w_2 t, t) = \frac{1}{2} V_2 \left(\frac{c_2^2 + w_2^2}{c_2^2 w_2}\right)\delta P_2(t). \tag{11.97}$$

By multiplying both sides of this equation with the total derivative, and describing the change in time of a moving fluid element on the shock surface, one gets

$$\left(\frac{\partial}{\partial t} + w_2 \frac{\partial}{\partial z}\right) u_{1,z}(z = w_2 t, t) = \frac{1}{2} V_2 \left(\frac{c_2^2 + w_2^2}{c_2^2 w_2}\right)\left(\frac{\partial}{\partial t} + w_2 \frac{\partial}{\partial z}\right)\delta P(z = w_2 t, t). \tag{11.98}$$

At this stage the mass and momentum equations (equations (11.87) and (11.88)) are necessary. However, before using these equations one has to calculate the x derivative of $u_{1,x}$.

The component of the fluid velocity $\mathbf{v}$, parallel to the shock surface, is continuous across this surface. Therefore, one can write to the first order in our perturbation theory (see figure 11.2(c)) (note $u_{1,x} = u_{2,x}$ and $u_{1,z} = u_{2,z}$):

$$u_{1,x}(w_2 t, t)\exp(\mathrm{i}kx) = u_3 \tan\phi$$
$$\tan\phi = \frac{\partial z}{\partial x} = \frac{\partial}{\partial x}[w_2 t + \zeta_2(t)\exp(\mathrm{i}kx)] = \mathrm{i}k\zeta_2(t)\exp(\mathrm{i}kx) \tag{11.99}$$
$$\Rightarrow \mathrm{i}k w_2 u_{1,x}(z = w_2 t, t) = -k^2 w_2 u_3 \zeta_2(t).$$

Adding this result to equation (11.98) and using the following mass and momentum equations for region 2 (similar to equations (11.87) and (11.88)):

$$\frac{\partial u_{1,z}}{\partial z} + \mathrm{i}k u_{1,x} = -\frac{V_2}{c_2^2}\frac{\partial \delta P}{\partial t}, \qquad -\mathrm{i}k\delta P = \frac{1}{V_2}\frac{\partial u_{1,x}}{\partial t} \tag{11.100}$$

one gets the following second boundary condition on the surface of the reflected shock wave:

$$\left(\frac{3}{2}w_2 + \frac{c_2^2}{2w_2}\right)\frac{\mathrm{d}}{\mathrm{d}t}(\delta P_2) = (w_2^2 - c_2^2)\frac{\partial}{\partial z}[\delta P(z = w_2 t, t)] + \frac{k^2 c_2^2 w_2 u_3}{V_2}\zeta_2(t). \tag{11.101}$$

A similar second boundary condition is given for the transmitted shock-wave surface:

$$\left(\frac{3}{2}w_1 + \frac{c_1^2}{2w_1}\right)\frac{\mathrm{d}}{\mathrm{d}t}(\delta P_1) = -(w_1^2 - c_1^2)\frac{\partial}{\partial z}[\delta P(z = -w_1 t, t)] + \frac{k^2 c_1^2 w_1 u_0}{V_1}\zeta_1(t). \tag{11.102}$$

The boundary conditions given in equations (11.101) and (11.102) describe the change in time of the shock-wave pressures. The first term on the right-hand side of these equations is the pressure gradient contribution behind the shock. The second term on the right-hand side of these equations describes the convergence or divergence of the shock-wave propagation due to the corrugation of the shock surfaces (see figure 11.2(c)).

In this analysis of the RM instability, we have discussed only the linear development of the flow using weak shock waves. The differential equations (11.89) are subject to the boundary equations described by equations (11.90), (11.95), (11.96), (11.101) and (11.102). It is evident that a proper solution of this problem requires the help of a computer. However, the solution of the complete nonlinear problem describing the full development of the RM instability needs two- and three-dimensional sophisticated numerical analysis.

11.7 Kelvin–Helmholtz Instability

The Kelvin–Helmholtz (KH) instability occurs (Kelvin (1910), Helmholtz (1881)) when two different layers of fluids are in relative motion, such as the generation of water waves by wind blowing over the surface of the water (see figure 11.3).

In laser–plasma interactions the KH instability may occur during the later stages of RT and RM instabilities, during the motion of the bubbles and the spikes. For example, the low-density bubbles move relative to the heavy fluid background with appropriate conditions to create KH instabilities.

The motion of an incompressible, inviscid (no viscosity) fluid streaming in the horizontal direction is now considered. The surface tension is neglected in this analysis, although it is straightforward to include this stabilizing effect. It is assumed that the streaming takes place in the x direction with a velocity U, where U is an arbitrary function of z. The fluid is accelerated in the z direction, or equivalently it moves in a potential described by the acceleration g (in the $-z$ direction). First-order perturbation is assumed with the following notation (see equation (11.11)):

1. The flow velocity is $\mathbf{v}(x, y, z, t) + U(z)\hat{\mathbf{x}}$, where the velocity components of $\mathbf{v} = (v_x, v_y, v_z)$ are first-order terms ($\mathbf{v}_0 = 0$ and $\mathbf{v}_1$ is denoted here by $\mathbf{v}$).
2. The fluid density is $\rho(x, y, z, t) = \rho_0(z) + \rho_1(x, y, z, t)$, where ρ_1 is a first-order term.

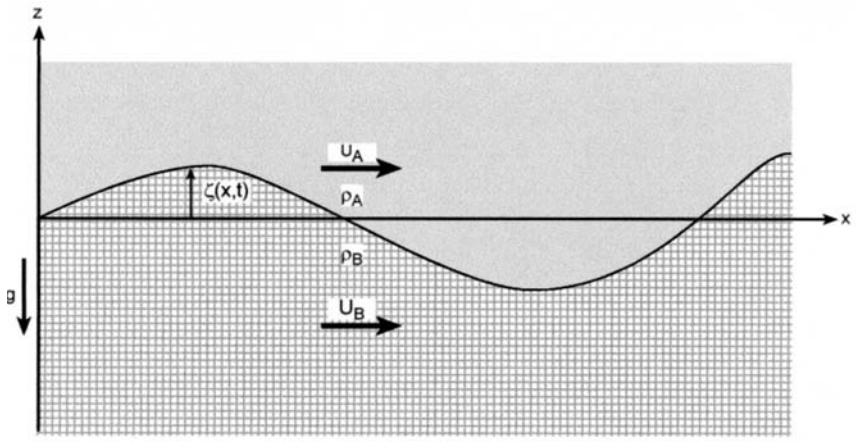

Figure 11.3. Two fluids A and B, with densities ρ_A and ρ_B, moving with different horizontal velocities U_A and U_B. The interface between the two media develops a disturbance with a wave number $k = 2\pi/\lambda$.

3. The pressure is $P = P_0 + P_1(x, y, z, t)$, with P_1 a first-order term.

The momentum conservation, mass conservation and the incompressible fluid assumption give five equations similar to those in (11.18). The following equations are derived by substituting $\mathbf{v}$ by $\mathbf{v} + \mathbf{U}$ in the conservation equations (11.9) and using a similar first-order perturbation theory, as has been done for example in section 11.2:

$$\begin{aligned}
\rho_0 \frac{\partial v_x}{\partial t} + \rho_0 U \frac{\partial v_x}{\partial x} + \rho_0 v_z \frac{\mathrm{d}U}{\mathrm{d}z} + \frac{\partial P_1}{\partial x} &= 0 \\
\rho_0 \frac{\partial v_y}{\partial t} + \rho_0 U \frac{\partial v_y}{\partial x} + \frac{\partial P_1}{\partial y} &= 0 \\
\rho_0 \frac{\partial v_z}{\partial t} + \rho_0 U \frac{\partial v_z}{\partial x} + \frac{\partial P_1}{\partial z} + g\rho_1 &= 0 \\
\frac{\partial \rho_1}{\partial t} + U \frac{\partial \rho_1}{\partial x} + v_z \frac{\mathrm{d}\rho_0}{\mathrm{d}z} &= 0 \\
\frac{\partial v_x}{\partial x} + \frac{\partial v_y}{\partial y} + \frac{\partial v_z}{\partial z} &= 0.
\end{aligned} \tag{11.103}$$

We assume that the interface between the fluids is initially at $z = 0$, the disturbance $\zeta(x, y, t)$ is in the z direction (also a first order perturbation term) and it obeys the following equation:

$$\frac{\partial \zeta}{\partial t} + U(z = \zeta)\frac{\partial \zeta}{\partial x} = v_z(z = \zeta). \tag{11.104}$$

This equation describes the velocity of the disturbance normal to the interface. Analysing the disturbance by its normal modes, one can look for the following solutions (note that here the time dependence is $\exp(\mathrm{i}\Gamma t)$, while in (11.19) it is $\exp(\gamma t)$):

$$\left.\begin{aligned}&\mathbf{v}(x,y,z,t)=\mathbf{u}(z)\\&\rho_1(x,y,z,t)=\delta\rho(z)\\&P_1(x,y,z,t)=\delta P(z)\\&\zeta(x,y,t)=\zeta_0\end{aligned}\right\}\times\exp[\mathrm{i}(k_x x+k_y y+\Gamma t)]. \tag{11.105}$$

Substituting (11.105) into equations (11.103) and (11.104), one gets accordingly

$$\begin{aligned}\mathrm{i}\rho_0(\Gamma+k_x U)u_x+\rho_0\left(\frac{\mathrm{d}U}{\mathrm{d}z}\right)u_z+\mathrm{i}k_x\delta P&=0\\ \mathrm{i}\rho_0(\Gamma+k_x U)u_y+\mathrm{i}k_y\delta P&=0\\ \mathrm{i}\rho_0(\Gamma+k_x U)u_z+\left(\frac{\mathrm{d}\delta P}{\mathrm{d}z}\right)+g\delta\rho&=0\\ \mathrm{i}(\Gamma+k_x U)\delta\rho+u_z\left(\frac{\mathrm{d}\rho_0}{\mathrm{d}z}\right)&=0\\ \mathrm{i}(k_x x+k_y y)+\left(\frac{\mathrm{d}u_z}{\mathrm{d}z}\right)&=0\end{aligned} \tag{11.106}$$

$$\mathrm{i}(\Gamma+k_x U_\zeta)\zeta_0=u_\zeta,\qquad U_\zeta\equiv U(z=\zeta),\qquad u_\zeta\equiv u(z=\zeta). \tag{11.107}$$

Similar to the algebra used to solve equations (11.20), the following differential equation is obtained for $u_z(z)$ by solving equations (11.106):

$$\begin{aligned}&\frac{\mathrm{d}}{\mathrm{d}z}\left\{\left[\rho_0(\Gamma+k_x U)\frac{\mathrm{d}}{\mathrm{d}z}\right]-\left[\rho_0 k_x\left(\frac{\mathrm{d}U}{\mathrm{d}z}\right)\right]\right\}u_z(z)\\ &\quad=\left[k^2\rho_0(\Gamma+k_x U)+\frac{gk^2}{(\Gamma+k_x U)}\left(\frac{\mathrm{d}\rho_0}{\mathrm{d}z}\right)\right]u_z(z).\end{aligned} \tag{11.108}$$

This differential equation is subject to boundary conditions such as that given in (11.24). Furthermore, from equation (11.107) it follows that

$$\frac{u_z(z=\zeta+0)}{\Gamma+k_x U(z=\zeta+0)}=\frac{u_z(z=\zeta-0)}{\Gamma+k_x U(z=\zeta-0)} \tag{11.109}$$

i.e. if one approaches the interface from below or from above, the same value of ζ_0 is obtained, or in other words, if U is continuous at the interface then u_z is also continuous there; however, if U is discontinuous, then the normal displacement on the interface at any point on the surface should be uniquely defined.

At this stage the 'jump' condition on the interface between the fluids is defined. For this purpose one has to integrate equation (11.108) across the

interface from $\zeta - \varepsilon$ to $\zeta + \varepsilon$ in the limit that ε goes to zero. As in (11.28), we define

$$\begin{aligned}
&\lim_{\varepsilon \to 0} \int_{\zeta-\varepsilon}^{\zeta+\varepsilon} \frac{\mathrm{d}}{\mathrm{d}z} F(z)\, \mathrm{d}z = \lim_{\varepsilon \to 0} [F(\zeta+\varepsilon) - F(\zeta-\varepsilon)] \equiv \Delta_\zeta \mathrm{F} \\
&\lim_{\varepsilon \to 0} \int_{\zeta-\varepsilon}^{\zeta+\varepsilon} G(z)\, \mathrm{d}z = 0, \qquad G(z) \text{ continuous at } z = \zeta \\
&\lim_{\varepsilon \to 0} \int_{\zeta-\varepsilon}^{\zeta+\varepsilon} \delta(z-\zeta)\, \mathrm{d}z = 1.
\end{aligned} \tag{11.110}$$

Integrating (11.108) and using (11.109) and (11.110), the following boundary condition (or as occasionally it is called, 'the jump' equation) is satisfied at the interface between the fluids:

$$\Delta_\zeta \left[\rho_0 (\Gamma + k_x U) \frac{\mathrm{d}u_z}{\mathrm{d}z} - \rho_0 k_x \left(\frac{\mathrm{d}U}{\mathrm{d}z} \right) u_z \right] = g k^2 \left(\frac{u_z}{\Gamma + k_x U} \right)_{z=\zeta} \Delta_\zeta \rho_0. \tag{11.111}$$

We calculate explicitly this equation for the following problem. Two uniform fluids, separated at the surface $z = 0$, have densities ρ_A and ρ_B (see figure 11.3). The upper fluid has a density ρ_A smaller than the lower fluid ρ_B, so that in this case we do not analyse the RT instability. Regarding the streaming, it is assumed that the upper fluid and the lower fluid stream have constant velocities U_A and U_B respectively.

Equation (11.108) for constant ρ_0 and U, i.e. anywhere except at the interface between the fluids, reduces to

$$\left(\frac{\mathrm{d}^2}{\mathrm{d}z^2} - k^2 \right) u_z(z) = 0. \tag{11.112}$$

The general solution of this equation is a linear combination of $\exp(kz)$ and $\exp(-kz)$. Taking into account that u_z vanishes at $\pm\infty$, and at $z = 0$ equation (11.109) must be satisfied, one obtains the solution

$$u_z(z) = \begin{cases} w(\Gamma + k_x U_\mathrm{B}) \exp(kz) & \text{for } z < 0 \\ w(\Gamma + k_x U_\mathrm{A}) \exp(-kz) & \text{for } z > 0. \end{cases} \tag{11.113}$$

Using (11.110), the jump relations relevant for this problem are

$$\begin{aligned}
\Delta_0 \left[\rho_0 (\Gamma + k_x U) \frac{\mathrm{d}u_z}{\mathrm{d}z} \right] &= k w [\rho_\mathrm{A} (\Gamma + k_x U_\mathrm{A})^2 + \rho_\mathrm{B} (\Gamma + k_x U_\mathrm{B})^2] \\
\Delta_0 \left[\rho_0 k_x \left(\frac{\mathrm{d}U}{\mathrm{d}z} \right) u_z \right] &= 0 \\
g k^2 \left(\frac{u_z}{\Gamma + k_x U} \right) \Delta_0(\rho_0) &= w g k^2 (\rho_\mathrm{A} - \rho_\mathrm{B}).
\end{aligned} \tag{11.114}$$

Substituting (11.114) into (11.111) yields the following quadratic equation in Γ:

$$\Gamma^2 + \frac{2k_x}{\rho_A + \rho_B}(\rho_A U_A + \rho_B U_B)\Gamma + \left[\frac{k_x^2}{\rho_A + \rho_B}(\rho_A U_A^2 + \rho_B U_B^2) - \frac{gk}{\rho_A + \rho_B}(\rho_B - \rho_A)\right] \tag{11.115}$$

with the solutions

$$\Gamma = -\frac{k_x}{\rho_A + \rho_B}(\rho_A U_A + \rho_B U_B) \pm \left[\frac{gk(\rho_B - \rho_A)}{\rho_A + \rho_B} - \frac{k_x^2 \rho_A \rho_B (U_B - U_A)^2}{(\rho_A + \rho_B)^2}\right]^{1/2}. \tag{11.116}$$

If the perturbations are perpendicular to the streaming, then the flow is stable:

$$k_x = 0: \quad \Gamma = \pm\sqrt{gk\left(\frac{\rho_B - \rho_A}{\rho_B + \rho_A}\right)}. \tag{11.117}$$

Since $\rho_B > \rho_A$, the solution of all perturbations behave like $\exp(i\Gamma t)$, Γ real, and therefore no instability.

If the perturbations are in any direction other than normal to the streaming, then instability occurs. Defining the angle θ between the vector $\mathbf{k}$ and the x axis, or more generally between the vectors $\mathbf{U}$ and $\mathbf{k}$,

$$\cos\theta = \frac{k_x}{k} = \frac{\mathbf{k}\cdot\mathbf{U}}{kU} \tag{11.118}$$

then instability occurs if Γ in equation (11.116) is complex, so that $\exp(i\Gamma t)$ increases exponentially. Instability exists when

$$k(U_B - U_A)^2 \cos^2\theta > g\left(\frac{\rho_B^2 - \rho_A^2}{\rho_B \rho_A}\right) \tag{11.119}$$

or equivalently the instability develops for any wave number k satisfying

$$k > k_{\min} \equiv g\left(\frac{\rho_B^2 - \rho_A^2}{\rho_B \rho_A}\right)\frac{1}{(U_B - U_A)^2 \cos^2\theta}. \tag{11.120}$$

It is interesting to point out that the KH instability occurs for any finite value of velocity jump across the interface, $U_B - U_A$, assuming that θ is not 90°. The stability of any static configuration becomes KH, unstable in the presence of a streaming difference (sharp gradient) across the interface of two fluids.